Vaccinia Virus Modulates the Host Cell Cycle to Promote Infection

Caroline Katharina Martin

A dissertation submitted in partial fulfilment of the requirements for

the degree of Doctor of Philosophy

University College London

MRC Laboratory for Molecular Cell Biology

Supervised by

Dr Jason Mercer and Dr Mark Marsh

September 2019

Declaration

I, Caroline Katharina Martin, confirm that the work presented in this thesis is my own. Where information has been derived from other sources, I confirm that this has been indicated in the thesis.

Signed

Date

Abstract

Vaccinia Virus (VACV) is well-known as the vaccine used for the eradication of smallpox. It serves as the model orthopox virus and has gained further clinical significance as an oncolytic virus. As a member of the poxvirus family, VACV is a double-stranded DNA virus that replicates exclusively in the cytoplasm of infected cells. Early research suggested that VACV alters the host cell cycle and inhibits cellular DNA synthesis. Later, VACV was described to modulate key cell cycle regulators during late timepoints of infection. However, the relevance of this cell cycle subversion to VACV replication and how it is achieved remains undefined. In this PhD project, I combined state of the art techniques with classical assays to determine the (viral) effector proteins, their mode of action, and the contribution of the host cell cycle to productive VACV infection. Using recombinant VACV strains, RNAi, biochemistry, and super-resolution microscopy, I demonstrate that VACV early gene expression inhibits cell proliferation after viral entry. Concurrently, the cellular CDK inhibitor p21 is upregulated, while the tumour suppressor p53 is targeted for degradation by the viral kinase B1 and/or its paralog pseudokinase B12. The second wave of viral gene expression shifts the cell cycle from G1 to S/G2/M, while still inhibiting cell proliferation. Additionally, the viral kinase F10 was shown to be necessary and sufficient to cause degradation of p21, and for activation of the cellular DNA damage response (DDR), a process known to be essential for viral DNA replication. By probing these cellular pathways with a small molecule inhibitor library I defined their requirement for the viral life cycle. Screening for defects in viral late gene expression, I found inhibition of Aurora Kinases, selected CDKs, ATR and Chk1/2 interferes with infection. Collectively, I demonstrate that VACV modulates cell cycle checkpoints and identify the viral kinases B1 and F10 as potential temporal controllers of the host cell cycle that serve to promote productive viral replication.

Impact statement

Cancer represents the second most prevalent cause of death worldwide, costing millions of lives each year. With over 18 million new cases in 2018 alone, it imposes an immense burden on global healthcare systems. Due to the high treatment-associated costs, the majority of deaths caused by cancer occur in low and middle income countries. There is therefore a great need for preventative treatments and novel, more effective anti-cancer therapies. Development of improved therapies relies on better understanding of the mechanisms that drive oncogenesis. These efforts have identified a small group of oncogenic viruses that drive cancer development, and current estimates by the WHO assume that viral infections account for 20% of human cancer cases. However, viruses have not only been recognized as a cause for cancer but also as a promising biotechnological tool for anti-cancer therapy. These virotherapies exploit a virus' natural or engineered preference for preferentially infecting and thereby destroying tumour cells. Several different virotherapies based on oncolytic viruses such as vaccinia virus (VACV) are currently being tested in clinical trials.

VACV is well-known as the model poxvirus and has gained clinical significance as the vaccine used to successfully eradicate smallpox. The causative agent of smallpox, variola poxvirus, remains the deadliest virus in human history, accounting for more than 500 million deaths. The smallpox vaccination campaign has been discontinued, which leaves the population at risk for smallpox re-emergence by bioterrorism, or zoonotic poxvirus infections such as monkeypox and cowpox. Limited treatment options for poxvirus infections necessitate continued research into this virus family to develop improved anti-virals and vaccines.

This study characterizes how VACV affects the division and growth program of its host cell, the so-called cell cycle. This process is tightly regulated in normal cells, whereas uncontrolled cell division is a hallmark of cancer. Several molecular checkpoints ensure that cells divide in a controlled manner. To study the interaction of VACV with the cellular checkpoint machinery, new methods were developed that can also be applied to study other viruses. Using these assays, VACV was found to activate cellular checkpoints and thereby prevents (cancer) cells from dividing. Apart from inhibiting cancer cell division, activation of the checkpoint machinery was also shown to be essential for VACV replication and production of infectious particles. Highlighting the complexity of host-pathogen interactions, these findings might not only help the advancement of improved anti-cancer virotherapies but also provide new drug targets for the development of anti-poxviral agents.

Acknowledgements

[redacted]

[redacted]

List of Figures

List of Tables

List of Cellular Proteins

Protein abbreviation	Protein name
Protein function	
Relevance to study	

α-Tubulin	α-Tubulin
Major component of microtubules which are part of the cellular cytoskeleton.	
Loading control for immunoblots.	
ATR	Ataxia telangiectasia and Rad3-related
Serine/threonine protein kinase. Sensor of (cellular) DNA damage and essential kinase in the DNA damage checkpoint. Activation due to double strand breaks, escalates the signal by phosphorylating downstream effectors, including the kinase Chk1. Results in inhibition of cellular DNA replication to promote DNA repair and/or apoptosis.	
VACV infection was found to activate Chk1, which is the downstream effector kinase of ATR. Previously, it has been published that VACV infection activates both ATR and ATM in the cytosol but only depends on ATR activation for viral genome replication (Postigo et al., 2017).	
ATM	Ataxia-telangiectasia-mutated
Serine/threonine protein kinase. Sensor of (cellular) DNA damage and essential kinase in the DNA damage checkpoint. Activation due to single strand breaks, escalates the signal by phosphorylating downstream effectors, including the kinase Chk2. Results in inhibition of cellular DNA replication to promote DNA repair and/or apoptosis.	
VACV infection was found to activate Chk2, which is the downstream effector kinase of ATM. Previously, it has been published that VACV infection activates both ATM and ATR in the cytosol but only depends on ATR activation for viral genome replication (Postigo et al., 2017).	
Aurora A	Aurora kinase A
Serine/threonine kinase. Critical regulator of key mitotic events such as spindle assembly, and centrosome separation. Assists progression through spindle checkpoint during mitosis.	
Chemical inhibition of the kinase for 24h prior to infection was found to prevent viral late gene expression but not viral early gene expression.	
Aurora B	Aurora kinase B
Serine/threonine kinase. Part of the chromosome passenger complex. Involved in key mitotic events such as chromosome condensation and alignment, as well as cytokinesis.	
Chemical inhibition of the kinase for 24h prior to infection was found to prevent viral late gene expression but not viral early gene expression.	
Cdc25	Cell division cycle 25
Tyrosine protein phosphatase	
Dephosphorylates CDK1, thus assisting in CDK1 activation and M phase entry. Involved in the DNA damage response ATR/ATM cascade to arrest the cell cycle.	
CDK1	Cyclin-dependent kinase 1
Serine/threonine kinase. Associates with Cyclin A to promotes G2 progression, then switches to Cyclin B binding which is required for M phase entry.	
CDK1 levels, as well as phosphorylation of CDK1 were analysed by immunoblot analysis over an infection timecourse of 24h. While VACV was not found to modulate CDK1 protein	

expression, it was observed that CDK1 in infected cells was more phosphorylated on Tyr15 (i.e. inhibited) than mock infected controls.	
CDK2	Cyclin-dependent kinase 2
Serine/threonine kinase. Associates with Cyclin E at the G1/S border to promote S phase entry, then binds Cyclin A which promotes S phase completion.	
Protein levels were analysed by immunoblot over an infection timecourse of 24h. No viral modulation of CDK2 levels was observed.	
CDK4	Cyclin-dependent kinase 4
Serine/threonine kinase. Promotes G1/S transition; phosphorylates and thus inhibits cellular Rb. Requires Cyclin D for cyclic activation.	
Protein levels were analysed by immunoblot over an infection timecourse of 24h. No viral modulation of CDK4 levels was observed.	
CDK6	Cyclin-dependent kinase 6
Serine/threonine kinase. Promotes G1/S transition; phosphorylates and thus inhibits cellular Rb. Requires Cyclin D for cyclic activation.	
Protein levels were analysed by immunoblot over an infection timecourse of 24h. CDK6 levels were observed to decrease upon infection, compared to mock infected controls.	
CDK7	Cyclin-dependent kinase 7
Serine/threonine kinase. Catalytic subunit of the CDK-activating kinase (CAK) complex which is required for activation of other cell cycle regulatory proteins including CDK1/2/4/6.	
Protein levels were analysed by immunoblot over an infection timecourse of 24h. No viral modulation of CDK7 levels was observed.	
Cdt1	Chromatin licensing and DNA replication factor 1
Cellular DNA replication licensing factor, essential for pre-replication complex assembly, loading of the MCM complex onto DNA	
Cell cycle-dependent expression exploited as a marker for G1 phase. Used both untagged in immunoblots and fluorescently tagged in the stable HeLa FUCCI cell line (Sakaue-Sawano et al., 2008).	
Chk1	Chk1
Serine/threonine-protein kinase. Effector kinase in the ssDNA damage response pathway: activated ATR propagates the signal by phosphorylating Chk1, which triggers a biochemical cascade that results in inhibition of S phase progression and prevents M phase entry. Modulates activity of key effectors such as the M phase promoting phosphatases Cdc25A and Cdc25C.	
VACV infection was shown to cause activation of Chk1, as was measured by phosphorylation of Chk1 at Ser345. Activated Chk1 was observed by immunofluorescence to be enriched in VACV replication sites. Chemical inhibition of Chk1 was found to inhibit viral late gene expression while allowing for viral early gene expression.	
Chk2	Chk2
Serine/threonine-protein kinase. Effector kinase in the dsDNA damage response pathway: activated ATM propagates the signal by phosphorylating Chk2, which triggers a biochemical cascade that results in inhibition of S phase progression and prevents M phase entry. Modulates activity of key effectors such as p53 and p21.	
The viral kinase F10 was shown to cause activation of Chk2, as was measured by phosphorylation of Chk2 at Thr68. Activated Chk2 was observed by immunofluorescence to be enriched in VACV replication sites. Chemical inhibition of Chk1/2 was found to inhibit viral late gene expression while allowing for viral early gene expression.	
Cyclin A	Cyclin A
CDK activating protein, S/G2 transition and G2 progression.	

VACV was previously reported to reduce Cyclin A expression (Wali and Strayer, 1999b). These findings were confirmed in this study and VACV infection was found to reduce Cyclin A levels compared to mock infected controls (measured by immunoblot analysis).	
Cyclin B	Cyclin B
CDK activating protein, G2/M transition and M phase progression.	
VACV was previously reported to alter expression of Cyclin B (Wali and Strayer, 1999b). However, immunoblot analysis in this study could not confirm these findings and Cyclin B levels were not measured to modulated by VACV infection (assessed by immunoblot analysis).	
Cyclin D	Cyclin D
CDK activating protein, G1 and G1/S - specific protein	
Required for G1 progression and S phase entry. Immunoblot analysis of VACV infected cells showed no viral modulation of Cyclin D protein levels compared to mock infected controls.	
Cyclin E	Cyclin E
CDK activating protein, G1/S - specific protein	
Cyclin E levels were analysed by immunoblot over an infection timecourse of 24h. No viral modulation of Cyclin E levels was observed.	
DNA-PK	DNA-dependent protein kinase catalytic subunit
Serine/threonine protein kinase.	
Sensor for (cellular) DNA damage. Part of the ssDNA damage response. Has been previously been reported to have anti-poxviral activity and is counteracted the by the VACV proteins C4 and C16 (Ferguson et al., 2012; Peters et al., 2013; Scutts et al., 2018). In this study, chemical inhibition of DNA-PK was not found to affect VACV replication.	
Geminin	Geminin
Cellular inhibitor of cellular DNA replication. Blocks association of the MCM complex with the pre-replication complex.	
Cell cycle-dependent expression exploited as a marker for S/G2/M phase. Used both untagged in immunoblots and fluorescently tagged in the stable HeLa FUCCI cell line (Sakaue-Sawano et al., 2008).	
MCM2	Minichromosome maintenance protein 2
Subunit of the MCM2-7 complex required for cellular DNA replication initiation and elongation	
Used as a marker to distinguish quiescent from dividing cells by immunoblot analysis.	
Mdm2	(Mouse) double minute 2
E3 ubiquitin-protein ligase	
Destabilizes the tumour suppressor p53 by ubiquitination and directs its proteasomal degradation in unstressed cells. VACV was found in this study to cause degradation of Mdm2 in a viral kinase B1 and/or viral pseudokinase B12 dependent manner.	
MEK1	Mitogen-activated protein kinase 1 (MAP2K1)
Serine/threonine kinase. Part of the MAP kinase signalling pathway. Extracellular factors (e.g. mitogens, growth factors, and cytokines) associate with the receptor Ras, which then activates Raf1. Raf1 promotes activation of MEK1. This regulates several cellular effects such cell growth, and cell division.	
The effect of chemical inhibition of MEK1 on VACV replication was tested. MEK1 inhibition was not found to negatively affect the viral life cycle at the tested concentrations.	
P21	P21, Waf1, Cip1
Member of the Cip/Kip family of CDK inhibitors (CKI). Context-dependent function: in the presence of mitogens assists G1/S transition. In the absence of cell cycle stimulatory factors inhibits CDKs, thus preventing cell cycle progression.	

VACV infection was found to dynamically regulate cellular levels of p21 (induction coinciding with viral early gene expression, degradation coinciding with viral late gene expression). F10 was shown to be sufficient and required to degrade p21 late during infection.	
P53	P53
Transcription factor and tumour suppressor. Relays and integrates signals from different cellular pathways in response to stresses such as DNA damage, hypoxia, and starvation. Induces cell cycle arrest to allow for e.g. DNA repair, or apoptosis if the damage is irreparable. Transcription factor for p21.	
VACV infection was observed to cause degradation of p53 (Wali and Strayer, 1999b; Yoo et al., 2008). However, p53 was found to be dispensable for the VACV-induced cell cycle arrest. The p53 stabilizing drug Nutlin-3 was shown to inhibit viral late gene expression and to prevent VACV from shifting the cell cycle.	
PCNA	Proliferating cell nuclear antigen
Subunit of the cellular DNA polymerase delta, processivity factor, and implicated in cellular DNA damage response.	
Used as a marker to distinguish quiescent from dividing cells by immunoblot analysis. Was reported to be involved in VACV genome replication (Postigo et al., 2017).	
PIM1	PIM1
Serine/threonine protein kinase	
Phosphorylates and stabilizes the CKI p21 (Wang et al., 2002). Shares sequence homology with the viral kinase B1.	
PIM2	PIM1
Serine/threonine protein kinase	
Phosphorylates and stabilizes the CKI p21 (Wang et al., 2010). Shares sequence homology with the viral kinase B1.	
Rb	Retinoblastoma-associated protein
Transcriptional repressor. Hypophosphorylated (active) Rb binds to the cellular transcription factor E2F1, prevents transcription of its target genes, thus inhibiting G1/S progression. Serine/threonine protein kinase	
Dysregulation of Rb activity is observed in several viral infections. VACV was shown to cause hypophosphorylation of Rb. However, Rb(hypo) was found to be inactivated by sequestration into a complex with the TFIIIB subunit Brf1 (Yoo et al., 2008).	
Wee1	Wee1
Tyrosine protein kinase	
Inhibitory phosphorylation of CDK1 on Tyr15, thus blocking M entry. Chemical inhibition of Wee1 was found to inhibit VACV replication after early and before late viral gene expression.	

List of Viral Proteins

Protein abbreviation	Protein name (gene name)	Viral expression
Protein function		
Relevance to study		

A24	DNA-directed RNA polymerase 133kDA polypeptide RPO132, A24 (A24R)	Early and prepackaged
Subunit of the DNA-dependent RNA polymerase. Required for early, intermediate, and late viral gene transcription.		
siRNA knockdown of A24 was used as an experimental mean to inhibit viral intermediate and late gene expression, while allowing for viral genome replication.		
B1	Serine/threonine protein kinase B1 (B1R)	Early and prepackaged
Promotes viral genome replication by phosphorylating and thus inhibiting the host antiviral factor BAF1, as well as the viral pseudokinase B12. Loss of B1 prevents viral genome replication (Olson et al., 2017; Wiebe and Traktman, 2007).		
siRNA knockdown of B1, or a temperature sensitive VACV mutant with a non-functional version of B1 were used as an experimental mean to inhibit viral genome replication and viral post-replicative gene expression while allowing for viral early gene expression. Additionally, B1 and/or its pseudokinase B12 were found to be required for VACV-mediated degradation of cellular p53 and Mdm2. B1 was found to be dispensable for both the observed VACV-induced cell cycle arrest and shift.		
B12	Probable serine/threonine protein kinase B12 (B12R)	Early
Paralog pseudokinase of B1. Represses viral genome replication in the absence of B1 through an unknown mechanism. B1 represses B12 (Olson et al., 2017, 2019).		
In this study a recombinant VACV strain (ΔB1mutB12) was used that lacks B1 and has an additional mutation in B12 which renders the virus replication competent. ΔB1mutB12 could no longer direct degradation of p53, nor Mdm2 but was found to still block host cell cycle progression.		
D5	Primase/helicase D5 (D5R)	Early and prepackaged
Required for VACV core degradation, genome uncoating and replication (Kilcher et al., 2014).		
siRNA knockdown of D5, or temperature sensitive VACV mutants with non-functional versions of D5 were used as an experimental mean to inhibit viral genome uncoating and post-uncoating steps while allowing for viral early gene expression.		
E9	DNA polymerase E9 (E9L)	Early
Viral DNA synthesis.		

siRNA knockdown of E9 was used as an experimental mean to inhibit viral genome replication and viral post-replicative gene expression while allowing for viral early gene expression and viral genome uncoating.		
F10	Serine/threonine protein kinase F10 (F10L)	Late and prepackaged
F10 is required for several steps during VACV morphogenesis: recruitment of cellular membranes to initiate crescent formation; transition of immature virions into mature virions (forms a dynamic phosphorylation network with H1). Additional function in modulation of the host cytoskeleton and stress fibre formation (Greseth et al., 2017; Novy et al., 2018; Punjabi and Traktman, 2005).		
This study has identified F10 as required and sufficient to activate the cellular DNA damage response as marked by phosphorylation of Chk2. Additionally, F10 was found to be required and sufficient to cause degradation of cellular p21 late during VACV infection.		
F17	Phosphoprotein (F17R)	Late and prepackaged
Required for virion maturation and infectivity (Wickramasekera and Traktman, 2010). Prevents cytosolic sensing by dysregulation of mTOR (Meade et al., 2018).		
Used as a marker for viral late gene expression in immunoblots		
H1	Dual specificity protein phosphatase H1 (H1L)	Late and prepackaged
Dephosphorylates the viral early transcription factor A7, which is required for transcriptional competence of the virus. Negatively regulates the viral protease I7, which is involved in VACV morphogenesis (Liu et al., 1995; Novy et al., 2018). Immunomodulatory functions: prevents Stat1 activation (Najarro et al., 2001).		
Genetic deletion of H1 was used as an experimental mean to test for the requirement of viral early gene expression and/or the phosphatase H1 itself in blocking and/or shifting the host cell cycle.		
I3	Protein I3 (I3L)	Early and intermediate
Single stranded DNA binding protein, interacting with viral genomes, undefined function in viral genome replication (Greseth et al., 2012, 2018).		
Used as a marker for viral early gene expression in immunoblots		

Table of Contents

1 Introduction

1 Poxviruses and vaccinia virus

1.1 Poxviruses: A general overview

Viruses are ancient, obligate intracellular parasites that have co-evolved with their hosts for millions of years. As such they have developed highly diverse morphologies, host range tropisms, and replication strategies.

Poxviruses are amongst the largest and most complex viruses known to date. They package a single, linear 120-360 kbp double-stranded DNA genome, which encodes over 200 ORFs (Moss, 2007). Owing to the large coding capacity, poxviruses replicate more autonomously from the host cell than other viruses. They encode and pre-package their own transcription and replication machinery which allows viral replication to occur in the cytoplasm (Cyrklaff et al., 2005; Moss, 2013). While poxviral DNA replication is independent of the nuclear DNA machinery, viral proteins are translated on host ribosomes. These viral proteins modulate and highjack (almost) every cellular pathway to promote productive infection. Horizontal gene transfer armed poxviruses with an arsenal of immune-modulatory factors that help to avoid detection by the immune system, as well as subversion of apoptotic pathways (McFadden et al., 1995).

Poxviruses have a broad host and cell tropism, although their primary cell type is thought to be epithelia (McFadden, 2005). Highlighting this, the *Poxviridae* family is subdivided into the *Chordopoxvirinae* that infect vertebrates, and the *Entomopoxvirinae* that infect insects (Figure 1-1). The *Chordopoxvirinae* are further subdivided into eight genera, including the Orthopoxviruses, Leporipoxviruses, and Molluscipoxviruses (Moss, 2007). The most well-studied genera are the Orthopoxviruses which comprise the etiological agent of smallpox variola virus (VARV), the prototype poxvirus vaccinia virus (VACV), and two poxviruses which are known to cause zoonotic infections, monkeypox (MPXV) and cowpox virus (CPXV).

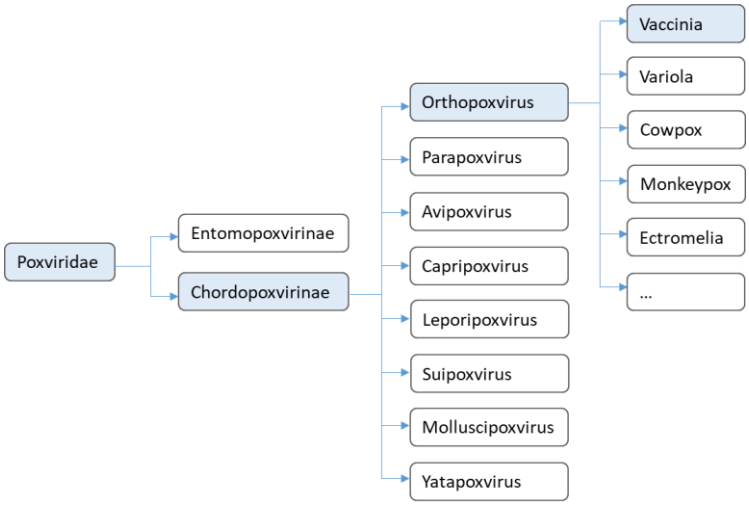

Figure 1-1 Poxviridae family phylogenetic tree.

Although the origin of poxviruses remains enigmatic, DNA sequencing and bioinformatics analysis showed the Poxviridae family to be closely related to other DNA virus families such as the Asfaviridae, Iridoviridae, Phycodnaviridae, and Mimiviruses (Iyer et al., 2001; Suzan-Monti et al., 2006).

1.2 Medical history of poxviruses

In 1980 the world witnessed the first and, to date, only eradication of a human pathogen: variola virus (VARV), the causative agent of smallpox. Smallpox infections start with non-specific symptoms such as fever and fatigue, before developing the characteristic virus filled lesions that spread across the entire body of an infected individual (Behbehani, 1983). With a mortality rate of 15-45% variola major killed 2-3 million people a year, amounting to 300 to 540 million casualties in the 20th century alone (Aylward and Birmingham, 2005; Behbehani, 1983; Selgelid, 2004). This makes smallpox the deadliest human pathogen that has been described (WHO).

Highlighting the social impact and ancient history of VARV, the Indian God Kakurani is dedicated to smallpox and descriptions of smallpox-like symptoms can be found already in ancient Indian and Chinese writings (Behbehani, 1983). Although the biological origins of VARV remain enigmatic, it is speculated that VARV might have evolved from Camelpox (Behbehani, 1983). Global traders and invaders brought the disease to Europe and North Africa around 570

AD. Spanish invaders spread smallpox across the Atlantic to the Americas where 3.5 millions Aztecs were killed by introduction of VARV.

The history of smallpox is closely linked to the history and discovery of vaccination as a preventative treatment. In 1122 BC China reported a novel immunization process against smallpox, so-called “variolation”. Susceptible individuals would sniff or swallow scab material from smallpox lesions in order to gain protective immunity. However, this early form of vaccination was associated with considerable risks and inoculated patients frequently developed smallpox infections. The breakthrough in combatting smallpox was made in England in the 18th century. Several physicians observed that dairy maids who were previously infected with cowpox seemed protected from subsequent smallpox infections (Behbehani, 1983). One of the physicians, Dr. Edward Jenner, systematically researched the protective immunization of cowpox and discovered that passaging of cowpox through a human host increased the effectiveness of immunization. In 1796 Dr. Edward Jenner coined the term variolae vaccinae (smallpox of the cow) which he used to describe the inoculation of individuals with cowpox to confer immunity against subsequent smallpox infection. Despite initial scepticism, vaccination became recognized as a safe and effective preventative treatment to combat smallpox (Behbehani, 1983). Almost 200 years after the invention of vaccination, smallpox was targeted for eradication in a world-wide vaccination program. The Smallpox Eradication Program from 1966-1980 spearheaded by the WHO immunized individuals with three different vaccines based on live, replicating poxvirus. Although the origin remains unknown, the virus has been isolated and was termed vaccinia (VACV). The WHO noted the last natural case in Somalia in 1977 before smallpox was officially declared eradicated in 1980 (Okwo-Bele and Cherian, 2011).

Although smallpox is eradicated, poxviruses are still recognized as a potential threat to global health (WHO, 2015). Recent advancements in synthetic biology allowed Noyce and co-workers to bring previously extinct horsepox back from the dead by recreating it from synthetic DNA fragments (Noyce et al., 2018). This opens up the possibility of reconstituting VARV and its use as a bioterrorist agent. However, poxviruses do not only pose a threat through deliberately re-created and released viruses: Zoonotic transmission of monkeypox has a reported fatality rate of 10-15%. Monkeypox is endemic in Africa but sporadic outbreaks have also been reported in the USA and in individual cases in the UK (Nolen et al., 2016; Vaughan et al., 2018). Treatment of poxvirus infections relied on non-poxvirus specific anti-virals such as cidofovir, which has originally been approved for treatment of cytomegalovirus. Limited specificity and bioavailability required the development of improved, specific anti-poxvirals (De Clercq,

2002). In 2018, the first orthopox-specific anti-viral was globally approved (Hoy, 2018). Tecovirimat (TPOXX) inhibits the wrapping protein F13 and therefore prevents formation and egress of EVs. Although a considerable advancement in poxvirus therapeutics, TPOXX remains the only orthopoxviral-specific compound approved by the FDA for use in humans. Given the continued threat to global health by poxviruses, further research of poxvirus - host interactions are essential in order to improve and expand current treatment options.

However, poxviruses have not only been recognized for their disease potential but also as a promising biotechnological vector for gene therapy (cf. section 2.3). Additionally, poxviruses have co-evolved with their cellular host for thousands of years and have developed strategies to manipulate and exploit almost every cellular pathway. Together with the possibility to genetically modify their genome, this makes poxviruses an excellent molecular tool to study host cell biology.

2 Vaccinia Virus

2.1 Morphology and composition of the virion

Poxviruses, including VACV, produce two types of infectious particles during infection: mature virions (MVs), and enveloped virions (EVs). Whereas MVs are wrapped in a single membrane which contains the viral fusion machinery, EVs contain an MV-like particle that is surrounded by a second lipid bilayer (Figure 1-2) (Payne, 1978, 1979; Smith et al., 2002). MV-like particles contained in EVs are distinct from MVs as they lack the viral protein A26 (Ulaeto et al., 1996). EVs are exocytosed from 8hpi onwards and mediate short range virus spread within a tissue (Payne, 1980). MVs on the other hand are released by cell lysis after ca. 72hpi and are required for long range host-to-host transmission (Moss, 2007; Smith et al., 2003).

VACV virions were first visualized by electron microscopy (EM) as large, brick-shaped particles, measuring 360 x 270 x 250 nm (Cyrklaff et al., 2005; Griffiths et al., 2001; Hollinshead et al., 1999; Nagler and Rake, 1948; Roos et al., 1996; Sodeik and Krijnse-Locker, 2002). MVs are composed of approximately 80 different structural proteins arranged into three main structural elements (Condit et al., 2006; Cyrklaff et al., 2005; Easterbrook, 1966; Goebel et al., 1990; Hollinshead et al., 1999; Ichihashi, 1996): the dumbbell shaped core containing the viral dsDNA genome and early transcription system, two lateral bodies (LBs) that flank the core, and a single-lipid bilayer membrane containing 26 membrane proteins, half of which are

dedicated to fusion (Bisht et al., 2008; Gray et al., 2018; Moussatche and Condit, 2015; Ojeda et al., 2006; Senkevich and Moss, 2005).

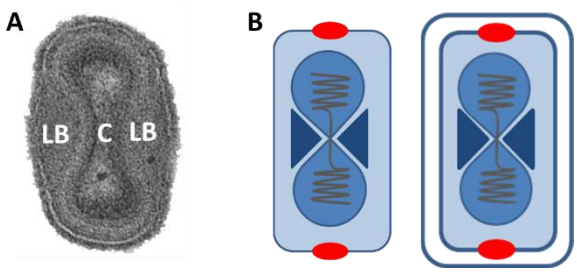

Figure 1-2 Vaccinia virion structure.

[A] VACV as seen by electron microscopy (image: Dr. Jason Mercer). The dumbbell-shaped core (C) contains the viral dsDNA genome and is flanked by two proteinaceous structures called lateral bodies (LB). The virion is surrounded by a lipid bilayer envelope. [B] Schematic representation of an MV (left) and an EV (right). Outlined are the viral genome, the dumbbell-shaped core, the two lateral bodies and the entry fusion complex (red) at the tips of the virions.

The virion core contains the 192 kbp VACV genome which encodes approximately 200 genes. Within the core, the genome is packed into highly condensed structures termed nucleoids, which assemble to form 30-40nm thick helical tubules, comparable to cellular chromosomes (Goebel et al., 1990; Griffiths et al., 2001; Holowczak et al., 1975; Malkin et al., 2003; Müller and Peters, 1963).

The LBs are two proteinaceous structures that reside on either side of the core. Although the exact composition and function of the LBs is unclear, they have been shown to pre-package (viral) effector proteins, including the main component F17, G4, and the viral phosphatase H1. Upon viral entry, the LBs are degraded in a proteasome-dependent manner to release the pre-packaged proteins that were proposed to function as cytoplasmic immune-modulators (Schmidt et al., 2013). Therefore, the LBs offer an immediate delivery system of pre-synthesised effector proteins that do not require de novo protein synthesis.

2.2 VACV replication cycle

The virus life cycle has co-evolved with its host cell to efficiently produce a large number of infectious progeny virions. VACV encodes over 200 proteins which allow the virus to highjack (almost) every cellular process to promote its own replication. Unique amongst DNA viruses, the poxvirus life cycle takes place only in the cytoplasm of infected cells, and no nuclear replication stage has been observed.

The complex VACV replication consists of temporally cascaded phases which each depend on completion of the previous step (Figure 1-3). The virus life cycle begins with attachment to the host cell where virions use apoptotic mimicry to trigger their own uptake by macropinocytosis (Mercer and Helenius, 2008a; Mercer et al., 2010; Schmidt et al., 2011a). However, a subset of virions is able to directly fuse at the plasma membrane, thus bypassing the endocytic internalisation step (Moss, 2006). Like all viruses that enter by endocytosis, VACV takes advantage of the environment within its endocytic carriers, macropinosomes, to facilitate infection. Acidification and macropinosome maturation promotes fusion of the viral and delimiting macropinosome membrane, which releases the viral core into the cytoplasm (Armstrong et al., 1973; Carter et al., 2005; Rizopoulos et al., 2015a). After entry into the host cytosol, lateral bodies are degraded to release pre-packaged (viral) effector proteins (Schmidt et al., 2013). The reducing environment of the cytosol stimulates expression of viral early genes within the intact core by the pre-packaged viral transcription machinery (Broyles et al., 1988; Gross and Shuman, 1996; Hu et al., 1998; Moss, 1990; Resch and Moss, 2005; Yang and Moss, 2009). The transcribed viral RNAs (vRNAs) are exported through pores in the core and are translated on host ribosomes into proteins required for viral DNA replication and uncoating (Kates and McAuslan, 1967; Kates et al., 1968; Kilcher et al., 2014; Munyon et al., 1967). After uncoating, the viral genome is released into the cytosol and accumulates in discrete cytosolic structures, so-called viral factories, where the viral DNA is replicated (Mercer et al., 2012; Schmidt et al., 2013; Welsch et al., 2003). Viral genome replication allows for viral intermediate and late gene expression. Intermediate genes mostly encode transcription factors that direct the late stage of viral gene expression, whereas the viral late genes encode structural proteins that form new progeny virions during morphogenesis. In addition to structural proteins, late genes also encode the viral early transcription machinery which is packaged in the assembling virions for the next round of infection (Moss, 2013). Assembly of the new virions occurs within electron-dense, perinuclear sites which localize close to the MTOC (Tolonen et al., 2001). Although only incompletely characterized, VACV morphogenesis is initiated by membrane crescent formation. These viral membranes were described to “scoop up” all the components required for formation of an infectious virion, the viroplasm, excluding the viral DNA (Szajner et al., 2003, 2004). These immature virions (IVs) are filled with viral DNA through an unknown mechanism. Maturation of IVs to MVs requires proteolytic processing of several viral proteins, as well as complex dynamic phosphorylation (Ansarah-Sobrinho and Moss, 2004; Byrd and Hruby, 2005; Byrd et al., 2002; Mercer and Traktman, 2005; Novy et al., 2018; Whitehead and Hruby, 1994). Once fully processed, MVs are either

stored until cell lysis, or they are wrapped in two additional Golgi-derived membranes to form wrapped virions (WVs) (Condit et al., 2006; Sivan et al., 2016). WVs are transported to the plasma membrane where they undergo egress by fusion of the outermost membrane to be released as extracellular enveloped virions (EEVs), thus completing one round of VACV replication.

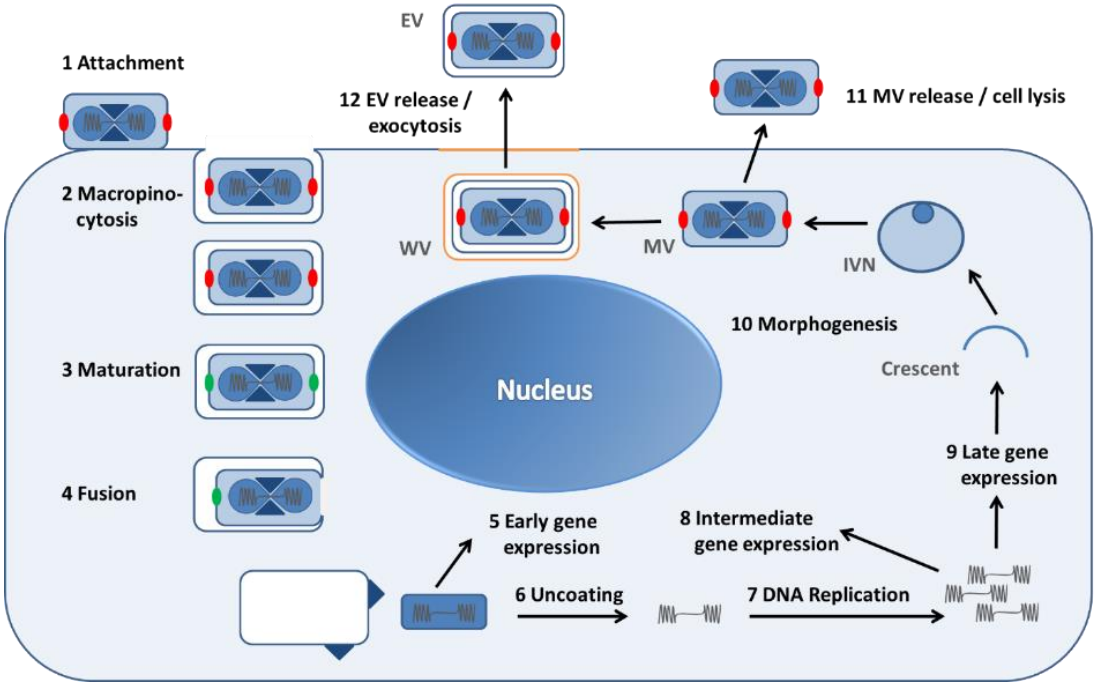

Figure 1-3 VACV replication cycle.

The VACV life cycle takes place only in the cytoplasm of infected cells. The virus life cycle begins with attachment to the host cell and uptake by macropinocytosis. Acidification and macropinosome maturation promote fusion, which releases the viral core into the cytoplasm. Viral early genes are expressed and promote genome uncoating. Released viral genomes are replicated in the cytosol, which allows for viral intermediate and late gene expression. Viral late gene expression is followed by morphogenesis which produces two different forms of infectious particles: the double wrapped enveloped virions (EVs), and the single wrapped mature virions (MVs).

2.2.1 VACV entry and fusion

Poxviral attachment and entry mechanisms have been controversially discussed and it was suggested that VACV strains differed in their entry mechanisms (Bengali et al., 2009). As I have been using the VACV strain Western Reserve (WR) throughout this study, this section focuses on the reported uptake mechanisms for WR.

During its life cycle, VACV produces two infectious forms of virions, MVs and EVs which show distinct but converging entry mechanisms (Figure 1-4). VACV entry is initiated by attachment of virions to the cell surface. MVs attach to glycosaminoglycans (GAGs) and extracellular laminin on the host cell surface. Binding requires the MV protein H3 that interacts with chondroitin sulfate, A26 which mediates attachment to laminin, as well as D8 and A27 which bind heparin sulfate (Chiu et al., 2007; Chung et al., 1998; Hsiao et al., 1998, 1999; Lin et al., 2000). While GAG binding is the primary mechanism for MV attachment, GAG-independent mechanisms have been described and were suggested to account for the broad VACV host cell tropism (Foo et al., 2009; McFadden, 2005). As MVs and EVs have distinct molecular surfaces they do not share any epitopes and were shown to rely on different factors for attachment. While no attachment factors for EVs have been described so far, the cellular protein Gas6 was hypothesised to link phosphatidylserine in the EV membrane to the cell surface receptor kinase Axl (Morizono et al., 2011; Vanderplasschen and Smith, 1997).

Virions that are attached to the cell surface trigger their own uptake by apoptotic mimicry (Mercer and Helenius, 2008a). Phosphatidylserine (PS) in the MV membrane allows virions to "pose" as apoptotic bodies which induces their uptake by macropinocytosis (Mercer and Helenius, 2008b; Zwartouw, 1964). Macropinocytotic uptake is paralleled by largescale actin and plasma membrane rearrangements, causing cell blebbing (Mercer and Helenius, 2008b). Fusion of the viral and macropinosome membrane, which releases the viral core into the cytoplasm, relies on macropinosome maturation (Rizopoulos et al., 2015b). VACV containing macropinosomes mature in parallel to classical endosomes, going through an early to late Rab5 to Rab7 exchange, phosphoinositide switch, and gradual acidification.

In order to deliver the viral core into the cytosol, the virus needs to fuse its envelope membrane with the delimiting membrane of the macropinosome. Poxviral fusion is catalysed by the entry fusion complex (EFC) which consists of 11 proteins that are structured into functional subdomains (Gray et al., 2018, 2016; Moss, 2006, 2012). Each EFC protein is individually required for fusion and deletion either causes a defect in hemifusion (A16, A21, F9, G3, G9, H2, J5, and O3), or full fusion (A28, L1, L5) (Moss, 2012). In the case of MV fusion, the acidic pH 4.5-5.0 of late macropinosomes activates the entry/fusion complex within the

MV membrane (Rizopoulos et al., 2015b; Townsley et al., 2006). Although this process is only incompletely understood, it has been suggested to involve pH-dependent inactivation of the fusion suppressor A26 (Chang et al., 2012).

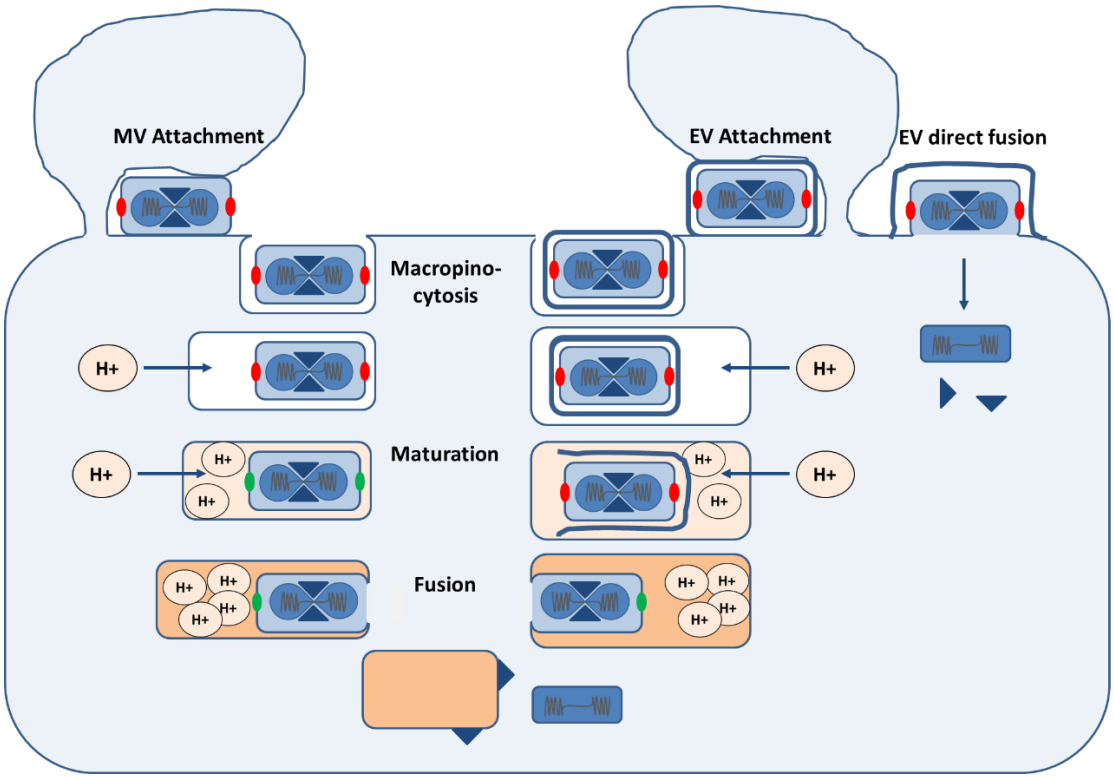

Figure 1-4 Entry mechanisms for MVs and EVs.

After attachment to the host cell plasma membrane MVs and EVs enter the cell by macropinocytosis. In case of the single-wrapped MVs acidification of the macropinosome activates the fusion machinery, located at the tips of the virions. Fusion with the delimiting membrane of the macropinosome releases the core into the host cell cytosol. As EVs have an additional membrane, acidification of the macropinosome is required to promote rupturing of the outer EV envelope in order to expose the underlying fusion machinery. EVs were also reported to enter the cell by direct fusion at the plasma membrane, thus directly releasing the core into the cytosol without prior acidification step.

Since EVs are surrounded by an additional membrane that shields the EFC, EV fusion requires an additional membrane rupture step. It has been shown that EV membrane rupture is acid mediated and also relies on macropinosome maturation (Schmidt et al., 2011b). While the molecular details remain unclear, the major EV membrane proteins A34 and B5 have been suggested to render the membrane susceptible to acidic destablilization (Roberts et al., 2009; Schmidt et al., 2011b). Removal of the EV membrane exposes the underlying EFC in the MV membrane to promote fusion and release the viral core (Schmidt et al., 2011b). In addition to pH-mediated fusion, EVs have been shown to fuse directly at the plasma membrane (Law et al., 2006; Roberts et al., 2009; Vanderplasschen et al., 1998).

Upon release into the cytosol, the two lateral bodies (LBs) that flank the core are degraded by the host cell proteasome. Degradation of the main LB component F17 was found to be required to release pre-package viral factors, such as the viral phosphatase H1 (Schmidt et al., 2013). Released H1 then dephosphorylates STAT1 to abrogate IFN-γ stimulated anti-viral immune responses (Najarro et al., 2001; Schmidt et al., 2013).

2.2.2 Viral early gene expression and core disassembly

During extracellular transmission, the viral dsDNA genome is supercoiled and protected within the proteinaceous virus core. The core needs to be disassembled to release the genome and allow for genome replication upon entry into the host cell. Therefore, the core has a context dependent role as either protective shell or a barrier to replication. Viruses have solved this problem by generating cores or capsids that exist in an intrinsically meta-stable state which responds to internal as well as external stability cues (Greber et al., 1994; Kilcher and Mercer, 2015). Poxviruses release their genome from the core in a unique two-step uncoating process.

The first step, core activation, occurs after release of the core into the cytosol. The redox environment of the host cytoplasm reduces and therefore breaks the disulphide bonds within the viral core (Locker and Griffiths, 1999; Schmidt et al., 2013). Core activation causes distinct morphological changes and expansion transforms the biconcave core into an oval structure. Prepackaged within the core is the viral early transcription machinery, including the viral DNA-dependent RNA polymerase subunit A24, L3, the RNA-helicase I8, and the viral early transcription factor A7 (Baroudy and Moss, 1980; Broyles et al., 1988; Gross and Shuman, 1996; Hooda-Dhingra et al., 1990; Hu et al., 1998; Moss, 1990; Resch and Moss, 2005; Yang and Moss, 2009). Deletion of any component of the transcription machinery was found to inhibit the formation of virus particles (Hu et al., 1998; Resch and Moss, 2005). Although not part of the transcriptional machinery, genetic deletion of the VACV phosphatase H1 produces infectious virions that are transcriptionally incompetent (Liu et al., 1995). Recently, H1 has been found to dynamically dephosphorylate the early transcription factor A7, which is critical for transcriptional competence of the progeny virions (Novy et al., 2018).

Upon core activation, preassembled complexes of viral RNA polymerase and early transcription factors are triggered to transcribe early genes while the core is still intact

(Broyles, 2003; Rohrmann et al., 1986; Yang and Moss, 2009). The ca. 80 different viral mRNAs are exported into the cytosol via pores in the viral core to be translated by host ribosomes (Chou et al., 2012; Yang and Moss, 2009). The early wave of genes encodes viral proteins that are required in subsequent viral DNA replication, such as the viral kinase B1, the viral AAA+ ATPase D5, and the viral polymerase E9; proteins that serve as intermediate transcription factors such as A24; and proteins that have immune-modulatory functions (Chou et al., 2012). Early gene expression triggers the second stage of core disassembly called core uncoating. Viral genome uncoating requires expression of the viral uncoating factor D5 and the ubiquitin-proteasome system, although the exact mechanism remains unknown (Kilcher et al., 2014; Mercer et al., 2012; Satheshkumar et al., 2009; Schmidt et al., 2013). Once uncoated, the genome is accessible for DNA replication factors and replication of the genome can start.

2.2.3 Viral DNA replication

VACV DNA replication occurs exclusively in the cytoplasm (Moyer, 1987) in distinct, electron dense structures termed viral factories (Kajioka et al., 1964; Katsafanas and Moss, 2007). These sites of viral DNA replication are transiently surrounded with ER membrane, which might serve to shield the viral genome from cellular DNA sensing (Tolonen et al., 2001).

Poxviruses encode an arsenal of proteins involved in all stages of DNA replication, including precursor metabolism, DNA replication and processing. These proteins include the viral polymerase E9, the helicase-primase D5, the Uracil DNA glycosylase D4, the processivity factor A20, the protein kinase B1, the late transcription elongation factor H5, and the single strand DNA binding protein I3 (Boyle et al., 2007; Czarnecki and Traktman, 2017; Hutin et al., 2016; Moss, 2013).

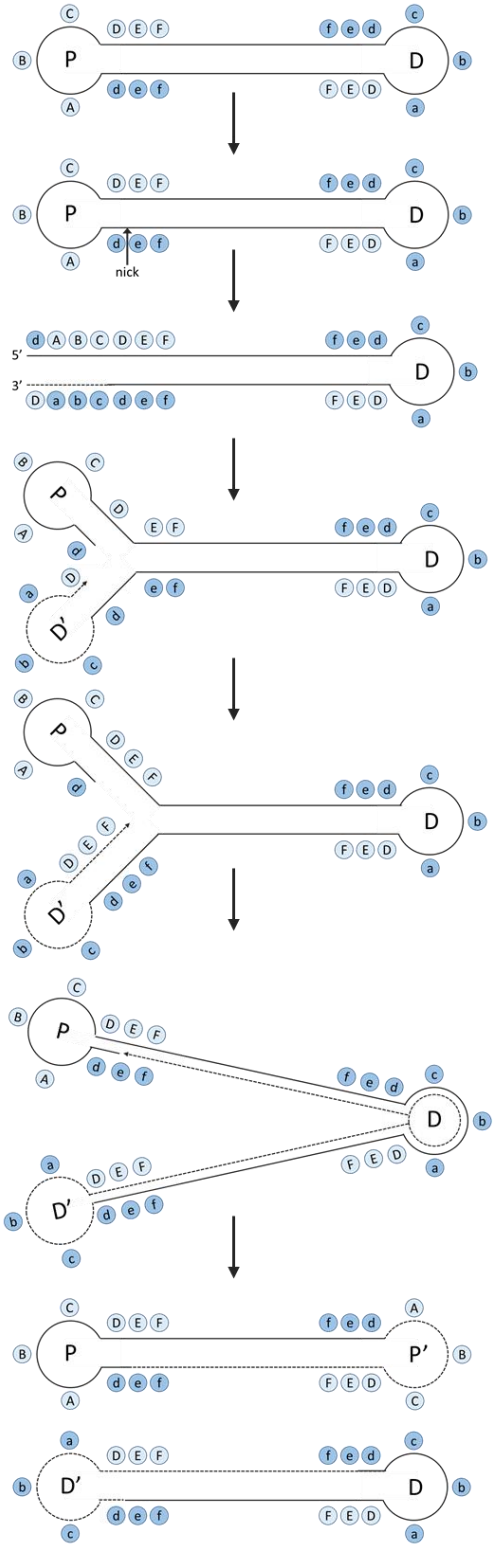

Figure 1-5 VACV genome replication by rolling hairpin strand displacement mechanism.

Figure adapted from (Moss, 2007). VACV genome replication is initated via self-priming by nicking the DNA near the hairpin termini. The replisome including the virally encoded polymerase E9 synthesises the new genome from 3' to 5' end. The new ends fold back onto themselves to reform the hairpins. As the rest of the genome is copied, a concatamer of two, or up to four genomes is formed which is then cleaved into single genomes by the viral resolvase A22.

Although the replication mechanism of poxviruses is incompletely understood, genome replication is generally thought to proceed via a rolling hairpin strand displacement mechanism (Du and Traktman, 1996; Moss, 2013; Pogo et al., 1984) (Figure 1-5). Once released from the core, the viral genome is coated with the viral ssDNA binding protein I3 and H5, which as of now has no clear function in viral DNA replication (Beaud and Beaud, 1997; Rochester and Traktman, 1998). Replication is initiated via self-priming: while the origin of the free 3' end remains unidentified, the viral DNA is thought to get nicked near the hairpin termini at one or both ends of the genome (Senkevich et al., 2015). They thus generated free 3' end to primes the viral replisome complex consisting of the DNA polymerase E9, the uracil-DNA glycosylase D4, and the accessory protein A20 (Moss, 2007). Sharing homology with eukaryotic polymerases, the viral E9 DNA polymerase then starts to synthesise VACV DNA from the 3' to the 5' end (Tattersall and Ward, 1976; Wang et al., 1989). As the ITR regions are complementary, the newly replicated DNA strand folds back on itself to form the hairpin for the newly synthesized genome. The replisome continues to copy the DNA, extending deoxynucleotides towards the distal hairpin terminus. As the remaining genome is copied, a concatamer of two, or up to four genomes is formed (Garcia et al., 2006; Moyer and Graves, 1981). The juxtaposed genomes remain joined at their hairpin termini until the onset of late viral gene transcription. The virally encoded Holliday junction resolvase A22 cleaves the concatamer in its terminal hairpins to release unit-length, individual genomes (DeLange and McFadden, 1987; Garcia et al., 2000).

Another viral protein required for viral genome replication is the viral kinase B1 (Figure 1-6). B1 is pre-packaged into VACV particles and is expressed early during infection. Although B1 is not directly involved in the synthesis or processing of viral DNA, genetic deletion or loss of its kinase activity prevents genome replication (Condit and Motyczka, 1981; Condit et al., 1983; Rempel and Traktman, 1992). B1 has been shown to promote viral genome replication by suppressing the host antiviral barrier to autointegration factor (BAF). In the absence of B1, BAF detects and binds to viral DNA in the cytosol thus inhibiting viral genome replication and intermediate viral gene transcription (Ibrahim et al., 2011, 2013; Wiebe and Traktman, 2007). Although the detailed mechanism of BAF-mediated inhibition remains to be established, it was suggested that BAF compacts and aggregates viral DNA, thus prevent efficient replication (Ibrahim et al., 2011). The antiviral activity of BAF depends on its ability to bind DNA, which can be inhibited by phosphorylation (Ibrahim et al., 2011; Wiebe and Traktman, 2007). B1-mediated phosphorylation of BAF prevents its association with viral DNA thus inhibiting its

antiviral function. Apart from BAF, the only described substrates of B1 are the viral DNA binding protein H5, p53, and the ribosomal protein Sa and S2 (Banham et al., 1993; Beaud et al., 1995; Brown et al., 2000; Santos et al., 2004). As these substrates have either been identified by in vitro phosphorylation assay, or by expressing only the B1 without the context of infection, the functional relevance of these modifications and substrates during the VACV life cycle remains to be established.

B1 shares sequence homology with the cellular vaccinia-related kinases (VRKs) and it was found that expression of VRK2, and to a lesser extent VRK1, can complement B1's function in viral genome replication (Boyle and Traktman, 2004; Nichols and Traktman, 2004; Olson et al., 2017). Interestingly, the ability of VRK2 and VRK1 to rescue viral DNA replication in the absence of B1, was described not to depend on the inactivation of BAF (Olson et al., 2017). This indicated that B1 and the VRKs share another substrate which is linked to viral DNA replication. Recently, this substrate has been identified as the viral pseudokinase B12 (Olson et al., 2019; Rico et al., 2019). B12 is a paralog of B1, also expressed early during infection but without any reported kinase activity. In the absence of B1 and VRKs, B12 inhibits viral genome replication through a not yet identified mechanism. Phosphorylation by B1 and/or VRK1/2 relieves the DNA block mediated by the repressor B12 (Rico et al., 2019).

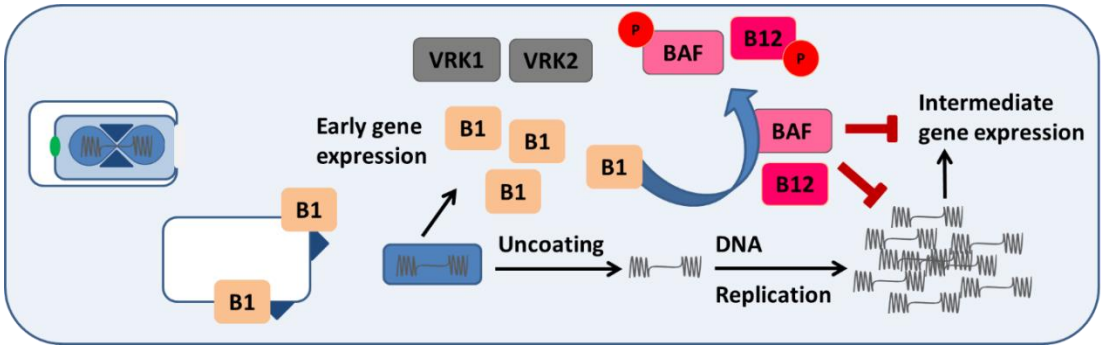

Figure 1-6 Viral kinase B1 promotes viral DNA replication by inhibiting viral B12 and cellular BAF.

Although not directly involved in viral DNA synthesis, the early expressed viral kinase B1 (orange) is required for viral genome replication. B1 has a dual suppressor function: it phosphorylates and inactivates the cellular antiviral restriction factor BAF, as well as the viral pseudokinase B12. How B12 represses viral genome replication in the absence of B1 is not known.

As poxviruses seemingly encode all the required factors, poxviral DNA replication has long been believed to be independent of the nuclear replication machinery. However, a recent report questions whether viral replication is really autonomous (Postigo et al., 2017). VACV

was shown to activate the cellular DNA damage response (DDR) pathway (cf. section 3.3.3) in a pre-uncoating step. Although the function of DDR activation remains unclear, it was shown to be essential for VACV DNA replication and late gene expression. In contrast to previous reports, the authors suggested a model whereby the cellular single strand binding protein RPA rather than the viral I3 is recruited to nicked viral DNA. Based on pulldown experiments, RPA was suggested to then form a complex with the viral polymerase E9, the proposed scaffold protein H5, and the cellular DDR activator protein TOPBP1, thus linking the replisome complex to the viral DNA. Supporting this idea, RPA was found to co-localize with H5 and E9 on AraC stabilized genomes. In addition to DDR activation, the cellular DNA polymerase processivity factor PCNA was also found to be essential for VACV replication. As VACV is not known to encode a viral sliding clamp protein, it was suggested that PCNA might function to stabilize the interaction between the polymerase E9 and the viral DNA. In support of this, PCNA was found to interact with E9 in pulldown experiments, however it could not be visualized on viral genomes. Although this study provides evidence that VACV replication is not completely autonomous from the nuclear replication machinery, the detailed mechanism and functional relevance of DDR activation for viral replication remains to be established.

2.2.4 Viral intermediate and late gene expression

Post-replicative viral gene expression is divided into intermediate and late gene expression, which together account for ca. 90 viral ORFs. Although this expression wave is described to occur after genome replication, it has been suggested that genome replication is not a requirement per se but the delay is rather a consequence of the inaccessibility of the viral genome for intermediate transcription factors prior to uncoating (Keck et al., 1990; Moss, 2007). However, since poxviral gene transcription is cascaded, intermediate expression requires early expression of essential transcription factors. The intermediate class of genes encodes the three viral transcription factors A1, A2, and G8 which are required for late gene expression (Keck et al., 1990; Yang et al., 2011), as well as the single strand binding protein I3 which is also expressed early (Tseng et al., 1999). Many of the intermediate genes were shown to have dual specificity promoters, allowing them also to be transcribed during the late expression wave (Yang et al., 2011). Transcription of intermediate genes is mediated by the viral RNA polymerase, the capping enzyme D1, the transcription elongation factor J3, the helicase A18, the viral intermediate transcription factor-1 (VITF-1) E4, and VITF-3 which is a heterodimer of A8 and A23 (Broyles, 2003; Moss, 2007; Sanz and Moss, 1999). In addition to

the viral proteins, the cellular proteins G3BP and p137 were shown to form a complex which can direct transcription of viral intermediate genes and was therefore named VITF-2 (Katsafanas and Moss, 2004; Rosales et al., 1994). It was speculated that VITF-2 might serve as a sensor of cell activation i.e. exit from quiescence in order to promote post-replicative gene expression only if the cellular environment is favourable. In addition to VITF-2, another cellular transcription factor, YY1, was shown to bind to the intermediate promoter of I3 (Broyles et al., 1999; Oh and Broyles, 2005). Thus, although VACV encodes most of the machinery involved in intermediate gene expression, it also recruits select cellular proteins to assist transcription.

While intermediate genes mostly encode transcription factors that direct the late stage of viral gene expression, viral late genes encode structural proteins that form new progeny virions during morphogenesis. In addition to structural proteins, late genes also encode the viral fusion proteins, the viral phosphatase H1, the viral kinase F10, and the viral early transcription machinery which is packaged in the assembling virions for the next round of infection (Lin and Broyles, 1994; Liu et al., 1995; Moss, 2007; Szajner et al., 2004). The major structural proteins that form the viral core, A3, A10, and L4 are expressed during this late transcriptional wave (Jesus et al., 2015; Katz and Moss, 1970; Resch et al., 2007), as well as major LB component F17 (Schmidt et al., 2011b; Wickramasekera and Traktman, 2010). Specific late viral transcription factors (VLTFs) direct transcription of late viral genes. Genetic studies have identified the viral A1, A2, and G8 proteins to serve as the VLTFs (Carpenter and Delange, 1992; Keck et al., 1990; Yang et al., 2011; Zhang et al., 1992). Additionally, the early expressed H5 has also been described to promote late gene expression (Moss, 2007). Again highlighting the involvement of host factors, a fifth transcription factor termed VLTF-X was found to be composed of the heterogeneous nuclear ribonucleoproteins A2/B1 and RBM3 (Gunasinghe et al., 1998; Wright et al., 2001). Additionally, the cellular transcription factors TATA binding protein (TBP), SP1 and YY1 were described to be recruited to sites of viral replication (Broyles et al., 1999; Knutson et al., 2006; Oh and Broyles, 2005). However, it remains to be established how these factors are recruited and how they support viral transcription.

2.2.5 Morphogenesis and spread

Assembly of the new virions occurs within electron-dense, perinuclear sites which localize close to the MTOC and contain viral DNA as well as viral late proteins (Tolonen et al., 2001).

VACV morphogenesis is a highly orchestrated assembly and maturation process that requires extensive proteolytic processing, as well as complex dynamic phosphorylation (Ansarah-Sobrinho and Moss, 2004; Byrd and Hruby, 2005; Byrd et al., 2002; Mercer and Traktman, 2005; Novy et al., 2018; Whitehead and Hruby, 1994). Due to its complexity, many processes remain incompletely understood.

Much of what is known today about VACV morphogenesis was discovered by electron microscopy (EM) (Condit et al., 2006; Dales and Siminovitch, 1961; Dales et al., 1978) (Figure 1-7). The assembly of new progeny virions is marked by the formation crescent-shaped structures composed of a single lipid bilayer and the viral scaffold protein D13 (Heuser, 2005; Szajner et al., 2005) (Figure 1-7, red). In addition to D13, this initial step of membrane diversion requires the activity of the viral kinase F10 (Condit et al., 1983; Wang and Shuman, 1995). Inactivation of F10 results in the loss of any discernible, morphogenesis-associated structures such as crescents, or electron-dense viroplasm. After F10-assisted membrane recruitment D13 organizes into a honeycomb lattice to stabilize the ER-derived membrane, assisted by additional viral proteins (Bahar et al., 2011; Moss, 2018; Weisberg et al., 2017). In order for crescent formation to occur, D13 requires anchoring to the ER membrane by interaction with the viral protein A17 (Bisht et al., 2009; Krijnse-Locker et al., 1996). A17 is a substrate for F10 phosphorylation and its deletion causes an accumulation of membranous material in the absence of any functional crescents (Betakova et al., 1999; Derrien et al., 1999; Mercer and Traktman, 2003; Rodríguez et al., 1995, 1998). While maintaining their curvature, crescents then grow into spherical IVs which scoop up dense viral matter that contains all essential viral building blocks apart from the viral DNA (Figure 1-7, blue). As crescents are growing to form IVs the membrane ends are capped by the viral protein A11. Capping prevents annealing of the lipid bilayer and is thought to be required for incorporation of the viral genome into the IVs. The mechanism of how viral genomes are trafficked and packaged into the IV has not yet been defined. Viral DNA replication however is known to occur independently of viral morphogenesis (Szajner et al., 2003, 2004). Packaged DNA then starts to condense within the IVs, forming so-called immature virions with nucleoid (IVNs) (Condit et al., 2006) (Figure 1-7, yellow).

Maturation of the IVNs into intracellular mature virions (IMVs) relies on the viral seven-protein complex (7PC), which includes the viral kinase F10 (Figure 1-7, green). Studies using temperature sensitive F10 VACV strains have shown that F10 not only functions in membrane recruitment but also in IMV formation (Derrien et al., 1999; Punjabi and Traktman, 2005;

Szajner et al., 2004). F10 kinase activity is required for association and incorporation of viroplasm into the IVs (Punjabi and Traktman, 2005). Each component of the 7PC, A15, A30, D2, D3, G7, and J1, has been shown to be individually required for virion morphogenesis (Cassetti et al., 1998; Chiu and Chang, 2002; Chiu et al., 2005). Again linking F10 kinase activity to correct progression of morphogenesis, the two 7PC components A30 and G7 were identified as F10 substrates and F10 phosphorylation is required for IV to IMV maturation (Mercer and Traktman, 2005; Szajner et al., 2001, 2003).

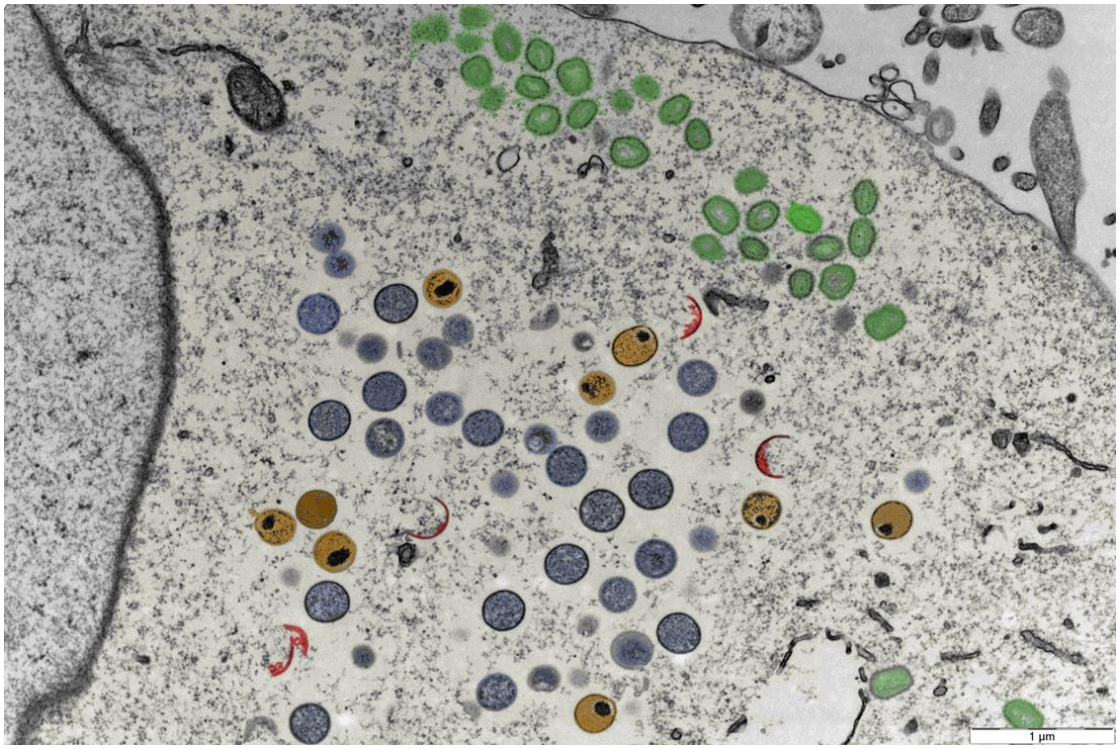

Figure 1-7 The different morphological stages during VACV assembly.

Electron microscopy image of an VACV infected cells (image: Dr. Jason Mercer). VACV morphogenesis is initiated by formation of membrane crescents (red). The crescents incorporate dense, viral matter (viroplasm) and grow into spherical immature virions (IVs, blue). Viral DNA is incorporated into IVs by an unidentified mechanism and starts to condense, forming immature virions with nucleoid (IVNs, yellow). IVNs mature into intracellular MVs (IMVs, green) through a complex process of dynamic phosphorylation and proteolytic processing which causes condensation of the viral core and lateral bodies.

Maturation of the brick-shaped core and lateral bodies requires disulphide bond formation in structural proteins of the core and membrane, as well as proteolytic processing which is regulated by complex dynamic phosphorylation (Byrd and Hruby, 2005; Byrd et al., 2002; Locker and Griffiths, 1999; Novy et al., 2018). Proteolytic cleavage is mediated by the viral proteases I7 and G1 and is temporally as well as spatially regulated (Moss and Rosenblum,

1973; Novy et al., 2018). Activation of I7 is regulated by Ser134 phosphorylation by F10 and dephosphorylation by the viral phosphatase H1 (Novy et al., 2018). After IVN formation F10 directs I7 proteolytic cleavage of A17 in order to allow for disassembly of the D13 scaffold. Activation of I7 by F10 is also required for subsequent cleaving of the core proteins p4a (A10), p4b (A3), G7, A12, and L4 (Ansarah-Sobrinho and Moss, 2004; Dyson et al., 1989; Katz and Moss, 1970; Mercer and Traktman, 2005; Novy et al., 2018; Sarov and Joklik, 1972; Unger et al., 2013; Vanslyke and Hruby, 1994; Vanslyke et al., 1991). H1 is a negative regulator of I7 protease activity and deletion of H1 causes hypercleavage the core proteins p4a, p4b, A12 and L4 (Novy et al., 2018). However, H1(-) virions are able to form and morphogenesis occurs without any visible defects. While hypercleavage of the core proteins does not seem to impact particle production, the absence of proteolytic processing causes severe morphogenesis defects (Heljasvaara et al., 2001; Vanslyke and Hruby, 1994; Vanslyke et al., 1991; Wittek et al., 1984). An additional player involved in correct processing of viral core proteins is the viral phosphoprotein F17 (Zhang and Moss, 1991). In the absence of F17, the major core components p4a and p4b fail to be cleaved which results in a morphogenesis block (Wickramasekera and Traktman, 2010; Zhang and Moss, 1991). As the major component of the core flanking lateral bodies, F17 has also been suggested to be implicated in lateral body condensation during morphogenesis.

Fully processed IMVs are marked by association of the attachment protein A27. IMVs accumulate in the cell cytoplasm where the majority of virions is stored until cell lysis at ca. 72hpi. However, a subset of IMVs is wrapped in two additional Golgi-derived membranes to form wrapped virions (WVs) (Condit et al., 2006; Hiller and Weber, 1985; Sivan et al., 2016). Although association of A27 assists in microtubular transport of the IMV and has been shown to be a requirement for wrapping, the molecular determinants that destine an IMV to become an WV have not been determined (Howard et al., 2008; Rodriguez and Smith, 1990; Sanderson et al., 2000). Since EVs lack the fusion suppressor protein A26, and show differences in their membrane composition compared to “non-wrapped” MVs, it has been suggested that a subset IMVs might be specifically premarked for wrapping (Howard et al., 2008; Ulaeto et al., 1996). Once the IMVs are wrapped, they are transported to the plasma membrane in a process that depends on several viral proteins and the host cell cytoskeleton. The viral protein complex F12/E2 has been shown to assist in tethering the virions to the kinesin-1 motor complex, thus promoting their transport along microtubules (Carpentier et al., 2015; Dodding et al., 2011). WVs undergo egress by fusion of the outermost membrane with the plasma membrane thus

releasing mature EVs (Leite and Way, 2015; Roberts and Smith, 2008; Smith et al., 2002). After egress, a majority of EVs stay attached to the plasma membrane as so-called cell-associated EVs (CEVs), whereas the rest is released as extracellular enveloped virions (EEVs). The EV protein A36 promotes CEV dissemination by inducing actin polymerization underneath the virion (Blasco and Moss, 1992; Horsington et al., 2013). Actin tail formation propels the CEVs away from the infected cell to spread the virions to uninfected neighbours. In addition, if a virion attaches to an already infected cell, actin tail formation prevents re-infection by repelling the virion in a process called superinfection exclusion (Doceul et al., 2012).

In summary, VACV infection produces two infectious forms of virions that differ in the number of wrapping membranes: the single-wrapped MVs, and the double-wrapped EVs. While EVs mediate short range spread of the virus within a tissue or host, MVs are required for long-range dissemination between different hosts.

2.3 Oncolytics

Cancer represents the second most prevalent cause of death worldwide, costing millions of lives each year. With over 18 million new cases in 2018 alone, it imposes an immense burden on global healthcare systems. Due to the high treatment-associated costs, the majority of deaths caused by cancer occur in low- and middle- income countries. There is therefore a great need for preventative treatments and novel, more effective anti-cancer therapies. Over the past decades, viruses have been recognized and developed as a promising biotechnological tool for anti-cancer therapy. These virotherapies exploit a virus' natural or engineered preference for infecting and thereby destroying tumour cells. Several different virotherapies based on oncolytic viruses, including VACV, are currently being tested in clinical trials (Breitbach et al., 2015; Yang et al., 2018).

The ideal oncolytic virus selectively infects and destroys cancer cells, spreads within a tumour and can disseminate to distant metastases, elicits a robust and targeted immune response against the cancer cells, and has minimal side effects (Kirn and Thorne, 2009; Thorne, 2014; Yang et al., 2018). The poxviral life cycle offers several intrinsic advantages that make VACV an effective oncolytic agent. First, the broad host tropism allows for high transduction efficiency (McFadden, 2005; Yang et al., 2018). Second, owing to VACV's fast replication kinetics, infected cells disseminate progeny virions within 8h of infection and are destroyed by cell lysis

within 48-72 hpi. Third, as VACV was used as the live vaccine to eradicate smallpox, the virus and its interaction with the human host has been extensively studied (Cono et al., 2003; Fenner et al., 1988). Furthermore, there are treatments available for adverse reaction to the vaccine, including the small molecule inhibitor Cidofovir (De Clercq, 2002). Additionally, VACV replicates exclusively in the cytosol of infected cells without incorporation of viral DNA into the host cell genome. This limits the risk of long-term latent effects or carcinogenesis due to host gene disruption (Shen and Nemunaitis, 2005). These aspects of VACV biology make it a uniquely safe viral system. Fourth, its large dsDNA genome is amenable to genetic modification and can accommodate transgenes without compromising viral integrity (Noyce et al., 2018; Thorne, 2014). VACV has been developed as a gene expression vector since the 1980s (Mackett et al., 1982) and it was demonstrated that expression of non-poxviral genes could elicit a specific host immune response (Bennink et al., 1984). Since then, more efficient tools to generate recombinant VACV strains have been developed based on CRISPR-Cas9 genome editing techniques (Okoli et al., 2018; Yang et al., 2018; Yuan et al., 2015). Fifth, VACV infection elicits a robust cytotoxic T-lymphocyte immune response as well as persistent, circulating neutralizing antibodies (Miller et al., 2008; Pütz et al., 2006). Sixth, the virion can be freeze dried and remains infective, thus facilitating storage and clinical use. Seventh, VACV EVs spread under the radar of the host immune system due to the additional viral membrane hiding most viral antigens. Together with the option of intravenous administration, this allows infection to spread to distant tumours and enables systemic treatment of metastatic cancers (Kirn and Thorne, 2009; Thorne, 2014; Yang et al., 2018).

Several different VACV strains have been developed as oncolytic viruses. These include the strains Wyeth, Lister, Copenhagen and Wester Reserve (WR) (Foloppe et al., 2008; Kim et al., 2006; Thorne et al., 2007; Zhang et al., 2007). Poxviruses have an inherent selectivity for cancer cells which has been further increased by genetic engineering of the virus. A common strategy is deletion of poxviral genes that make infection more dependent on cancer-specific host factors (Kirn and Thorne, 2009). VACV has an natural advantage in cancer cells, as viral replication relies on EGFR-Ras signalling which is intrinsically upregulated in most human cancers (Hanahan and Weinberg, 2000; Katsafanas and Moss, 2004). To further increase selectivity of VACV replication, deletion of the viral thymidine kinase (J2) renders infection dependent on host cell expression of thymidine kinase, which is also known to be induced in cancers (Gnant et al., 1999; Hengstschläger et al., 1994). Based on this principle, the oncolytic WR strain vvDD was engineered with a double deletion, missing both the viral thymidine kinase (J2R) and the viral growth factor (VGF). This oncolytic VACV strain induced an increased

cytopathic effect in mouse xenographs, compared to the single deletion virus (Thorne et al., 2007).

While deletion of viral genes increases tumour selectivity, introduction of immuno-stimulatory, and so-called suicide genes increases the oncolytic efficiency. The VACV oncolytic strain JX-594 (Pexa-Vec) expresses granulocyte-macrophage colony stimulating factor (GM-CSF) in a thymidine kinase negative background. Using this oncolytic VACV strain has produced promising results in phase I and II clinical trials, as it was able to disrupt tumour perfusion in hepatocellular carcinoma (Breitbach et al., 2015). Additionally, selective expression of pro-drug converting enzymes (suicide genes) renders the infected cancer cell susceptible to treatment with the pro-drug whereas uninfected, normal tissue is not affected.

In summary, VACV is a highly promising platform for oncolytic therapies owing to its unique replication characteristics and previous use as live vaccine in the smallpox eradication campaign. While different VACV-derived oncolytic strains are already tested in clinical trials, more detailed understanding of the virus host interaction will help the development of improved oncolytic strains.

3 Host cell cycle

The cell cycle describes the tightly controlled growth and division program of the cell. The active part of the cell cycle is divided into four consecutive stages: gap phase 1 (G1), DNA synthesis phase (S), gap phase 2 (G2), and mitosis (M). These four stages ensure that the cellular genome is copied faithfully and divided equally into two progeny cells. During G1, the cell monitors whether conditions are favourable to enter the cell cycle. In the presence of cell cycle stimulating factors, so-called mitogens, the cell will enter the replicative stage. During S phase the DNA replication machinery copies the genome, which is then proofread during the following G2 phase. Once all mistakes are corrected, the cell is cleared to enter mitosis, the

actual division stage of the cell cycle. During mitosis, the DNA is condensed into chromosomes and equally partitioned into two progeny cells. If cells are no longer required to divide and/or are terminally differentiated, they enter the fifth stage of the cell cycle, G0. In the presence of mitogens, quiescent, non-replicating G0 cells can re-enter the active cell cycle in G1.

A complex signalling network ensures the correct and timely succession of each stage. The engine of the cell cycle, the core cell cycle machinery is fine-tuned by positive and negative regulators. Several molecular checkpoints monitor completion of the previous cell cycle phase and survey the cell for any damage. If any damage is detected, the checkpoints will either pause the cell cycle to allow for repair, or induce apoptosis if the incurred damage is irreparable. Although precisely regulated, accumulating errors in the control machinery can lead to aberrant cell division and cancer.

In the following I am going to introduce the molecular constituents of the core cell cycle machinery, the positive and negative regulators, as well as the major checkpoints. For simplicity I am summarizing the mammalian system only and am going to focus on somatic cell division.

3.1 The core cell cycle machinery: CDKs and cyclins

Cell cycle progression is driven by the cyclin-dependent kinases (CDKs), which belong to the family of serine / threonine protein kinases. There are four main CDKs known: CDK1, CDK2, CDK4, and CDK6. Each CDK is associated with a different stage of the cell cycle (Figure 1-8). CDK4 and CDK6 are required during early G1, while CDK2 is required in late G1 and helps S phase completion, where CDK1 takes over to promote transit through G2 and M phase. While expression of CDKs is stable throughout the cell cycle, their activity is restricted to specific phases. Cyclic activation of the CDKs requires association with periodically expressed cyclins and phosphorylation of the resulting protein complex by the CDK-activating kinase (CAK) CDK7. Phosphorylation by CDK7 at conserved Thr residues promotes cyclin binding through a conformational change in CDKs. The conserved residues are Thr 172 on CDK4, Thr 160 on CDK2, and Thr 161 on CDK1 (Vermeulen et al., 2003). As CDK7 is localized in the cell nucleus, CDK - cyclin complexes require nuclear translocation for full activation.

There are four distinct types of cyclins that associate with CDKs, cyclins D, E, A, and B (Figure 1-8). An additional cyclin H binds and activates the CAK CDK7. The D-type cyclins (D1, D2, and D3) activate CDK4 and CDK6 (Sherr, 1993, 1994), cyclin E associates with CDK2 (Ohtsubo et al., 1995), cyclin A binds to CDK2 as well as CDK1, and cyclin B forms a complex with CDK1 (Girard et al., 1991; Walker and Maller, 1991). When the cell cycle has progressed past the stage where the respective cyclin was required, it is rapidly degraded by the proteasome, thus ensuring that the cell cycle only progresses in one direction.

Cell cycle stage-specific cyclin degradation is mediated by two E3 ubiquitin ligases, the anaphase promoting complex / cyclosome (APC/C) and the SCF (Skp1/cullin/F-box protein) complex. While SCF controls the transitions between G1/S and G2/M phases, APC/C mediates progression through mitosis by enabling separation of the sister chromosomes during Anaphase. Activity of the APC/C is cell cycle dependent and requires association with its cofactors Cdc20, and Cdh1, respectively. Cdc20 activates APC/C early during mitosis and is then replaced by Cdh1 to keep the APC/C active throughout late mitosis and the transition from G1 to S. Association of its cofactors and activation of APC/C is regulated by cell cycle stage specific phosphorylation: phosphorylation of APC/C by CDK1 during early mitosis is required for association of Cdc20. On the other hand, CDK2 and CDK1 mediated phosphorylation of the second APC/C activator, Cdh1 prevents its binding to APC/C, thus keeping the complex inactive during S and G2 phase. Creating a reciprocal feedback loop, APC/C controls activity of CDKs by targeting cyclin A for degradation during G2 and M phase, and cylin B during late mitosis.

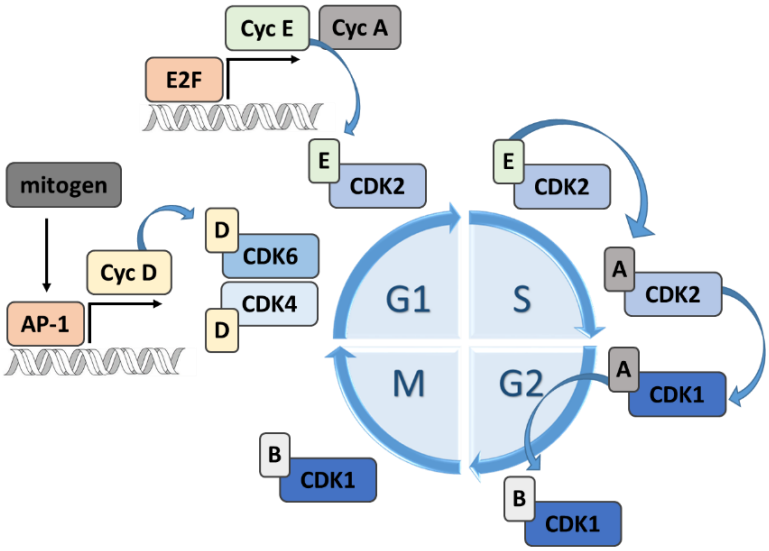

Figure 1-8 Schematic summary of the core cell cycle machinery.

The cell cycle is regulated by CDKs (blue) and periodically expressed cyclins (yellow, green, grey, light grey). The activity of CDKs is controlled by association with a cell cycle stage specific cyclin and phosphorylation by CAK. The cell cycle is initiated by mitogen-induced (dark grey) expression of cyclin D (yellow) during early G1 phase.

SCF uses different F-box proteins for substrate recognition. If the complex contains the F-box protein Skp2 (SCF-Skp2) it recognizes the CDK inhibitors p27 and p21 (cf. section 3.2) and promotes their proteasomal degradation. In complex with the F-box protein hCdc4, the SCF-hCdc4 complex regulates the transition from G1 to S phase by degradation of cyclin E after entry into S phase (Spruck and Strohmaier, 2002). If complexed to the F-box protein β-TrCP (SCF- β-TrCP) it promotes entry into M phase by targeting the APC/C inhibitor Emi for degradation, as well as the M phase inhibiting kinase Wee1.

Together, CDKs and cyclins represent the core cell cycle machinery that drives cell growth and division. Sequential succession of the distinct phases is mediated by phase-specific activation of the CDKs through the periodic rise and fall of cyclins (Bagga and Bouchard, 2014; Harper and Brooks, 2005; Vermeulen et al., 2003). G1 phase associated organelle duplication and protein synthesis is initiated by expression of cyclin D. The transcription of cyclin D is stimulated upon mitogen signalling and therefore acts as a sensor of optimal conditions for cell growth and division. Activation of the mitogen-activated protein kinase (MAPKs) and the Ras-Raf-MEK-ERK pathway stimulate expression of AP-1 transcription factors, which then in turn direct transcription of *CCND* gene (Albanese et al., 1995; Balmanno and Cook, 1999). Cyclin D activates CDK4 and CDK6, which directs expression of S phase inducing proteins such as cyclin E, and cyclin A (Sherr, 1993, 1994). During late G1 cyclin E associates with CDK2 to promote G1/S transition (cf. section 3.2) (Ohtsubo et al., 1995). While CDK2 – cyclin E activity initiates synthesis of DNA and chromatin structural proteins, exchanging cyclin E for cyclin A is required for completion of S phase. Once the cells entered G2, cyclin A dissociates from CDK2 and switches to binding CDK1 to drive G2 progression and DNA repair. The last cyclin switch happens at the G2/M checkpoint where CDK1 replaces cyclin A with cyclin B. Association of cyclin B with CDK1 is required for transit through G2/M and entry into mitosis (Girard et al., 1991; Walker and Maller, 1991). If cells pass the spindle-checkpoint in mid-M phase, the cell cycle is reset at the end of M phase by the destruction of cyclin B.

3.2 Negative regulators of cell cycle progression

While cyclins and the CAK drive cell cycle progression by activating CDKs, they are counteracted by CDK inhibitors (CKIs) that repress CDK activity (Figure 1-9). There are two distinct families of CKIs, the INK4 (inhibitor of CDK4) family, and the Cip (CDK-interacting protein) / Kip (kinase inhibitor protein) family. The INK4 family consists of four members: p15 (INK4b), p16 (INK4a), p18 (INK4c), and p19 (INK4d) (reviewed in (Guan et al., 1994; Hannon and Beach, 1994; Serrano et al., 1993)). On the other hand, Cip/Kip family members include p21 (Waf1, Cip1), p27 (Kip1), and p57 (Kip2) (Dulić et al., 1994; El-Deiry et al., 1993; Matsuoka et al., 1995; Polyak et al., 1994a, 1994b).

The INK4 CKIs specifically bind and inhibit the G1-associated kinases CDK4 and CDK6 (Harper and Brooks, 2005; Vermeulen et al., 2003). Expression of INK4 family members is incompletely understood but p15 has been shown to be induced by TGF-β (Hannon and Beach, 1994; Reynisdóttir and Massagué, 1997; Reynisdóttir et al., 1995). Cells accumulate p16 as they age through an unknown mechanism, while p18 and p19 are expressed during a narrow time window in foetal development and have been associated with terminal cell differentiation (Alcorta et al., 1996; Morse et al., 1997; Phelps and Xiong, 1998; Zindy et al., 1997).

The Cip/Kip family members show broader specificity and bind cyclins as well as CDKs (Chen et al., 1995, 1996; Nakanishi et al., 1995; Sherr and Roberts, 1999; Warbrick et al., 1995). Association with CDK2 and CDK1 inhibits their enzymatic activity. On the other hand, the effect of Cip/Kip CKIs on CDK4 and CDK6 appears to depend on the stoichiometry of the resulting complex, as well as the phosphorylation status of the CKIs. At equimolar ratios, p21 and p27 assist in the assembly of CDK4/6 with cyclin D, thus promoting CDK activity (Sherr and Roberts, 1999).

The two CKI families form a regulatory network that dictates the transition from G1 to S phase, as well as progression through the remaining cell cycle (Sherr and Roberts, 1999) (Figure 1-9). Successful entry from G1 into S phase requires sequential activation of CDK4/6 and CDK2 (cf. section 3.3.1). In the absence of cell cycle inducing mitogens Cip/Kip members inhibit CDK2/1 activity by direct interaction with the kinases. This negative regulation is relieved during G1, as p21 and p27 are sequestered into a complex with CDK4/6, and thus dissociate from CDK2/1. This process is started during early G1 when mitogens induce expression of cyclin D, as well as p21 and p27. Cyclin D is bound by p21/p27 that then contact CDK4/6 to facilitate CDK4/6 - cyclin D complex formation. CDK4/6 activation is thought to be further promoted by p21/p27

through stabilization and nuclear localization of the resulting complex. Translocation into the nucleus is essential for full activation as it requires phosphorylation by the nuclear CAK CDK7 (Chen et al., 1996; Hall et al., 1995; LaBaer et al., 1997; Sherr and Roberts, 1999). CDK4/6 activation triggers subsequent activation of CDK2, which phosphorylates p27 at Thr187 to promote its degradation (Sheaff et al., 1997; Vlach et al., 1997). Therefore, sequestration of the Cip/Kip proteins by CDK4/6 allows for full activation of CDK2 and progression into S phase (Polyak et al., 1994a; Sherr and Roberts, 1999). P21 and p27 remain bound to CDK4/6 for the remainder of the cell cycle, thus preventing inhibition CDK2, and CDK1 (Nourse et al., 1994; Polyak et al., 1994a; Toyoshima and Hunter, 1994). Although the mechanism is incompletely understood, p21 and p27 mediated inhibition is restored after degradation of cyclin E and cyclin A in S and G2 phase, respectively (Sherr and Roberts, 1999). Additionally, in the absence of mitogens, Cip/Kip family members are displaced from CDK4/6 by INK4 CKIs. This is thought to liberate Cip/Kip CKIs to interact with and inhibit CDK2/1 which causes cells to arrest in G1 (Guan et al., 1994; Koh et al., 1995; McConnell et al., 1999; Medema et al., 1995; Mitra et al., 1999; Reynisdóttir et al., 1995).

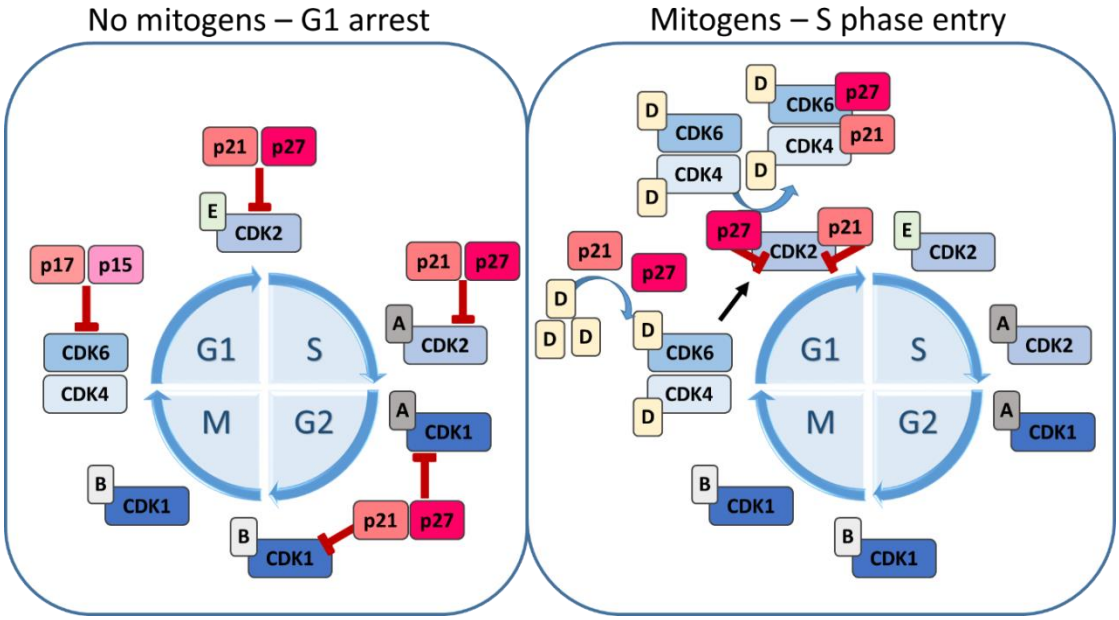

Figure 1-9 Schematic overview of negative cell cycle inhibitors and their cell cycle targets.

Cell cycle progression is regulated by the two CDK inhibitor families INK4 and Cip/Kip (pink and red). In the absence of cell cycle stimulatory mitogens, INK4 family member p17 and p15 inhibit G1 CDKs (blue), and Cip/Kip family

member p21 and p27 inhibit S/G2/M CDKs (blue). This systemic inhibition causes a G1 arrest. On the other hand, in the presence of mitogens, p21 and p27 are sequestered into a complex with CDK4/6 which relieves the inhibition and the cell cycle progresses.

In addition to the above described process, inhibition by Cip/Kip CKIs is fine-tuned by phosphorylation. Dynamic phosphorylation of p21 and p27 has been shown to regulate their substrate specificity, inhibitory function, as well as subcellular localization. The two kinases CDK2 and GSK3β phosphorylate p21 on Thr57 which has the dual effect of facilitating binding to CDK1-cyclin B while repressing p21's inhibitory function, thus promoting M phase progression (Dash and El-Deiry, 2005). A similar regulatory mechanism has been reported for p27, where phosphorylation switches its function as a CDK4 inhibitor to a CDK4 activator (James et al., 2008; Kardinal et al., 2006). Apart from regulation by post-translational modification, the activity of CKIs is also modulated by cellular factors such as Set/TAF1 nuclear protein which switches p21 from inhibiting CDK2 to inhibiting CDK1 (Canela et al., 2003).

The Cip/Kip family of CKIs has not only been shown to function in G1/S transition but also in control of cellular DNA synthesis and repair (Ando et al., 2001; Luo et al., 1995; Nallamshetty et al., 2005; Waga et al., 1994; Watanabe et al., 1998). Binding of p21 to the DNA polymerase δ processivity factor PCNA in response to DNA damage prevents cellular DNA synthesis (Ando et al., 2001). Additionally, the interaction between p21 and PCNA inhibits the phosphatase Cdc25, thus preventing progression through G2/M (cf. section 3.3.2).

In summary, the two CKI families INK4 and Cip/Kip are key regulators of cell cycle progression as well as integrators that link the G1/S and G2/M checkpoints to the core cell cycle machinery.

3.3 Cell cycle checkpoints

3.3.1 G1/S transition checkpoint

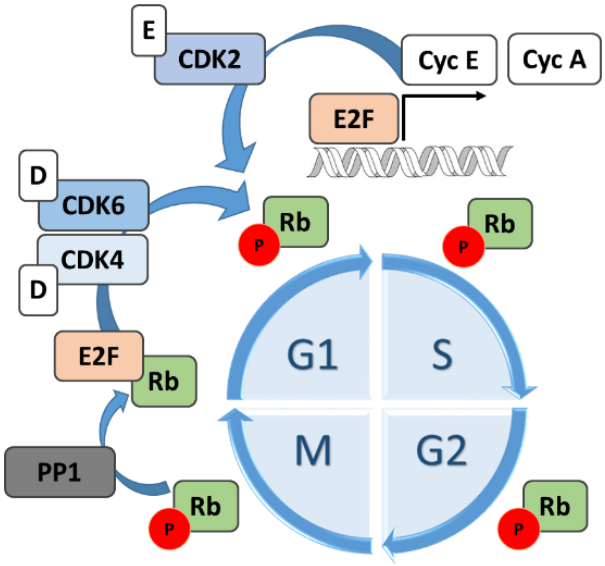

Figure 1-10 Schematic summary of the molecular mechanism of the G1/S checkpoint.

The G1/S checkpoint is regulated by the tumour suppressor Rb (green). During early G1 it binds and represses the transcription factor E2F (orange). Activation of CDK4/6 (blue) by cyclin D (white, indicated by "D") stimulates the complex to phosphorylate Rb, thus disrupting E2F binding. E2F dissociates and translocates to the nucleus where it initiates transcription of S phase genes, including cyclin A and B (white, indicated by "E" and "A"). Cyclin E mediated activity of CDK2 (blue) further promotes phosphorylation of Rb. Rb is dephosphorylated and activated by the PP1 phosphatase (grey) at the end of M phase.

Transition from G1 into S phase is regulated by the tumour suppressor Retinoblastoma protein (Rb) (Figure 1-10). Rb acts as the gatekeeper between G1 and S phase by preventing transcription of S phase genes. In its active, unphosphorylated form Rb complexes the S phase transcription factor E2F, thus inhibiting its transcriptional activity. The active CDK4/6 – cyclin D complex mono-phosphorylates Rb at different residues during early G1, which disrupts Rb binding to E2F (Narasimha et al., 2014). E2F is released and can translocate to the nucleus where it directs transcription of cyclin E and cyclin A. Cyclin E then forms a complex with CDK2 to further hyperphosphorylate and inactivate Rb (Lundberg and Weinberg, 1998; Narasimha et al., 2014). The combined action of Rb inhibition and increased cyclin E/A expression forms a positive feedback loop that initiates G1/S transition. At the end of M phase, Rb is dephosphorylated by the phosphatase PP1, which restores E2F repression (Ma et al., 2003).

3.3.2 G2/M checkpoint

Transit from G2 into M phase requires full activation of the CDK1 - cyclin B complex (Figure 1-11). This stepwise process is initiated by binding of cyclin B in the cytosol which stimulates

CDK1 activity. Upon translocation into the nucleus the partially activated CDK1 phosphorylates bound cyclin B. Full activation of the complex relies on additional phosphorylation of CDK1 at Thr161 by the CAK CDK7 (Fesquet et al., 1993; Poon et al., 1993).

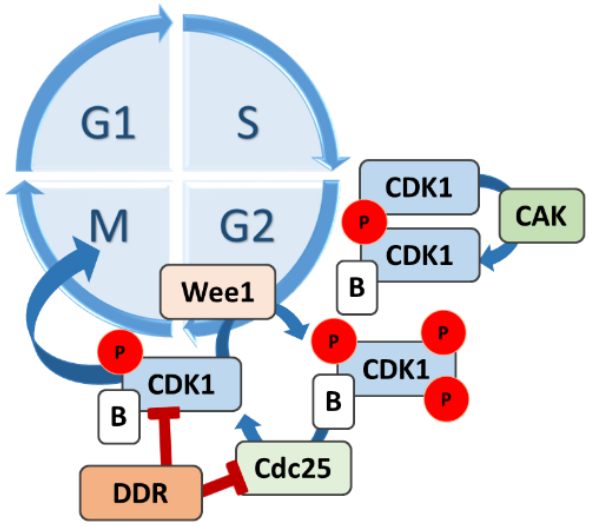

Figure 1-11 Schematic summary of the molecular mechanism of the G2/M checkpoint.

CDK1 (blue) activity requires binding to cyclin B (white, "B"), translocation to the nucleus, and phosphorylation by the CAK CDK7 (dark green). During G2, the CDK1 - cyclin B complex is kept in an inactive state by Wee1 (orange) and Myt1 which phosphorylate CDK1 at Tyr15 and Thr14, respectively. In the absence of DNA damage, the phosphatase Cdc25 (light green). Thus fully activated, CDK1 - cyclin B induces M phase entry. Triggering of the DNA damage response prevents M phase entry by blocking CDK1 - cyclin B activation.

In order to ensure a long enough G2 phase to assess and repair any DNA damage, CDK1 - cyclin B is kept inactive throughout G2 by additional phosphorylation at residues Tyr15 and Thr14 on CDK1. These two inhibitory phosphorylations are directed by the kinases Wee1 and Myt1, respectively (Booher et al., 1997; Liu et al., 1997; Parker and Piwnica-Worms, 1992). In the absence of DNA damage, the phosphatase Cdc25 then relieves the inhibition by dephosphorylating both residues at the border between G2/M (Draetta and Eckstein, 1997). Thus, fully activated CDK1 - cyclin B induces phosphorylation of downstream substrates promoting entry into M phase. However, in the presence of unrepaired DNA damage, the DNA damage response is triggered to prevent M phase entry through several pathways (cf. section 3.3.3).

3.3.3 DNA damage response

The cell closely monitors DNA damage that might occur during the cell cycle. In case any damage is detected, a complex molecular signalling cascade is activated that either pauses the cell cycle to allow for DNA repair, or if the damage is irreparable induces apoptosis. This DNA damage response (DDR) is composed of sensor proteins that detect the DNA damage, transducer proteins that then propagate the signal, and effector proteins which mount an appropriate response. The DDR is divided into two branches, depending on whether a single strand DNA break (SSB), or a double strand DNA break (DSB) occurred. These two branches of the DDR are controlled by the two signal transducing kinases Ataxia telangiectasia and Rad3-related (ATR), and Ataxia-telangiectasia-mutated (ATM), respectively (Figure 1-12).

ssDNA breaks are sensed by the replication protein A (RPA) which coats the exposed ssDNA and assists in the recruitment and activation of ATR and the ATR interacting protein (ATRIP) (Ashton et al., 2013; Awasthi et al., 2015; Cimprich and Cortez, 2008; Maréchal et al., 2014; Zou and Elledge, 2003). The ATR/ATRIP/RPA complex associates with the DNA-damage-specific RAD9-RAD1-HUS1 (9-1-1) clamp (Ellison and Stillman, 2003). The 9-1-1 complex assists ATR kinase activity by recruiting TopBP1 which binds ATR and stimulates its kinase activity (Delacroix et al., 2007). Activated ATR propagates the signal by phosphorylating its effector kinase Chk1 at Ser residues 317 and 345 (Liu et al., 2000; Zhao and Piwnica-Worms, 2001), thus triggering a biochemical cascade that results in inhibition of S phase progression and prevents M phase entry (reviewed in (Awasthi et al., 2015; Lukas et al., 2004)). Chk1 mediated phosphorylation of CDC25 negatively regulates S phase progression. Additionally, cytoplasmic sequestration of the isoform CDC25C and degradation of CDC25A prevents dephosphorylation of CDK1 (cf. section 3.3.2). Hyperphosphorylated CDK1 remains inactive and fails to induce G2/M transition (Mailand et al., 2002; Nghiem et al., 2001; Peng et al., 1997; Sanchez et al., 1997). Activation of the SSB response therefore influences both the G1/S and G2/M checkpoint.

On the other hand, how dsDNA breaks are sensed is not as well-understood. Activation of ATM in response to dsDNA breaks involves recruitment by the Mre11-Rad50-Nbs1 (MRN) complex (Carson et al., 2003; Dupré et al., 2006; Hartlerode et al., 2015; Lee and Paull, 2004, 2005; You et al., 2005). Recruitment by MRN and subsequent acetylation stimulate autophosphorylation of ATM at Ser1981 which is required for full activation and stabilization at sites of DNA damage (Bakkenist and Kastan, 2003; So et al., 2009; Sun et al., 2007). Similarly to the ATR signalling

cascade, ATM escalates the signal by phosphorylating its effector kinase Chk2 at residue Thr68 (Chaturvedi et al., 1999; Matsuoka et al., 1998, 2000), which triggers further downstream events that pause cell cycle progression (reviewed in (Awasthi et al., 2015; Lukas et al., 2004)).

A key effector protein in DDR signalling is the tumour suppressor p53. In unstressed cells, p53 is rapidly turned over by proteasomal degradation, which is mediated by its negative regulator, the E3 ubiquitin ligase Mdm2 (Haupt et al., 1997; Kubbutat et al., 1997). Upon DNA damage, p53 is phosphorylated on several residues by ATR and ATM (Ser15), as well as their effectors Chk1/2 (Thr18 and Ser20) which inhibits binding to Mdm2 (reviewed in (Ashcroft et al., 1999; Hafner et al., 2019)). Additionally, p53 is further stabilized by ATR/ATM directed degradation of Mdm2 (Khosravi et al., 1999; Maya et al., 2001). P53 which is no longer bound to Mdm2 is acetylated by the acetylases CBP and p300, thus promoting p53's transcriptional activity (Gu and Roeder, 1997; Sakaguchi et al., 1998). Activated p53 then promotes transcription of p53-responsive genes such as *CDN1A,* which encodes the above discussed CKI p21 (Waf1/Cip1) (Dornan et al., 2003; Sherr and Roberts, 1999; Waldman et al., 1995). While arrest at the G1/S checkpoint was found to depend on p53, the G2/M arrest proceeds both through a p53-dependent and a p53-independent mechanism (Agarwal et al., 1995; Kastan et al., 1991; Taylor and Stark, 2001). P53 is thought to mediate a long-term G2 arrest by downregulating transcription of CDK1 as well as its M phase promoting cyclin B (Clifford et al., 2003; Taylor et al., 2001). CDK1 activity is further inhibited by p53-mediated expression of Gadd45. Gadd45 binds CDK1 and thereby displaces cyclin B which hinders activation of CDK1(Jin et al., 2000; Zhan et al., 1999).

In summary, DNA damage is sensed by the kinases ATM and ATR which trigger a complex signalling cascade that results in cell cycle inhibition, or apoptosis. The key effector protein is the transcription factor p53 which initiates a transcriptional program that can arrest cells in G1/S and/or G2/M.

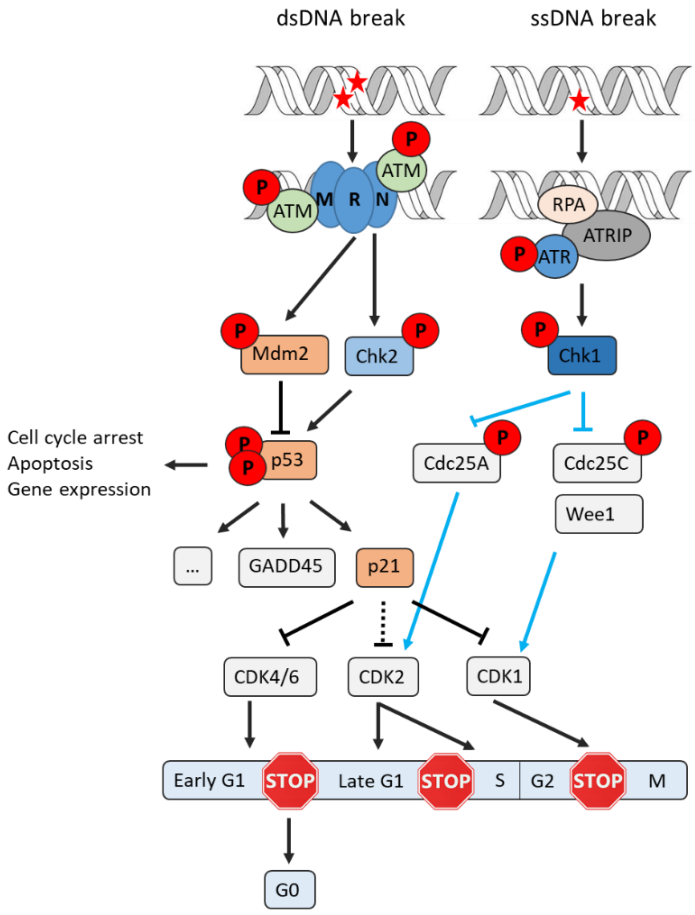

Figure 1-12 Schematic overview of the SSB and DSB DNA damage response.

Adapted from (Awasthi et al., 2015; Lukas et al., 2004). DNA damage can appear in the form of double strand, or single strand breaks. In the event of DSB, the MRN complex recruits and activates ATM to sites of DNA lesions. Activated ATM then cascades the signal through phosphorylation of its effector kinase Chk2, and other downstream effectors such as Mdm2 and p53. Transcriptional activation of p53 leads to cell cycle inhibition by preventing CDK activity. Similarly, SSB are recognized by the ssDNA binding protein RPA which leads to the recruitment and activation of ATR. ATR escalates the signal by phosphorylating Chk1. Activated Chk1 inhibits Cdc25 phosphatase activity, thus preventing full activation of CDK2 and CDK1.

4 Viral modulation of the host cell cycle

As obligate intracellular parasites, viruses are highly dependent on the host cell environment for productive viral replication. Therefore, they have evolved strategies to make host factors more abundant and accessible, while evading the host's immune response. A common viral strategy is subversion of the host cell's division and growth program, the so-called cell cycle.

This process is tightly regulated in normal, uninfected cells and several molecular checkpoints ensure that cells divide in a controlled manner. Uncontrolled division, however, is a hallmark of cancer and cell cycle dysregulation is a major cause for cancer development. Efforts to better understand the mechanisms that promote oncogenesis have identified a small group of oncogenic viruses that drive cancer development. Current estimates by the WHO assume that viral infections account for 20% human cancers worldwide and virus-induced cell cycle dysregulation has been the focus of intense research over the past years (reviewed in (Bagga and Bouchard, 2014; Fan et al., 2018)). In the following I summarize how three selected nuclear replicating viruses alter host cell cycle progression.

4.1 HPV: G1/S dysregulation

HPV is a member of the papillomaviruses and encodes its 8kb genome as circular double stranded DNA. Like all papillomaviruses, adenoviruses and polyomaviruses, HPV is classified as a small DNA tumour virus (Howley and Livingston, 2009). While HPV infection can drive oncogenesis of cervical, anal and neck cancers, different genotypes of HPV vary in their oncogenicity (Gatza et al., 2005). For example, 70% of global cervical cancer cases are estimated by WHO to be caused by the genotypes HPV16 and HPV18.

Two characteristics of HPV are thought to have selected for its oncogenic properties: the limited coding capacity and the preference to infect non-dividing quiescent cells. As HPV does not encode its own DNA replication machinery, it has to rely on the cellular enzymes to replicate the viral genome (Flemington, 2001). The cell replicates its own genome during S phase and all factors required for DNA synthesis, including high dNTP pools and DNA polymerase, are therefore upregulated during S phase. Despite HPV's dependency on the host DNA machinery, it predominantly infects non-replicating, quiescent cells that have low levels of dNTPs and don't offer a favourable environment for viral DNA replication (Helt et al., 2005). HPV has therefore evolved to promote S phase entry of its host cell (Helt et al., 2005; Lavia et al., 2003). During infection HPV disarms the G1/S transition checkpoint by inhibition of the tumours suppressors Rb and p53, and deactivation of the CKI p27 (Bagga and Bouchard, 2014; Helt et al., 2005). In uninfected, normal cells active Rb prevents uncontrolled entry into S phase by sequestering the cellular transcription factor E2F into a complex (Harper and Brooks, 2005). E2F is only released upon phosphorylation of Rb by the G1 CDK4 and CDK6. The HPV protein

E7 has been shown to associate with Rb, disrupt the interaction with E2F and thereby release the transcription factor (Harper and Brooks, 2005). Thus, E7 binding decouples Rb activation from regulation by CDK4/6 (Chellappan et al., 1992; Pagano et al., 1992). Additionally, E7 has been shown to cause proteasomal degradation of the three Rb family members, Rb, p107, and p130, thus further promoting E2F-dependent transcription of S phase inducing genes (Boyer et al., 1996; Dyson et al., 1989; Helt et al., 2005). The CKI p27 normally prevents activity of CDKs, thus inhibiting cell cycle progression. E7 counteracts the negative regulation by binding and inactivating p27 (Bagga and Bouchard, 2014; Fan et al., 2018).

Replicating viral DNA might set off the DNA damage response pathway by activation of p53. To counteract its activity, the HPV E6 protein recruits the ubiquitin ligase E6AP-100K to stimulate proteasomal degradation of p53 (Scheffner et al., 1993). Additionally, E6 binding also inhibits p53 transcriptional activity by inducing a conformational change and sequestering it in the cytosol (Mantovani and Banks, 2001; Patel et al., 1999; Zimmermann et al., 1999). It has been hypothesized that the HPV E6 protein prevents premature apoptosis by inhibiting the transcriptional activity of p53.

In summary, HPV evolved several mechanisms, including deactivation of Rb and p53, to induce S phase entry and promote its own replication, which continues into G2 (Reinson et al., 2015).

4.2 KSHV: G1/S disregulation and G2 arrest

Kaposi's sarcoma-associated herpesvirus (KSHV), also known as human herpesvirus-8 (HHV-8), is a member of the γ - subgroup of Herpesviruses (Zmasek et al., 2019). KSHV has been characterized as a human oncogenic virus and is the causative agent of Kaposi sarcoma (KS). KSHV infections can cause lymphoproliferative disorders in immunocompromised individuals and accounts for the majority of cancer cases in untreated HIV-1 patients (Cai et al., 2012; Dittmer and Damania, 2013; Mesri et al., 2010). While palliative treatments are available, neither curative therapies, nor a vaccine are available to-date (Chauhan et al., 2019).

As a herpesvirus, KSHV encodes its genes as a large double-stranded DNA genome. Similar to poxviruses, Herpesvirus gene expression is temporally cascaded and encodes for many proteins involved in dNTP biogenesis and DNA replication. KSHV infection is divided into a latent phase, where only a subset of genes is expressed, and a lytic phase where the progeny virions are produced (Järviluoma and Ojala, 2006; Sarid et al.). While latent viral gene expression drives oncogenesis by dysregulating cell cycle checkpoints and inducing cell cycle progression, lytic gene expression is implicated in arresting the host cell cycle (Direkze and Laman, 2004; Moore, 2007).

In normal, uninfected cells transition from G1 into S is regulated by the G1/S checkpoint mediated by the tumour suppressors Rb and p53 (cf. section 3.3.1). Controlled S phase entry requires activation of CDK4/6 via CAK phosphorylation and association with cyclin D (cf. section 3.3.1). Cyclin D is only expressed in response to mitogen stimulation, thereby ensuring favourable conditions for cell growth and division. KSHV promotes uncontrolled S phase entry by activating CDK4/6 and simultaneously inhibiting the G1/S checkpoint. Herpesviruses have evolved to express their own version of cyclin D, called virus cyclin (v-cyclin) (Järviluoma and Ojala, 2006; Moore, 2007). Mimicking cellular cyclin D, v-cyclin binds to and activates CDK4 and CDK6 (Chang et al., 1996). However, different to its cellular homolog, v-cyclin activates CDK4/6 independently of phosphorylation by a CAK (Kaldis et al., 2001). Further promoting uncontrolled activation, the v-cyclin CDK4/6 complex does not respond to inhibition by the cellular CKIs p21, p27, and p16 (Swanton et al., 1997). V-cyclin CDK4/6 induces entry into S phase by phosphorylating and thereby inactivating Rb, as well as the CKIs p21 and p27 (Chang et al., 1996; Järviluoma and Ojala, 2006; Sarek et al., 2006). Rb activity is further inhibited by the KSHV protein LANA-1 which binds Rb (Radkov et al., 2000). CKI degradation and direct phosphorylation of CDK2 by v-cyclin CDK4/6 together act to induce cell cycle progression and cellular DNA replication (Direkze and Laman, 2004; Ellis et al., 1999; Godden-Kent et al., 1997; Sarek et al., 2006). However, the effect of v-cyclin might be dependent on cell types and expression status of p53: studies in primary cells as well as mice showed that v-cyclin arrests cell growth in a p53-dependent manner but confirmed the pro-proliferative effect of v-cyclin in the absence of p53 (Ojala et al., 1999; Verschuren et al., 2002, 2004). Three KSHV proteins have been reported to target p53 and inhibit its transcriptional activity: LANA-1, LANA-2, and viral interferon regulatory factor 1 (vIRF1) (Friborg et al., 1999; Nakamura et al., 2001; Rivas et al., 2010; Seo et al., 2001; Si and Robertson, 2006). In summary, the latency associated KSHV protein LANA-1 and v-cyclin dysregulate the G1/S checkpoint to stimulate cell cycle progression into S phase.

While KSHV infection has a pro-proliferative effect during latency, its lytic phase has been reported to arrest the host cell cycle. The block in host cell cycle has been attributed to the KSHV encoded transcription factor K-bZIP (Moore, 2007; Seaman et al., 1999). Upon entry of the lytic replication cycle, K-bZIP induces expression of the CKI p21, and the cellular transcription factor CCAAT/enhancer binding protein-α (Wang et al., 2003a, 2003b). It was further suggested that K-bZIP directly interacts and inhibits cyclin A-CDK2, thus preventing S phase entry and locking the cells in G1 (Izumiya et al., 2003). While it remains to be established how a G1 arrest might benefit viral replication, the block was hypothesised to prevent apoptosis from the stress induced by virion production.

Taken together, although KSHV encodes many enzymes involved in DNA precursor synthesis, which reduces the dependency on host factors for viral replication, infection abolishes the G1/S checkpoint during latency to drive cells into S phase. On the other hand, lytic infection is paralleled by an arrest in G1 which might protect cells from the virus replication induced stress. While many of the above findings were discovered by expressing KSHV proteins, their behaviour and function in the context of a full KSHV infection remains to be further investigated (Bagga and Bouchard, 2014).

4.3 HIV: G1-like state and G2/M arrest

HIV is the causative agent of acquired immunodeficiency syndrome (AIDS) and classifies as a lentivirus. As a member of the family of Retroviruses, HIV encodes its proteins as a positive sense, single stranded RNA (+ ssRNA) genome (Freed and Martin, 2013). There are two types of HIV: HIV-1 and HIV-2. As HIV-1 represents the majority of HIV infections and is the more virulent of the two types, the following summery will focus on how HIV-1 interacts with the host cell cycle (Freed and Martin, 2013; Gilbert et al., 2003; Sharp and Hahn, 2011). While HIV-1 infection has been shown to induce a G1-like state in quiescent cells, it was shown to arrest replicating cells in G2/M, thus demonstrating a cell-type dependent response.

HIV-1 successfully replicates in terminally differentiated macrophages which are in the G0 phase of the cell cycle (Mlcochova et al., 2017). Replication in quiescent G0 cells is counteracted by the dNTP hydrolase SAMHD1. SAMHD1 functions as a host restriction factor by reducing cellular dNTP levels during quiescence (Goldstone et al., 2011; Lahouassa et al., 2012; Schmidt et al., 2015). In actively dividing cells SAMHD1 is deactivated by CDK1/2 mediated phosphorylation thus creating an environment that is permissive for viral DNA replication (Cribier et al., 2013; White et al., 2013). While HIV-2 encodes a viral effector, Vpx, that causes degradation of SAMHD1, HIV-1 lacks a Vpx-like protein and has evolved a different mechanism to avoid SAMHD1 restriction (Hrecka et al., 2011; Kaushik et al., 2009; Laguette et al., 2011; Mlcochova et al., 2017). HIV-1 infection of G0 macrophages has been shown to induce a G1-like state as marked by the expression of MCM2, and cyclins A, E, D1/D3 (Mlcochova et al., 2017). While the cellular markers were upregulated, the cells did not re-enter the active cell cycle. SAMHD1 deactivation in this G1-like state was attributed to phosphorylation by upregulated CDK1. Regulation of the host cell cycle therefore allows HIV-1 to replicate in non-dividing cells and expand its host tropism.

HIV-1 has also been shown to inhibit cell cycle progression in dividing cells, including fission yeast, which has mostly been attributed to the multifunctional viral protein R (Vpr) (Bagga and Bouchard, 2014; Zhao et al., 2011). How Vpr induces cells to arrest at the G2/M border is incompletely understood and several different models have been proposed.

One model suggests Vpr-mediated activation of the DDR as the underlying mechanism for the G2/M arrest. In support of this model, Vpr was reported to trigger the ssDNA break DDR response, causing activation of ATR and Chk1 (Lai et al., 2005; Roshal et al., 2003). While ATR and Chk1 were found to be essential to arrest infected cells in G2, the dsDNA damage response, mediated by ATM, was not required (Bartz et al., 1996; Li et al., 2007, 2010a;

Mansky, 1996; Roshal et al., 2003; Zhao and Elder, 2005; Zimmerman et al., 2006). Although the mechanism of Vpr-mediated ATR activation remains to be established, DNA replication stress indicated by stalled replication forks was suggested as a potential inducer (Andersen et al., 2008; Zimmerman et al., 2006). Additionally, progression through S phase was proposed to be essential for Vpr-mediated activation of Chk1. Distinguishing viral activation of Chk1 from the canonical DDR pathway, cells do not arrest in S phase but progress into G2 where they arrest at the G2/M border (Li et al., 2010a). Furthermore, Vpr was reported to cause deactivation of M-phase promoting CDK1 (Zhao and Elder, 2005; Zhao et al., 2011). CDK1 activity is inhibited by phosphorylation on Tyr15. Vpr causes hyperphosphorylation of CDK1 by inhibiting the phosphatase Cdc25, and simultaneously activating the kinase Wee1 (Bartz et al., 1996; Elder et al., 2001; Goh et al., 2004; He et al., 1995; Kamata et al., 2008; Re et al., 1995; Yuan et al., 2004). However, it remains unclear whether inhibition of CDK1 activity is a direct effect of Vpr, or results from upstream activation of the DDR.

In addition to the DDR, the HIV-1 induced G2/M arrest also requires the activity of the host proteasome (DeHart et al., 2007; Tan et al., 2007; Zhao et al., 2011). Vpr recruits and assists the assembly of the E3 ubiquitin ligase complex cullin4A-DDB1-DCAF1 (DeHart et al., 2007), which is thought to facilitate G2/M arrest by promoting degradation of the cellular DNA replication factor MCM10 (Romani et al., 2015). HIV-1 is suggested to arrest the host cell cycle because the HIV promoter, long terminal repeat (LTR), was proposed to be most active during G2. Thus, a cell cycle arrest in G2 would generate an optimal environment for maximal HIV RNA production (Bagga and Bouchard, 2014; Zhao et al., 2011).

In summary, HIV-1 creates a pro-viral environment by inducing a G1-like state in quiescent cells, and arresting proliferating cells in G2.

5 Poxviridae and modulation of the host cell cycle

Research efforts to understand how viruses modulate the host cell cycle have been mostly focused on oncogenic viruses that infect humans such as HPV, KSHV, and EBV. In comparison, relatively little is known about poxvirus subversion of the host cell cycle.

Poxviruses are not generally described as oncogenic in humans. To-date only a single report linked poxvirus infection to human cancer and described the formation of malignant tumours at sites of smallpox vaccination scars in 24 individuals (Marmelzat, 1968). However, some

poxviruses including fowlpoxvirus (FWPV), the monkey-infecting Yaba poxvirus, the human poxvirus Molluscum contagiosum, and rabbit Shope Fibromavirus (SFV) have been described to cause tumour-like hyperplasia in infected animals (Cheevers et al., 1968; MD, 1970; Niven et al., 1961; Shope, 1932). This poxvirus-induced tissue hyperplasia has been linked to secretion of virally encoded growth factors but has not been studied in the context of molecular control of the host cell cycle (McFadden, 2005; Moss, 2007).

Myxoma virus (MV) is a rabbit specific poxvirus. It has been shown to alter cell cycle progression by expressing the protein M-T75 (Johnston et al., 2005) which was linked to cell cycle exit from G0/G1 and accumulation in G2/M of infected, serum starved cells. The change in cell cycle distribution was attributed M-T75 dependent regulation of the cellular E3 ligase cullin-1. M-T75 was shown to interact with cullin-1 and was suggested to stimulate E3 ligase activity. Cullin-1 is involved in cell cycle control as it controls proteasomal degradation of several cell cycle regulators, such as the CKI p27 (Kip1). While p27 did not change during infection in the presence of M-T75, deletion of M-T75 caused an increase in p27 and apoptosis. Preventing p27 accumulation and cell cycle arrest was therefore suggested to counteract antiviral responses such as induction of apoptosis.

Malignant rabbit fibroma virus (MRV) is a chimeric poxvirus, combining sequences from SFV and the previously discussed Myxoma virus (MV). While MRV is highly virulent and tumorigenic in rabbits, SFV infection causes benign fibromyxoma that is usually cleared within a few weeks. Comparing determinants of virulence, it was observed that MRV infection decreases cell proliferation, regulates p53 transcription via a poxviral transcription factor (C7), and prolongs the G2/M phase of the cell cycle (Wali and Strayer, 1996, 1999a). Although this study suggests a connection between virulence and the ability to control cell cycle progression, molecular understanding of how these changes are induced remain to be investigated.

Orf virus, the prototype parapoxvirus was found to encode a viral protein that negatively regulates the APC/C, which was accordingly named PACR (poxvirus APC/cyclosome regulator (Mo et al., 2009). APC/C is an ubiquitin ligase which is required for correct cell cycle progression. While it is essential in promoting exit from mitosis, it requires deactivation for cells to transit from G1 into S phase. The Orf PACR was defined as a RING-H2 protein which shares sequence similarity with the APC/C subunit APC11. PACR works as a dominant/negative regulator of APC/C by binding to the APC2 subunit of the complex. However, PACR lacks ubiquitin ligase activity and thereby impairs APC/C function. Consistent with inhibited APC/C activity, cell lines stably expressing PACR showed increased G2/M cell fractions at the expense

of G1 phase. This shift in cell cycle distribution was paralleled by increased cyclin A and cyclin B levels. Based on these results, PACR was suggested to arrest cells at the border between G2 and M phase, thus inhibiting cell proliferation and inducing apoptosis. While PACR was not found to be essential for the virus life cycle, genetic deletion drastically decreased viral fitness and growth. However, it remains to be established how PACR expression promotes productive viral infection. Additionally, PACR was found to be encoded not only by Orf virus but by a subset of poxviruses, including the two genera parapoxviruses and molluscipoxviruses, as well as Crocodile and Squirrel poxvirus.

5.1 Vaccinia and modulation of the host cell cycle

VACV was first described to alter cell cycle progression in the 1960s. Infection was observed to inhibit cell proliferation and DNA synthesis immediately after infection, reducing DNA replication to 25% of control levels by 6hpi. In addition to blocking cellular DNA synthesis, VACV also prevented entry into mitosis and no mitotic cells were observed in infected cultures after 7hpi (Jungwirth and Launer, 1968; Kit and Dubbs, 1962; Magee and Sagik, 1959; Magee et al., 1960). Although it was suggested that inhibition required viral entry and early gene expression, conclusions from infections with cowpox and VACV were inconclusive and contradictory (Kit and Dubbs, 1962; Magee and Sagik, 1959; Magee et al., 1960). In addition to these conflicting results, mechanistic insights remained inaccessible due to experimental limitations. First, viral DNA was not readily distinguishable from cellular DNA given that classical studies indirectly determined cellular DNA synthesis rates by pulsed radiolabelling with ^{14}C-thymidine. Since VACV is a dsDNA virus, ^{14}C-thymidine is also incorporated into replicating viral genomes. Differentiation of the two DNA species required physico-chemical separation of the nuclear (cellular) from the cytosolic (viral) DNA fraction (Jungwirth and Dawid, 1967). Second, initial experiments aimed at studying the minimal viral requirement to block the cell cycle relied on UV or heat inactivated VACV (Jungwirth and Launer, 1968). These inactivation methods result in a poorly defined and highly variable inhibition of the virus life cycle (Tsung et al., 1996).

After these initial observations that VACV inhibited cellular DNA synthesis and cell cycle progression, it took 30 years till the topic was revisited. In 1999 a report was published that linked VACV infection to changes in cell cycle progression and expression of several cell cycle

regulators (Wali and Strayer, 1999b). VACV was shown to significantly increase the S phase cell fraction at 24hpi at the expense of G1 in rabbit kidney fibroblasts that were released from a serum starvation block. Although the G2/M fraction was also slightly increased, the change was not significant. The change in cell cycle distribution was suggested to be caused by increased CDK1 activity at 36hpi, as well as altered protein and transcript levels of cell cycle regulators in response to VACV infection. While CyclinA and p53 were found to be upregulated between 4-12hpi, the protein levels fell below mock controls during late infection (12-60 hpi). Similarly, p27, CDK1 and CDK2 levels were suggested to decline between 36-60hpi. Mirroring the reduction in protein abundance at late timepoints, VACV was indicated to first induce *CDK2* and *CyclinB* transcription between 2-12hpi before reducing it again later on. Similar results were obtained for transcript levels of Cyclins A2, C, D1, G1, and H in a more recent microarray study: VACV infection increased transcript abundance in unsynchronized HeLa cells at 2hpi, before causing a reduction at 6 and 16hpi, compared to mock controls (Guerra et al., 2003). Taken together, the study by Wali and Strayer showed that VACV altered cell cycle progression at late stages of infection (>24hpi) and provided first suggestions of molecular changes in the host cell. However, (molecular) changes in host cell cycle progression during early VACV infection (0-12hpi), implications for the virus life cycle, as well as the required viral effectors remained undefined.

VACV was further reported to alter cell cycle progression by dysregulating G1/S transcription and an increased fraction of S and G2/M cells was observed after 30hpi (Yoo et al., 2008). Transcription of S phase inducing genes relies on RNA polymerase III (pol III) and its associated transcription factors TFIIIB and TFIIIC (Mauck and Green, 1974; White et al., 1995). VACV infection was shown to induce expression of both TFIIIB and TFIIIC, thereby promoting tRNA synthesis (Yoo et al., 2008). In uninfected cells, pol III transcriptional activity is negatively affected by the tumour suppressors Rb and p53, which bind to TFIIIB and TFIIIC subunits (Crighton et al., 2003; Larminie et al., 1997; White, 2004). It was suggested that VACV-mediated inactivation of both Rb and p53 caused the observed increase in the populations of S and G2/M phase cells (Yoo et al., 2008). Rb was found to be hypo-phosphorylated upon VACV infection, while total protein levels remained unchanged. This result was surprising as hypo-phosphorylated Rb is known to prevent G1/S transcription and S phase entry (cf. section 3.3.1 of this chapter). However, hypo-phosphorylated Rb was observed to be sequestered and inactivated in a complex with the TFIIIB subunit Brf1. Additionally, infection was shown to deactivate p53 by inducing its complex formation with another TFIIIB subunit TBP, as well as its degradation. Degradation of p53 was suggested to be promoted by VACV-induced

upregulation of *Mdm2* transcription, which is known as a negative regulator of p53 stability. To summarize, this report suggests that late VACV infection (>30hpi) increases the S and G2/M cell cycle fractions by deactivating Rb and p53 thus inducing G1/S transcription. The same study reported a pro-proliferative effect of VACV infection on 143B osteosarcoma cells, thus contradicting previous report and indicating cell-type dependent differences. In summary, although changes in cellular regulators pathways were described, the viral effector protein and the effect on productive infection remain to be defined.

The VACV kinase B1 is the only viral protein that has been implicated in regulating progression of the host cell cycle (Santos et al., 2004). During infection, B1 is expressed as an early protein and has critical functions in viral genome replication (cf. Introduction section 2.2.3.). Linking B1's kinase function with host cell cycle control, expression of B1 in uninfected cells was shown to be sufficient to promote degradation of p53 (Santos et al., 2004). In this system, B1 hyperphosphorylated p53 at several N-terminal residues, including Ser15 and Thr18, which modulate p53 stability (Haupt et al., 1997; Kubbutat et al., 1997). B1-induced degradation of p53 depended on proteasome activity, and the E3 ligase Mdm2 which is a known negative regulator of p53. In the absence of Mdm2, B1 expression caused an increase in p53, rather than its degradation. While this demonstrates that B1 phosphorylates p53 and causes its degradation, it remains to be investigated whether B1 has the same function in the context of VACV infection.

5.2 Involvement of the host cell cycle in productive VACV infection

Although the publications described above indicate that VACV alters host cell cycle progression and manipulates key cell cycle regulators, it has not been discovered how this benefits viral replication.

Encoding over 200 proteins, Poxviruses are known as master regulators that highjack and control (nearly) every process in their host cells. As a member of the poxvirus family, VACV encodes its own DNA replication and transcription machinery, as well as enzymes involved in nucleotide metabolism (Black and Hruby, 1991; De Silva and Moss, 2008; Gammon et al., 2010; Paoletti and Moss, 1974). The vast coding capacity allows VACV to replicate exclusively in the cytosol, and more independently from its host cell than other viruses. However, the notion that VACV replication proceeded without nuclear involvement was disproven when it was

observed that enucleated cells did not support production of infectious virions (Pennington and Follett, 1974). While viral DNA replication and transcription proceeded with normal timing, viral factories contained fewer IVs, and viral DNA condensation as well as virus particle maturation was inhibited (Hruby et al., 1979; Pennington and Follett, 1974; Prescott et al., 1971). Further suggesting nuclear involvement in replication, siRNA knockdown of nuclear pore components, and inhibition of nuclear transport was found to mimic the enucleation phenotype (Mercer et al., 2012; Sivan et al., 2013). It was further shown that the nuclear pore complex proteins Nup358 and Nup62 are directly recruited to sites of VACV replication and are involved in productive infection (Khuperkar et al., 2017).

Highlighting the importance of host factors in the VACV life cycle, several nuclear factors in addition to Nups have been described to localize to viral factories and assist in either genome replication or viral gene transcription (cf. sections 2.2.3 and 2.2.4). These cellular factors include the transcription factors YY1, TBP, and SP1, the heterogeneous nuclear ribonucleoproteins A2/B1 and RBM3, as well as cellular translation factors G3BP1, eIF4E, and eIF4G (Broyles et al., 1999; Gunasinghe et al., 1998; Katsafanas and Moss, 2004; Knutson et al., 2006; Oh and Broyles, 2005; Rosales et al., 1994; Rozelle et al., 2014; Walsh et al., 2008).

Recently, VACV has been shown to exploit the cellular DNA damage response (cf. section 2.2.3), thus linking a key component of the cell cycle machinery to productive infection for the first time (Postigo et al., 2017). While the paper did not investigate activation of the DDR in context of cell cycle regulation, it found DDR activation to be essential for VACV genome replication. It was suggested that VACV recruits the cellular single strand binding protein RPA to replicating genomes to serve as a platform for the assembling replisome and activated DDR components. Within the replisome, the viral polymerase E9 was found to interact with the DDR activating protein TOPBP1 and the cellular sliding clamp PCNA. While activation of the DDR kinases ATR and Chk1 was found to be essential, their role in VACV genome replication has not been established. It was suggested, however that they might function in facilitating viral genome replication.

Mass spectrometry analysis of the proteome associated with replicating VACV genomes (IPOND-MS) indicated that VACV might exploit several cellular pathways dedicated to DNA repair in addition to DDR (Reyes et al., 2017). The proteome was found to be enriched in cellular factors involved in Non-Homologous End Joining (NHEJ), Base Excision Repair (BER), Nucleotide Excision Repair (NER), Interstrand Crosslink (ICL) repair, and Homologous Recombination Repair (HRR). While neither ATR nor Chk1 were confirmed to associate with

VACV DNA, PCNA was strongly enriched, as well as all subunits of the mini-chromosome maintenance MCM2-7 replicative helicase complex, the HRR components BLM, MRE11, NBS1, and Ku70, as well as topoisomerase I/II which was previously shown to facilitate VACV replication (Lin et al., 2008). While this dataset provides interesting new links between VACV replication and the host cell machinery, it remains to be investigated how these different DNA repair pathways interact with the VACV life cycle.

However, the DDR has not only been described to benefit infection. The ssDNA branch of the DDR is mediated by two kinases: ATM and DNA-PK (cf. section 3.3.3). While activation of ATM and its downstream effector kinase Chk1 were implicated in assisting VACV genome replication, DNA-PK is known as a cytoplasmic DNA sensor with anti-poxviral activity (Ferguson et al., 2012). VACV encodes several proteins, including C4 and C16, which directly inhibit the antiviral effect of DNA-PK by preventing its DNA binding activity (Peters et al., 2013; Scutts et al., 2018). The opposing effects of ATM and DNA-PK mediated DDR highlight the dual role of checkpoint activation in the viral life cycle, as well as the complexity of viral modulation of host cellular pathways.

5.3 Summary

VACV has been shown to inhibit cellular DNA synthesis, as well as to alter host cell proliferation and cell cycle distribution. While deactivation of the tumour suppressors Rb and p53 were described to facilitated entry into S phase during late infection, detailed mechanistic insights remain to be investigated. VACV infection has further been implicated to activate and harness the cellular DNA damage response for its own genome replication. However, how the DDR assists in viral DNA replication is still undefined and it remains to be elucidated VACV-induced DDR activation affects host cell cycle progression.

6 Aims of the PhD

Poxviruses are known as master regulators that highjack and control (nearly) every process in their host cells. As the model poxvirus, VACV has been extensively studied over the past decades. While infection has been linked to alterations in cell cycle progression and activation of cellular checkpoints, the relevance of this cell cycle subversion to VACV replication and how it is achieved remains undefined.

Cell cycle progression is tightly regulated in normal, uninfected cells and several molecular checkpoints ensure that cells divide in a controlled manner. Uncontrolled division, however, is a hallmark of cancer and cell cycle dysregulation is a major cause for cancer development. Recently, viruses have been recognized as a promising biotechnological tool for anti-cancer therapy. These virotherapies exploit a virus' natural or engineered preference for infecting and thereby destroying tumour cells. Several different virotherapies based on oncolytic viruses, including VACV are currently being tested in clinical trials.

VACV is well-known as the model poxvirus and has gained clinical significance as the vaccine used to successfully eradicate smallpox. The causative agent of smallpox, variola virus, remains the deadliest pathogen in human history, accounting for more than 500 million deaths. The smallpox vaccination campaign has been discontinued, which leaves the population at risk for smallpox re-emergence by bioterrorism, or zoonotic poxvirus infections such as monkeypox and cowpox. Limited treatment options for poxvirus infections necessitate continued research into this virus family to develop improved anti-virals and vaccines.

Better understanding of how VACV interacts with the host cell cycle will help the advancement of improved anti-cancer virotherapies and provide new drug targets for the development of anti-poxviral agents.

This PhD project therefore aims to provide a more comprehensive understanding of how VACV alters the host cell cycle during infection.

AIM 1: Characterization and description of VACV induced cell cycle changes.

AIM 2: Identification of the required VACV life cycle stages and viral effector proteins.

AIM 3: Identification of the cellular co-effector proteins and signalling pathways

AIM 4: Definition of host cell cycle contribution to productive infection.

2 Materials and Methods

1 General material and methods

1.1 Cell Culture

Cells were grown in Dulbecco's Modified Eagle Medium (DMEM, Life Technologies) supplemented with cell line specific additives (Table 1). Cell cultures were maintained under standard conditions at 37°C and 5% CO_2. When reaching a 80-90% confluency, cells were passaged using Phosphate-buffered Saline (PBS) and Trypsin/EDTA (2.5 g Trypsin/litre, 0.2 g EDTA/litre). All cell culture reagents (1x PBS, Trypsin, and media) are pre-warmed to 37 °C prior to use, unless specified otherwise. Handling of non-fixed cells was exclusively conducted in laminar-flow.

Cell line	Specification	Medium composition	Source
HeLa	Human, cervical cancer	DMEM (Life Technologies) 10% Foetal Bovine Serum (FBS, Life Technologies) 1 % Gluta-Max (Gibco) 1% Penicillin-Streptomycin (Life Technologies) 1% Non-essential amino acids (NEAA, Gibco)	ATCC
HeLa Kyoto H2B-mCherry	Human, cervical cancer. Expressing exogenous histone H2B C-terminally tagged with mCherry.	HeLa medium	Murielle Serres (Paluch Lab, LMCB, UCL)
HeLa FUCCI	Human, cervical cancer. Expressing XX	HeLa medium	RIKEN Cell Bank
A549	Adenocarcinomic human alveolar basal epithelial cells	HeLa medium	ATCC
HCT116	Human, colorectal cancer	HeLa medium	M. Wilson (Saiardi Lab, LMCB, UCL)
HCT116 p53-/-	Human, colorectal cancer. Homozygous p53 knockout.	HeLa medium	M. Wilson (Saiardi Lab, LMCB, UCL)
BSC40	Green monkey kidney cells	HeLa medium supplied with 1 % Sodium Pyruvate (Life Technologies)	ATCC

Table 1 Cell lines used in this study

1.1 Viruses

Recombinant VACV strains used in this study are part of the Mercer Lab collection and have either been obtained elsewhere (cf. Table 2), or were generated through homologous recombination as previously described (Mercer and Helenius, 2008b). BSC40 cells were infected with the backbone VACV of choice and transfected with linearized plasmid 4hpi. Cells were harvested at 48hpi and the recombinant virus was plaque purified over several rounds, using fluorescence as a marker. Plaques from the final round were sequenced to confirm construct insertion in the correct locus. Insertions in the thymidine kinase (TK) locus were generated using vectors derived from the plasmid pJS4 (Chakrabarti et al., 1997). Insertions in other loci, including endogenous insertions were generated using vectors based on the commercial plasmid pBluescript II KS (ThermoFisher Scientific).

Virus Type	Description	Source / Reference
VACV WT WR	Wild-type VACV Western Reserve strain	Jason Mercer
WR E EGFP	VACV WR encoding EGFP under the J2R early promoter in the TK locus	(Chakrabarti et al., 1997; Stiefel et al., 2012)
WR L EGFP	VACV WR encoding EGFP under the F17R late promoter in the TK locus	(Chakrabarti et al., 1997; Schmidt et al., 2013; Stiefel et al., 2012)
WR HA-D5	VACV WR encoding an endogenous HA-D5 fusion protein in the TK locus	(Kilcher et al., 2014)
WR Cts2	VACV WR encoding a thermolabile, endogenous B1 protein. Permissive temp: 31°C, non-permissive temp: 39.7°C	(Condit et al., 1983)
WR Cts24	VACV WR encoding a thermolabile, endogenous D5 protein. Permissive temp: 31°C, non-permissive temp: 39.7°C	(Condit et al., 1983; Kilcher et al., 2014)
WR F10-SH EL EGFP	VACV WR encoding EGFP under a viral early late promoter in the TK locus, and a F10-Streptavidin-HA fusion protein in the endogenous F10L locus	Jason Mercer
vL1Ri EL EGFP	VACV WR encoding L1 under an IPTG inducible LacZ promoter	(Bisht et al., 2008)
v*ind*H1	VACV WR encoding H1 under an IPTG inducible LacZ promoter. 5mM IPTG	(Liu et al., 1995)
ΔB1mutB12-A1 / -A3	VACV WR B1R deletion virus which encodes a mCherry cassette instead of the B1R gene and contains an additional mutation in the B12R locus, which renders the virus replication competent.	(Olson et al., 2019)

Table 2 VACV recombinants used in this study

1.2 Reagents and antibodies

1.2.1 Kits

The following kits were used according to manufacturer's instructions, unless specified otherwise. The Click-iT EdU kit was used with 5-Ethynyl-2'-deoxycytidine (5-EdC) purchased from Abcam instead of the supplied EdU. Cytotoxicity was determined using the Pierce LDH Cytotoxicity Assay Kit with a reaction volume of 3 x 25 µl instead of the described 3 x 50 µl.

Kit	Company
Click-iT™ EdU Alexa Fluor™ 488 Imaging Kit	Invitrogen
Pierce LDH Cytotoxicity Assay Kit	Thermo Scientific
QIAquick PCR Purification Kit	Qiagen
QIAquick Gel Extraction Kit	Qiagen
QIAprep Spin Miniprep Kit	Qiagen
Plasmid Maxi Kit	Qiagen

Table 3 Kits used in this study

1.2.2 Western blot and immunofluorescence antibodies

Table 4 summarizes the primary antibodies that were used to detect cellular proteins either by immunoblot or immunofluorescence.

Target	Species	Dilution	Reference/Company
ATM	Mouse	1:1000	GeneTex GTX70103
ATR	Rabbit	1:1000	Abcamab2905
Aurora A	Rabbit	1:1000	Abcam ab1287
Aurora B	Rabbit	1:1000	Abcam ab2254
CDK1	Mouse	1:1000	Cell Signaling #9116
CDK2	Rabbit	1:1000	Cell Signaling #2546
CDK4	Rabbit	1:1000	Cell Signaling #12790
CDK6	Rabbit	1:1000	Cell Signaling #13331
CDK7	Mouse	1:1000	Cell Signalling #2916
CDk9	Rabbit	1:1000	Cell Signalling #2316
Cdc25C	Rabbit	1:1000	Cell Signalling #4688
Phospho-Cdc25C (Thr48)	Rabbit	1:1000	Cell Signalling #9527
Phospho-Cdc25C (Ser216)	Rabbit	1:1000	Cell Signalling #4901

Cdt1	Mouse	1:1000	Millipore 04-1524
Chk1	Mouse	1:1000	Santa Cruz sc-56291
Phospho-p53 (Thr18)	Rabbit	1:1000	Elabscience 20958ELA
Geminin	Rabbit	1:1000	Santa Cruz sc-13015
Chk2	Mouse	1:1000	Cell Signalling #3440
Cyclin A	Mouse	1:1000	Santa Cruz sc-71682
Cyclin B1	Rabbit	1:1000	Cell Signalling #4138
Cyclin D1	Rabbit	1:1000	Cell Signaling #2978
Cyclin E	Mouse	1:1000	BD Pharmingen 551160
INCENP	Mouse		Abcam ab23956
Lamin B1	Rabbit	1:1000	Abcam ab133741
MCM2	Mouse	1:1000	Cell Signaling #12079
Mdm2	Mouse	1:1000	Abcam ab16895
p53	Mouse	1:1000	
Phospho-AurorA (Thr228) / 68hosphor-AuroraB (Thr232) / 68hosphor-AuroraC (Thr198)	Rabbit	1:1000	Cell Signalling #2914
Phospho-CDK1 (Tyr15)	Rabbit	1:1000	Cell Signaling #4539
68Phospho-Chk1 (Ser345)	Rabbit	1:1000	Cell Signaling #2348
Phospho-Chk2 (Thr68)	Rabbit	1:1000	Cell Signaling #2197
Phospho-Histone H2A.X Ser139	Rabbit	1:1000	Cell Signaling #9718
Phospho-p53 (Ser15)	Mouse	1:1000	Cell Signaling #9286
Phospho-Rb (Ser795)	Rabbit	1:1000	Cell Signaling #9301
Phospho-Rb (Ser807/811)	Rabbit	1:1000	Cell Signaling #8516
α-Tubulin	Rabbit	1:2000	Cell Signaling #
α-Tubulin	Mouse	1:2000	Cell Signaling #
PCNA	Mouse	1:1000	Santa Cruz sc-25280
HA	Mouse	1:2000	BioLegend
HA	Rabbit	1:2000	BioLegend
Phospho-ATR			
Phospho-ATM (Ser1981)	Mouse	1:1000	Cell Signaling #4526
Rb			
SAMHD1	Mouse	1:1000	Abcam ab67820
YY1	Rabbit	1:1000	Abcam ab109237
p21			

Table 4 Primary cellular antibodies used in this study

Table 5 summarizes the primary antibodies that were used to detect viral proteins by immunoblot analysis.

Target	Species	Dilution	IF Fixation	Reference/Company
F17	Rabbit	1:1000	-	Paula Traktman (Liu et al., 1995)
I3	Rabbit	1:1000	-	Paula Traktman (Rochester and Traktman, 1998)

Table 5 Primary viral antibodies used in this study

Table 6 summarizes the secondary antibodies that were used to visualize cellular and viral proteins either by immunoblot (chemiluminescence and near-infrared fluorescence), or by immunofluorescence.

Target	Species	Dilution	Application	Reference/Company
Anti-mouse IgG, HRP-linked	Horse	1:2000	WB	Cell Signalling #7076
Anti-rabbit IgG, HRP-linked	Goat	1:2000	WB	Cell Signalling #7074
Anti-mouse IgG, IRDye 680RD	Donkey	1:10000	WB	LI-COR 926-68072
Anti-rabbit IgG, IRDye 680RD	Donkey	1:10000	WB	LI-COR 926-68073
Anti-rabbit IgG, IRDye 800CW	Donkey	1:10000	WB	LI-COR 926-32213
Anti-mouse IgG, IRDye 800CW	Donkey	1:10000	IF	LI-COR 926-32212
Anti-rabbit IgG, AlexaFluor 488	Goat	1:400	IF	Thermo Fisher
Anti-mouse IgG, AlexaFluor 594	Goat	1:400	IF	Thermo Fisher
Anti-rabbit IgG, AlexaFluor 594	Goat	1:400	IF	Thermo Fisher
Anti-mouse IgG, AlexaFluor 488	Goat	1:400	IF	Thermo Fisher
Anti-mouse IgG, AlexaFluor 647	Goat	1:400	IF	Thermo Fisher
Anti-rat IgG, AlexFluor 647	Goat	1:400	IF	Thermo Fisher

Table 6 Secondary antibodies used in this study

1.2.3 Small molecule inhibitors

The inhibitors used in this study are summarized in Table 7 and Table 8. The compounds were dissolved and stored as recommended by the manufacturer. Mevinolin (Lovastatin) was activated by dissolving the prodrug in 70% EtOH to convert it into its active form (JavanMoghadam-Kamrani and Keyomarsi, 2008).

Name	Final concentration	Company
Cytosine arabinoside (AraC)	10 µM	Sigma-Aldrich
Cycloheximide (CHX)	50 µM	Sigma-Aldrich
Mevinolin (Lovastatin)	20 µM	LKT Labs
DL-Mevalonic acid lactone (Mevalonate)	6 mM	Sigma-Aldrich
Hydroxyurea (HU)	2.5 mM	Sigma-Aldrich
RO3306	10 µM	Sigma-Aldrich
Tissue-culture grade DMSO	-	Sigma-Aldrich

Table 7 Inhibitors used in this study

Table 8 summarized the custom-made small molecule inhibitor library that was screened for anti-viral activity (described in methods section 3.1.1-3.1.2). The pre-dissolved library was obtained from Selleckchem.

Cat. No.	Name	Target	IC50 in cell free assays (Selleckchem)	Tested concentration range
S1008	Selumetinib, AZD6244	Mek1	14 nM	97.66 nM – 50µM
S1048	VX-680	pan-Aurora	9.9 nM (mostly AuroraA)	2.54 nM – 50µM
S1092	KU-55933	ATM	12.9 nM	97.66 nM – 50µM
S1116	Palbociclib, PD-0332991	CDK4/6	11 nM / 16 nM	39.06 nM – 20µM
S1145	SNS-032, BMS-387032	CDK2/7/9	48 nM / 62 nM / 4 nM	39.06 nM – 20µM
S1153	Roscovitine Seliciclib, CYC202	CDK1/2/5	0.65 µM / 0.7 µM / 0.16 µM	97.66 nM – 50µM
S1249	JNJ-7706621	Pan-CDK (effect on AurK)	9 nM (CDK1) 4 nM (CDK2)	2.54 nM – 50µM
S1525	MK-1775	Wee1	5.1 nM	39.06 nM – 20µM
S1532	AZD7762	Chk1/2	5 nM	39.06 nM – 20µM
S1572	BS-181 HCL	CDK7	21 nM	39.06 nM – 20µM
S1896	hydroxyurea	DNA synthesis	32 µM	78.13 nM – 40µM
S2248	Silmitasertib, CX-4945	CK2	1 nM	78.13 nM – 40µM
S2683	CHIR-124	Chk1	0.3 nM	39.06 nM – 20µM
S2893	NU7026	DNA-PK	0.23 µM	97.66 nM – 50µM
S7102	VE-822	ATR	19 nM	39.06 nM – 20µM
S8007	VE-821	ATR	26 nM	97.66 nM – 50µM
S8050	ETP-46464	ATR	25 nM	97.66 nM – 50µM
S1107	Danusertib , PHA-739358	pan-Aurora	13nM / 79 nM / 61 nM	2.54 nM – 50µM
S1147	Barasertib, AZD1152-HQPA	AuroraB	0.37nM (3700 fold more selective over B than A)	2.54 nM – 50µM
S1451	Aurora A Inhibitor I	AuroraA	3.4 nM (1000 fold more selective over A than B)	78.13 nM – 40µM

Table 8 Small molecule inhibitor library screened in this study

2 Virus methods

For amplification of the virus, confluent 60 mm dishes of BSC40 cells were infected with the desired VACV strain at multiplicity of infection (MOI) of 1. After incubation under standard conditions for 2 days, cells were harvested by scraping into 1 mM Tris pH 9.0 and lysed by freeze-thawing three times in liquid nitrogen. This cell extract was then used to infect two 15

cm dishes of confluent BSC40 cells which were again incubated under standard conditions for 2days. As before, infected cells were harvested in 1 mM Tris pH 9.0. After freeze-thawing three times, the lysate was used to infect 15 x 15cm dishes of BSC40 cells which were harvested after 2 days of incubation. The cells were scraped into PBS and pelleted by centrifugation at 300 x g for 5min.

The cell pellet was resuspended in 12mL 10mM Tris pH 9.0 and kept on ice for 5min. Cell membranes were disrupted with 25 strokes in a tight-fitting douncer (Wheaton) and the resulting cytosolic extract was centrifuged at 2000 x g for 10 min at 4°C. To remove cell debris from the cell extract, the supernatant was centrifuged again. Next, the cytosolic extracts were sedimented through a 36% sucrose cushion (20 mM Tris pH 9.0) by ultracentrifugation in a SW 32 Ti Rotor (Beckman Coulter) at 43'000 x g for 80 min at 4°C. The resulting virus pellet was resuspended in 300µL 1mM Tris pH 9.0 and was stored at -80°C.
For further purification, the sedimented virus was vortexed, sonicated, and layered onto a 25-40 % sucrose gradient, which was prepared using a Gradient Master (Biocomp) set at 81.5°, 18 rpm, 3 min in 10 mM Tris 9.0. Sedimented virus was banded through ultracentrifugation at 12'000 x g at 4°C for 40 min. The banded virus was extracted from the SW41 ultracentrifuge tube (Beckman Coulter) using a hypodermic needle and was resuspended in 1 mM Tris pH 9.0 and stored at -80°C. The titer of the purified virus stocks was then determined by plaque assay (materials and methods section 2.2).

2.1 Virus titration and MOI

2.1.1 Virus titration

Virus yields or virus titers of purified virus stocks were determined by plaque assay. The virus yield or stock (2µL) were serially diluted in DMEM(-) (998 µl) to a final dilution of 10^{-9} and tittered on confluent monolayers of BSC40 cells. 500 µl inoculum was added per well of a 6 well plate and incubated at standard conditions, gently rocking the plates every 15min. After 1h, the infection medium was replaced with 1.5 ml BSC40 growth medium. After incubation for 2 days, the medium was aspirated and cells were fixed with staining solution (0.1% crystal violet and 2% paraformaldehyde (PFA)). Plaques were manually counted (excluding satellite plaques) to calculate the plaqueforming units per millilitre (pfu/ml).

2.1.2 MOI for different cell lines

The virus stocks were titered in BSC40 cells and the MOI was adjusted for the different cell lines. Since, BSC40 cells are more permissive than HeLa cells, a ten times higher MOI is required in HeLa cells to match the infection level in BSC40 cells. In the following, the indicated MOI represents the cell line adjusted MOI i.e. if BSC40 cells are described to have been infected with an "MOI 50" the same amount of virus particles used to infect HeLa cells is indicated as "MOI 5".

2.1.3 MOI equivalents for non-plaqueforming VACV strains

VACV strains that are defective in viral replication do not form plaques and therefore cannot be titered by plaque assay. Instead of calculating the multiplicity of infection based on plaqueforming units, the amount of input virions was matched between different VACV strains. In order to determine the virion concentration, the DNA absorbance at 260/280nm was measured on a NanoDrop (Thermo Scientific). The absorbance of WT VACV with a known pfu/ml titer was used to calculate the corresponding "pfu equivalent" for the non-replicating VACV strain. Based on the "pfu equivalent titer", the MOI equivalent (MOI eq.) was calculated for the non-replicating VACV strains L1(-) and H1(-).

3 Pharmacological assays

3.1 Cell cycle inhibitor screen

3.1.1 24h drug pretreatment: viral early and late gene expression

18'000 HeLa or A549 cells 18'000 were seeded in 100 µl growth medium in the inner wells of 96-well plates (Greiner Bio-one) and the outer wells were filled with PBS. Cells were grown under standard conditions for approximately 16 hrs. The medium was replaced with 75 µl fresh growth medium and the inhibitors were added in 25 µl DMEM(-) from a 4x stock dilution. The cells were incubated in the diluted 1x inhibitor medium under standard conditions for 24h. Samples were infected with either WR E EGFP, or WR L EGFP at MOI (5) in 100 µl DMEM (-) to ensure > 90% infection. After 1h incubation under standard conditions, unbound virus was

aspirated and wells were fed with 75 µl fresh growth medium before adding the inhibitors in 25 µl DMEM(-) from a 4x stock dilution. Plates were incubated at standard conditions and harvested at either 6hpi or 16 hpi for early and late EGFP viruses, respectively. The samples were then prepared for analysis by flow cytometry (methods section 8).

3.1.2 30min acute pretreatment:

18'000 HeLa or A549 cells 18'000 were seeded in 100 µl growth medium in the inner wells of 96-well plates (Greiner Bio-one) and the outer wells were filled with PBS. Cells were grown under standard conditions for approximately 16 hrs. The medium was replaced with 25 µl fresh growth medium and the inhibitors were added in 25 µl DMEM(-) from a 4x stock dilution. The cells were incubated in the diluted 2x inhibitor medium 30min at standard conditions. Samples were infected by adding 50 µl DMEM(-) with either WR E EGFP, or WR L EGFP (MOI 5) to ensure > 90% infection. After 1h incubation under standard conditions, unbound virus was aspirated and wells were fed with 75 µl fresh growth medium before adding the inhibitors in 25 µl DMEM(-) from a 4x stock dilution. Plates were incubated at standard conditions and harvested at either 6hpi or 16 hpi for early and late EGFP viruses, respectively. The samples were then prepared for analysis by flow cytometry (methods section 8).

3.1.3 Calculation of EC90 values

Viral early and viral late gene expression was quantified by flow cytometry and either measured as mean fluorescence intensity of the entire cell population (MFI), or as the percentage of infected (EGFP positive) cells. To determine the dose response curves, the MFI or percentage of infected cells were plotted against the inhibitor concentrations using Prism7 (GraphPad). The inbuilt analysis tool was used to fit a non-linear regression curve with a variable slope (four parameters) to the input data (inhibitor concentration vs. response), according to the following model:

$$y(x) = y_{min} + [y_{max} - y_{min}]/[1 + \left(\frac{x^H}{IC50^H}\right)]$$

x : inhibitor concentration

y_{max} : maximum value for infection parameter (at minimal inhibitor concentration)

y_{min} : minimum value for infection parameter (at maximal inhibitor concentration)

H : Hill Slope, describes steepness of fitted curve

$IC50$: concentration of inhibitor that results in 50% of maximal inhibition

Next, the IC50 values were calculated from the fitted dose-response curve. The IC50 value refers to the inhibitor concentration that induces a half-maximal response i.e. 50% of maximum viral inhibition. Similarly, the IC90 values reflect the inhibitor concentration that elicits a 90% response i.e. 90% of maximum viral inhibition. The IC90 values were calculated for the hits from the small molecule screen using the adapted Hill equation:

$$EC_F = \left(\frac{F}{100 - F}\right)^{1/H} \cdot EC_{50}$$

F : percent response (e.g. 90 for EC_{90} values)

EC_F : inhibitor concentration that leads to F % of maximal inhibition

H : Hill Slope, describes steepness of fitted curve

$EC50$: concentration of inhibitor that results in a half maximal inhibition, for the purposes of this thesis the EC50 = IC50

3.1.4 Cytotoxicity assay

To test for cell viability after VACV infection or drug treatment, the cytotoxicity was determined via Lactate Dehydrogenase assay using the Pierce™ LDH Cytotoxicity Assay Kit (Thermo Scientific). The assay indirectly measures cell viability by the amount of extracellular LDH. Viable cells have an intact plasma membrane barrier that prevents cytoplasmic content from leaking out of the cell. Upon cell death, the plasma membrane integrity is compromised and cytosolic contents such as the enzyme LDH are released. Manufacturer's instructions were followed while using half the suggested volume for every reaction. Briefly, the assay of interest was carried out in 96-well plates (Greiner Bio-one) in a total volume of 100 µl. At assay-dependent times post infection or post treatment, 25 µl supernatant from each well was transferred to a clear bottom 96-well plate (Greiner Bio-one). To each sample, 25 µl Pierce™ LDH Reaction Mix was added and incubated at RT in the dark for 30min. The LDH reaction was

stopped with 25 µl Stop Solution, and the absorbance at 490 nm and 650 nm was read with VersaMax Microplate Reader (Molecular Devices) using SoftMax Pro software. The 490nm absorbance signal was background corrected by subtracting the absorbance at 650nm. Measurements were normalized against a "maximum cell death" control where cells were lysed for 45min at standard conditions.

Drug No.	Pre-incubation time	Virus	EC90 (µM)	Toxic at EC90
S1008	30min	E EGFP	-	
		L EGFP	0.12	-
	24h	E EGFP	-	
		L EGFP	68.02	
S1048	30min	E EGFP	11.16	No
		L EGFP	16.19	No
	24h	E EGFP	12.53	No
		L EGFP	0.09	No
S1092	30min	E EGFP	-	
		L EGFP	101.41	-
	24h	E EGFP	-	
		L EGFP	46.19	-
S1116	30min	E EGFP	-	
		L EGFP	16.21	-
	24h	E EGFP	-	
		L EGFP	94.14	-
S1145	30min	E EGFP	-	
		L EGFP	-	
	24h	E EGFP	0.36	No
		L EGFP	2.86	No
S1153	30min	E EGFP	-	
		L EGFP	13.72	-
	24h	E EGFP	-	
		L EGFP	-	
S1249	30min	E EGFP	17.95	No
		L EGFP	5.75	No
	24h	E EGFP	7.55	No
		L EGFP	20.4	No
S1525	30min	E EGFP	-	
		L EGFP	9.80	No
	24h	E EGFP	0.30	No
		L EGFP	0.83	No
S1532	30min	E EGFP	-	
		L EGFP	19.26	-
	24h	E EGFP	4.99	-
		L EGFP	1.07	No

S1572	30min	E EGFP	-	
		L EGFP	10.30	No
	24h	E EGFP	-	
		L EGFP	36.18	-
S1896	30min	E EGFP	-	
		L EGFP	0.12	No
	24h	E EGFP	-	
		L EGFP	93.72	-
S2248	30min	E EGFP	-	
		L EGFP	48.39	-
	24h	E EGFP	-	
		L EGFP	51.10	-
S2683	30min	E EGFP	61.71	Yes (> 47%)
		L EGFP	5.23	No
	24h	E EGFP	7.49	No
		L EGFP	0.2	No
S2893	30min	E EGFP	-	
		L EGFP	0.27	No
	24h	E EGFP	-	
		L EGFP	28.00	-
S7102	30min	E EGFP	-	
		L EGFP	45.36	Yes (> 95%)
	24h	E EGFP	5.72	No
		L EGFP	5.31	No
S8007	30min	E EGFP	-	
		L EGFP	43.63	-
	24h	E EGFP	-	
		L EGFP	14.47	-
S8050	30min	E EGFP	-	
		L EGFP	0.16	-
	24h	E EGFP	-	
		L EGFP	42.00	-
S1107	30min	E EGFP	6.71	No
		L EGFP	57.83	Yes (> 67%)
	24h	E EGFP	-	
		L EGFP	0.61	No
S1147	30min	E EGFP	-	
		L EGFP	83.24	-
	24h	E EGFP	--	
		L EGFP	0.05	No
S1451	30min	E EGFP	-	
		L EGFP	25.67	-
	24h	E EGFP	-	
		L EGFP	2.62	No

Table 9 Summary of EC90 values for early and late inhibitors

4 Cell cycle assays

4.1 Cell cycle shift assays

Asynchronous HeLa FUCCI cells were infected with VACV, or a recombinant VACV strain (MOI 2). Samples were harvested at assay-dependent times post infection and prepared for flow cytometry as described in section 8. Using the flow cytometry analysis software InCyte (Merck Milipore), cells were gated according to their fluorescence as either no fluorescence, red only, red and green, or green only (outlined in Figure 3-7). The percentage of each cell fraction was displayed as the percentage of total cell counts.

4.2 Cell cycle synchronization assays

HeLa FUCCI cells were synchronized in G1 with Lovastatin as previously described (JavanMoghadam-Kamrani and Keyomarsi, 2008; Ma and Poon, 2011). Briefly, cells were synchronized with Lovastatin (20 µM) for 24h. Cells were washed twice before being either mock infected, or infected with WT VACV (MOI 2). To fully release the cells, the infection inoculum was replaced with medium supplemented with mevalonate (6 mM) and samples were harvested at 0, 8, and 24hpi. The cell cycle distribution was assessed by flow cytometry using the gating strategy outlined above (Figure 3-7).

For S phase arrest, cells were incubated with 2.5mM HU (Sigma Aldrich) for 16hrs. Then processed as described for Lovastatin, with the difference that the feeding medium did not contain mevalonate.

For G2 arrest, cells were incubated with 10µM RO3306 (Sigma Aldrich) for 16hrs. Then processed as described for Lovastatin, with the difference that the feeding medium did not contain mevalonate.

5 Cell proliferation assays

For all cell proliferation assays, cells were counted using the automatic cell counter Cellometer (Nexcelom) and seeded into 6 well plates in 1.5 ml growth medium per well. After incubated at standard conditions overnight, the samples were infected with an MOI 5 and harvested at assay-dependent times post infection. To harvest the samples, the medium was aspirated and cells were detached by incubation with 500 µl Trypsin/EDTA (2.5 g Trypsin/litre, 0.2 g EDTA/litre) for 5min at standard conditions. Trypsin activity was quenched with 500 µl 5% FBS in PBS and cells were fixed by adding 1 ml 4% PFA in PBS. To reduce clumping, the cell suspensions were briefly sonicated in a sonicator bath. Cell counts were determined by two individual measurements per sample using Cellometer (Nexcelom). To assess relative cell proliferation, all cell counts were normalized to the respective baseline at 0hpi.

The generation time *G* for each cell line was determined by measuring the cell number at t_0 (x(0)) and after a specific time interval Δt at t_{end} (x(end)). These values were then used in the following calculation:

$$G = \frac{\Delta t}{3.3 * \log(\frac{x(end)}{x(0)})}$$

5.1 EdC incorporation assay with WT and temperature sensitive VACV mutants

HeLa Kyoto H2B-mCh were seeded on 13mm glass coverslips. Cells were allowed to attach and grow overnight, then coverslips moved into 24 well dish. Samples were either mock infected, or infected with WR HA-D5 (MOI8) in 600 µl DMEM(-). After 1h, the inoculum was replaced with 600µl HeLa growth medium. 15 min before fixation, cells were fed with either 200 µl 4x concentration EdC (4x = 40 µM), or 200 µl 4x concentration EdU (4x = 40 µM). This diluted the EdC/EdU concentration to a final concentration of 10µM. Cells were fixed at 0.5 hpi, 1 hpi, 4 hpi, 5 hpi, 6 hpi, 8 hpi, 24 hpi by washing them once with PBS, and fixing with 4 % PFA at RT for 15min, followed by another 2 PBS washes and storage overnight at 4°C in the dark in PBS.

Fixed samples were stained for EdC / EdU incorporation using the Click-iT™ EdU Alexa Fluor™ 488 Imaging Kit (Invitrogen), according to manufacturer's instructions with minor changes (60 µl per coverslip, permeabilization with PBS 5% FBS, 0.1% Triton-X, washes with plain PBS). Coverslips were mounted with Immu-Mount (Thermo Scientific), and dried overnight in the dark at RT.

Images were acquired using a 100x oil immersion objective (NA 1.45) on a VT-iSIM microscope (Visitech; Nikon Eclipse TI), using 405nm, 488 nm, and 561 nm laser frequencies for excitation. Images were analysed using ImageJ, where nuclei were counted manually and either scored as red only, or EdC/EdU positive (i.e. green channel). A minimum of 5 different locations per coverslip were imaged (3x3 frames per tiled image) and a minimum of 450 nuclei were counted per sample. The ratio of S Phase nuclei to total nuclei was calculated per image with Excel, and the average ratio per sample was determined. The infection data are normalized against mock infected samples.

6 siRNA silencing

HeLa cells passaged at subconfluency were reverse transfected with Lipfectamine RNAiMAX (Invitrogen) according to the maunfacturer's protocol. Briefly, siRNA (stock 10μM) and RNAiMAX were individually diluted in DMEM(-). The two components were combined and incubated for 1hr at RT. 250'000 HeLa cells were counted for each well (6well dish) and added in full HeLa growth medium to the siRNA / RNAiMAX solution, diluting the siRNA to a final concentration of 20-40 nM, depending on the siRNA. The cells were grown in the incubator at standard conditions for 48hrs (viral gene), and 72hrs (cellular gene) prior to infection.

Target	Sequence 5'-3' (sense strand)	Conc.	Time	Modification	Reference
siATM	CUUAGCAGGAGGUGUAAAU	40 nM	72 h	[dT][dT]	Sigma Aldrich
siATR	CCUCCGUGAUGUUGCUUGA	40 nM	72 h	[dT][dT]	(Postigo et al., 2017)
allStar Negative	Proprietary Sigma Aldrich	40 nM	72 h	n.a.	Sigma Aldrich

Table 10 Cellular siRNA used in this study

Target	Sequence 5'-3' (sense strand)	Conc.	Time	Modification	Reference
siD5R	GAAACCAUGCGACAAUCAU	20 nM	48 h	[dT][dT]	(Kilcher et al., 2014)
siE9L	GUAUAAGGAUUAUAAUCUA	20 nM	48 h	[dT][dT]	(Kilcher et al., 2014)

siF10L	AACUGGUAUUACGAUUUCCAUU	20 nM	48 h	[dT][dT]	Unpublished
siA24R	CUGCUAAGCCGUACAACAA	20 nM	48 h	[dT][dT]	(Kilcher et al., 2014)
siB1R	GGUAUCUUGCCAUGGACUA	20 nM	48 h	[dT][dT]	(Kilcher et al., 2014)
allStar Negative	Proprietary Sigma Aldrich	20 nM	48 h	n.a.	Sigma Aldrich

Table 11 Viral siRNA used in this study

7 Protein overexpression

HeLa or BSC40 cells were seeded in 6 well dishes overnight at standard conditions. Cells were transfected with the lipofectamine 2000 and the indicated amount of plasmid DNA. Per well of a 6 well plate, a total of 500 µl DMEM(-) was mixed with 10 µl lipofectamine 2000 and between 0.5 -2 µg plasmid DNA. The reaction mixture was incubated for 5min at RT before being added to the cells. Samples were then incubated for 30 min under standard conditions and occasional rocking. Next, 1 ml of HeLa or BSC40 growth medium was added and cells were incubated for an assay-dependent time. Each overexpression experiment also contained a pMAX GFP expression vector control (Lonza).

8 Flow cytometry

8.1 Sample preparation

8.1.1 96 well plates

HeLa, HCT116, and HCT116 p53-/- infection assays were carried out as described. The following volumes are per well in a 96 well plate. Samples were washed once with 200 µl PBS and cells were detached with 80 µL trypsin/EDTA (0.25 % trypsin, 0.02 % EDTA). After incubation at 37°C for 10min, trypsin activity was quenched with 40 µl 5%FBS in PBS. To fix samples, 40 µl 4% PFA in PBS was added and incubated at RT for 10min. Samples were either directly analysed by flow cytometry or stored at 4°C in the dark (no longer than 1 day).

8.1.2 6 well plates

HeLa, and HeLa FUCCI infection assays were carried out as described. The following volumes are per well in a 6 well plate. Samples were washed once with 1 ml PBS and cells were detached with 500 µL trypsin/EDTA (0.25 % trypsin, 0.02 % EDTA). After incubation at 37°C for 5min, trypsin activity was quenched with 500 µl 5%FBS in PBS. To fix samples, 500 µl 4% PFA in PBS was added and incubated at RT for 10min. Samples were either directly analysed by flow cytometry or stored at 4°C in the dark (no longer than 1 day).

8.1.3 Propidium iodide staining for cell cycle analysis

Cells were stained with propidium iodide as described elsewhere (Darzynkiewicz et al., 2017). Briefly, cells were washed with PBS and detached with 500 µL trypsin/EDTA (0.25 % trypsin, 0.02 % EDTA). After incubation at 37°C for 5min, trypsin activity was quenched with 500 µl 5%FBS in PBS. Cells were collected by centrifugation at 300 g 4°C for 5 min. The supernatant was aspirated and cells were fixed with 0.5 ml 80% EtOH in ddH_2O. Dropwise addition of the fixative and vortexing was used to prevent clumping. Samples were stored on ice for 30 min before stored at -20 °C. Cells were washed twice with PBS, each time spinning at 850g for 5min at RT. In order to digest RNA, 50 µl of a 100 µg/ml RNAse (QIAGEN) stock solution was added, before staining with 200 µl PI (Sigma Aldrich) of a 50 µg/ml stock solution. To ensure complete staining, cells were left overnight at 4°C before being analysed by flow cytometry.

8.2 Flow cytometry acquisition and analysis

Infection levels were assessed by flow cytometry using GUAVA easyCyte HT (Merck Millipore, UK) according to manufacturer's manual. Acquired data were analysed using InCyte 3.1.1 (Merck Millipore, UK), Excel (Microsoft, USA), and Prism 7 (GraphPad, USA).

Samples stained with propidium iodide for cell cycle distribution analysis were analysed with a BD cytometer using the BS FACSDIVA software for acquisition and FlowJo for sample analysis.

9 Immunoblotting

9.1 Sample preparation

The medium was aspirated and samples were scraped in PBS. Cells were collected by centrifugation at 4°C 300g for 5min. The supernatant was removed and samples were resuspended in 45 µl lysis buffer with protease inhibitor (per well of a 6 well plate, or equivalent). Cell lysis was allowed to proceed for at least 30min on ice before samples were either frozen at -80°C for long-term storage, or before processing for immunoblotting. Thawed samples were centrifuged at 4°C, 20'000g for 10min to separate the protein lysate from cell debris. The supernatant was added to 15 µL of 4x loading dye with 4x DTT and the samples were boiled at 95°C for 5min. After cooling on ice, sonication for 5-15min was used to disrupt genomic DNA and prevent smearing.

9.2 Immunoblot analysis

Protein samples were loaded onto 4-12% Bis-Tris polyacrylamide gels and rand with MES SDS buffer (both Thermo Fisher Scientific) at 70V, 2.5-3.5 hrs. Proteins were transferred onto 0.2µM nitrocellulose membrane (Invitrogen) by wet transfer (Biorad) at 15V for 1hr with transfer buffer contain MeOH (NuPAGE buffer, Thermo Fisher Scientific). Membranes were blocked with 5% non-fat milk in TBS-T (Sigma Aldrich) for 1h before blotting. Primary antibodies were diluted in blocking solution at a concentration indicated in Table 4 and Table 5, and incubated overnight at 4°C on a rolling bed. Membranes were washed 3x in TBS-T before incubation with secondary antibodies which were diluted in blocking solution at a concentration indicated in Table 6. Membrane were incubated in secondary antibody for 2hrs at RT, then washed 3x in TBS-T and analysed. HRP-secondary antibodies were analysed with ImageQuant LAS 4000 Mini (GE Life Sciences) and Luminata Forte Western HRP Substrate (Merck) for detection. IRDye secondary antibodies were images with a LiCOR ImageQuant. Independent of the detection method, protein intensities were quantified using the software StudioLite (LiCOR). Where applicable, samples were normalized against an internal α-Tubulin loading control.

3 VACV arrests the host cell cycle

1 VACV infection arrests the host cell cycle

The cell cycle describes the tightly regulated succession of cell growth and division. Dysregulation of any of these steps can cause hyperproliferation (cancer), or arrest the cell cycle and induce apoptosis. Many viruses have been shown to alter the host cell cycle by either promoting cell cycle entry (oncogenic viruses such as HPV (Banerjee et al., 2011), HTLV-1 (Iwanaga et al., 2008) , EBV (Knight and Robertson, 2004), SV40 (Lehman et al., 2000), and KSHV (Moore and Chang, 1998)), or arresting cell proliferation (e.g. HIV-1 (Zimmerman et al., 2006), and IBV (Dove et al., 2006)). VACV was shown to inhibit cell proliferation of mouse fibroblasts (Kit and Dubbs, 1962), as well as cellular DNA and protein synthesis in HeLa cells (Jungwirth and Launer, 1968). Conversely, a pro-proliferative effect was reported for VACV infected 143B osteosarcoma cells (Yoo et al., 2008).

In addition to these conflicting results, mechanistic insights remained inaccessible due to experimental limitations. First, viral DNA was not readily distinguishable from cellular DNA given that classical studies indirectly determined cellular DNA synthesis rates by pulsed radiolabelling with ^{14}C-thymidine. Since VACV is a dsDNA virus, ^{14}C-thymidine is also incorporated into replicating viral genomes. Differentiation of the two DNA species required physico-chemical separation of the nuclear (cellular) from the cytosolic (viral) DNA fraction (Jungwirth and Dawid, 1967). Second, initial experiments aimed at studying the minimal viral requirement to block the cell cycle relied on UV or heat inactivated VACV (Jungwirth and Launer, 1968). These inactivation methods result in a poorly defined and highly variable inhibition of the virus life cycle (Tsung et al., 1996).

For this chapter, I aimed to characterize VACV induced changes in host cell cycle progression, to measure the kinetics of these changes, and to define which virus life cycle stage is essential to induce the changes. To address these questions, I monitored proliferation of WT infected HeLa and BSC40 cells. Additionally, I developed a radioactive-free, microscopy-based assay to specifically measure cellular DNA synthesis in infected cells. To define which step of the VACV life cycle altered host cell cycle progression, I combined well-characterized temperature sensitive VACV mutants and RNAi for targeted depletion of viral proteins. Together, this combination of classical assays and novel techniques show that VACV early gene expression rapidly blocks host cell proliferation and cellular DNA synthesis.

1.1 VACV infection inhibits host cell proliferation in BSC40, and HeLa cells

Cell numbers double with every round of mitotic cell division, dividing one mother cell into two daughter cells. Cell proliferation describes the overall change in cell numbers and depends on the opposing effects of cell division and cell death. To characterize the effect of VACV (strain WR) infection on cell proliferation, BSC40 cells were either mock infected, or infected with WT VACV (MOI 5). Cells were harvested and counted at 0, 12, 24, and 48hpi (Figure 3-1, A). Mock infected cells divide approximately once every 18h, whereas infected cells fail to proliferate. Compared to baseline cell numbers at 0hpi, mock controls tripled by 48hpi (3.1 ± 0.4 fold) whereas WT infected samples remained unchanged (1.0 ± 0.1 fold). Comparable results were obtained for HeLa, and HCT116 cells (please refer to chapter 5 of this thesis).

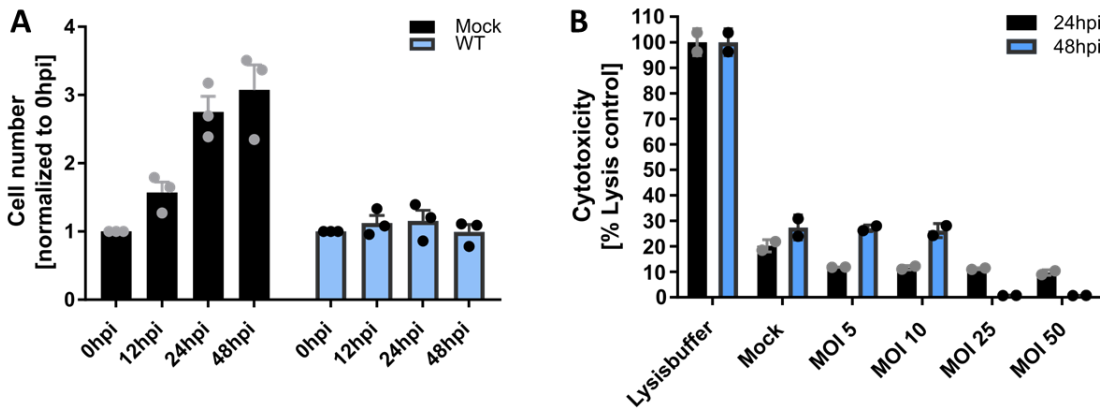

Figure 3-1 VACV infection inhibits host cell proliferation.

[A] Relative increase in cell numbers in mock an VACV WT infected BSC40 cells. Unsynchronized BSC40 cells were mock infected, or infected with WT VACV (MOI 5) and automatically counted at 0, 12, 24, and 48hpi. Cell counts were normalized to 0hpi. Data represent three biological replicates with two technical replicates each and are displayed as mean ± S.E.M. [B] Percentage of apoptotic cells, measured by Pierce LDH Cytotoxicity assay. BSC40 cells were infected with either mock, or WT VACV (MOI 5, 10, 25 and 50). Cytotoxicity was measured with the LDH Cytotoxicity assay at 24, and 48 hpi. Background (680nm) corrected absorbance at 490nm for each sample was normalized to a lysis buffer positive control. Data represent one biological replicate with two technical replicates each and are displayed as mean ± S.D.

Reduced cell proliferation rates can result from decreased cell division and/or increased cell death. To determine the contribution of cell death to inhibiting proliferation in infected samples, the cytotoxicity of different MOIs was measured by lactate dehydrogenase (LDH) assay at 24, and 48 hpi (Figure 3-1, B). This assay measures the extracellular LDH enzyme concentration as a biomarker for membrane integrity which is compromised in apoptotic cells. Complete cell lysis was used as a positive control. The baseline LDH activity in mock infected

samples was measured to be 20.2 ± 2.4 % (24hpi), and 27.4 ± 4.9 % (48hpi) of the cell lysis control, respectively. Similarly, VACV infected samples (MOI 5) showed 11.8 ± 0.1 % (24hpi), and 27.1 ± 1.3 % (48hpi) LDH activity, respectively. Furthermore, even at an MOI 50 VACV did not cause more than 10% cell death, neither at 24, nor 48 hpi. This shows that VACV infection causes only low levels of apoptosis which cannot explain the observed block in cell proliferation. Therefore, this data indicates that VACV inhibits proliferation by arresting the host cell cycle, and not by increasing cell death.

1.2 VACV infection blocks cellular DNA replication

1.2.1 Establishing a protocol to measure cellular DNA synthesis during VACV infection

In the previous section I showed that VACV inhibits cell proliferation over 48hpi. Next, I aimed to develop a protocol to measure the kinetics of the VACV-induced block with better time resolution. As the doubling time for BSC40 cells is approx. 18h, the desired resolution cannot be achieved with cell proliferation as a readout. Focusing instead on progression through a single cell cycle stage allows for increased time resolution. A previous study assessed the mitotic index of VACV infected cell populations and found that VACV reduces the number of mitotic cells from 3hpi onwards (Kit and Dubbs, 1962). However, since mitosis is a very rapid process less than 10% of asynchronous cells are mitotic at any given time. Therefore, measuring the mitotic index results in a limited dynamic range. On the other hand, approx. 20-40% of uninfected cells are in S phase which allows for a broader dynamic range. Additionally, S phase cells are actively synthesising DNA and are therefore readily identified by pulse-labelling with nucleotide analogues such as BrdU and EdU (Ma and Poon, 2011). Incorporated analogues can be visualized by antibody labelling or covalent linking to a fluorophore (“Click chemistry”). The amount of S phase cells (labelling index) can then be determined by microscopy, or flow cytometry (Alberts et al., 2002).

Nucleotide analogues are incorporated both into newly synthesised cellular and viral DNA which leads to two technical challenges. First, EdU inhibits production of infectious VACV particles at 10µM, which is the concentration required for incorporation into cellular DNA (Wang et al., 2013). Second, an additional marker is required to distinguish viral from cellular DNA synthesis.

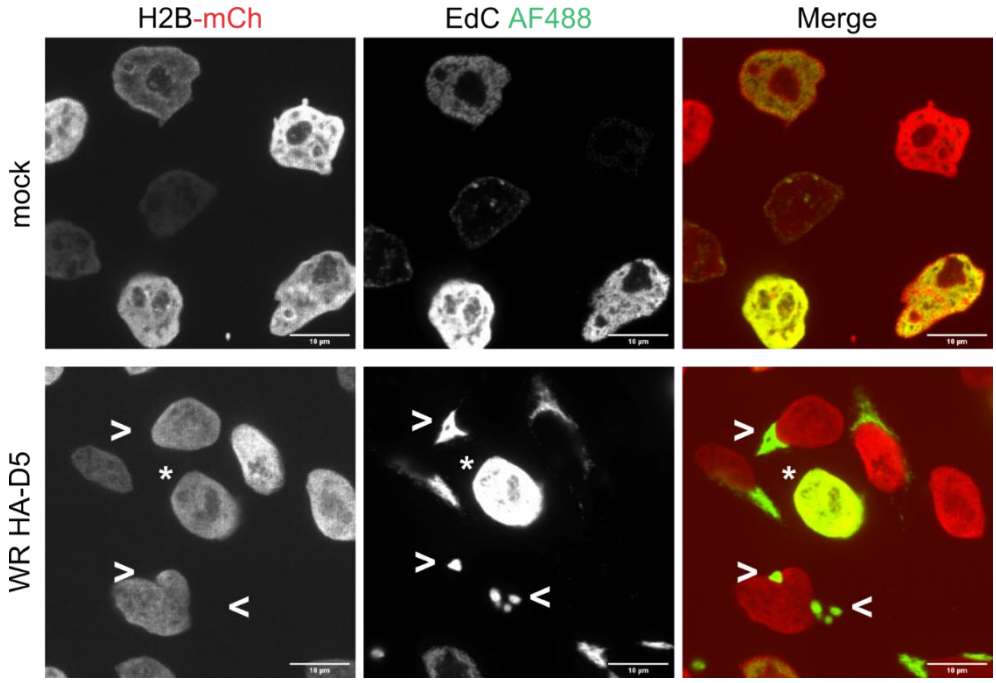

Figure 3-2 The nucleotide analogue EdC is incorporated into cellular and viral DNA.

HeLa Kyoto H2B-mCh were either mock infected, or infected with WR HA-D5 (MOI 2) in the presence of the nucleotide analogue EdC (10µM). Samples were fixed in 4% PFA at 8hpi and incorporated EdC was visualized via covalent conjugation with AlexaFluor 488. EdC was incorporated in newly synthesized viral (**>**) and cellular (*) DNA. Representative images of mock and WR HA-D5 infected samples 8hpi. Scale bar represents 10 µm.

To replace EdU, I searched for an alternative nucleotide analogue that is readily incorporated into cellular DNA, permissive for VACV infection, and compatible with Click chemistry. EdC used at 10 µM fulfils these three requirements: it was previously shown not to affect VACV infectivity (Wang et al., 2013), and I detected incorporated EdC in cellular and viral DNA using Click chemistry (Figure 3-2). Since spatial information is essential to score EdC positive DNA as viral or cellular I analysed samples by confocal microscopy. To distinguish between foci of viral and cellular DNA synthesis, I exploited the distinct subcellular localization of the two DNA species. Viral DNA is exclusively cytoplasmic whereas cellular DNA is nuclear. To detect the cell nucleus, I used a HeLa Kyoto cell line that exogenously expresses an mCherry tagged version of the histone H2B (H2B-mCh) (kindly provided by Dr. Murielle Serres). Additionally, to label the viral DNA, I used a recombinant virus expressing an HA-tagged version of the viral AAA+ ATPase D5 (WR HA-D5) which was shown to localize to sites of viral DNA replication (Kilcher et al., 2014). This system allowed me to detect DNA synthesis in infected cells and distinguish cellular DNA replication from viral DNA replication.

1.2.2 VACV infection inhibits cellular DNA synthesis

Having established a protocol to monitor cellular DNA synthesis in VACV infected cells (Figure 3-2) , I set out to use this assay to characterize the kinetics of the VACV-induced cell cycle arrest during a timecourse of infection (workflow outlined in Figure 3-3, A). HeLa Kyoto H2B-mCh cells were grown on coverslips and either mock infected, or infected with the recombinant virus WR HA-D5 (MOI 8). Cells were pulse-labelled with the nucleotide analogue EdC (10µM) for 15min prior to fixation at 0.5, 1, 2, 4, 5, 6, 8, and 24hpi. Incorporated EdC was visualized by covalent conjugation to AlexaFluor 488. Tiled overview images were acquired by confocal, optical superresolution microscopy (iSIM) (Figure 3-3, B) . Per sample a minimum of 300 nuclei was counted manually and either scored as EdC positive (S phase cells), or EdC negative (non-S phase cells). The percentage of S phase cells was calculated for mock and infected samples (Figure 3-3, C). To account for fluctuations in cell cycle progression due to sample manipulation, the percentage of S phase cells in infected samples was further normalized to their respective mock control (Figure 3-3, D). While the fraction of S phase cells in mock controls only moderately fluctuated, it decreased rapidly in infected samples. With the onset of viral early gene expression around 2hpi, the amount of S phase cells dropped to 50 % of control levels at 4hpi, and was further reduced to 15% at 8hpi. By 24hpi there was no more cellular DNA synthesis detectable in infected samples. This indicates that VACV infection causes a profound block of cellular DNA synthesis, starting at 2hpi and culminating in a full block by 24hpi.

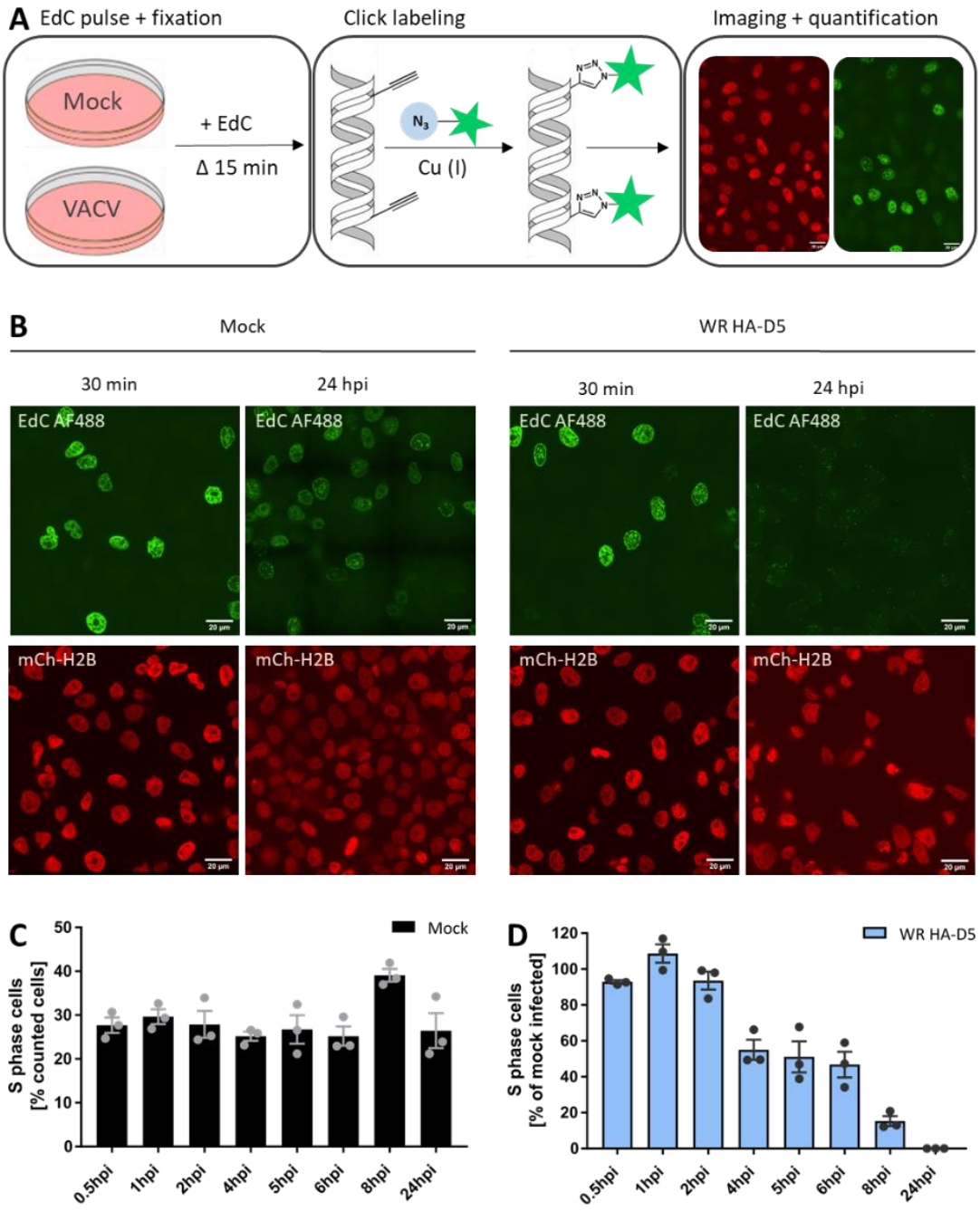

Figure 3-3 VACV infection inhibits host cell DNA replication.

[A] Experimental set-up: HeLa H2B-mCh were either mock infected, or infected with WR HA-D5 (MOI 8). Cells were pulse-labelled with the nucleotide analogue EdC (10µM) for 15min prior to fixation at 0.5, 1, 2, 4, 5, 6, 8, and 24hpi. Incorporated EdC was covalently conjugated to AlexaFluor488 and tiled overview microscopy images were acquired. A minimum of 300 nuclei was counted per sample and scored as EdC positive (S phase) or negative (non S phase). **[B]** Representative images of mock and WR HA-D5 infected samples at 30min and 24 hpi. Scale bar represents 20 µm. **[C]** The percentage of S phase (i.e. EdC positive) cells in mock infected samples. **[D]** Bars represent the percentage of S phase cell in infected samples over time, normalized to the respective mock control. **[C-D]** Data represent three biological replicates and are displayed as mean ± S.E.M.

2 VACV causes a systemic cell cycle arrest

The experiments described above show that VACV inhibits cell cycle progression but do not specify in which cell cycle stage the block occurs. From this assay it cannot be differentiated whether VACV induces a systemic block that freezes cells in their current cell cycle stage; or whether infection establishes a specific block by allowing cells to progress to, but not beyond, a specific cell cycle stage (Figure 3-4). To address this question, I aimed to establish a reliable method to monitor the cell cycle stages in infected cells and to develop an assay that would allow me to distinguish between a systemic and a specific viral block.

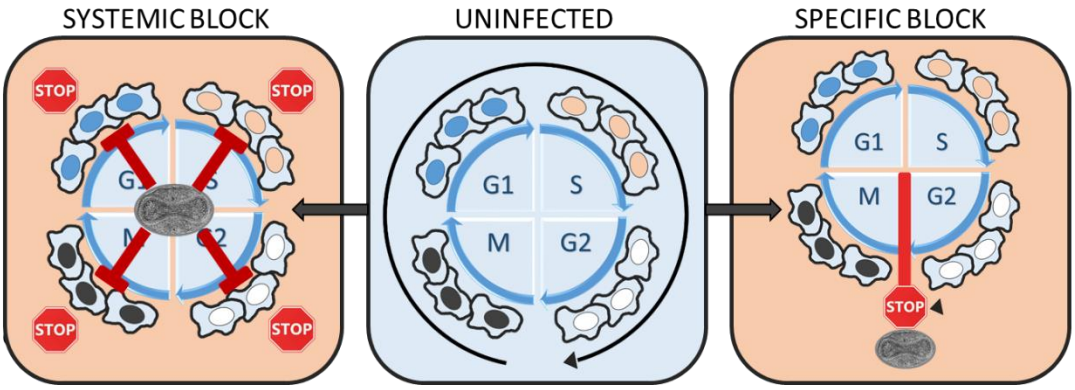

Figure 3-4 model for two different VACV-induced cell cycle blocks.

VACV infection inhibits cell cycle progression through an undefined mechanism. Infection could either establish a systemic block that arrests cell independently of their cell cycle stage; or cause a specific block in a distinct phase of the cell cycle.

2.1 A method to analyse cell cycle distribution in VACV infected cells

Cell cycle analysis methods can be grouped into two categories: methods that are based on monitoring cellular DNA (content and/or morphology), and methods that rely on a protein marker. These methods can either be used individually, or in combination to allow for more in-depth characterization of cell cycle changes (Darzynkiewicz et al., 1996; Pozarowski and Darzynkiewicz, 2004).

Analysis of cellular DNA morphology allows to determine the fraction of mitotic cells by microscopy (mitotic index). M phase cells are characterized by condensed chromosomes, which are distinct from the relaxed chromatin in interphase cells (G1, S, G2) (Figure 3-5, A). Non-mitotic cells can be further separated into individual G1, S, and G2/M fractions by flow

cytometric analysis of the cellular DNA content (Dilla et al., 1969, 1975). As cells progress from G1 to G2, new DNA is synthesised in S phase and the amount of cellular DNA doubles. DNA quantification with a stoichiometric DNA-binding dye allows to classify cells as diploid (G1), tetraploid (G2/M), or an intermediate state (S phase) based on their fluorescence intensity (Figure 3-5, B).

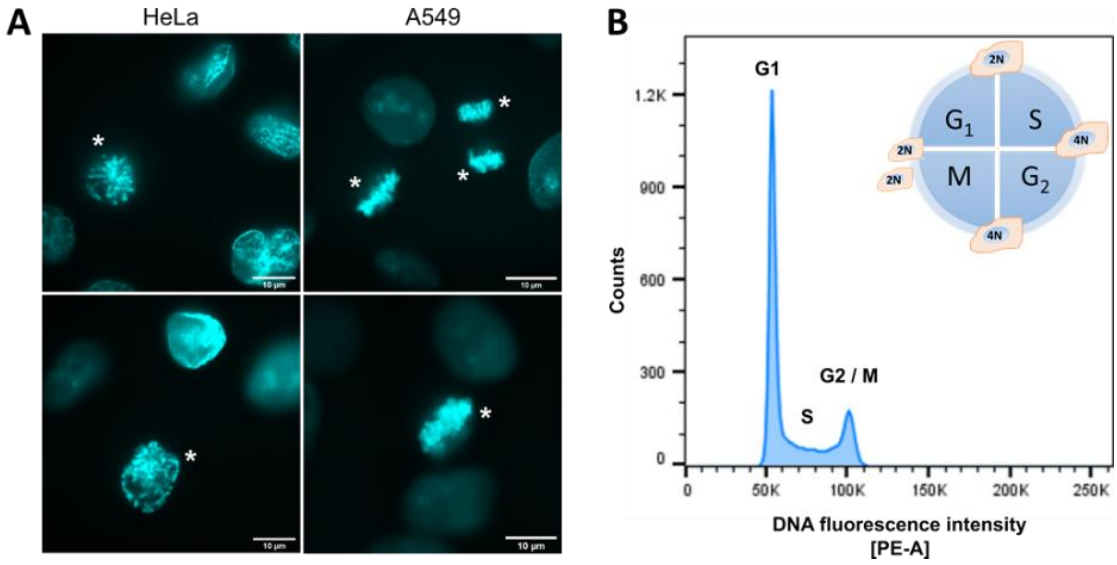

Figure 3-5 DNA-based cell cycle analysis methods.

[A] Microscopy images of fixed, uninfected HeLa and A549 cells. Cellular DNA was visualized with the DNA stain Hoechst. Condensed chromatin is a marker for mitotic cells (*). Scale bar represents 10 µm. [B] DNA content distribution of fixed, uninfected HeLa cells. Nuclear DNA was stained with the stoichiometric dye propidium iodide (PI) and quantified by flow cytometry. The fluorescence intensity is proportional to the total DNA mass and separates the diploid G1 cells from the tetraploid G2/M cells. S phase cells are actively synthesising DNA and lie between the G1 and G2/M peaks.

2.1.1 VACV genome replication distorts DNA-based cell cycle analysis methods

First, I set out to establish a method to evaluate and quantify cellular DNA content by flow cytomtery in order to perform cell cycle analysis of VACV infected cells. Analysis of the cell cycle distribution by measuring whole cell DNA content relies on stoichiometric DNA staining. VACV infection results in the production of viral DNA which is also stained by nuclear DNA stains such as propidium iodide and Hoechst. To test whether accumulating viral DNA contributes to the DNA content seen in the flow cytometry analysis, I monitored the shift upon inhibition of viral genome replication. siRNAs targeting either the viral AAA+ ATPase D5 (siD5R), or the viral DNA-dependent DNA polymerase E9 (siE9L) were used to knock down the

respective proteins. Loss of the uncoating factor D5 inhibits core degradation (Kilcher et al., 2014) whereas deletion of E9 prevents replication of the released viral genome. HeLa cells were reverse transfected with scrambled control siRNA (Scr), siD5R, or siE9L. After 48h, cells were either mock infected, or infected with WT VACV (MOI 1). Samples were harvested at 0, 8, and 24hpi and the DNA content was analysed by flow cytometry and plotted as frequency histograms (Figure 3-6, A). Knockdown of D5 and E9 was indirectly confirmed by immunoblot analysis of the viral early protein I3, and the late viral protein F17 (Figure 3-6, B). While viral early genes are expressed prior to genome release, late viral gene transcription requires replication of the released genome (Oda and Joklik, 1967). Expression of I3 was observed in all samples, whereas F17 expression was undetectable after siD5R knockdown, and was profoundly reduced upon siE9L RNAi. This indicates effective knockdown of D5 and E9, respectively, and that viral genome replication was successfully inhibited.

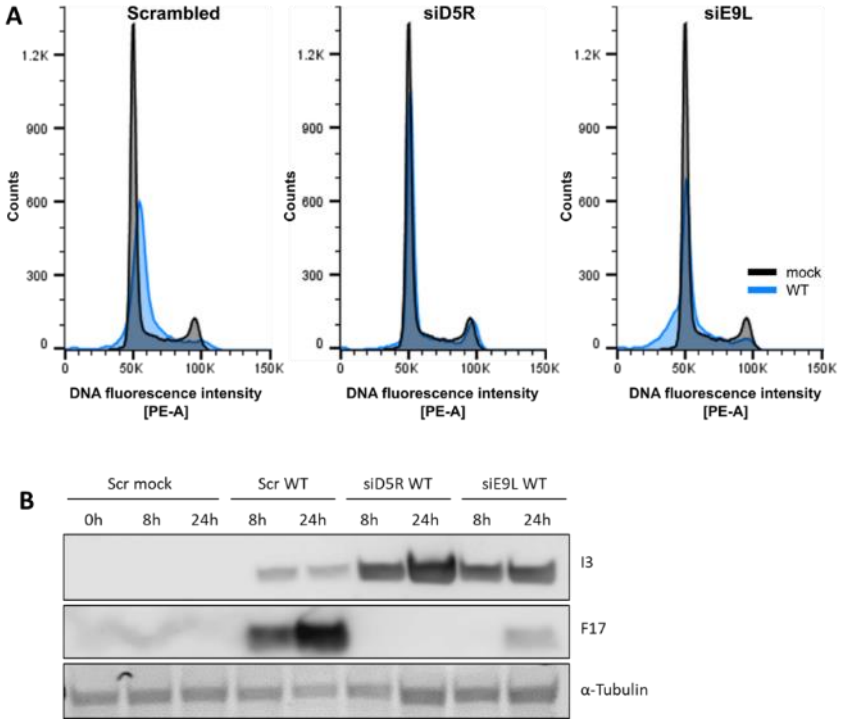

Figure 3-6 The effect of WT VACV genome replication on whole cell DNA content.

HeLa cells were reverse transfected with either scrambled control siRNA (Scr), or siD5R targeting the viral uncoating factor D5, or siE9L targeting the viral DNA polymerase. After 48h, cells were either mock infected, or infected with WT VACV (MOI 1) and samples were harvested at 0, 8, and 24hpi. [A] The whole cell DNA content was stained with PI and analysed by flow cytometry. The plots represent DNA content histograms of mock (grey) or WT infected (blue) cells treated with either scrambled siRNA, siD5R, or siE9L at 24hpi. [B] Whole cell lysates were resolved via SDS-PAGE and immunoblotted for the viral early protein I3, the viral late protein F17, and α-tubulin as a loading control. The blot represents the viral gene expression profile of mock or WT infected samples, treated with either scrambled siRNA, siD5R, or siE9L at 8 and 24hpi.

2.1.2 The FUCCI system for cell cycle analysis of VACV infected cells

Cell cycle progression is coordinated by temporally controlled expression and degradation of numerous regulatory proteins. Additionally, key enzyme activities are fine-tuned by an intricate network of feedback loops, including the reciprocal inhibition of the E3 ligase complexes APC^{Cdh1} and SCF^{Skp2} (Benmaamar and Pagano, 2005; Wei et al., 2004). Due to the complexes' antiphasic oscillation, their respective activity is restricted to distinct phases of the cell cycle: while APC^{Cdh1} ubiquitinates its substrates in late M and G1, SCF^{Skp2} functions in S and G2 (Vodermaier, 2004). The cellular DNA replication regulators Geminin and Cdt1 are targeted for degradation by APC^{Cdh1} and SCF^{Skp2}, respectively (Figure 3-7, A) . Ubiquitination by APC^{Cdh1} during late M phase ensures that Geminin is only expressed and active outside of G1 (McGarry and Kirschner, 1998). Inversely, SCF^{Skp2}- mediated ubiquitination restricts Cdt1 activity and expression to G1 and early S phase (Nishitani et al., 2004, 2006).

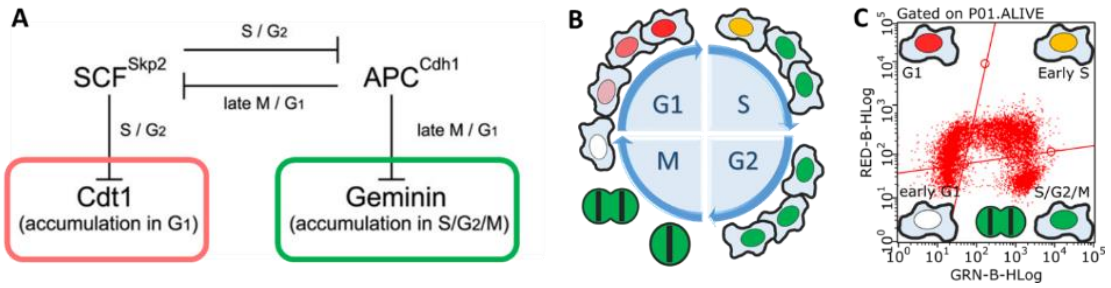

Figure 3-7 The HeLa FUCCI system for cell cycle analysis.

The HeLa FUCCI cell line stably expresses fluorescently tagged fragments of human Geminin (mAG-hGem(1-100), green) and Cdt1 (mKO2-hCdt1(30-120), red). Due to the antiphasic expression of the fragments, the relative abundance marks distinct phases of the cell cycle. [A] Simplified regulation of the cellular proteins Cdt1 and Geminin during different stages of the cell cycle. Adapted from (Sakaue-Sawano et al., 2008). [B] Cell cycle stage-dependent changes in fluorescence of the HeLa FUCCI cell line. [C] Schematic flow cytometry fluorescence plot indicating the gating strategy used to group cells as either early G1 (no fluorescence), G1 (red), early S (green + red =yellow), and S/G2/M (green).

Making use of the antiphasic expression of Geminin and Cdt1, Sakaue-Sawano and colleagues developed the fluorescence, ubiquitination-based cell cycle indicator (FUCCI) system that allows for realtime analysis of cell cycle progression (Sakaue-Sawano et al., 2008). Briefly, they generated a stable HeLa S cell line (HeLa FUCCI) that exogenously expresses fluorescently tagged fragments of human Geminin (mAG-hGem(1-100), green) and Cdt1 (mKO2-hCdt1(30-120), red). As cells progress through G1 they accumulate Cdt1 which is marked by increasing red fluorescence. While Cdt1 levels fall again with the onset of S phase, Geminin levels start to rise which causes cells to appear orange (green and red fluorescence). Towards the end of S phase, only the green fluorescence of Geminin is detectable, which persists throughout G2

before being degraded at the end of M phase (Figure 3-7, B). Concluding, the FUCCI system distinguishes 4 different cell cycle phases based on fluorescence: early G1 (colourless), G1 (red), early S (orange), S / G2 / M (green) (Figure 3-7, C).

In order to be used as a tool to monitor cell cycle stages in infected cells, HeLa FUCCI cells need to be permissive for VACV infection. Therefore, I compared the expression profile of viral early and late genes in HeLa and HeLa FUCCI cells. The cells were infected with WT VACV (MOI 1), and samples were harvested at 0, 2, 4, 5, 6, 8, 10, and 24hpi. Whole cell lysates were resolved by SDS-PAGE and immunoblotted for the viral early protein I3, and the viral late protein F17 (Figure 3-8). With a slight delay of 2hrs, HeLa FUCCI cells expressed comparable amounts of I3 and F17 as HeLa cell. Concluding, HeLa FUCCI cells are permissive for VACV infection.

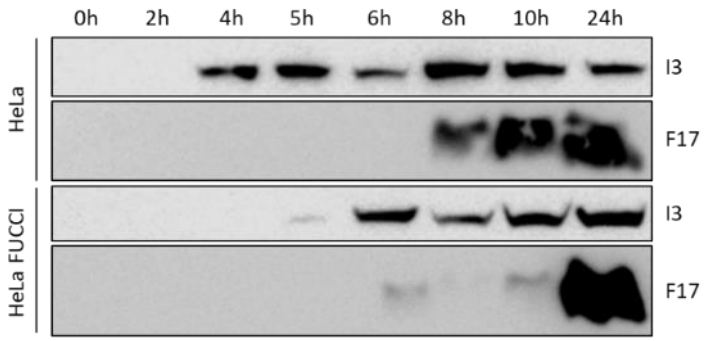

Figure 3-8 Viral gene expression profile in HeLa and HeLa FUCCI cells.

HeLa and HeLa FUCCI cells, respectively, were infected with WT VACV (MOI 1), and samples were harvested at 0, 2, 4, 5, 6, 8, 10, and 24hpi. Whole cell lysates were resolved by SDS-PAGE and immunoblotted for the viral early protein I3, and the viral late protein F17.

Since VACV has been shown to repress host protein synthesis, I assessed whether the FUCCI reporter proteins continued to be expressed in VACV infected cells (Kit and Dubbs, 1962). Unsynchronized HeLa FUCCI were either mock infected, or infected with WT VACV (MOI 2) and samples were harvested at 0, 2, 4, 6, 8, 10, 12, and 24hpi. To compare the expression levels of the mKO2-hCdt1 and mAG-hGeminin reporter constructs, the mean fluorescence intensity (MFI) was measured by flow cytometry for the red (Cdt1) and green (Geminin) channel (Figure 3-9). While expression levels of both constructs were found to fluctuate, they were comparable in mock and WT infected cells. I therefore concluded that VACV infection does not prevent expression of the FUCCI reporter constructs.

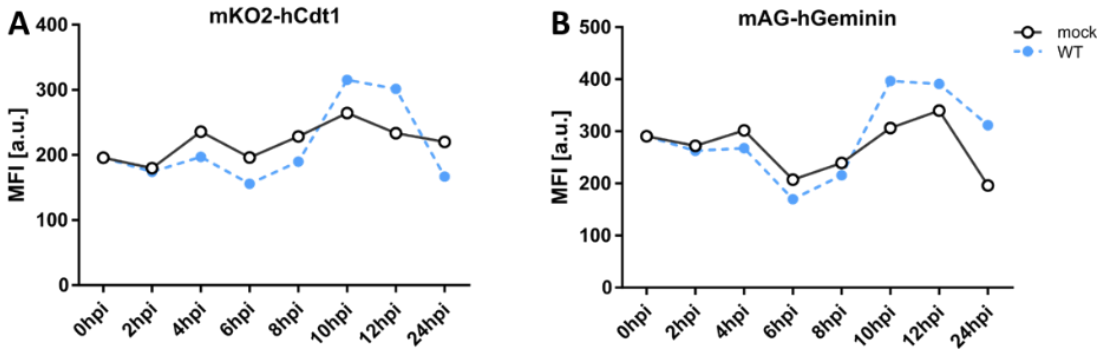

Figure 3-9 Mean fluorescence intensity of the FUCCI reporter constructs mKO2-Cdt1 and mAG-Geminin in mock and WT infected samples.

Unsynchronized HeLa FUCCI were either mock infected, or infected with WT VACV (MOI 2) and samples were harvested at 0, 2, 4, 6, 8, 10, 12, and 24hpi. To compare the expression levels of the mKO2-hCdt1 and mAG-hGeminin reporter constructs, the mean fluorescence intensity (MFI) was measured by flow cytometry.

2.2 VACV induced cell cycle arrest in G1, S, and G2 synchronized cells

Having established the tools to analyse cell cycle changes in infected cells, I next focused on gaining more mechanistic insight into the VACV induced block.

In section 1 of this chapter, I showed that VACV infection inhibits cellular DNA synthesis and cell proliferation. However, these assays do not specify where the cell cycle is halted: measuring DNA synthesis by EdC incorporation cannot distinguish between a block in S phase progression, and reduced S phase entry because the cells are locked in another cell cycle stage. Therefore, I next investigated if VACV could arrest cells in any given cell cycle stage.

To address this question, I infected pre-synchronized cells and monitored the cell cycle distribution over time. Once released, uninfected cells re-enter the cell cycle as a synchronous population that reverts to asynchrony after a few rounds of division. Infected cell populations were anticipated to be either retained in the pre-synchronized cell cycle stage, or to re-enter the cell cycle and get stopped in a distinct cell cycle stage (Figure 3-10). Pre-synchronizing cells in different phases of the cell cycle (e.g. G1 and G2) allows to distinguish between a systemic and a specific VACV induced cell cycle block. While a systemic block predicts VACV to freeze cells in any given pre-synchronized cell cycle stage, a specific block forecasts VACV to trap cells only in one specific stage.

In the following, HeLa FUCCI cells were synchronized in either G1, S, or G2, released and simultaneously infected with WT VACV. The cell cycle distribution was then assessed at 8, and 24hpi.

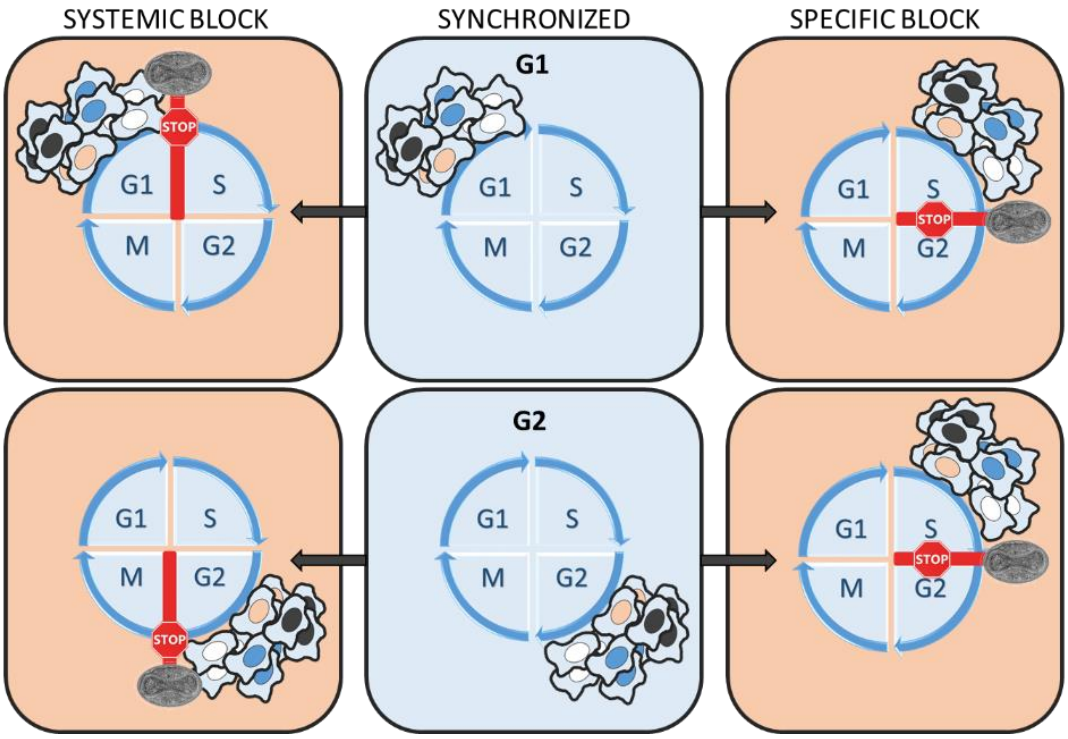

Figure 3-10 Experimental design to distinguish between a systemic and a specific virus-induced block.

To test whether VACV systemically inhibits the cell cycle, or whether it blocks progression at a specific stage, synchronized cells (blue panels) were released and immediately infected. At 24hpi, the cell cycle distribution was expected to show one of two patterns: infected cells fail to re-enter the cell cycle, independent of their pre-synchronized state (systemic block). Second, dependent on the pre-synchronized stage, infected cells re-enter the cell cycle and accumulate in a distinct phase (specific block).

2.2.1 VACV blocks S phase entry of G1 synchronized cells

The HMG-CoA reductase inhibitor Lovastatin (Mevinolin) mediates a G1 arrest by inhibiting the proteasome (Rao et al., 1999) which causes accumulation of the CDK2 inhibitors p21 and/or p27 (Gray-Bablin et al., 1997). Addition of mevalonate releases synchronized cells from G1 by re-stimulating proteasome activity (Rao et al., 1999).

To test whether VACV can block cells in G1, HeLa FUCCI cells were synchronized in G1 with Lovastatin as previously described (JavanMoghadam-Kamrani and Keyomarsi, 2008; Ma and Poon, 2011). Briefly, cells were synchronized with Lovastatin (20 µM) for 24h. Cells were washed twice before being either mock infected, or infected with WT VACV (MOI 2). To fully

release the cells, the infection inoculum was replaced with medium supplemented with mevalonate (6 mM) and samples were harvested at 0, 8, and 24hpi. The cell cycle distribution was assessed by flow cytometry using the gating strategy outlined above (Figure 3-7).

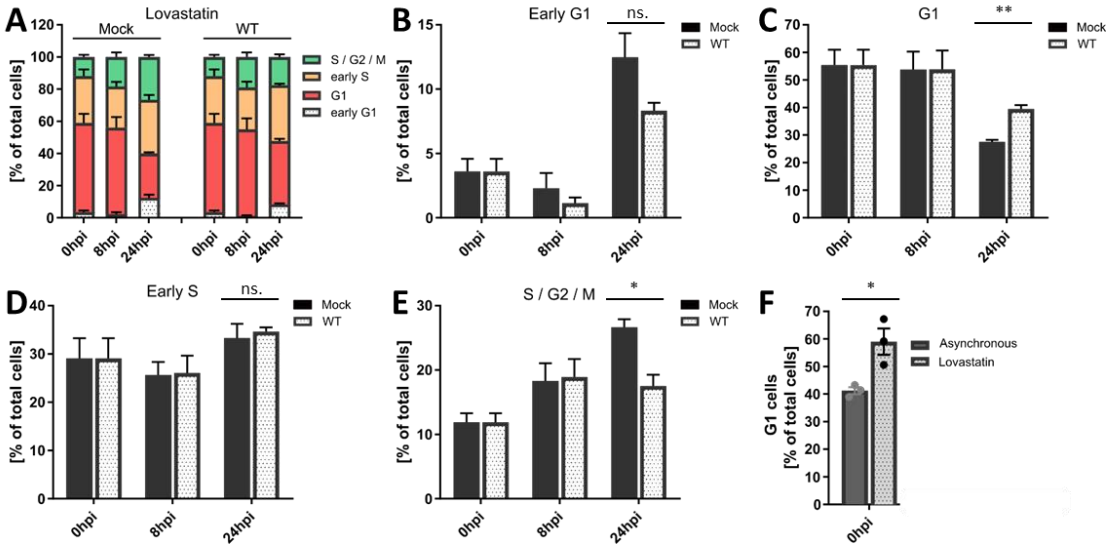

Figure 3-11 VACV infection arrests Lovastatin synchronized cells in G1.

HeLa FUCCI cells were synchronized in G1 with Lovastatin (20 µM) for 24h. Released cells were immediately infected with WT VACV (MOI 2) and harvested at 0, 8, and 24hpi. Using flow cytometry, cells were classified as early G1, G1, early S, or S / G2 / M. [A] Combined cell cycle stage distribution of mock infected and WT VACV infected samples. Individual cell cycle fractions are compared in [B-E]. [B] Percentage of early G1, [C] G1, [D] early S, and [E] S / G2 / M cell fractions in mock and WT VACV infected samples. [F] Synchronization effectiveness: the total G1 fraction in asynchronous and Lovastatin synchronized cell populations. Data represent three biological replicates with one technical replicate each and are displayed as mean ± S.E.M. Parametric, unpaired, two-tailed t-test for significance. ns. $p > 0.05$, * $p < 0.033$, ** $p < 0.0021$, *** $p < 0.0002$, **** $p < 0.0001$

Synchronization with Lovastatin significantly enriched cells in the G1 cell cycle phase from 41.2 ± 1.3% to 59.1 ± 4.7% (Figure 3-11, F). 8h after release, mock infected cells showed a 1.54-fold increase in the S/G2/M fraction compared to 0hpi, which occurred the expense of G1 and early S phase cells (Figure 3-11, E). The cell cycle distribution of WT VACV infected samples followed the same trend. 24h after release, the G1 fraction of mock infected samples was reduced to 27.6 ± 0.7% of the total cell population (Figure 3-11, C), while the S/G2/M fraction further rose to 26.6 ± 1.3% of the total cell population (Figure 3-11, E). On the contrary, only 17.5 ± 1.7% of WT infected cells were observed in the S/G2/M fraction while the G1 fraction was decreased just 1.15-fold to 47.8 ± 1.1%. Thus, while mock treated cells were found to re-enter the cell cycle, VACV infection significantly blocked progression from G1 into S/G2/M phase at 24hpi.

2.2.2 VACV blocks M phase entry of S phase synchronized cells

The small molecule drug hydroxyurea (HU) blocks (cellular) DNA synthesis which reversibly arrests cells in early S phase (Bacchetti and Whitmore, 1969; Fallon and Cox, 1979). HU acts by inhibiting the enzyme ribonucleotide reductase (RNR) which is required for synthesis of deoxyribonucleotides as precursors for DNA synthesis (Krakoff et al., 1968; Young and Hodas, 1964).

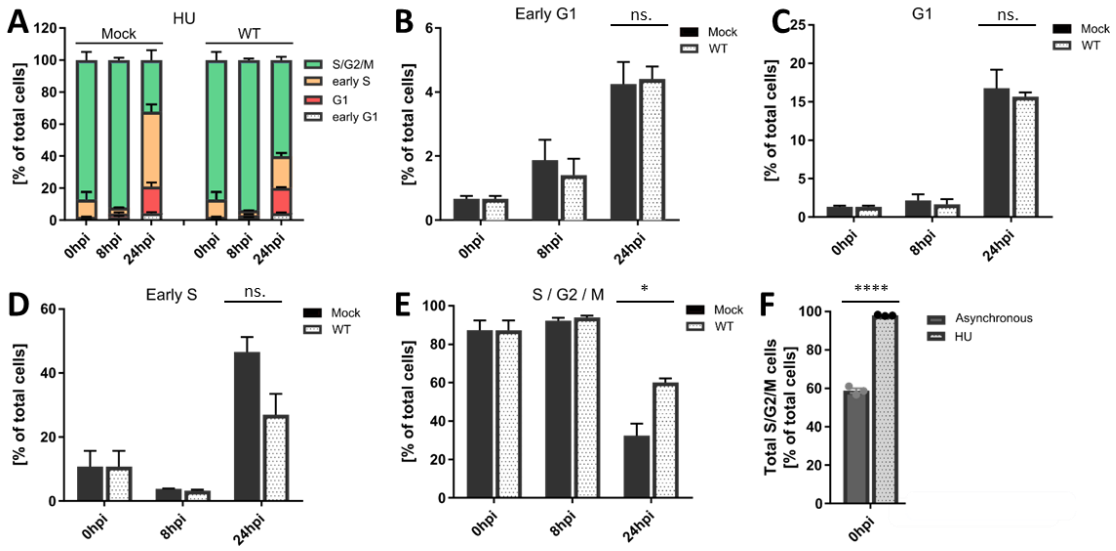

Figure 3-12 VACV infection arrests Hydroxyurea (HU) synchronized cells in S / G2 / M.

HeLa FUCCI cells were synchronized in S phase with HU (2.5 mM) o.n. Released cells were immediately infected with WT VACV (MOI 2) and harvested at 0, 8, and 24hpi. Using flow cytometry, cells were classified as early G1, G1, early S, or S / G2 / M. [A] Combined cell cycle stage distribution of mock infected and WT VACV infected samples. Individual cell cycle fractions are compared in [B-E]. [B] Percentage of early G1, [C] G1, [D] early S, and [E] S / G2 / M cell fractions in mock and WT VACV infected samples. [F] Synchronization effectiveness: the total S/G2/M fraction in asynchronous and HU synchronized cell populations. Data represent three biological replicates with one technical replicate each and are displayed as mean ± S.E.M. Parametric, unpaired, two-tailed t-test for significance. ns. $p > 0.05$, * $p < 0.033$, ** $p < 0.0021$, *** $p < 0.0002$, **** $p < 0.0001$

To test whether VACV can retain cells in S phase, HeLa FUCCI cells were synchronized with HU (2.5 mM) overnight. Cells were released and immediately either mock infected, or infected with WT VACV (MOI 2). Samples were harvested at 0, 8, and 24hpi and the cell cycle distribution was assessed by flow cytometry using the gating strategy outlined above (Figure 3-7).

Synchronization with HU increased the S/G2/M (including early S) cell cycle fraction from 58.8 ± 1.3% to 98.0 ± 0.2% (Figure 3-12, F). 8h after release, mock infected cells showed a moderate increase in the early G1 and G1 fractions (Figure 3-12, B, C), which occurred at the expense of early S phase (Figure 3-12, D). A similar trend was observed for the distribution of WT infected samples. 24h after release, the early S fraction of mock infected samples was increased 4.3-fold to 46.0 ± 4.7% of the total cell population (Figure 3-12, D), while the S/G2/M fraction was reduced to 32.4 ± 6.2% of the total cell population (Figure 3-12, E). Contrarily, only 19.9 ± 2.0% of WT infected cells were observed in the early S fraction, while the S/G2/M fraction remained significantly increased at 60.1 ± 2.1% compared to mock control. Concluding, mock treated cells were found to re-enter the cell cycle, whereas VACV infection significantly blocked progression from S/G2/M phase at 24hpi.

2.2.3 VACV reduces G1 entry of G2 synchronized cells

Cell cycle progression is orchestrated by periodically activated cyclin-dependent kinases (CDKs). CDK1 is activated after completion of S phase and induces progression through G2 and entry into M phase (Girard et al., 1991; Walker and Maller, 1991). Targeting CDK1 activity with the small molecule inhibitor RO3306 reversibly arrests cells at the border of G2/M (Vassilev et al., 2006).

To test whether VACV can trap cells in late G2, HeLa FUCCI cells were synchronized with RO3306 (10 µM) as previously described (Ma and Poon, 2011). Briefly, cells were incubated overnight with RO3306, released and immediately mock infected, or infected with WT VACV (MOI 2). Samples were harvested at 0, 8, 24hpi and the cell cycle distribution was assessed by flow cytometry using the gating strategy outlined above (Figure 3-7).

Synchronization with RO3306 increased the S/G2/M cell cycle fraction from 21.8 ± 1.8% to 61.3 ± 3.9% (Figure 3-13, F). Mock infected cells re-entered the cell cycle as was observed by moderately increased early G1 and G1 fractions at 8hpi (Figure 3-13, B, C) which was mirrored by slightly reduced early S phase levels (Figure 3-13, D). By 24hpi, uninfected cells had further transitioned from S/G2/M into G1 which was reflected by the reduction in S/G2/M to 25.9 ± 7.7% of the total cell population. Contrarily, 48.1 ± 3.7% of WT infected cells remained in the S/G2/M after 24hpi. Although not statistically significant, these data suggest that WT infection reduces G1 entry by trapping cells in G2 at 24hpi.

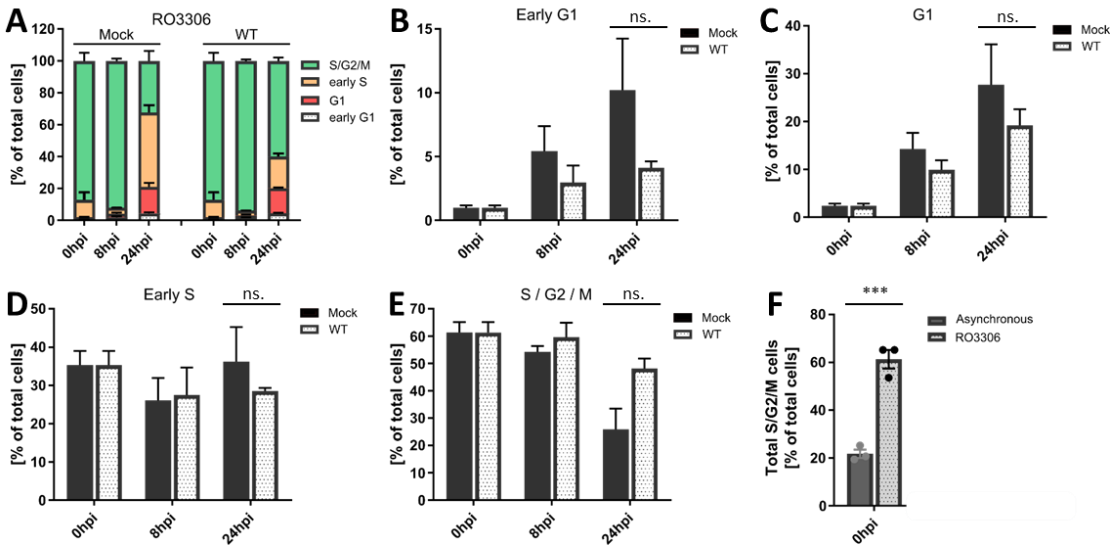

Figure 3-13 VACV infection increases the S / G2 / M cell fraction in RO3306 synchronized cells.

HeLa FUCCI cells were synchronized in G2 phase with the CDK1 inhibitor RO3306 (10 µM) o.n. Released cells were immediately infected with WT VACV (MOI 2) and harvested at 0hpi, 8hpi, and 24hpi. Using flow cytometry, cells were classified as early G1, G1, early S, or S / G2 / M. [A] Combined cell cycle stage distribution of mock infected and WT VACV infected samples. Individual cell cycle fractions are compared in [B-E]. [B] Percentage of early G1, [C] G1, [D] early S, and [E] S / G2 / M cell fractions in mock and WT VACV infected samples. [F] Synchronization effectiveness: the total S/G2/M fraction in asynchronous and HU synchronized cell populations. Data represent three biological replicates with one technical replicate each and are displayed as mean ± S.E.M. Parametric, unpaired, two-tailed t-test for significance. ns. $p > 0.05$, * $p < 0.033$, ** $p < 0.0021$, *** $p < 0.0002$, **** $p < 0.0001$.

3 VACV early gene expression is required and sufficient to block the host cell cycle

Having found that VACV inhibits host cell proliferation and cellular DNA synthesis, I next aimed to determine how VACV blocks progression of the cell cycle. To gain better understanding of the viral-induced block, I probed the virus life cycle to define the essential infection step. Similar to the cell cycle, VACV replication consists of temporally cascaded phases which each depend on completion of the previous step. As illustrated in Figure 3-14, the virus life cycle starts with attachment to the cell where the virus induces its own uptake by macropinocytosis. Next, acidification of the macropinosome activates the viral fusion machinery which mediates fusion of the virus and macropinosome membrane to release the viral core into the cytosol. After entry, pre-packaged lateral body proteins are released, and viral early genes are expressed within the core. The early protein D5 then causes core degradation and viral genome uncoating in a proteasome-dependent manner (Kilcher et al., 2014). The uncoated genome is replicated in the cytosol, allowing for viral intermediate and late gene expression.

Viral late genes mostly give rise to structural proteins which then form new progeny virions during morphogenesis. The infectious particles are released either in the form of double-wrapped EVs, or exit the cells by cell lysis as single-wrapped MVs.

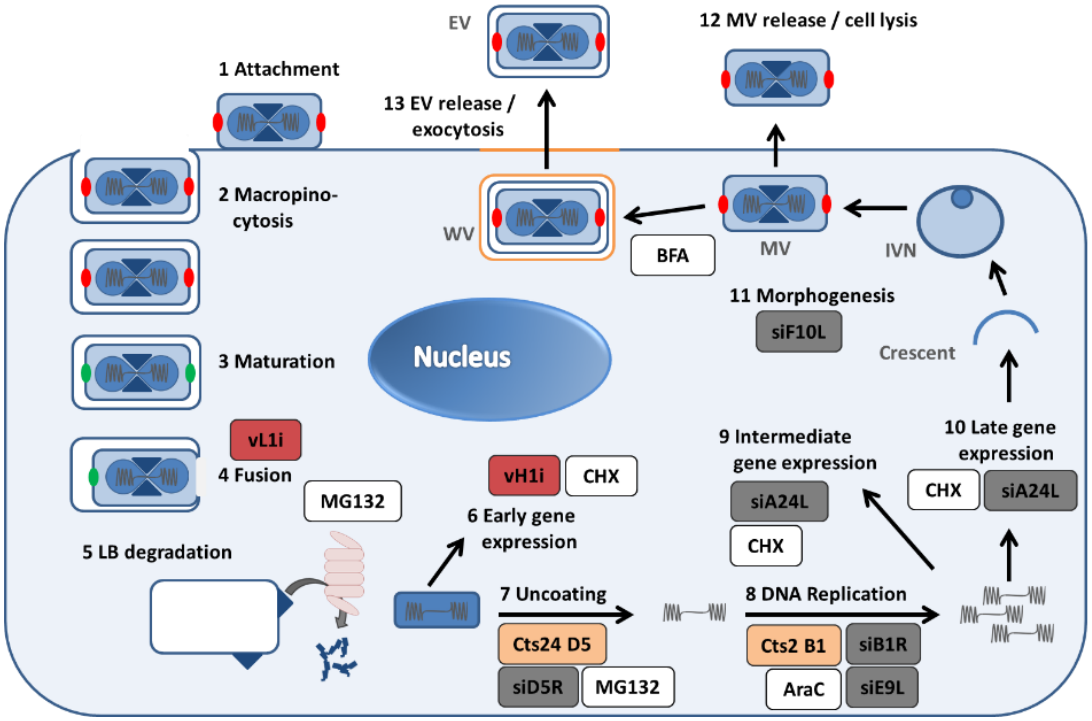

Figure 3-14 Schematic representation of the VACV replication cycle and different inhibition strategies.

VACV replication consists of temporally cascaded events which require completion of the respective preceding steps. The virus life cycle can be probed with different tools including pharmacological inhibitors (white), temperature sensitive (orange) and recombinant (red) VACV mutants, and RNAi targeting cellular or viral mRNAs (grey). This schematic summarizes the strategies used in this thesis and indicates the inhibited virus life cycle step.

To address which stage of VACV replication was required to block the host cell cycle, I needed tools to probe/manipulate the virus life cycle while allowing for unperturbed host cell cycle progression. There are many tools used in the VACV field to inhibit specific stages of the virus life cycle. These include pharmacological inhibitors, temperature sensitive and recombinant VACV mutants, and RNAi targeting either cellular or viral proteins. Some of these tools and where they block the virus life cycle are summarized in (Figure 3-14).

3.1 Classical pharmacological viral inhibitors directly inhibit the host cell cycle

Individual steps of the virus life cycle can be inhibited with the peptide aldehyde MG132, or the small molecules Cytosine arabinoside (AraC), and Cycloheximide (CHX). MG132 (25 µM)

reversibly inhibits the cellular proteasome and thereby prevents viral uncoating, while still allowing for viral early gene expression (Kilcher et al., 2014; Lee and Goldberg, 1998; Mercer et al., 2012; Schmidt et al., 2013). AraC (10µM) interferes with viral DNA synthesis by competing with its corresponding triphosphate dCTP as a substrate for the viral DNA polymerase (Furth and Cohen, 1968; Jr, 1968). Infection in the presence of AraC proceeds through early gene expression and genome uncoating but fails at replication of the uncoated genomes and therefore intermediate and late gene expression (Jr, 1968; Kilcher et al., 2014). However, the inhibitory effect of AraC is not specific for viral DNA synthesis but also prevents cellular DNA replication through the same mechanism (Furth and Cohen, 1968). Similarly, CHX prevents viral and cellular protein synthesis by interfering with the translational elongation step of the host ribosomes (McMahon, 1975).

Since I showed that VACV inhibits the host cell cycle, I next wanted to test whether these well-established inhibitors can be used to identify the essential stage of the virus life cycle. To address this question, BSC40 and HeLa cells were either mock infected, or infected with WT VACV (MOI 5) in the presence or absence of MG132 (25 µM), or AraC (10µM). Cells were harvested and counted at 0, 12, 24, and 48hpi (Figure 3-15, A and B). As observed before, WT infection inhibited cell proliferation, whereas untreated mock controls nearly tripled in cell numbers by 48hpi. On the other hand, samples that were treated with either MG132 or AraC failed to proliferate, independent of their infection status. These results reflect previous reports that highlight the importance of proteasomal degradation in regulating cell cycle progression (Han et al., 2009; Rao et al., 1999). Similarly, developed as an anti-cancer drug, AraC inhibits cellular DNA synthesis, thereby arrests cell proliferation, and induces apoptosis (Lucas-Lenard and Cohen, 1966; Rustum and Raymakers, 1992). Concluding, neither MG132 nor AraC can be used to characterize the required step in the virus replication cycle to block host cell proliferation.

To test whether CHX could be used to probe the virus life cycle, I assayed whether there was a CHX concentration that was anti-viral without affecting cell proliferation. To this end, HeLa cells were either mock infected, or infected with WR E/L EGFP expressing EGFP under an early/late promoter (MOI 5) in the presence of increasing concentrations of CHX. Mock infected cells, incubated with different CHX concentrations, were harvested and counted at 0, and 24hpi (Figure 3-15, C). Additionally, WR E/L EGFP infected samples were harvested at 24hpi and the percentage of infected cells were analysed by flow cytometry. The overlay of infectivity and cell numbers show that cell proliferation is inhibited by lower CHX

concentrations than viral gene expression. Concluding, as for MG132 and AraC, CHX cannot be used to characterize the essential virus life cycle step that blocks host cell proliferation.

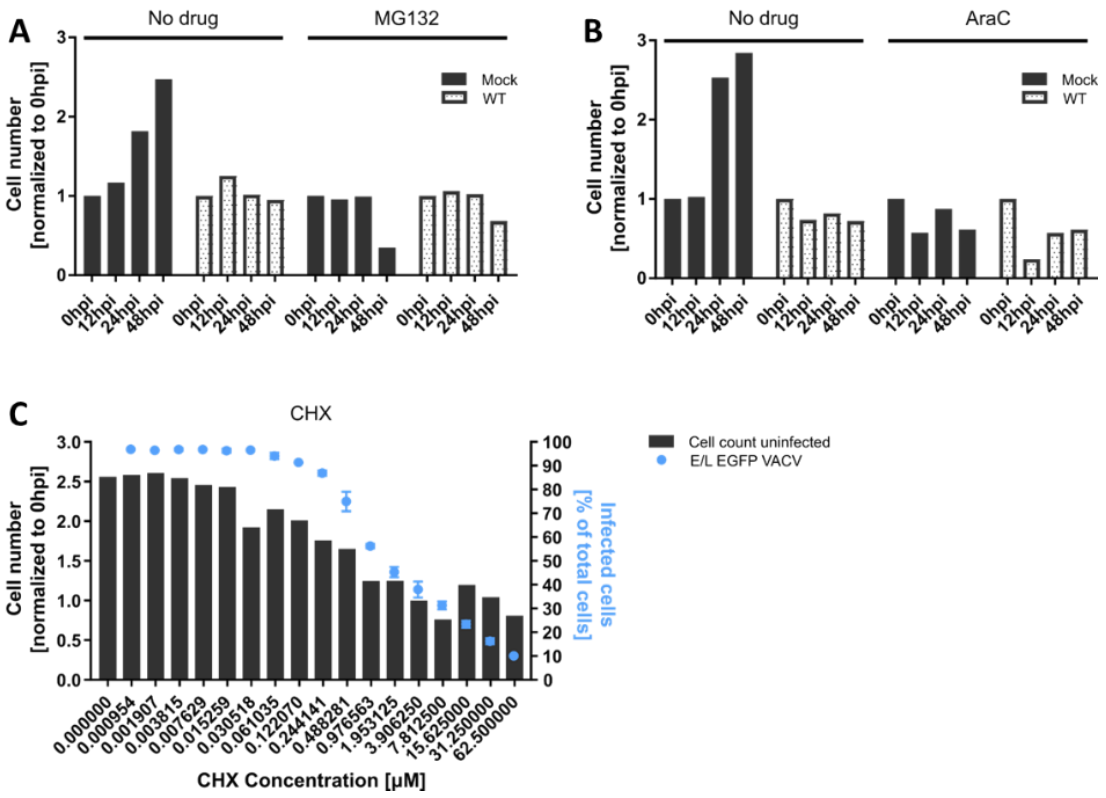

Figure 3-15 CHX, MG132, and AraC inhibit host cell proliferation.

[A-B] HeLa and BSC40 cells were either mock infected, or infected with WT VACV (MOI 5) in the presence of either the proteasome inhibitor MG132 (6,25 µM, [A]), or the DNA synthesis inhibitor AraC (10µM, [B]). Samples were automatically counted at 0, 12, 24, and 48hpi. Cell counts were normalized to 0hpi. Data represent the mean of two technical replicates of one biological replicate. [C] Overlay of cell count and viral gene expression for different CHX concentrations. HeLa cells were infected with either WT, or WR E/L EGFP in the presence of different concentrations of the translation inhibitor CHX. Samples were harvested at 0, and 24hpi and either counted, or analysed for viral gene expression by flow cytometry. Cell counts were normalized to 0hpi. Viral gene expression is displayed as the percentage of EGFP positive cells (blue dots). Data represent one biological replicate.

Since the pharmacological inhibitors MG132, AraC, and CHX directly block cell cycle progression, I needed a different strategy to specifically probe the virus life cycle while leaving the host cell cycle unperturbed. Therefore, I changed the approach from targeting cellular components to targeting viral proteins directly. VACV is amenable to genetic manipulation which allows for generation of various VACV recombinants. The recombinant VACV mutants can be grouped into three different classes: first, deletion mutants where a viral gene of interest was knocked out by e.g. insertion of a reporter cassette into the gene locus (Olson et al., 2017). Second, inducible mutants where the endogenous viral gene is put under control of

the *E. Coli lac* operator. Insertion of the *lac* operator into the viral genome allows to experimentally control the expression of the viral gene of interest by adding the inducer isopropylthiogalactopyranoside (IPTG) (Liu et al., 1995). Third, temperature-sensitive (ts) mutants which contain lesions in the viral genome that cause the resulting viral protein to become thermolabile at increased temperatures (Chernos et al., 1978; Condit and Motyczka, 1981; Condit et al., 1983). While ts mutants replicate productively at the lower, permissive temperature (31.5°C), viral replication becomes defective at the higher, non-permissive temperature (39.5°C). Inducible and ts recombinants allow to study the function of essential VACV proteins as the expression and protein activity, respectively, can be experimentally controlled. On the other hand, deletion viruses require transient complementation, if the deleted gene is essential to the virus life cycle.

In the following sections, I made use of inducible VACV strains (vL1i, v*ind*H1) and ts mutants (Cts2, Cts24) to define which stage of the viral life cycle is essential to block the host cell cycle.

3.2 VACV entry is required to arrest the host cell cycle

To identify the essential virus replication step, I tested different VACV mutants for their ability to inhibit host cell proliferation. Here, I aimed to define whether VACV entry was required. VACV entry is a two-step process. First, virions attach to the host cell and trigger their own uptake by macropinocytosis. Next, the virus fuses with the limiting membrane of the macropinosome to release the core with its lateral bodies into the cytosol. This second step is mediated by the VACV Entry Fusion Complex (EFC) which consists of several proteins, including the viral protein L1 (Bisht et al., 2008). Deletion of L1 disrupts the EFC and prevents viral entry into the cytosol (Bisht et al., 2008; Gray et al., 2018). The VACV strain vL1i encodes L1 under an IPTG inducible promoter and allows for production of virions lacking L1 (L1(-)). Since the L1(-) virus is entry incompetent, it cannot be titered by plaque assay. However, to guarantee a comparable infection, the amount of input virus needs to be matched. Therefore, L1(-) particle numbers were indirectly determined by measuring the DNA absorbance at 260/280nm and compared to the absorbance of a VACV prep with a known plaque titer. By correlating the DNA content to virus particle concentration, the MOI equivalent (MOI eq.) can be calculated for non-infectious VACV strains such as L1(-).

To test the effect of VACV entry on cell cycle progression, BSC40 cells were either mock infected (± IPTG), or infected with either WT VACV (MOI 5), L1(-) (MOI eq. 5), or its parental strain L1(+) (MOI 5, + IPTG). Samples were counted at 0, 12, 24, and 48hpi and cell counts were normalized to 0hpi (Figure 3-16). Cell proliferation was not affected by IPTG and uninfected cell numbers roughly tripled independent of the presence of IPTG. WT VACV infection, as well as infection with the parental L1(+) strain inhibited cell cycle progression and cell counts remained stable over 48hpi. On the other hand, the entry deficient L1(-) strain did not block cell proliferation and cell numbers increased 2.7-fold to a comparable level with uninfected controls. Concluding, this data demonstrates that VACV entry is required to establish a block in host cell cycle progression.

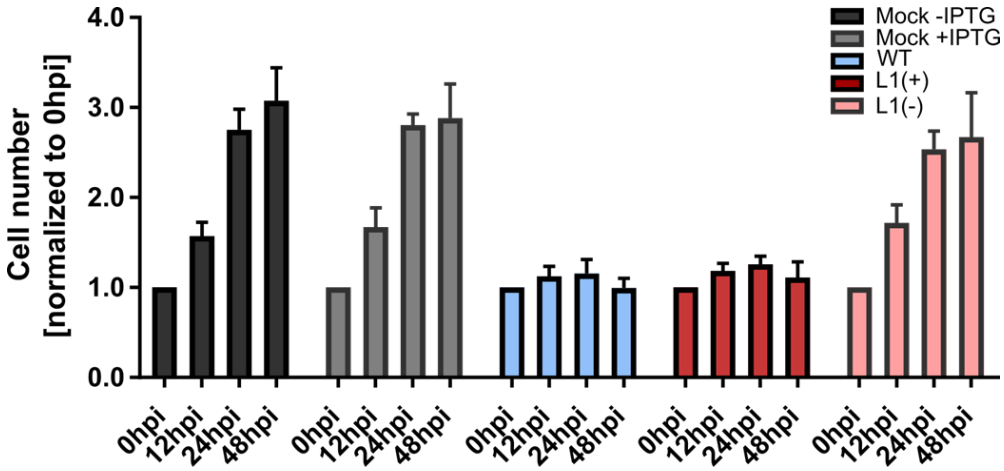

Figure 3-16 VACV entry and fusion are required to block host cell proliferation.

Relative increase in cell numbers after mock, WT, L1(+), L1(-) infection. Subconfluent BSC40 cells were mock infected (+/- the inducer IPTG), or infected with WT VACV (MOI 5), L1(+) VACV (MOI 5,+ the inducer IPTG), L1(-) (MOI 5 equivalents). Samples were automatically counted at 0, 12, 24, and 48hpi. Cell counts were normalized to 0hpi. Data represent three biological replicates with two technical replicates each and are displayed as mean ± S.E.M.

3.3 Does the VACV-induced cell cycle arrest require expression of viral early genes?

Having found that VACV entry is essential for inhibiting the host cell cycle, I next tested the role of early viral gene expression. After entry into the host cytosol, the two viral structures flanking the core, called lateral bodies, are degraded to release pre-packaged (viral) effector proteins (Schmidt et al., 2013). Concurrently, viral early mRNAs are synthesised within the still intact viral core by VACV-encoded enzymes, including L3, the RNA-helicase I8, and the viral early transcription factor A7 (Broyles et al., 1988; Gross and Shuman, 1996; Hu et al., 1998;

Moss, 1990; Resch and Moss, 2005; Yang and Moss, 2009). Since the transcription machinery is pre-packaged in the virus particle, generation of a transcriptionally incompetent virus requires genetic deletion of an essential viral enzyme. However, so far, deletion of any component of the transcription machinery was found to inhibit the formation of virus particles (Hu et al., 1998; Resch and Moss, 2005). Although not part of the transcriptional machinery, genetic deletion of the VACV phosphatase H1 produces infectious virions that are transcriptionally incompetent (Liu et al., 1995). Recently, H1 has been found to dynamically dephosphorylate the early transcription factor A7, which is critical for transcriptional competence of the progeny virions (Novy et al., 2018). To address the importance of viral early gene expression in inhibiting cell cycle progression and proliferation, I used the inducible H1 VACV (v*ind*H1, (Liu et al., 1995). Growing the virus without the inducer IPTG produces transcriptionally incompetent H1(-) virions, which enter the host cell but are severely attenuated for early gene expression. Virus prepared in the presence of the inducer IPTG (H1(+)), is fully replicative and shows normal viral gene expression levels, as long as IPTG is present in the medium. Similarly to the experiments described in section 2.2 of this chapter, I first assayed whether the deletion virus H1(-) was able to trap cells in any pre-synchronized cell cycle stage. Second, I monitored proliferation of asynchronous cell populations after infection with either the deletion H1(-) virus, or its parental H1(+) virus.

3.3.1 H1(-) is permissive for cell cycle progression of G1 synchronized cells

To test whether viral early gene expression is required to block cells in G1, HeLa FUCCI cells were synchronized in G1 with Lovastatin as previously described (JavanMoghadam-Kamrani and Keyomarsi, 2008; Ma and Poon, 2011). Briefly, cells were synchronized with Lovastatin (20 µM) for 24h. Cells were washed twice before being either mock infected, or infected with either H1(-) (MOI eq. 2, -IPTG), or parental H1(+) (MOI 2, + IPTG). To fully release the cells, the infection inoculum was replaced with medium supplemented with mevalonate (6 mM) and samples were harvested at 0, 8, and 24hpi. The cell cycle distribution was assessed by flow cytometry using the gating strategy outlined above (Figure 3-7).

Infection with H1(+) mirrored the previous observations for infection with WT virus (Figure 3-11). Uninfected cells re-entered the cell cycle and progressed from G1 into the S/G2/M fraction by 24hpi (Figure 3-17, E) , whereas H1(+) infected cells were retained in G1 as highlighted by the 1.6-fold increase in G1 cells compared to mock (Figure 3-17, C). On the other hand, H1(-) infection failed to trap cells in G1 and the cell cycle distribution paralleled the spread in uninfected controls. At 24hpi, 32.5 ± 1.0 % of H1(-) infected cells were measured in G1 phase, compared to 27.6 ± 0.7 % of uninfected cells, and 43.9 ± 3.2% of H1(+) infected cells, respectively. The S/G2/M fraction represented 26.6 ± 1.3 % of uninfected cells, and 26.6 ± 1.9 % of H1(-) infected cell populations, which constitutes a significant 1.6-fold increase compared to H1(+) samples. These data demonstrate that H1(-) cannot block cell cycle progression of G1 synchronized cells in the absence of viral early gene expression.

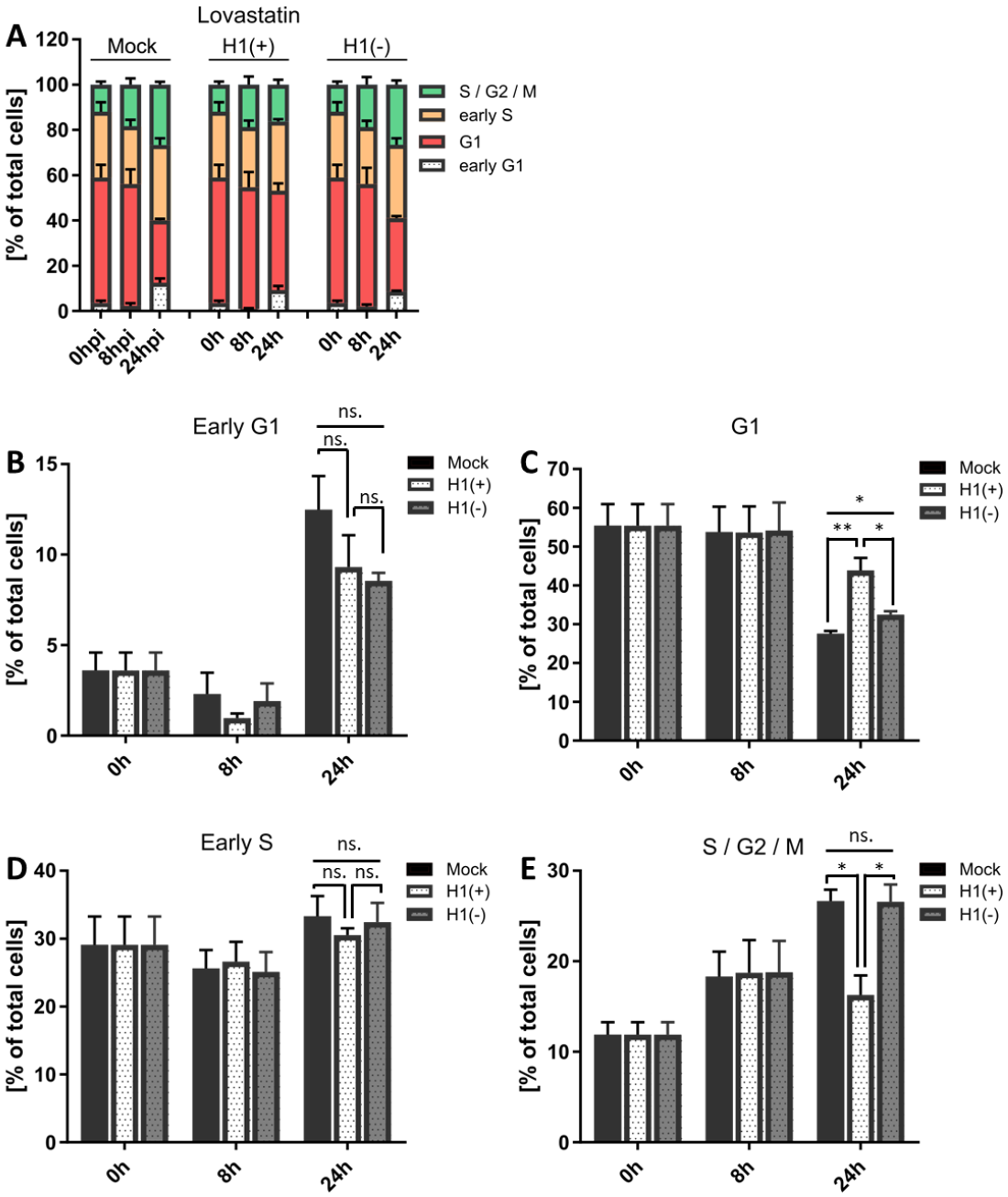

Figure 3-17 VACV early gene expression is required to arrest Lovastatin synchronized cells in G1.

HeLa FUCCI cells were synchronized in G1 with Lovastatin (20 µM) for 24h. Released cells were immediately infected with H1(-) VACV (MOI eq. 2, no inducer IPTG), or with H1(+) VACV (MOI 2, + inducer IPTG 5mM). Samples were harvested at 0hpi, 8hpi, and 24hpi. Using flow cytometry, cells were classified as early G1, G1, early S, or S / G2 / M. [A] Combined cell cycle stage distribution of mock infected, H1(-), and H1(+) VACV infected samples. Individual cell cycle fractions are compared in [B-E]. [B] Percentage of early G1, [C] G1, [D] early S, and [E] S / G2 / M cell fractions in mock, H1(-), and H1(+) VACV infected samples. Data represent three biological replicates with one technical replicate each and are displayed as mean ± S.E.M. Parametric, unpaired, two-tailed t-test for significance. ns. $p > 0.05$, * $p < 0.033$, ** $p < 0.0021$, *** $p < 0.0002$, **** $p < 0.0001$

3.3.2 H1(-) is permissive for cell cycle progression of S phase synchronized cells

To test whether viral early gene expression is essential to trap cells in S phase, HeLa FUCCI cells were synchronized with HU (2.5 mM) o.n. Cells were released and immediately either mock infected, or infected with either H1(-) (MOI eq. 2, -IPTG), or parental H1(+) (MOI 2, + IPTG). Samples were harvested at 0, 8, and 24hpi and the cell cycle distribution was assessed by flow cytometry using the gating strategy outlined above (Figure 3-7).

Infection with H1(+) mirrored the previously observed changes in cell cycle distribution with WT virus (Figure 3-12). While uninfected cells re-entered the cell cycle and progressed into G1 and early S phase by 24hpi (Figure 3-18, C, D), H1(+) infected cells remained in S/G2/M as marked by the 2.3-fold increase in the S/G2/M fraction compared to mock (Figure 3-18, E). Contrarily, H1(-) infection failed to trap cells in S phase and the cell cycle distribution paralleled the spread in uninfected controls. At 24hpi, 28.7 ± 5.8% of H1(-) infected cells were measured in S/G2/M, compared to 32.4 ± 6.2% of uninfected cells, and 73.5 ± 5.3% of H1(+) infected cells, respectively. However, H1(-) infected cells were found to transit through the cell cycle with slower kinetics than uninfected cells. H1(-) caused more accumulation of G1 cells (25.1 ± 2.9%) 24hpi, than mock infection (16.7 ± 2.4%), and H1(+) infection (9.3 ± 2.0%), respectively. The slower progression of H1(-) infected cells was further mirrored in reduced early S phase fraction in H1(-) samples compared to uninfected controls. From this I conclude that H1(-) infection cannot arrest pre-synchronized cells in S phase in the absence of viral early gene expression.

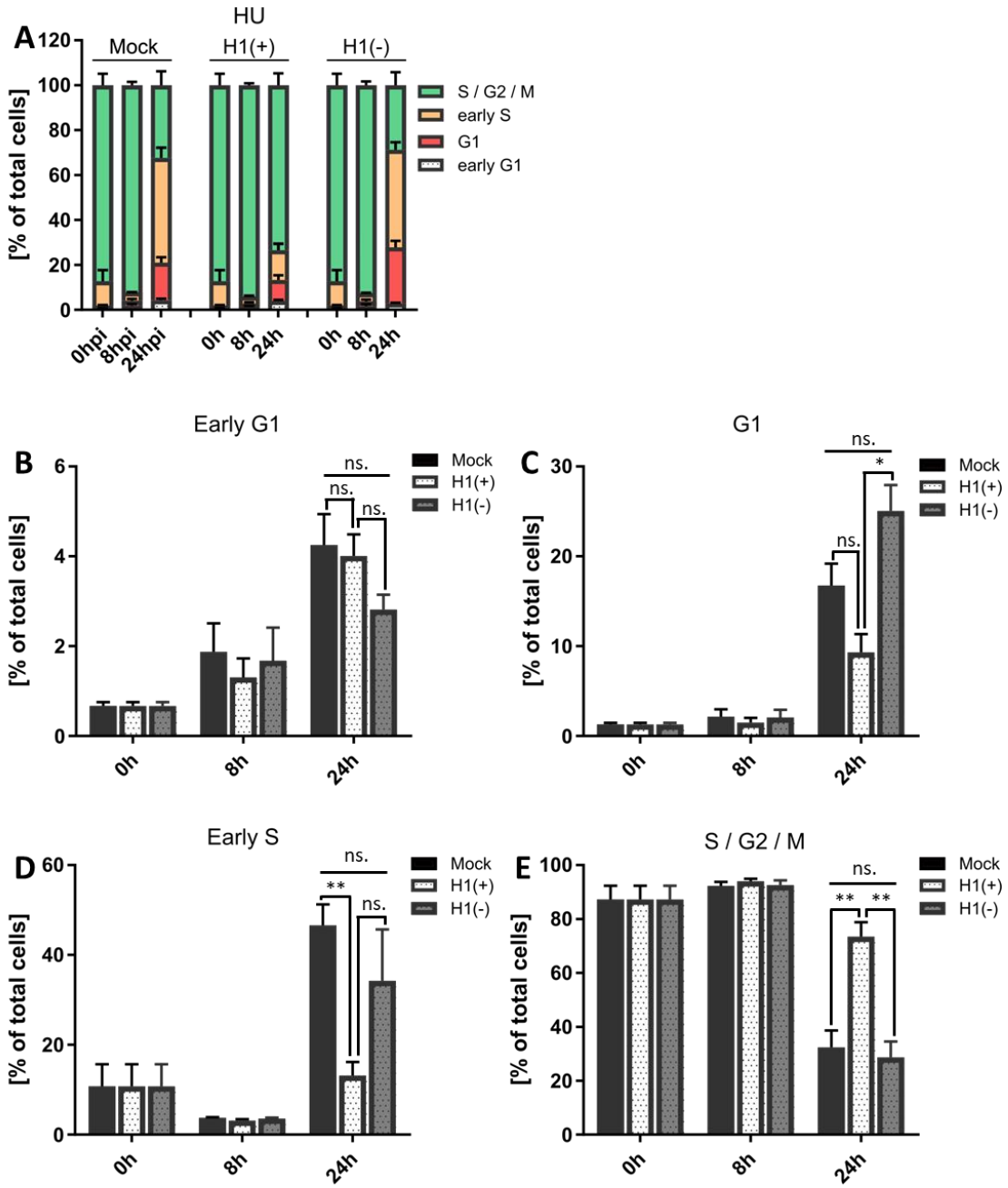

Figure 3-18 VACV early gene expression is required to arrest Hydroxyurea (HU) synchronized cells in S / G2 / M.

HeLa FUCCI cells were synchronized in S phase with HU (2.5 mM) o.n. Released cells were immediately infected with H1(-) VACV (MOI eq. 2, no inducer IPTG), or with H1(+) VACV (MOI 2, + inducer IPTG 5mM). Samples were harvested at 0hpi, 8hpi, and 24hpi. Using flow cytometry, cells were classified as early G1, G1, early S, or S / G2 / M. [A] Combined cell cycle stage distribution of mock infected, H1(-), and H1(+) VACV infected samples. Individual cell cycle fractions are compared in [B-E]. [B] Percentage of early G1, [C] G1, [D] early S, and [E] S / G2 / M cell fractions in mock, H1(-), and H1(+) VACV infected samples. Data represent three biological replicates with one technical replicate each and are displayed as mean ± S.E.M. Parametric, unpaired, two-tailed t-test for significance. ns. $p > 0.05$, * $p < 0.033$, ** $p < 0.0021$, *** $p < 0.0002$, **** $p < 0.0001$

3.3.3 H1(-) is permissive for cell cycle progression of G2 phase synchronized cells

To test whether viral early gene expression is required to arrest cells in G2, HeLa FUCCI cells were synchronized with the CDK1 inhibitor RO3306 (10 µM) o.n. Cells were released and immediately either mock infected, or infected with either H1(-) (MOI eq. 2, -IPTG), or parental H1(+) (MOI 2, + IPTG). Samples were harvested at 0, 8, and 24hpi and the cell cycle distribution was assessed by flow cytometry using the gating strategy outlined above (Figure 3-7).

Infection with H1(+) copied the effect previously observed for WT infection (Figure 3-12): while uninfected cells re-entered the cell cycle and progressed into G1 and early S phase by 24hpi (Figure 3-18, C, D), H1(+) infected cells remained in S/G2/M as indicated by the significant 2.1-fold increase in the S/G2/M fraction compared to mock (Figure 3-18, E). Contrarily, H1(-) infection failed to trap cells in G2 phase and the cell cycle distribution paralleled the spread in uninfected controls. At 24hpi, 26.3 ± 4.8% of H1(-) infected cells were measured in S/G2/M, compared to 25.9 ± 7.7% of uninfected cells, and 55.4 ± 4.6% of H1(+) infected cells, respectively. However, H1(-) infected cells seemed to transit through the cell cycle with slightly slower kinetics than uninfected cells. H1(-) caused more cells to accumulate in G1 (35.9 ± 7.6%) 24hpi, than mock infection (27.7 ± 8.5%), and significantly more than H1(+) infection (13.0 ± 2.6%), respectively. These results show that H1(-) infection cannot arrest pre-synchronized cells in G2 phase in the absence of viral early gene expression.

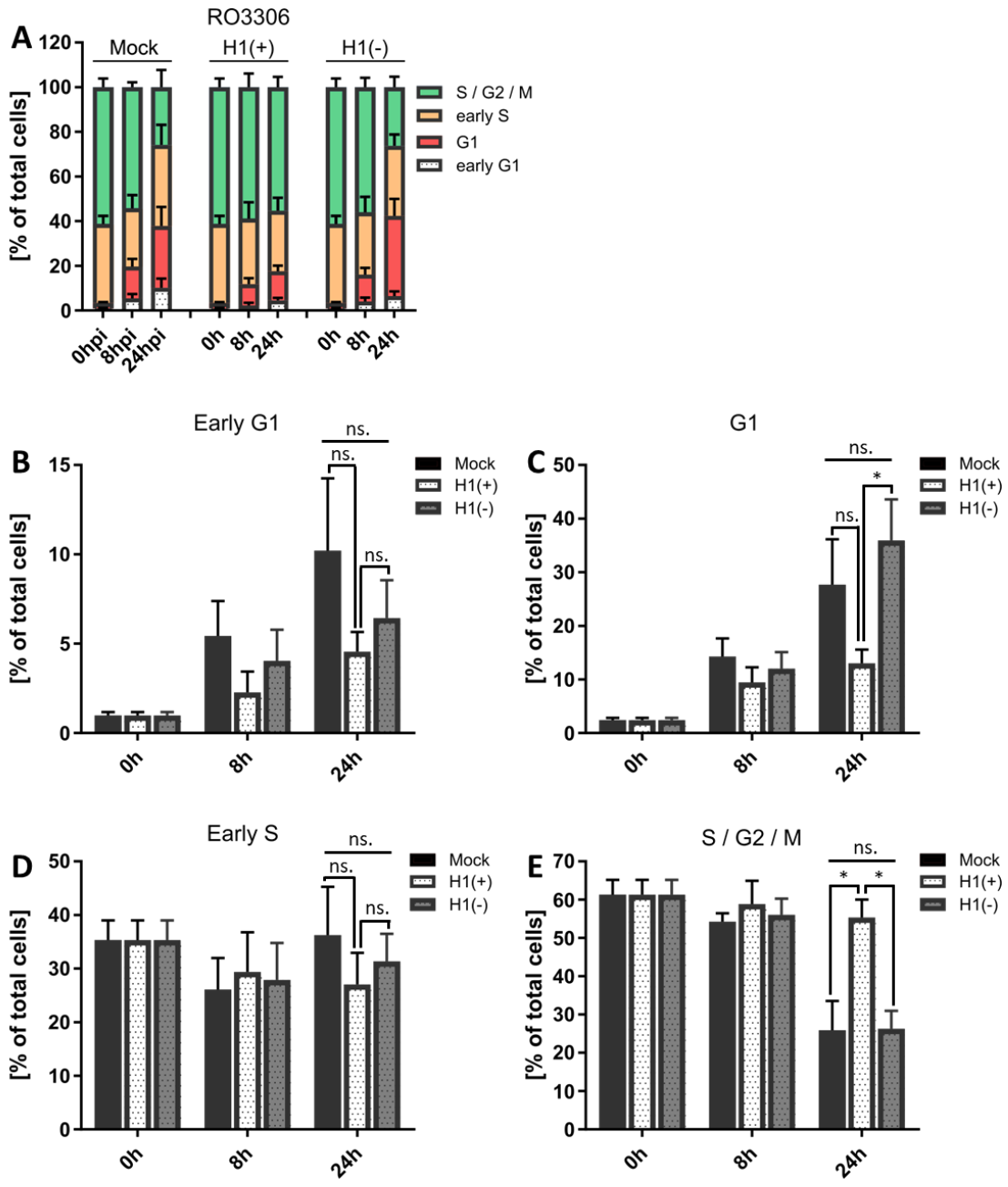

Figure 3-19 VACV early gene expression is required to arrest RO3306 synchronized cells in S / G2 / M.

HeLa FUCCI cells were synchronized in G2 phase with the CDK1 inhibitor RO3306 (10 µM) o.n. Released cells were immediately infected with H1(-) VACV (MOI eq. 2, no inducer IPTG), or with H1(+) VACV (MOI 2, + inducer IPTG 5mM). Samples were harvested at 0hpi, 8hpi, and 24hpi. Using flow cytometry, cells were classified as early G1, G1, early S, or S / G2 / M. [A] Combined cell cycle stage distribution of mock infected, H1(-), and H1(+) VACV infected samples. Individual cell cycle fractions are compared in [B-E]. [B] Percentage of early G1, [C] G1, [D] early S, and [E] S / G2 / M cell fractions in mock, H1(-), and H1(+) VACV infected samples. Data represent three biological replicates with one technical replicate each and are displayed as mean ± S.E.M. Parametric, unpaired, two-tailed t-test for significance. ns. $p > 0.05$, * $p < 0.033$, ** $p < 0.0021$, *** $p < 0.0002$, **** $p < 0.0001$

3.3.4 H1 is not required for inhibition of cell proliferation

In the previous sections (3.3.1 - 3.3.3), I showed that viral early gene expression and/or H1 is required to inhibit cell cycle progression of pre-synchronized cells. Next, I aimed to assay whether expression of viral early genes was also essential to block proliferation of unsynchronized cells. To address this question, BSC40 cells were either mock infected, or infected with either H1(-) (MOI eq. 2, -IPTG), or parental H1(+) (MOI 2, + IPTG). Cells were harvested and counted at 0, 12, 24, and 48hpi (Figure 3-20, A). As observed before, uninfected cells divide once approximately every 18h, whereas WT/H1(+) infected cells fail to proliferate. Mirroring its parental virus, H1(-) was also found to inhibit host cell proliferation and cell numbers of H1(-) infected samples remained constant over 48hpi. This data suggested that H1 and viral early gene expression is dispensable to block the host cell cycle.

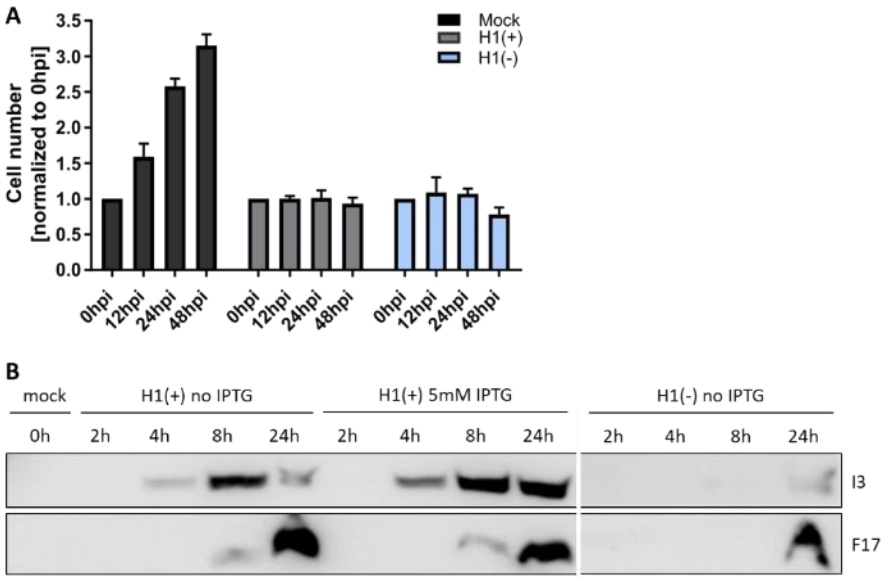

Figure 3-20 Transcriptionally attenuated H1(-) inhibits host cell proliferation.

[A] Relative increase in cell numbers in mock, WT and H1(-) infected BSC40 cells. Unsynchronized BSC40 cells were mock infected, or infected with either WT VACV (MOI 5), or H1(-) (MOI eq. 5) and counted at 0, 12, 24, and 48hpi. Cell counts were normalized to 0hpi. Data represent three biological replicates with two technical replicates each and are displayed as mean ± S.E.M. [B] Viral gene expression profile of the transcriptionally attenuated H1(-) virus compared to the parental H1(+) virus. HeLa cells were infected with H1(-) (MOI eq. 1, -IPTG), or with H1(+) (MOI 1, +/- IPTG) and samples were harvested at 0, 2, 4, 8, 24hpi. Whole cell lysates were resolved via SDS-PAGE and immunoblotted for the viral early protein I3 and the viral late protein F17.

As this finding contradicts the previous conclusion that early gene expression is essential to block pre-synchronized cells, I next looked to explain this discrepancy. To this end, I first analysed the viral gene expression profile during H1(-) infection, since both experiments exploit the transcriptional attenuation of H1(-). HeLa cells were either mock infected, or infected with H1(-) (MOI eq. 1), or H1(+) (MOI 1) in the presence or absence of IPTG. Samples were harvested at 0, 2, 4, 8, and 24hpi. To monitor viral early and late gene expression, whole cell lysates were resolved via SDS-PAGE and immunoblotted for the early protein I3, as well as the late protein F17 (Figure 3-20, B). In H1(+) infected samples, early gene expression was detected from 4hpi onwards, followed by late gene expression at 8hpi, independent of the presence of absence of IPTG. In contrast, no viral gene expression was observed in H1(-) infected cells between 0 and 8hpi, confirming the transcriptional defect of the virus recombinant. However, by 24hpi early and late gene products were measured with H1(-), demonstrating that the virus is transcriptionally attenuated but not completely inactive.

The “leaky” transcription of H1(-) at late infection timepoints might explain the opposing results in the synchronization and cell proliferation assay. The two assays differ in their time resolution, due to the distinct readouts parameters: while changes in cell cycle distribution were detectable already at 8hpi, changes in cell numbers had to be measured over 12-48hpi. Therefore, the cell cycle changes mostly happened before viral gene products could significantly accumulate and affect the cell cycle progression. However, due to the prolonged timecourse of the proliferation assay, infected cells were probably expressing both viral early and late genes when they were counted. This suggests that the proliferation block observed during H1(-) infection is an artefact of “leaky” viral gene expression. Concluding, although further experiments are required, the above described observations suggest that viral early gene expression or the H1 phosphatase are required to inhibit the host cell cycle.

3.4 VACV uncoating is not required to inhibit the host cell cycle

The previous findings suggested that expression of viral early genes is essential for inhibiting the host cell cycle. Therefore, I next tested whether the following viral life cycle stage, viral genome uncoating, is also required. VACV genome uncoating proceeds in two consecutive steps. First, activation of the viral cores triggers expression of viral early genes, including the viral uncoating factor D5. Next, together with the proteasome, D5 assists in degrading the viral core to release the viral genome into the cytosol (Kilcher et al., 2014; Mercer et al., 2012; Schmidt et al., 2013). To assay whether release of the viral genome was involved in inhibition of the host cell cycle, I made use of the temperature sensitive (ts) VACV strain Cts24 (Condit and Motyczka, 1981). Cts24 encodes a thermolabile mutant of D5 that is nonfunctional at non-permissive temperature (40°C) and thus prevents viral uncoating (Boyle et al., 2007; Evans and Traktman, 1992; Kilcher et al., 2014). In the following sections, I infected cells with Cts24 under permissive and non-permissive conditions to characterize the effect of viral genome release on host cell cycle progression.

3.4.1 VACV uncoating is not required to block cellular DNA synthesis

In section 1.2 of this chapter, I have described an assay to specifically measure cellular DNA synthesis in VACV infected cells and found VACV to progressively inhibit host cell DNA synthesis during infection (Figure 3-3). Using the same protocol to monitor the amount of S phase cells during infection, I characterized the role of viral uncoating in inhibiting host cell cycle progression.

HeLa Kyoto H2B-mCh cells were grown on coverslips and either mock infected, or infected with the ts mutant Cts24. After viral entry at the permissive temperature, cells were either kept at 31°C, or shifted to 40°C. Cells were pulse-labelled with the nucleotide analogue EdC (10µM) for 15min prior to fixation at 0.5, 1, 2, 4, 5, 6, 8, and 24hpi. Incorporated EdC was visualized by covalent conjugation to AlexaFluor 488. Tiled overview images were acquired by confocal, optical superresolution microscopy (iSIM) (Figure 3-21, A). Per sample a minimum of 300 non-apoptotic nuclei was counted manually and either scored as EdC positive (S phase cells), or EdC negative (non-S phase cells). The percentage of S phase cells was calculated for mock and infected samples (Figure 3-21, B-E). To account for fluctuations in cell cycle progression due to sample manipulation, the percentage of S phase cells in infected samples was further normalized to their respective mock control (Figure 3-21, C, E).

Uninfected cells were able to synthesize DNA at both the permissive (31°C) and the non-permissive (40°C) temperature. However, cell cycle progression was found to be accelerated at 40°C compared to 31°C: initially, the amount of S phase cells in uninfected populations was comparable for both temperature conditions. Between 5hpi and 24hpi, the S phase fraction at 41°C steadily increased from 33.3 ± 2.9 % to 59.8 ± 1.1 %, whereas it slightly decreased from 30.5 ± 3.1 % to 24.7 ± 0.6 % if cells were incubated at 31°C. On the other hand, infected cells ceased to synthesise cellular DNA by 24hpi, independent of the temperature conditions, although the kinetics of the virus-induced shutoff differed. Under permissive conditions, the amount of S phase cells in Cts24 infected populations fluctuated between 76.0 ± 4.7% and 107.7 ± 13.7% before decreasing after 5hpi. At the non-permissive temperature, the cellular DNA synthesis was already inhibited from 2hpi onwards, reducing the amount of S phase cells from over 100% of mock levels at 2hpi to 19.9 ± 3.2% at 8hpi. The difference in inhibition efficiency probably reflects the acceleration of cell cycle progression, as well as viral replication kinetics at higher temperatures. Concluding, this data show that neither viral uncoating, nor the viral uncoating factor D5 are required to block cellular DNA synthesis during infection.

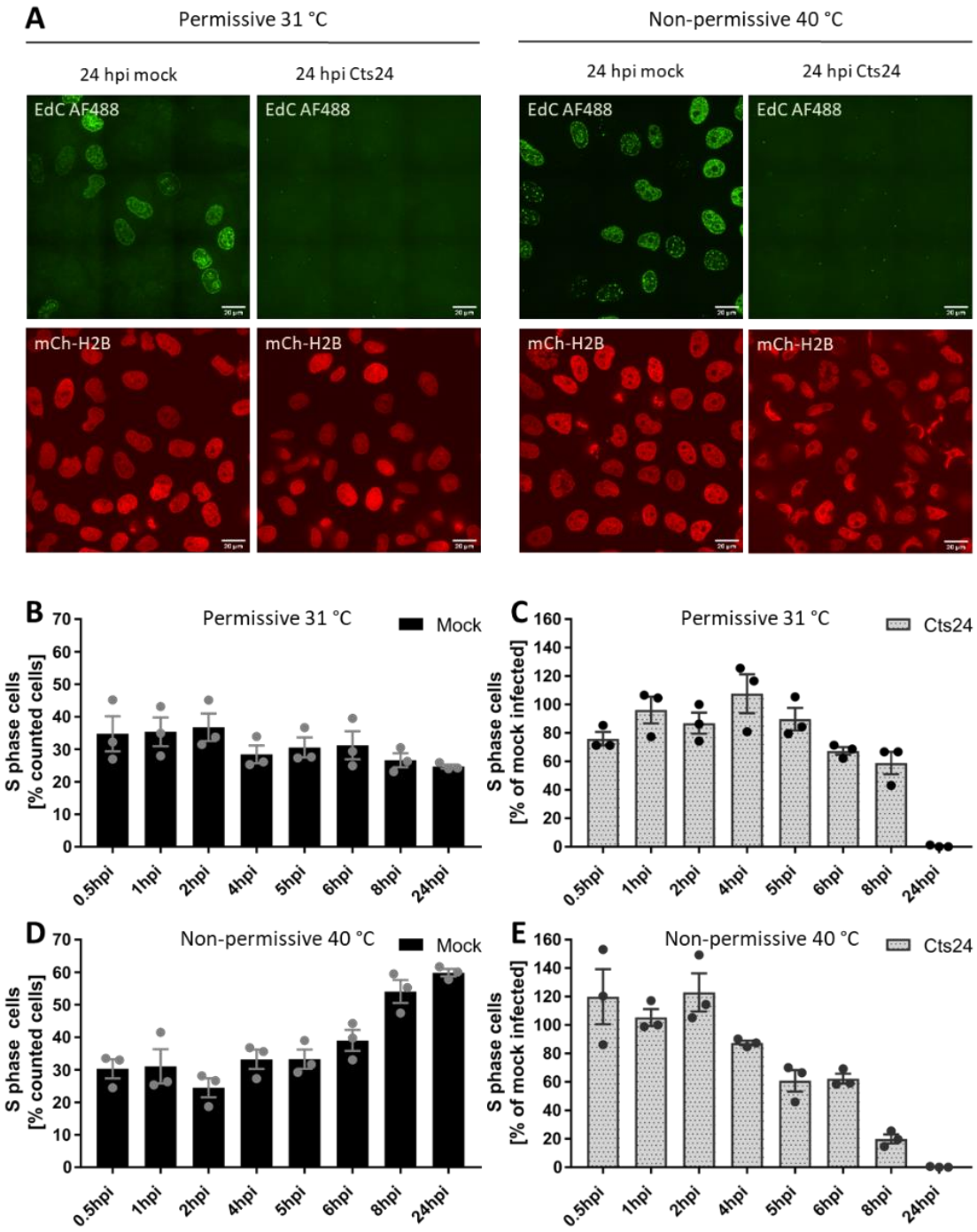

Figure 3-21 VACV inhibition of host cell DNA synthesis is independent of viral genome uncoating.

HeLa H2B-mCh were either mock infected, or infected with the temperature sensitive VACV strain Cts24 (MOI 8) either at the permissive, or non-permissive temperature. Cells were pulse-labelled with the nucleotide analogue EdC (10μM) for 15min prior to fixation at 0.5, 1, 2, 4, 5, 6, 8, and 24hpi. Incorporated EdC was covalently conjugated to AlexaFluor488 and tiled overview microscopy images were acquired. A minimum of 300 nuclei was counted per sample and scored as EdC positive (S phase) or negative (non S phase). [A] Representative microscopy images of mock and Cts24 infected cells at either the permissive, or non-permissive temperature at 24hpi. Scale bar represents 20 μm. [B-C] The percentage of S phase cells at 31°C in [B] mock infected samples, and [C] in infected samples, normalized to the respective mock control. [D-E] The percentage of S phase cells at 40°C in [D] mock infected samples, and [E] in infected samples, normalized to the respective mock control. Data represent three biological replicates and are displayed as mean ± S.E.M.

3.4.2 VACV uncoating is not required to inhibit host cell proliferation

I have shown that cellular DNA synthesis is inhibited independent of viral genome release. Next, I tested the role of viral genome uncoating in inhibiting host cell proliferation. As before, BSC40 cells were either mock infected, or infected with the ts mutant Cts24 (MOI 5). After viral entry at the permissive temperature, cells were either kept at 31°C (Figure 3-22, A), or shifted to 40°C and samples were counted at 0, 10, 24, and 48hpi (Figure 3-22, B). While uninfected cells were found to proliferate faster at 40°C than at 31°C, neither of the temperature regimes inhibited cell proliferation. On the other hand, infected cells failed to proliferate, independent of the temperature conditions. Under permissive conditions, infected cell numbers multiplied 1.2-fold, compared to a 1.8-fold increase in uninfected samples. Similarly, under non-permissive conditions, Cts24 infected cell numbers increased 1.5-fold, whereas uninfected controls tripled during 48h. Concluding, this data demonstrates that neither viral uncoating, nor the viral uncoating factor D5 are involved in arresting host cell proliferation.

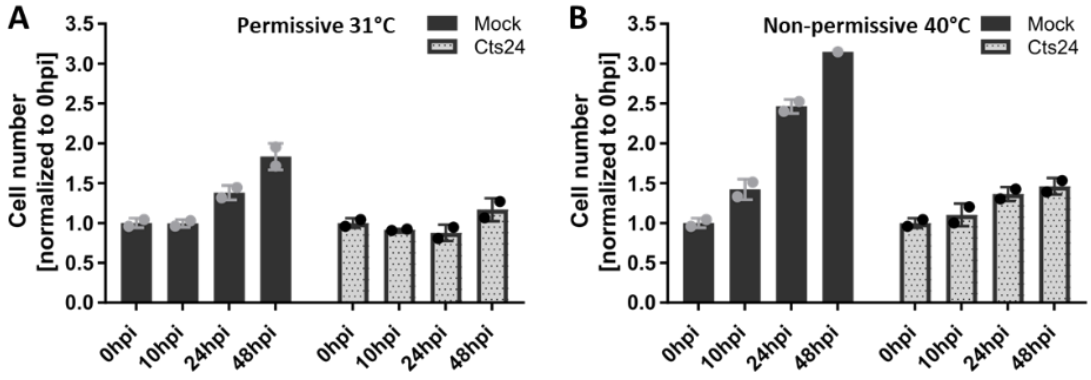

Figure 3-22 VACV inhibition of host cell proliferation does not require viral genome uncoating.

BSC40 cells were either mock infected, or infected with the temperature sensitive VACV strain Cts24 (MOI 5) either at the permissive, or non-permissive temperature. Cells were counted at 0, 10, 24, and 48hpi and counts were normalized to 0hpi. [A] Normalized counts of mock (black) and infected (grey) samples at the permissive temperature (31°C). [B] Normalized counts of mock (black) and infected (grey) samples at the non-permissive temperature (40°C). Data represent one biological replicate with two technical replicates and are displayed as mean ± S.D.

4 Summary Chapter 3

In this chapter I showed that VACV inhibits host cell proliferation, and that this inhibition depends on viral entry but not viral genome uncoating (Figure 3-23). Although previous work already suggested that VACV interfered with cell cycle progression, mechanistic insights remained elusive due to technical limitations. Here, I combined state of the art novel techniques with classical virology to gain more mechanistic understanding of VACV-induced alterations of the cell cycle.

First, I aimed to define the kinetics of the virus-induced cell proliferation block. Therefore, I developed a direct, image-based assay to visualize cellular DNA synthesis in VACV infected cells. Using this assay, I found that VACV rapidly inhibits synthesis of cellular DNA from 2hpi onwards and thereby completely blocks S phase progression by 24hpi.

Next, I characterized whether the S phase inhibition was specific, or part of a systemic cell cycle arrest. To address this question, I established a protocol to analyse the cell cycle distribution of productively infected cells. As viral DNA replication was found to interfere with DNA content-based analysis methods, I switched to the Fluorescent, Ubiquitination-based Cell Cycle Indicator (FUCCI) system. Using the HeLa FUCCI reporter cell line, I showed that VACV is able to trap synchronized cells in G1, S, and G2 phase of the cell cycle, suggesting that the virus causes a systemic cell cycle block.

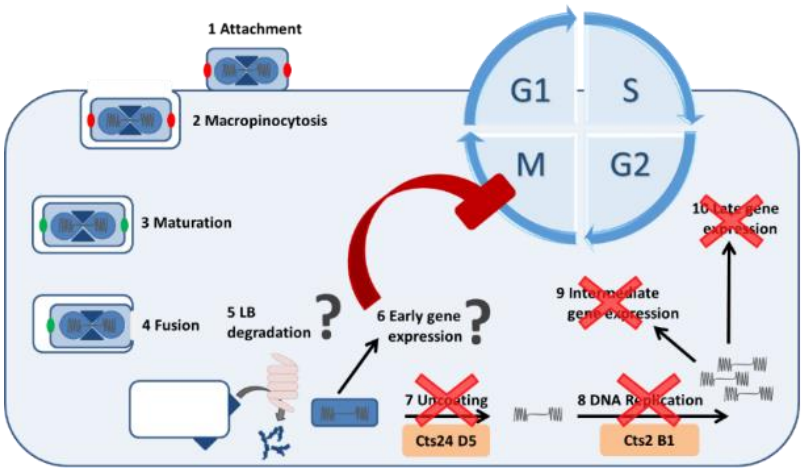

Figure 3-23 VACV early gene expression and/or lateral body delivery block the host cell cycle.

Schematic figure of the virus life cycle, summarizing results presented in chapter 1. Using different VACV mutants, viral entry was found to be essential to inhibit host cell proliferation, whereas viral genome uncoating is not required. Further experiments are needed to definitively distinguish between the contribution of pre-packaged effector proteins and expression of viral early genes.

Last, I aimed to identify the VACV life cycle stage that is essential to arrest the host cell cycle. To probe the virus life cycle, I used a combination of RNAi targeting viral mRNAs, temperature sensitive and recombinant VACV mutants. Infection with fusion defective L1(-) virus demonstrated that viral entry is required to prevent host cell cycle progression. Similarly, transcriptionally attenuated H1(-) virus could not trap synchronized cells in G1, S, or G2 phase of the cell cycle, suggesting that viral early genes, or H1 itself play a role in cell cycle inhibition. On the contrary, Cts24 retained the ability to arrest cellular DNA synthesis and proliferation, even under conditions where the viral genome was not uncoated. Taken together, these data indicate that a viral early protein(s) is required and sufficient to arrest the host cell cycle.

4 VACV shifts the host cell cycle

In chapter 3 I demonstrated that VACV infection arrests host cell proliferation, and that this inhibition depends on viral entry but not viral genome uncoating. Additionally, I have shown that VACV is able to trap synchronized cells in the G1, S, and G2 phase of the cell cycle, suggesting that the virus causes a systemic cell cycle block.

Using Lovastatin to reversibly synchronize cells in G1, I found infected cells to be retained in G1, even at 24hpi (Figure 3-11). These findings are contradictory to previous reports that synchronized cells in G1 by serum starvation. Both studies infected the G1 cells upon release, and monitored their cell cycle distribution at 24-48hpi by DNA quantification. Infection was found to increase the fraction of S and G2/M phase cells in 143B osteosarcoma cells (Yoo et al., 2008), as well as rabbit kidney fibroblasts (Wali and Strayer, 1999b). Concurrently, changes were observed in protein abundance, gene transcription, and posttranslational modifications of major cell cycle regulators such as CDKs 1/2/4/6, Cyclins A/B, and the tumour suppressors Rb and p53 (Wali and Strayer, 1999b; Yoo et al., 2008). Based on these observations, VACV was suggested to stimulate cell cycle progression and proliferation of 143B osteosarcoma cells. Similarly, in rabbit kidney fibroblasts, VACV was proposed to increase the transit through G1, while slowing but not blocking S phase progression. However, as cell numbers were not measured, neither study could relate the shift in cell cycle to cell proliferation. The published results cannot distinguish between an increase in S phase due to a block in S phase, and an increase caused by slowed S phase progression.

The discrepancy between my findings and the published data could be explained by differences in methodology and cell types. While I synchronized cells with Lovastatin, the previous studies synchronized cells by serum starvation, which might cause different lag times before cell cycle re-entry. As VACV was found to inhibit the cell cycle within 8hpi (Figure 3-3), infection could act like a timer on released cells: the observed increase in S phase, and G1, respectively, might reflect faster release kinetics after serum starvation than after Lovastatin treatment.

Moreover, the published shift in cell cycle distribution was measured by quantifying whole cell DNA content of infected cells. As discussed in chapter 3, I observed a similar progression from G1 into S phase in infected cells using DNA content as a readout (Figure 3-6). However, this apparent shift was lost when viral DNA synthesis was inhibited by RNAi knockdown of viral

proteins required for viral replication (Figure 3-6). Therefore, the reported shift might represent an artefact of the analysis method.

Similarly, the results from my synchronization experiments only demonstrate that VACV has the potential to arrest the cells in any cell cycle stage but do not necessarily reflect the natural infection state in untreated cells. Therefore, I next focused on characterizing the cell cycle distribution of unsynchronized cells during VACV infection, using the FUCCI reporter system and analysing a panel of major cell cycle regulators by immunoblot. Additionally, if a shift in cell cycle was observed, I aimed to identify the virus life cycle stage required for this.

1 VACV infection increases the S/G2 cell fraction at the expense of G1 and M

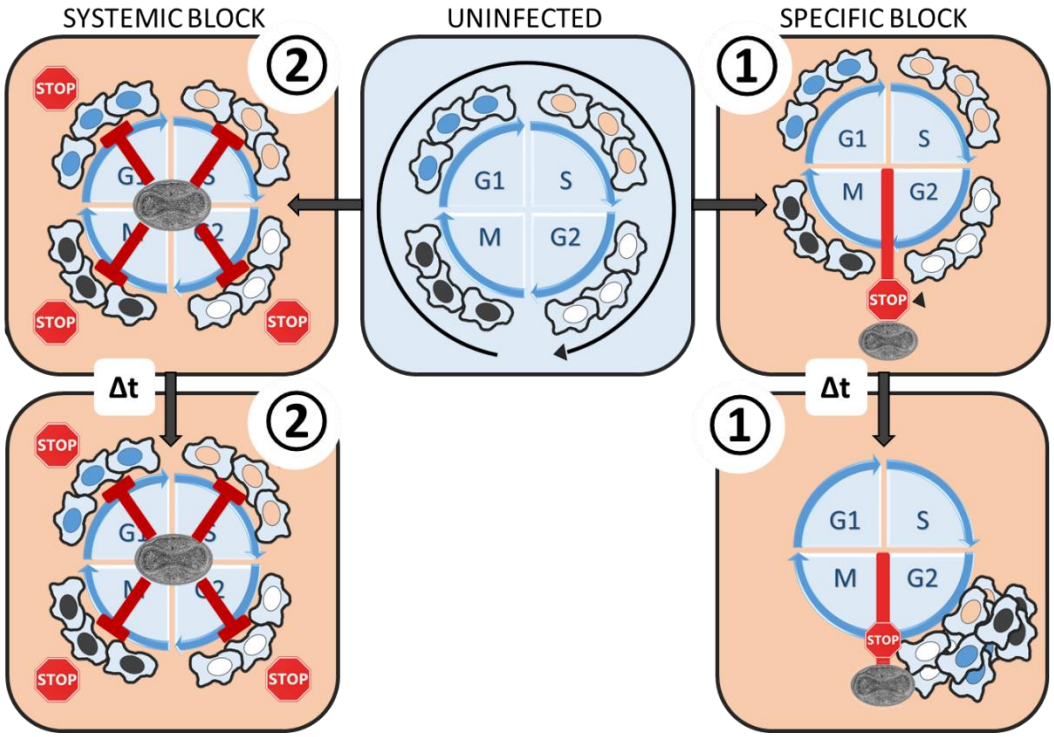

Figure 4-1 Predicted cell cycle distributions for an unspecific and a specific VACV-induced proliferation block.

Asynchronous cell populations are distributed between the four stages of the cell cycle (blue box). The redistribution of virus-arrested cells indicates which phase(s) of the cell cycle are inhibited by VACV infection. If progression of all phases is blocked, the cell cycle distribution is expected to remain unchanged ("systemic block"). On the other hand, if only progression of a specific phase is prevented, trapped cells will accumulate in this stage, and the distribution is expected to shift.

Here, I characterized the cell cycle distribution of unsynchronized cells during VACV infection. The distribution after infection was expected to reflect the nature of the virus-induced block. A systemic block, arresting each phase of the cell cycle individually, was hypothesized not to

change the cell cycle distribution. On the other hand, a specific block was predicted to accumulate cells in a particular cell cycle stage, thereby shifting the distribution (Figure 4-1).

Since I found VACV capable of trapping cells in G1, S, as well as G2, I hypothesised VACV to inhibit cell cycle progression by blocking each cell cycle stage individually. Therefore, my findings predicted no change in cell cycle distribution during VACV infection. Conversely, published reports suggested VACV to shift cells into S phase, indicating a specific block (Wali and Strayer, 1999b; Yoo et al., 2008).

To address this question, the cell cycle distribution of asynchronous HeLa FUCCI cells was monitored during VACV infection. Cells were either mock infected, or infected with WT VACV (MOI 2) and harvested at 0, 2, 4, 6, 8, 10, 12, and 24hpi. The cell cycle distribution was analysed by flow cytometry using the gating strategy outlined above (Figure 3-7): based on their fluorescence pattern, cells were classified as either early G1, G1, early S, or S / G2 / M (Figure 4-2, A, B).

Mock infected populations were measured to accumulate cells in G1, which increased the G1 fraction non-significantly from 23.1 ± 4.3% at 0hpi to 31.1 ± 6.2% at 24hpi (Figure 4-2, D). Concurrently, the amount of cells in S / G2 / M significantly decreased between 0 and 24hpi (Figure 4-2, F). Whereas this fraction represented 17.2 ± 2.2% of mock infected cells at 0hpi, it made up only 10.1 ± 2.1 % at 24hpi. Neither the early G1, nor the early S phase fraction was found to fluctuate significantly in mock infected samples (Figure 4-2, C, E).

Conversely, VACV infected samples showed the opposite trend: the fraction of S / G2 / M cells nearly doubled from 17.2 ± 2.2% of the infected cell population at 0hpi to 31.3 ± 2.9% at 24hpi (Figure 4-2, F). This significant increase occurred at the expense of G1 cells which decreased from representing 23.1 ± 4.3% of total cells at 0hpi, to 18.7 ± 4.0 % at 24hpi (Figure 4-2, D). Additionally, fewer cells were measured in early G1 as infection progressed, indicating either reduced G1 entry, or faster transit through G1.

Concluding, using the FUCCI reporter system, I found that VACV significantly shifted the cells from the G1 phase of the cell cycle into the S / G2 / M phase by 24hpi. On the other hand, mock infected cells showed the opposite trend and shifted from S / G2 / M into G1.

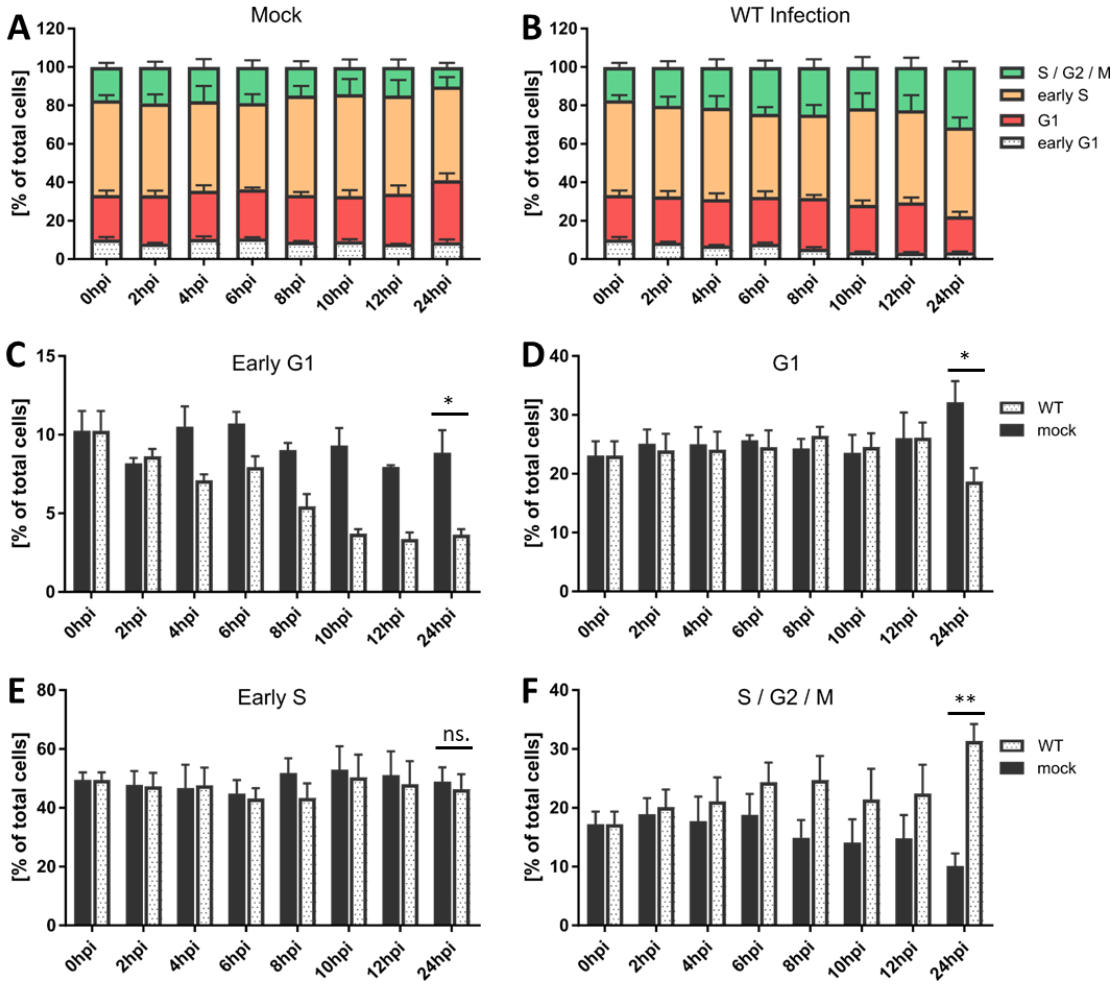

Figure 4-2 VACV infection increases the S / G2 cell fraction.

HeLa FUCCI cells were either mock infected, or infected with WT VACV (MOI 2) and harvested at 0, 2, 4, 6, 8, 10, 12, and 24hpi. Using flow cytometry, cells were classified as early G1, G1, early S, or S / G2 / M. [A-B] Combined cell cycle distribution of mock, and WT VACV infected samples, respectively. Individual cell cycle fractions are compared in [C-F]. [C] Percentage of early G1, [D] G1, [E] early S, and [F] S / G2 / M cell fractions in mock (black bars) and WT VACV (white bars) infected samples. Data represent three biological replicates with one technical replicate each and are displayed as mean ± S.E.M. Parametric, unpaired, two-tailed t-test for significance. ns. $p > 0.05$, * $p < 0.033$, ** $p < 0.0021$, *** $p < 0.0002$, **** $p < 0.0001$.

Since mock infected cells continue to proliferate, they grow denser and slowly deplete the available nutrients during the infection timecourse. These suboptimal growth conditions

might explain the increased fraction of cells in the resting state G1 at 24hpi. On the other hand, VACV infection shifted cells into the S / G2 / M fraction while inhibiting overall cell proliferation. These observations support two different models for how VACV modulates the host cell cycle (Figure 4-3) . First, VACV induces a specific block in the S or G2 phase of the cell cycle, but does not affect cells in G1. As cells progress from G1 they are trapped in S and/or G2, which causes a shift in the cell cycle distribution. Second, the VACV induced cell cycle shift and block are two individual steps. Infection first establishes a (systemic) cell cycle block and only then shifts the cells into the S and/or G2 phase.

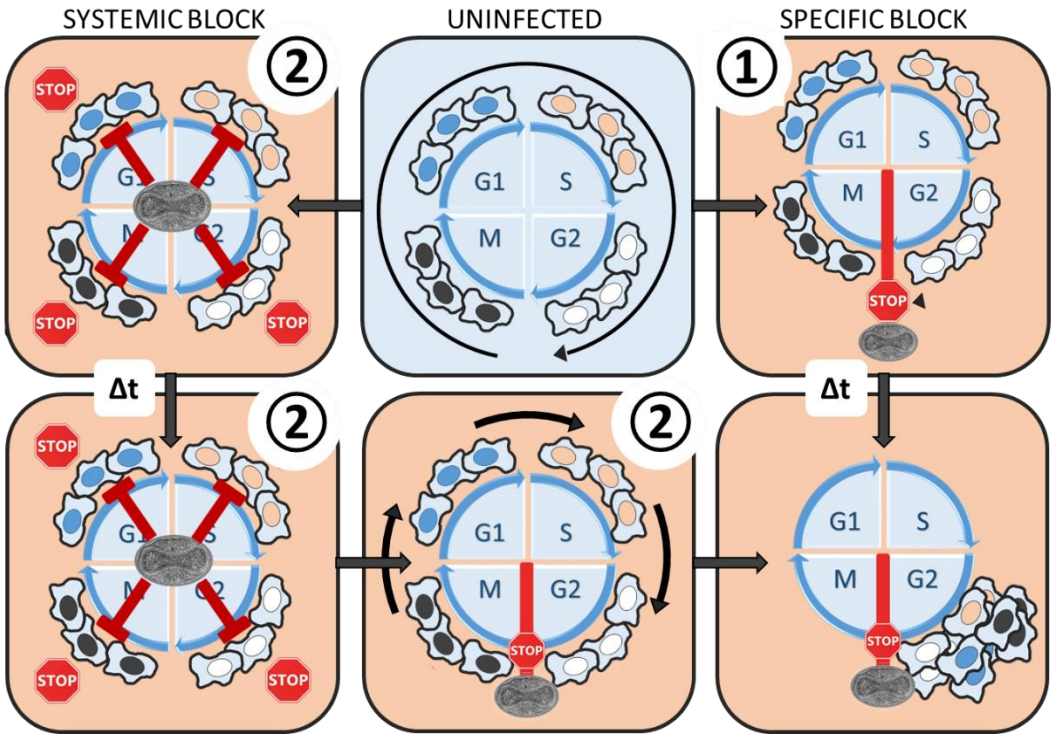

Figure 4-3 Two models of how VACV infection alters the cell cycle distribution.

VACV accumulates infected cells in the S/G2/M phases of the cell cycle. This shift in cell cycle distribution could either be achieved in a single step by specifically trapping infected cells in S/G2/M, or in two distinct steps where cells are first arrested non-specifically in their current phase before being shifted into S/G2/M.

The FUCCI system makes use of the antiphasic expression of the two cell cycle regulators Geminin and Cdt1 (please refer to Chapter 3). The stable HeLa FUCCI cell line exogenously expresses fluorescently tagged fragments of human Geminin (mAG-hGem(1-100), green) and

Cdt1 (mKO2-hCdt1(30-120), red). Using this cell line as a cell cycle reporter, I found VACV to shift cells from G1 into the S / G2 / M phase of the cell cycle. To confirm that the shift was not an artefact of exogenously expressing Geminin and Cdt1, I measured the endogenous protein levels in HeLa cells during VACV infection. To this end, asynchronous HeLa cells were either mock infected, or infected with WT VACV (MOI 2) and harvested at 0, 1, 2, 4, 5, 6, 8, 10, and 24 hpi. Whole cell lysates were resolved via SDS-PAGE and immunoblotted for Geminin, Cdt1, and α-Tubulin as loading control (Figure 4-4, A, B). The protein abundance was quantified, corrected for the total loading amount, and normalized to the baseline level at 0hpi (Figure 4-4, C, D). Confirming the results measured with the HeLa FUCCI cell line, VACV infection decreased Cdt1 levels (G1) while increasing Geminin levels (S / G2 / M) at 24hpi compared to 0hpi.

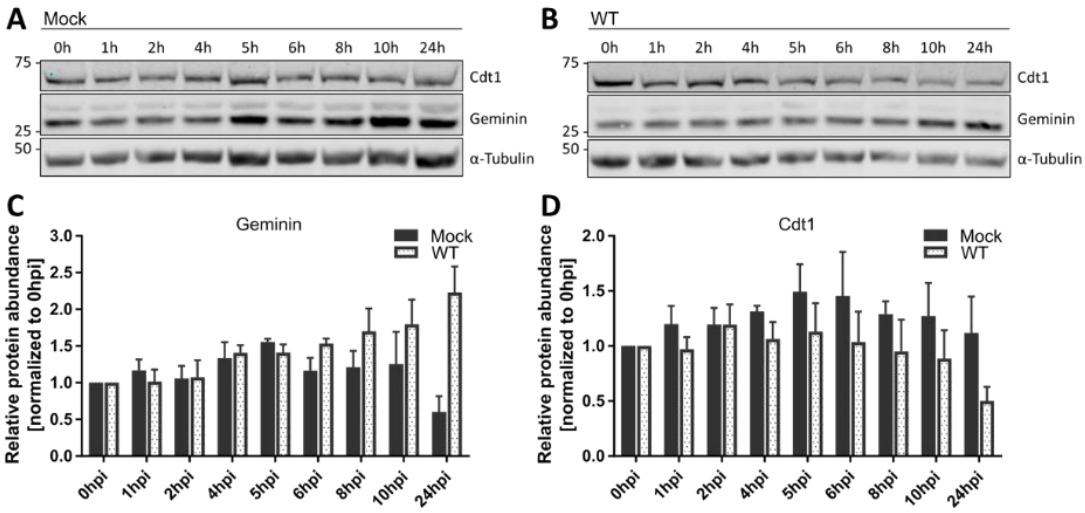

Figure 4-4 Geminin and Cdt1 protein levels during VACV infection.

Asynchronous HeLa cells were either mock infected, or infected with WT VACV (MOI 5) and samples were harvested at 0, 1, 2, 4, 5, 6, 8, 10, and 24 hpi. Whole cell lysates were resolved via SDS-PAGE and immunoblotted for Geminin, Cdt1, and α-Tubulin as loading control. [A-B] A representative blot of three biological replicates is shown. [C-D] Protein abundance was quantified and normalized to 0hpi. Data represent three biological replicates with one technical replicate each and are displayed as mean ± S.E.M.

2 VACV infection alters the abundance of cell cycle regulatory proteins

In the previous section I showed that VACV infection shifts the cell cycle from G1 into S/G2/M. To gain more mechanistic understanding of this virus-induced change, I next investigated whether infection also altered the expression of cell cycle regulating proteins. Progression of the cell cycle is tightly regulated by intra- and extracellular factors, including five different cellular cyclin-dependent kinases (CDKs): CDK4 and CDK6 are activated during early G1 before CDK2 is switched on in late G1 to help S phase progression. After completion of S phase, CDK1 takes over and steers the cell cycle from G2 through mitosis. The activity of CDKs is precisely controlled and depends on association with their cyclin partner as well as phosphorylation of the resulting protein complex by the CDK activating kinase (CAK) CDK7. While CDKs are evenly expressed during the cell cycle, cyclin levels change concurrently with the phase of the cell cycle. The timed waves of cyclin expression and proteasomal degradation periodically activate the CDKs (Bagga and Bouchard, 2014; Harper and Brooks, 2005; Vermeulen et al., 2003). The D-type Cyclins (D1, D2, and D3) promote entry into G1 by activating CDK4 and CDK6 (Sherr, 1993, 1994). Next, CyclinE is required to associate with CDK2 to enable transition from G1 into S phase (Ohtsubo et al., 1995). As the cell cycle continues, CyclinE is exchanged for CyclinA, which further drives S phase progression. During G2, CyclinA dissociates from CDK2 and binds to CDK1 instead which commits the cells to enter mitosis. Completion of mitosis is controlled by CDK1 switching from binding CyclinA to binding CyclinB (Girard et al., 1991; Walker and Maller, 1991).

Previous studies reported that VACV infection changed the expression of cellular proteins involved in cell cycle regulation (Wali and Strayer, 1999b) (Yoo et al., 2008). Reduced CDK4 and CDK6 protein levels in infected 143B osteosarcoma cells at 30hpi were suggested to promote the G1/S transition and thereby facilitate cell cycle progression (Yoo et al., 2008). Similarly, changes in the expression of CDK1, CDK2, CyclinA and CyclinB were proposed to explain the accumulation of S phase cells observed after VACV infection (Wali and Strayer, 1999b). Protein levels of CyclinA and CDK1 decreased late in infection (12 -60hpi), which was also reflected by a reduction in CDK1 mRNA levels. Protein and mRNA levels of CyclinB and CDK2 were initially upregulated before also dropping below uninfected control levels later in infection (12-60hpi). Concluding, these studies indicate that VACV infection changes cell cycle progression by altering the expression of cellular regulatory proteins.

However, both reports were biased towards late stages of infection and data either reflects a single 30hpi timepoint, or a timecourse measured at 4, 8, 12, 24, 36, 48, and 60hpi. Additionally, in either study cells were synchronized in G1 by serum starvation before being infected with VACV, therefore the observed changes do not necessarily reflect the infection of

an unperturbed, asynchronous cell population. Generalized conclusions were further hampered by technical limitations such as antibody specificity and detection sensitivity (Wali and Strayer, 1999b). Therefore, I next characterized how the protein levels of cell cycle regulators changed in asynchronous cells during early stages of VACV infection.

2.1 Alterations of G1-associated cellular protein levels

First, I measured the protein levels of the G1-associated cellular proteins CyclinD, CDK4, CDK6 and the CAK CDK7 during VACV infection. Unsynchronized HeLa cells were either mock infected, or infected with WT VACV (MOI 5) and samples were harvested at 0, 1, 2, 4, 5, 6, 8, 10, and 24hpi. Whole cell lysates were resolved via SDS-PAGE and immunoblotted for CyclinD, CDK4, CDK6, CDK7, and α-Tubulin (Figure 4-5, A-C). Protein abundance was either measured by near-infrared fluorescence intensity (LI-COR) (Figure 4-5, A, B) , or by chemiluminescence intensity (ECL) (Figure 4-5, C) for low abundance proteins and the intensities were internally normalized against the corresponding loading control α-Tubulin. To visualize relative changes in protein levels, the samples were further normalized against the 0hpi timepoint (Figure 4-5, D-F).

Contrary to published data, CDK4 levels were not reduced during VACV infection. The large spread of protein levels in both infected and uninfected samples reflect the normal fluctuations in protein levels and indicate that VACV does not regulate the expression of CDK4. On the contrary, CDK6 levels at 24hpi were reduced 2-fold compared to 0hpi, confirming previously published reports. Similar to CDK4, the levels of CyclinD expression varied considerably between different repeats both in mock and infected samples (Figure 4-5, C). The lack of a clear trend suggests that infection does not modulate CyclinD expression. Similarly, CDK7 expression was not observed to be regulated by VACV and CDK7 levels were found to increase throughout the timecourse both in infected and uninfected samples. Concluding, I found that VACV infection reduces CDK6 levels over 24hpi while having no effect on the other assessed G1-associated proteins CDK4, CDK7, and CyclinD.

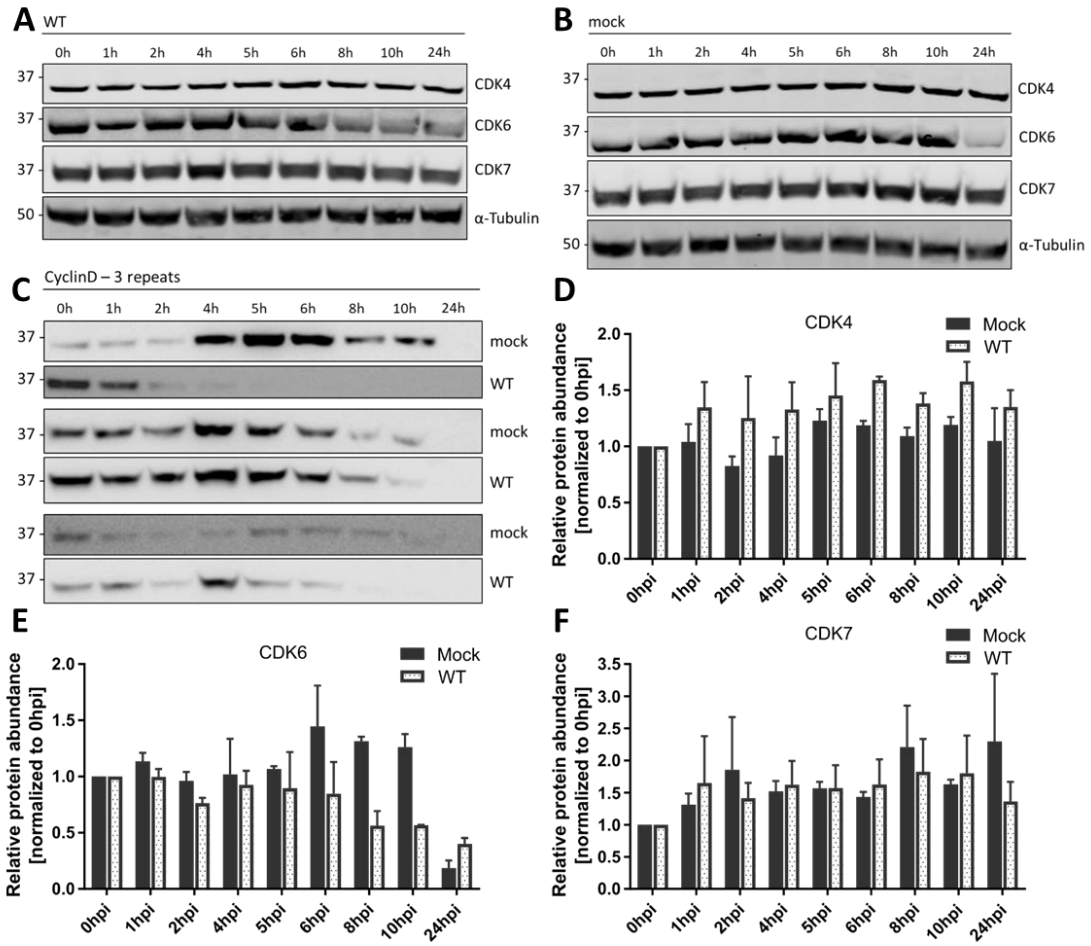

Figure 4-5 Alterations of G1-associated cellular protein levels.

Unsynchronized HeLa cells were either mock infected, or infected with WT VACV (MOI 5) and samples were harvested at 0, 1, 2, 4, 5, 6, 8, 10, 24hpi. Whole cell lysates were resolved via SDS-PAGE and immunoblotted for CDK4, CDK6, CDK7, CyclinD, and α-Tubulin as loading control. [A-B] A representative blot of three (CDK4), or two (CDK6), or one (CDK7) biological replicates is shown. [C] The blots from 3 biological repeats are shown for CyclinD. [D-F] Protein abundance of infected samples was quantified and normalized to 0hpi. Data represent three (CDK4, CDK7 WT), or two (CDK6, CDK7 mock) biological replicates with one technical replicate each and are displayed as mean ± S.E.M.

2.2 Alterations of S phase associated protein levels

Next, I measured the protein levels of the S phase associated cellular proteins CyclinE, and CDK2 during VACV infection. As described before, unsynchronized HeLa cells were either mock infected, or infected with WT VACV (MOI 5) and samples were harvested at 0, 1, 2, 4, 5, 6, 8, 10, and 24hpi. Whole cell lysates were resolved via SDS-PAGE and immunoblotted for CyclinE, and CDK2 (Figure 4-6, A, B). Protein abundance was measured by near-infrared fluorescence intensity (LI-COR) and the intensities were internally normalized against the corresponding α-Tubulin loading control. To visualize relative changes in protein levels, the samples were further normalized to the 0hpi timepoint (Figure 4-6, C, D).

Contrary to previous reports, I did not observe any significant changes in CDK2 levels after VACV infection (Figure 4-6, C). The protein levels in both infected and uninfected samples fluctuated to a comparable extent over 24hrs, indicating that VACV does not regulate the expression of CDK2. Similarly, the levels of CyclinE expression varied considerably between different repeats, both in infected and uninfected samples (Figure 4-6, D). The absence of a significant trend suggests that infection does not affect CyclinE expression. Concluding, these findings show that VACV infection does not influence expression S phase-associated proteins CDK2, and CyclinE.

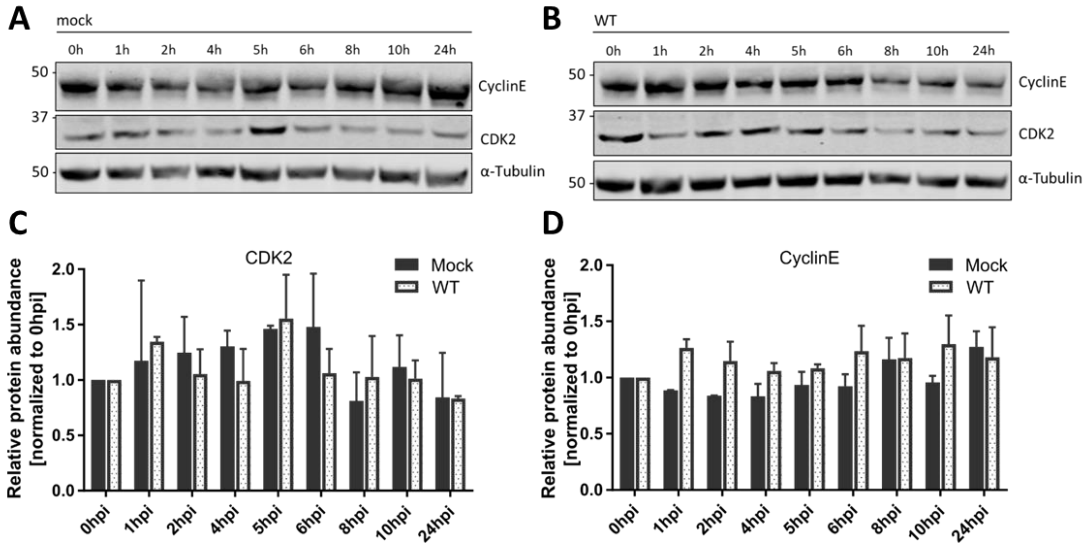

Figure 4-6 Alterations of S phase-associated cellular protein levels.

Unsynchronized HeLa cells were either mock infected, or infected with WT VACV (MOI 5) and samples were harvested at 0, 1, 2, 4, 5, 6, 8, 10, 24hpi. Whole cell lysates were resolved via SDS-PAGE and immunoblotted for CyclinE, CDK2, and α-Tubulin as loading control. [A-B] A representative blot of three biological replicates is shown. [C-D] Protein abundance of WT infected samples was quantified and normalized to 0hpi. Data represent three (cyclin E), or two (CDK2) biological replicates with one technical replicate each and are displayed as mean ± S.E.M.

2.3 Alterations of G2/M phase associated protein levels

Next, I measured the protein levels of the G2 and M phase associated cellular proteins CyclinA, CyclinB, and CDK1 during VACV infection. Additionally, I monitored the level of CDK1 phosphorylation on Tyr15 which inhibits CDK1 activity (Booher et al., 1997; Liu et al., 1997). As described before, unsynchronized HeLa cells were either mock infected, or infected with WT VACV (MOI 5) and samples were harvested at 0, 1, 2, 4, 5, 6, 8, 10, and 24hpi. Whole cell lysates were resolved via SDS-PAGE and immunoblotted for CyclinA, CyclinB, CDK1, and pCDK1 Tyr15 (Figure 4-7, A, B). Protein abundance was measured by near-infrared fluorescence intensity (LI-COR) and the intensities were internally normalized against the corresponding α-Tubulin loading control. To visualize relative changes in protein levels, the samples were further normalized to the 0hpi timepoint (Figure 4-7, C-F).

Contrary to published data, neither CDK1, nor CyclinB levels differed significantly between uninfected and VACV infected cells (Figure 4-7, D, E). CDK1 protein levels in both infected and uninfected conditions fluctuated to a comparable extent over 24hrs, indicating that VACV does not regulate the expression of CDK1.

While total CDK1 levels remained unchanged, the proportion of CDK1 phosphorylated on Tyr15 showed opposing trends in infected versus uninfected samples (Figure 4-7, F, G). 1h after infection, the inhibitory phosphorylation initially dipped below 0hpi baseline levels, and then gradually increased up until 4hpi where levels stayed 2.5-fold elevated compared to 24hpi mock. In contrast, uninfected cells initially showed an increase between 0 and 4hpi, before CDK1 Tyr15 was steadily dephosphorylated to reach 36.7 ± 0.1 % of initial levels at 24hpi.

In line with previous reports, between 0 and 10hpi CyclinA levels were consistently decreased in infected samples, compared to the respective mock controls (Figure 4-7, C). CyclinA expression gradually dropped below baseline levels from 6hpi onwards. At 24hpi, CyclinA levels were comparable in infected and uninfected cells. As discussed before, while infected samples arrest, uninfected samples continue to proliferate, grow denser and slowly deplete the available nutrients during the infection timecourse. These suboptimal growth conditions might explain the decreased CyclinA levels in mock samples at 24hpi.

Summarizing, infection decreased CyclinA levels from 6hpi onwards, while expression of CyclinB was not affected. Additionally, VACV did not alter total CDK1 levels compared to mock

infection but was found to cause increased phosphorylation on CDK1 Tyr15, which inhibits CDK1 activity.

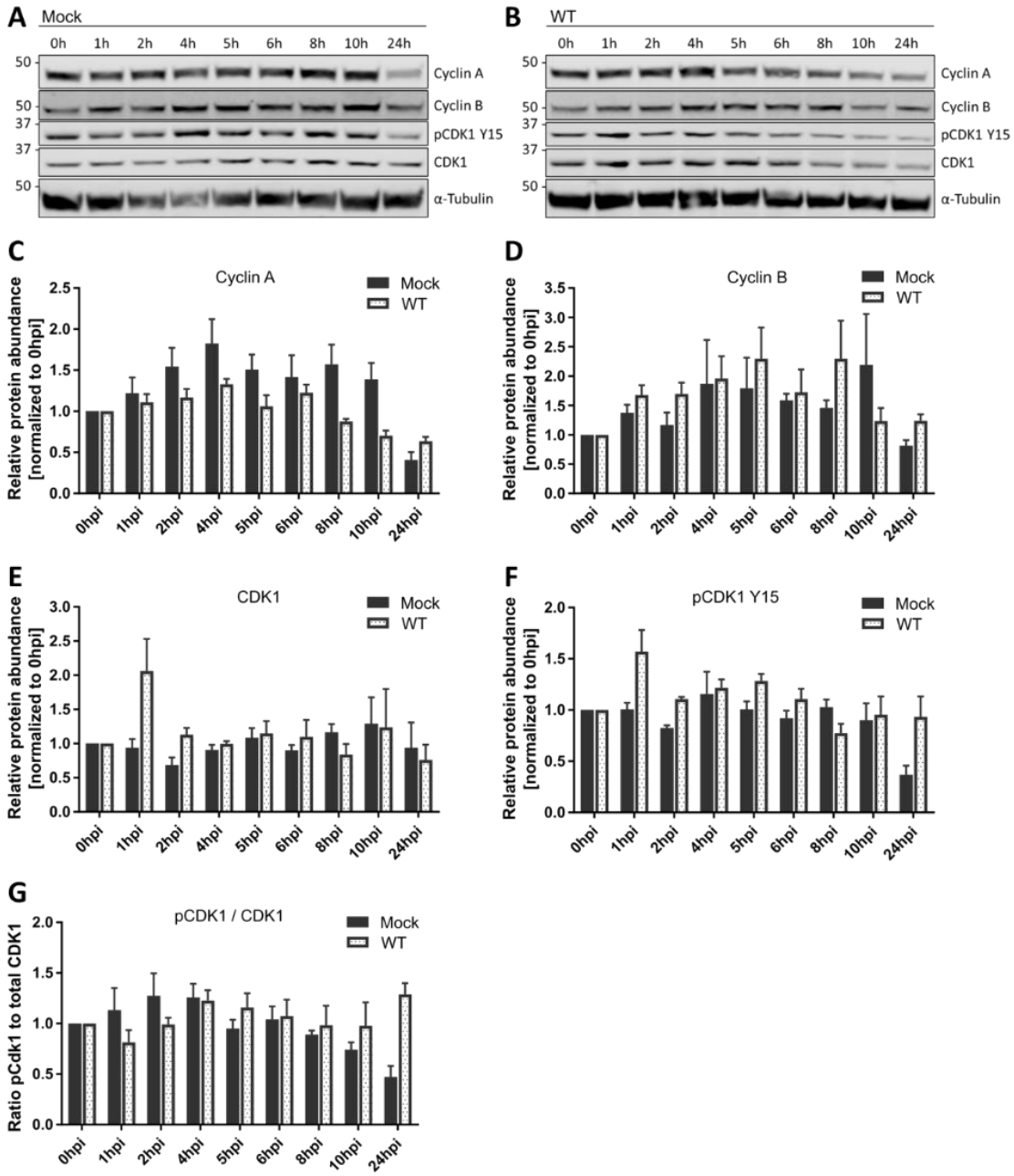

Figure 4-7 Alterations of G2/M phase-associated cellular protein levels.

Unsynchronized HeLa cells were either mock infected, or infected with WT VACV (MOI 5) and samples were harvested at 0, 1, 2, 4, 5, 6, 8, 10, 24hpi. Whole cell lysates were resolved via SDS-PAGE and immunoblotted for CyclinA, CyclinB, CDK1, pCDK1 Y15, and α-Tubulin as loading control. [A-B] A representative blot of three biological replicates is shown. [C-F] Protein abundance of mock and WT infected samples was quantified and normalized to 0hpi. [G] The amount of phosphorylated CDK1 is plotted as the ratio of pCDK1 Y15 and CDK1. Data represent three biological replicates with one technical replicate each and are displayed as mean ± S.E.M.

3 Viral late gene expression is required to shift the cell cycle

Having shown that infection alters the cell cycle distribution, I next aimed to determine how VACV shifts the cells from G1 into the S/G2 phases. To gain better understanding of the viral requirements, I probed the virus life cycle with recombinant VACV mutants, and siRNAs silencing essential viral genes.

3.1 VACV early gene expression is required to shift the cell cycle

First, I tested whether the host cell cycle shift required expression of viral early genes. To address this question, I monitored the cell cycle changes during infection with the inducible H1 VACV (v*ind*H1 (Liu et al., 1995)). As described before, the viral phosphatase H1 is essential for transcriptional competence of the virus by regulating the VACV early transcription factor A7 (Liu et al., 1995; Novy et al., 2018). Growing the virus without the inducer IPTG produces transcriptionally incompetent H1(-) virions, which enter the host cell but are severely attenuated for early gene expression. Virus prepared in the presence of the inducer IPTG [H1(+)], is fully replicative and shows normal viral gene expression levels, as long as IPTG is present in the medium.

Asynchronous HeLa FUCCI cells were infected with either H1(-) (MOI eq. 2, -IPTG), or parental H1(+) (MOI 2, + IPTG) and harvested at 0, 2, 4, 6, 8, 10, 12, and 24hpi. The cell cycle distribution was determined by flow cytometry using the gating strategy outlined above (Figure 3-7): based on their fluorescence pattern, cells were classified as either early G1, G1, early S, or S/G2/M (Figure 4-8).

As previously observed with WT virus, H1(+) infection nearly doubled the fraction of S / G2 / M cells from 17.2 ± 2.2% of the infected cell population at 0hpi to 33.7 ± 3.2% at 24hpi (Figure 4-8, F). This significant increase occurred at the expense of G1 cells: whereas this fraction represented 23.1 ± 2.5% of total cells at 0hpi, it made up only 16.9 ± 1.4% at 24hpi (Figure 4-8, D). Additionally, fewer cells were measured in early G1 as infection progressed, indicating either reduced G1 entry, or faster transit through G1 (Figure 4-8, C).

Conversely, H1(-) infected populations were measured to accumulate cells in G1, which increased the G1 fraction significantly from 23.1 ± 2.5% at 0hpi to 32.0 ± 3.5% at 24hpi (Figure 4-8, D). The S/G2/M fraction remained unchanged after 24h of H1(-) infection (Figure 4-8, F).

Neither the early G1, nor the early S phase fraction was found to fluctuate significantly in H1(-) infected samples (Figure 4-8, C, E).

In summary, H1(+) VACV caused a redistribution from G1 into the S/G2/M phase by 24hpi. On the other hand, H1(-) infection failed to shift cells into S/G2/M but caused an accumulation in G1 instead.

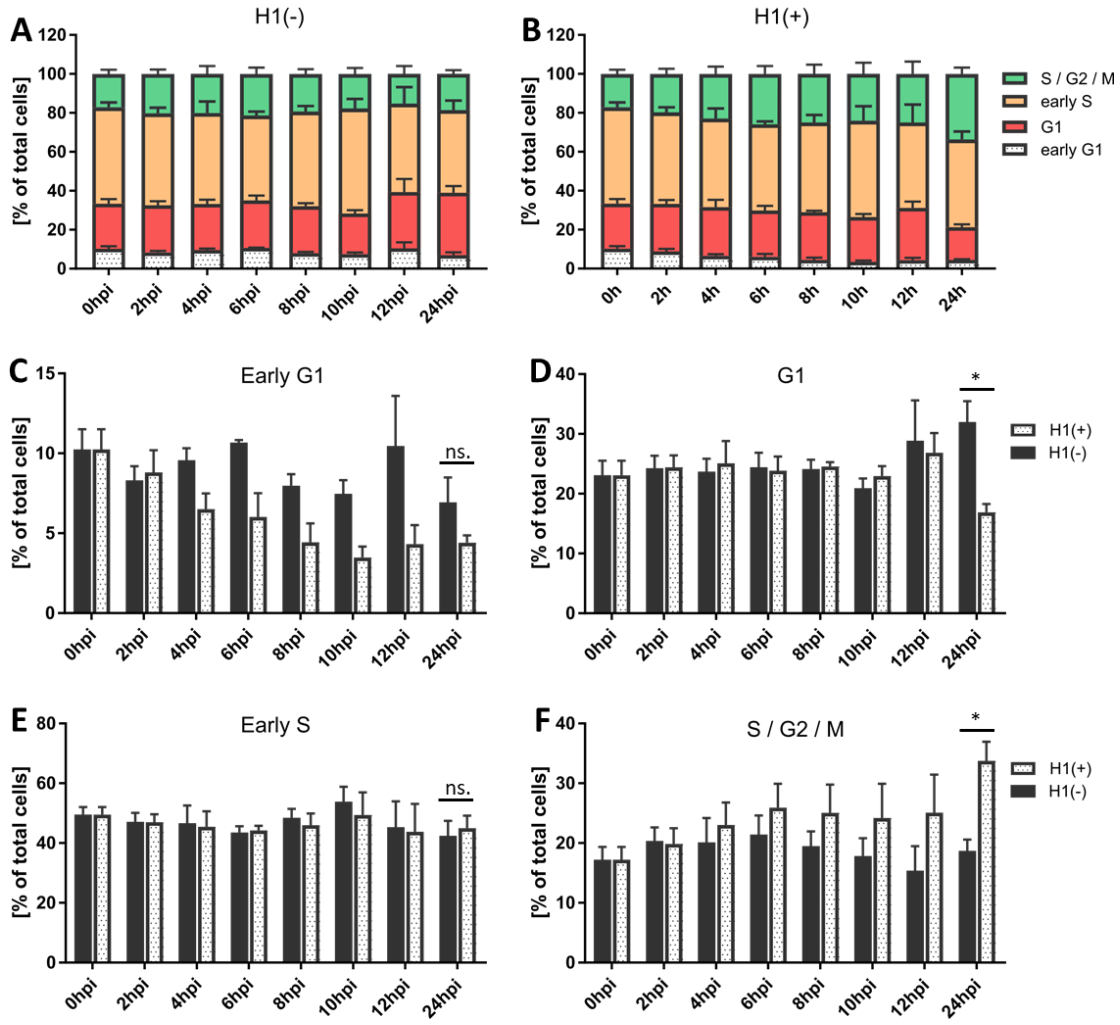

Figure 4-8 The viral phosphatase and/or viral early gene expression is required to shift the host cell cycle.

HeLa FUCCI cells were either mock infected, or infected with H1(-) (MOI eq 2, - IPTG), or parental H1(+) VACV (MOI 2, +IPTG). Samples were harvested at 0, 2, 4, 6, 8, 10, 12, and 24 hpi. [A-B] Combined cell cycle distribution of H1(-), and H1(+) VACV infected samples, respectively. Individual cell cycle fractions are compared in [C-F]. Percentage of cells in early G1 [C], G1 [D], early S [E], and S / G2 / M [F] in H1(-) (black bars) and H1(+) VACV (white bars) infected samples. Data represent three biological replicates with one technical replicate each and are displayed as mean ± S.E.M. Parametric, unpaired, two-tailed t-test for significance. ns. $p > 0.05$, * $p < 0.033$, ** $p < 0.0021$, *** $p < 0.0002$, **** $p < 0.0001$

Next, I compared the cell cycle distribution of mock and WT infected cells with the distribution observed after H1(+), and H1(-) infection, respectively (Figure 4-9). WT and H1(+) were found to be identical in their ability to shift the cell cycle, both causing significant increase in the S/G2/M fraction at the expense of the G1 fraction (Figure 4-9, B, D) . On the other hand, H1(-) cell cycle distribution mirrors the pattern observed in mock infected controls: cells accumulated in the G1 phase and failed to shift into S/G2/M. Distinguishing H1(-) from uninfected samples, the S/G2/M cell population remained unchanged after virus addition between 0 and 24hpi, whereas it was reduced in mock controls (Figure 4-9, D).

Concluding, deletion of the viral phosphatase H1 rescues the WT VACV induced S/G2/M cell cycle shift. This suggests that either H1 itself is essential, or that a step post viral entry is required to shift the cell cycle.

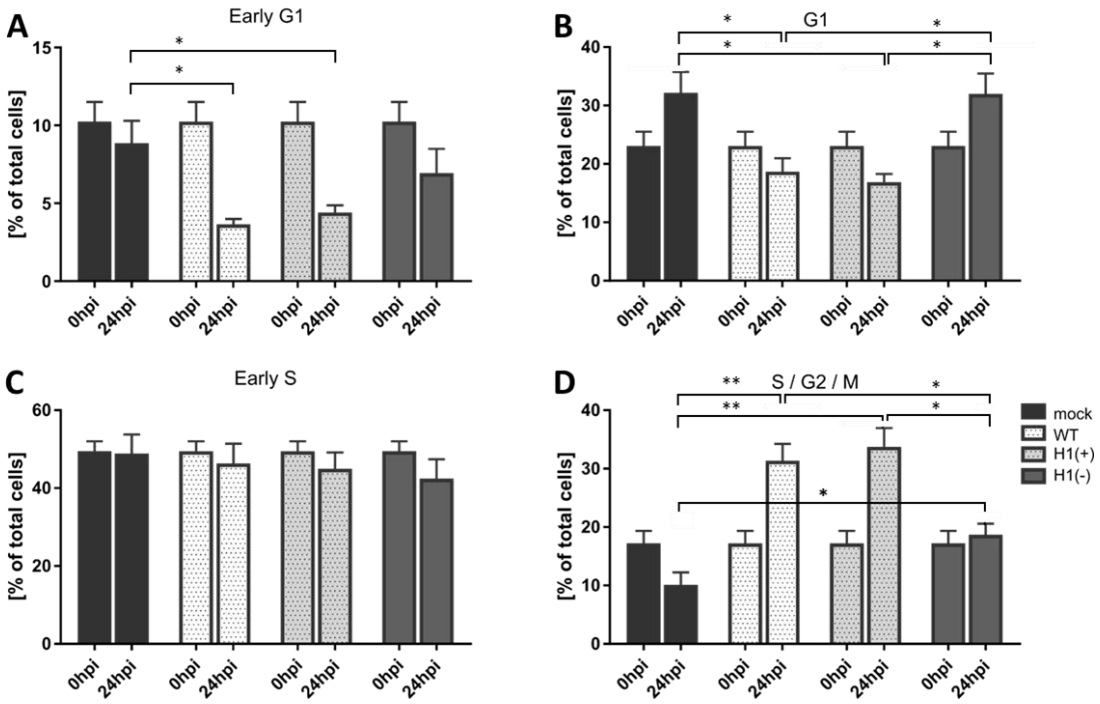

Figure 4-9 Cell cycle distribution after mock, WT, H1(+) and H1(-) infection.

This figure summarizes the cell cycle changes between 0 and 24hpi as described in section 1 and section 2.1. [A-D] Individual cell cycle fractions of mock, WT, H1(-), and H1(+) (MOI 2) infected samples are compared. Percentage of cells in early G1 [A], G1 [B], early S [C], and S / G2 / M [D]. Data represent three biological replicates with one technical replicate each and are displayed as mean ± S.E.M. Parametric, unpaired, two-tailed t-test for significance. ns. $p > 0.05$, * $p < 0.033$, ** $p < 0.0021$, *** $p < 0.0002$, **** $p < 0.0001$

3.2 VACV late gene expression is required to shift host cells into S / G2

Infection with H1(-) indicated that either the phosphatase H1 itself or a step post viral entry was required to shift the host cell cycle. Therefore, I aimed to determine whether viral genome uncoating, and/or viral intermediate gene expression was required to accumulate cells in S/G2/M. To address this question, I monitored the cell cycle distribution upon inhibition of either viral genome uncoating, or viral intermediate and late gene expression. The viral AAA+ ATPase D5 (siD5R), and the viral DNA-dependent RNA polymerase subunit A24 (siA24R) were silenced by siRNA knockdown (Figure 4-10, E). As described before, loss of the uncoating factor D5 inhibits core degradation but allows for viral early gene expression (Kilcher et al., 2014). As part of the DNA-dependent RNA polymerase polypeptide, A24 directs viral early, intermediate, and late gene transcription (Baroudy and Moss, 1980; Hooda-Dhingra et al., 1990). Nonetheless, siRNA knockdown of A24 does not inhibit viral early transcription, since the polymerase complex is pre-packaged in the virus core, ready to transcribe early genes before uncoating (Baroudy and Moss, 1980; Resch et al., 2007). On the other hand, viral late, and probably intermediate transcription require de novo expression of A24 during infection (Hooda-Dhingra et al., 1990).

HeLa FUCCI cells were reverse transfected with scrambled control siRNA (Scr), siD5R, or siA24R. After 48h, cells were either mock infected, or infected with WT VACV (MOI 1). Samples were harvested at 0, 7, 10, and 24hpi and the cell cycle distribution was analysed by flow cytometry as outlined above (Figure 3-7): based on their fluorescence pattern, cells were classified as either early G1, G1, early S, or S / G2 / M (Figure 4-10). Knockdown of D5 and A24 was indirectly confirmed by immunoblot analysis of the viral early protein I3, and the late viral protein F17 (Figure 4-10, F). While viral early genes are expressed before uncoating, late viral gene transcription requires replication of the released genome (Oda and Joklik, 1967). Therefore, viral late but not early gene transcription is dependent on D5 expression. As discussed above, A24R silencing also allows for early gene expression, while late gene expression is inhibited. D5R and A24R silencing was confirmed by expression of early I3 and the absence of late F17.

Reverse transfection of scrambled siRNA did not affect the cell cycle distribution in mock, or in VACV infected cells. As observed before, infected cells were found to shift from G1 into S/G2/M which made up 33.1 ± 1.0% of the cell population by 24hpi. However, silencing of either D5R, or A24R resulted in failure of the virus to accumulate cells in S/G2/M, leaving this fraction to represent ca. 20% of total cells at all assessed timepoints (Figure 4-10, D). Opposite

to the scrambled WT control, knockdown of either D5, or A24 resulted in accumulation of cells in G1 at the expense of early S phase between 0-10hpi: compared to 0hpi, the G1 fraction increased from 31.8 ± 2.0% to 53.9 ± 2.7% (siD5R), and to 49.3 ± 8.1% (siA24R), respectively at 7hpi (Figure 4-10, B). Concurrently, the S phase fraction was sharply reduced from 38.0 ± 1.1% to 21.4 ± 3.0% in siD5R samples, and more moderately to 27.8 ± 7.1% in siA24R samples (Figure 4-10, C). By 24hpi, the distribution returned to initial S phase levels in both siRNA conditions. In summary, knockdown of either D5 or A24 inhibits the virus-induced increase of the S/G2/M fraction.

Concluding, since viral early gene expression and replication were found to be insufficient to accumulate cells in S/G2/M, this indicates that a viral late (or intermediate) gene product is essential for inducing the shift.

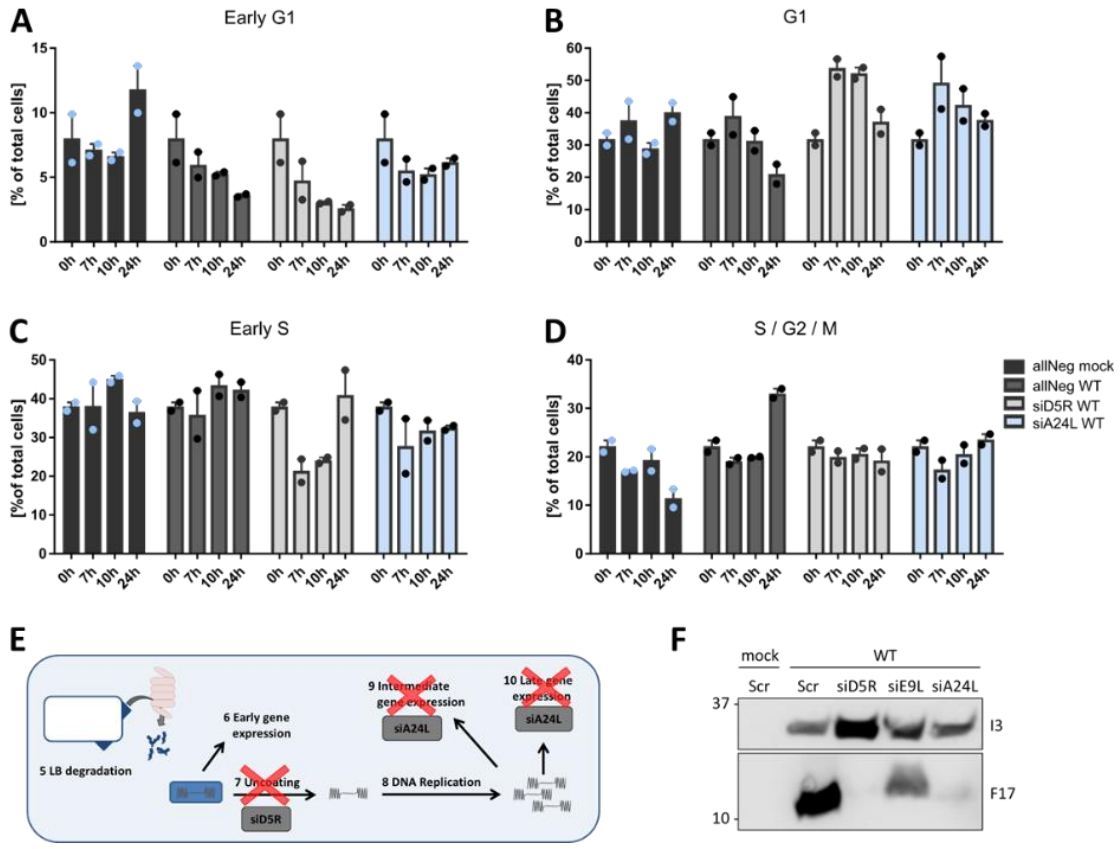

Figure 4-10 Expression of viral late genes is required to shift the host cell cycle. Asynchronous

HeLa FUCCI cells were reverse transfected with a scrambled siRNA control, siD5R, or siA24R (40 nM final). Cells were either mock infected, or infected with WT VACV (MOI 1) and samples were harvested at 0, 7, 10, and 24hpi. The cell cycle distribution was determined by flow cytometry. [A-D] Individual cell cycle fractions of Scr, siD5R, and siA24R silenced samples. Percentage of cells in early G1 [A], G1 [B], early S [C], and S / G2 / M [D]. [E] Schematic representation of the RNAi inhibited virus life cycle stage. [F] D5, A24, and E9 knockdown validation by immunoblot analysis. Whole cell lysates (24hpi) were resolved via SDS-PAGE and immunoblotted for I3 (viral early gene expression), F17 (viral late gene expression. A representative blot of two biological replicates is shown. Data represent two biological replicates with one technical replicate each and are displayed as mean ± S.D.

4 Summary chapter 4

VACV was suggested to increase S phase entry of G1 synchronized cells (Wali and Strayer, 1999b; Yoo et al., 2008), although the viral requirements were not explored. In this chapter, I have demonstrated that VACV shifts unsynchronized cells into S/G2/M and that the shift depends on viral late gene expression. On the other hand, I found in chapter 3 that the VACV-induced cell cycle arrest did only require viral entry and was independent of viral late genes. This indicates that inhibition and shift of the host cell cycle are two distinct viral effects. Considering that the cell cycle arrest is observed prior to the cell cycle shift, and that VACV can arrest cells in G1, S, and G2 phase of the cell cycle, I propose the following two-step model (Figure 4-11): VACV entry freezes the host cell in its current stage of the cell cycle, preventing cellular DNA synthesis and cell proliferation. As the virus starts expressing its late genes, it promotes exit from G1, while still inhibiting overall cell cycle progression, and thereby shifts the cell cycle into S/G2/M.

To gain more molecular understanding of how VACV alters the host cell cycle, I monitored the protein levels of key cell cycle regulators and found reduced expression of CyclinA and CDK6 after 6hpi. Consistent with the known function of CyclinA in S phase progression and M phase entry, reduced CyclinA levels could cause accumulation of infected cells in S/G2/M. CDK6 and its homolog CDK4 regulate the transition from G1 into S phase and reduced expression of CDK6 might contribute to the initial cell cycle arrest by decreasing entry into S phase.

However, as CDKs are consistently expressed during normal cell cycle conditions the protein abundance does not necessarily reflect kinase activity. CDKs are periodically activated by Cyclins and a complex pattern of phosphorylation. Therefore, further experiments characterizing the phospho-status of CDKs are required for a more complete understanding of how VACV manipulates the host cell cycle.

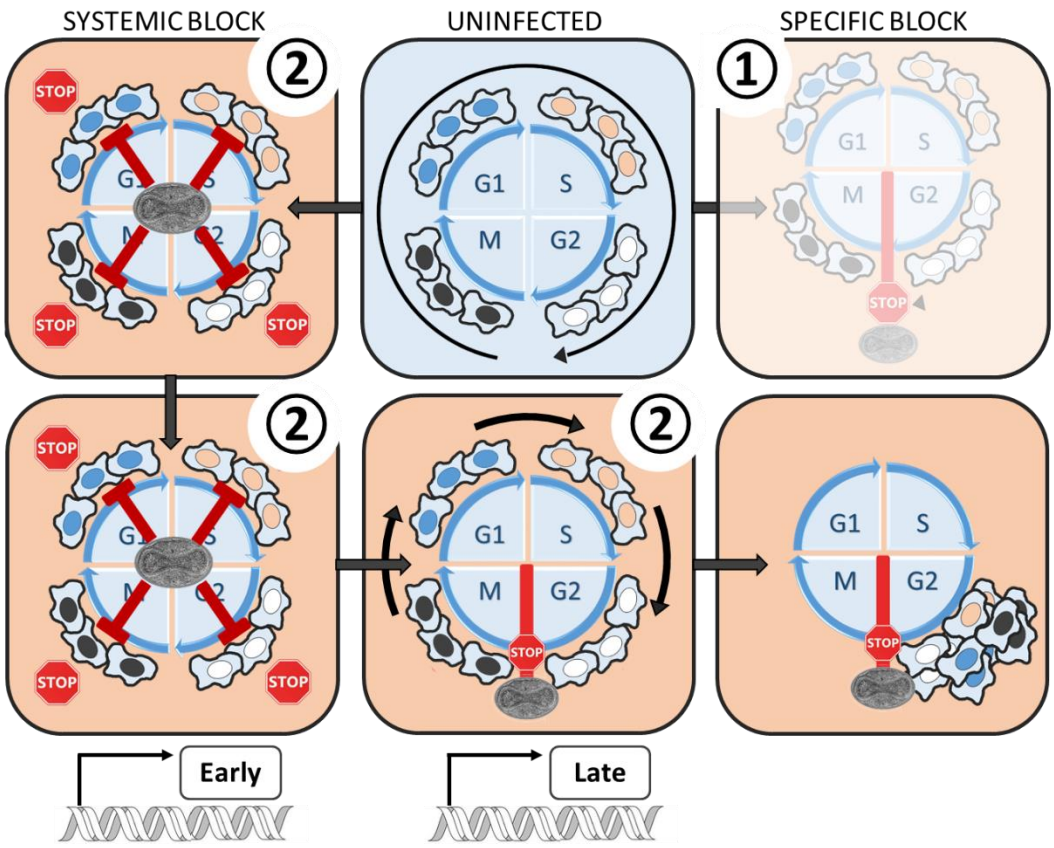

Figure 4-11 Model of VACV-induced cell cycle alterations.

Data discussed in Chapter 3 and 4 indicated that VACV early gene expression or the viral phosphatase H1 establish a systemic cell cycle block, trapping infected cells in their current stage of the cell cycle. As the virus life cycle progresses, expression of an unidentified late viral protein promotes infected cells to transit from G1 into S/G2/M while cell proliferation is still inhibited, thus creating a shift in cell cycle distribution.

5 The viral kinases B1 and F10 modulate host cell cycle checkpoints

In the previous two chapters I have described VACV-induced alterations of the host cell cycle and defined the essential stages of the virus life cycle needed for these. I demonstrated that VACV early gene expression and/or H1 inhibit cell cycle progression after viral entry, and that the second wave of viral gene expression shifts the cell cycle from G1 to S/G2/M, while still inhibiting cell proliferation. However, the relevance of cell cycle subversion for VACV replication and how it is achieved has remained undefined. Therefore, I next aimed to define the essential cellular machinery, as well as the need for cell cycle subversion for the virus life cycle.

The cell cycle serves the purpose of precisely duplicating the genome and dividing it equally into two daughter cells. Highlighting its importance, cell cycle progression is tightly regulated and several molecular checkpoints ensure that cells divide in a controlled manner. Each checkpoint consists of an intricate network of sensor proteins that survey cell cycle progression, and transducer proteins that amplify and propagate the signal to the effector proteins. Sensor proteins are triggered by danger signals such as DNA damage, absence of cell cycle promoting mitogens, or incorrect attachment of chromosomes during mitosis. Activated sensors then induce a complex signalling cascade which can pause or fully arrest the cell cycle machinery, depending on the severity of the incurred damage. If the damage is irreparable and the cell cycle block cannot be resolved, cells will undergo senescence-induced apoptosis (reviewed in (Lukas et al., 2004; Terzi et al., 2016)).

There are four major checkpoints, each operating in a different stage of the cell cycle (cf. Introduction section 3.3): the G1/G0 checkpoint promotes cell cycle exit in the absence of mitogens; the restriction point inhibits transition from G1 to S phase; the DNA damage checkpoint blocks entry into mitosis at the end of G2; and the spindle checkpoint prevents anaphase until all chromosomes are correctly aligned. Since these checkpoints have evolved to arrest cell cycle progression, I decided to investigate whether VACV subverts their molecular machinery to control the host cell cycle during infection. Supporting this hypothesis, previously published data indicate that VACV modulates the G1/S checkpoint (Yoo et al., 2008), and activates the cellular DNA damage response to promote viral genome replication (Postigo et al., 2017).

1 VACV infected cells do not enter G0

Cells have several intrinsic checkpoints where cell cycle progression can be stopped if conditions are not favourable. In the absence of cell cycle stimulating mitogens, or essential nutrients, cells can reversibly exit the cell cycle during G1 and enter the quiescent state G0 (reviewed in (Terzi et al., 2016)). Quiescent cells are hallmarked by CDK inactivity, dephosphorylation of retinoblastoma protein (Rb), reduced levels of the cell cycle regulators proliferating cell nuclear antigen (PCNA) and MCM2, as well as the absence of cell proliferation (Coller et al., 2006; Narasimha et al., 2014; So and Cheung, 2018). Since VACV also caused a non-proliferative state, I assayed whether infection drives cells into quiescence. To address this, I measured the expression of PCNA and MCM2 as markers for quiescence. As the name implies, PCNA identifies proliferating cells and its expression is reduced upon entry into G0 (Zerjatke et al., 2017). Similarly, levels of the DNA replication licencing factor MCM2 remain constant in actively cycling cells but are decreased upon cell cycle exit (Mlcochova et al., 2017; Musahl et al., 1998; Tsuruga et al., 1997).

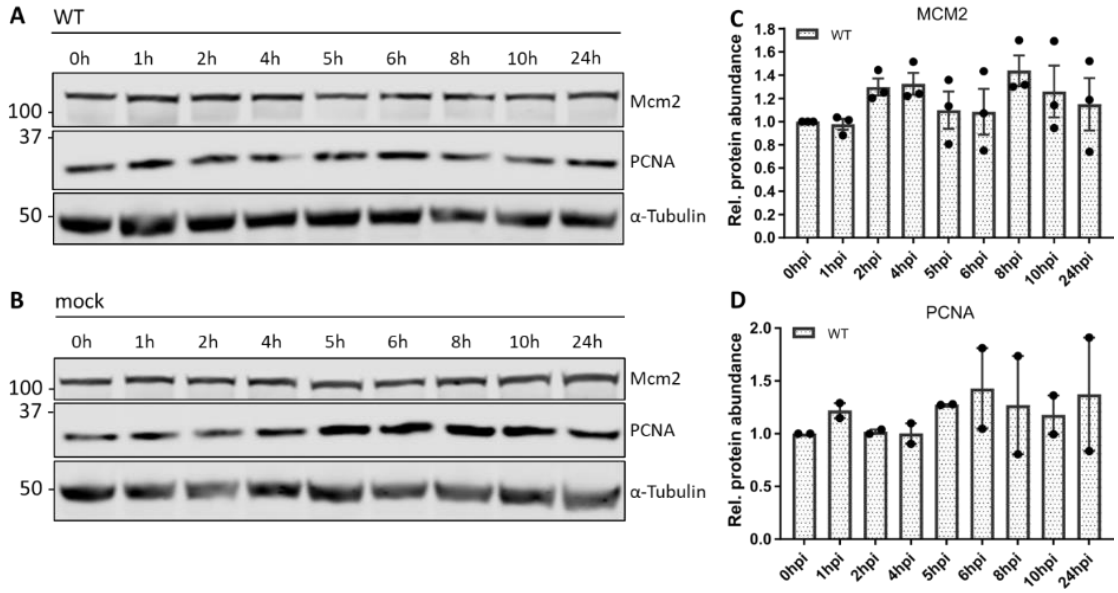

Figure 5-1 VACV infected cells do not enter the quiescent state G0.

Unsynchronized HeLa cells were either mock infected, or infected with WT VACV (MOI 5) and samples were harvested at 0, 1, 2, 4, 5, 6, 8, 10, 24hpi. Whole cell lysates were resolved via SDS-PAGE and immunoblotted for PCNA, MCM2, and α-Tubulin as loading control. [A-B] A representative blot of three (MCM2), or two (PCNA) biological replicates is shown. [C-D] The protein abundance of infected samples was quantified and normalized to 0hpi. Data represent three (MCM2), or two (PCNA) biological replicates with one technical replicate each and are displayed as mean ± S.E.M.

In order to analyse the protein expression during infection, HeLa cells were either mock infected, or infected with WT VACV (MOI 2) and harvested at 0, 1, 2, 4, 5, 6, 8, 10, and 24 hpi. Whole cell lysates were resolved via SDS-PAGE and immunoblotted for MCM2, PCNA, and α-Tubulin as loading control (Figure 5-1, A, B). The protein abundance was quantified, corrected for the total loading amount, and normalized to the baseline level at 0hpi (Figure 5-1, C, D). While expression of both MCM2 and PCNA was found to fluctuate over the period of 24hpi, protein levels never dropped below uninfected levels at 0hpi. This data suggests that VACV does not drive cells into quiescence, and that the infection induced non-proliferative state is distinct from G0.

2 VACV kinase F10 activates the cellular DNA Damage Response

Having shown that infected cells do not exit the cell cycle, I next focused on characterizing how VACV affects the G1/S and G2/M checkpoints. While these checkpoints inhibit different phases of the cell cycle, they are both activated by cellular DNA damage (Figure 1-12). DNA damage can occur in the form of single-strand (ss), or double-strand (ds) DNA breaks. These two branches of the DDR are controlled by the two signal transducing kinases Ataxia telangiectasia and Rad3-related (ATR), and Ataxia-telangiectasia-mutated (ATM), respectively. ssDNA breaks are sensed by the replication protein A (RPA) which coats the exposed ssDNA and assists in the recruitment and activation of ATR (Ashton et al., 2013; Awasthi et al., 2015; Cimprich and Cortez, 2008; Maréchal et al., 2014; Zou and Elledge, 2003). Activated ATR propagates the signal by phosphorylating its effector kinase Chk1 at residues Ser317 and Ser345 (Liu et al., 2000; Zhao and Piwnica-Worms, 2001), thus triggering a biochemical cascade that results in inhibition of S phase progression and prevents M phase entry (reviewed in (Awasthi et al., 2015; Lukas et al., 2004)).

On the other hand, how dsDNA breaks are sensed is not as well-understood. Activation of ATM in response to dsDNA breaks involves recruitment by the Mre11-Rad50-Nbs1 (MRN) complex (Carson et al., 2003; Dupré et al., 2006; Hartlerode et al., 2015; Lee and Paull, 2004, 2005; You et al., 2005). Recruitment by MRN and subsequent acetylation stimulate autophosphorylation of ATM at Ser1981 which is required for full activation and stabilization at sites of DNA damage (Bakkenist and Kastan, 2003; So et al., 2009; Sun et al., 2007). Similarly to the ATR signalling

cascade, ATM escalates the signal by phosphorylating its effector kinase Chk2 at residue Thr68 (Chaturvedi et al., 1999; Matsuoka et al., 1998, 2000), which triggers further downstream events that pause cell cycle progression (reviewed in (Awasthi et al., 2015; Lukas et al., 2004)).

A recent publication linked VACV infection to the cellular DDR in which VACV was shown to trigger canonical ATR signalling in a pre-uncoating step (Postigo et al., 2017). Activation of ATR and its downstream effectors was further suggested to be required for viral genome replication, as pharmacological inhibition of ATR and/or Chk1 prevented viral late gene expression. While ATR was found to be essential for VACV replication, VACV neither seemed to activate, nor to rely on the ATM branch of the DDR. However, it remained unclear how VACV selectively activates ATR and how activation assisted in viral genome replication.

2.1 VACV infection activates the ATR and ATM DNA damage response

The ATR-mediated dsDNA break response was shown to be activated and required for productive VACV infection (Postigo et al., 2017). While it was suggested that ATR and ATR-interacting proteins associated with the viral genome, these findings were not supported by mass spectrometry data published in the same year. While neither ATR nor RPA were found in the viral genome-associated proteome, the MS analysis showed that ATM as well as the ATM recruiting proteins KU70 (XRCC6) and Mre11 are associated with VACV DNA (Reyes et al., 2017). Although these studies reported conflicting results regarding the importance of the ATM and ATR branch, they strongly suggest a link between VACV infection and cellular DDR. Additionally, neither of the studies characterized the involvement of the DDR in the context of cell cycle progression. Therefore, I decided to revisit the changes in DDR signalling during infection and investigate whether activation was involved in VACV-mediated cell cycle arrest.

To address these questions, I first monitored activation of Chk1 and Chk2 during VACV infection. To this end, HeLa cells were either mock infected, or infected with WT VACV (MOI 5) and samples were harvested at 0, 1, 2, 4, 5, 6, 8, 10, and 24hpi. Whole cell lysates were resolved via SDS-PAGE and immunoblotted for phosphorylated Chk1 (Ser345), Chk1, phosphorylated Chk2 (Thr68), Chk2, ATM, a marker for cellular DNA damage (p-γH2AX Ser139), and α-Tubulin as loading control (Figure 5-2, A, B). Total and phosphorylated protein abundance was quantified and normalized to 0hpi, or 24hpi respectively (Figure 5-2, C-F).

In mock infected samples, only low levels of Chk2 activation were observed, whereas no activation of Chk1 was detectable. These findings were also reflected by the absence of cellular DNA damage as was marked by the lack of γH2AX phosphorylation (Figure 5-2, A, B). Conversely, VACV infection promoted robust phosphorylation of Chk1 at residue Ser345, and Chk2 at residue Thr68. While total protein levels for Chk1 and Chk2 were comparable (Figure 5-2, C, E), phosphorylation of Chk1 was less pronounced and was detected later than phosphorylation of Chk2 (Figure 5-2, D, F). In contrast to previously published findings which reported Chk1/2 activation as early as 1hpi, I observed activation of Chk1 and Chk2 only after 8hpi and 6hpi, respectively (Postigo et al., 2017). This discrepancy in timing might either reflect the difference in sensitivity and/or specificity of the two assays. Whereas I directly blot for activating phosphorylation of the kinases, the previous study monitored SQ/TQ motif phosphorylation of Chk1/2 substrates as a proxy for kinase activation. However, my results confirm the previous observation that VACV infection does not incur any cellular DNA damage as there was no significant increase in γH2AX phosphorylation, even after 24hpi.

These findings show that VACV infection promotes phosphorylation and activation of the DDR effector kinases Chk1 and Chk2 during late timepoints of infection, independently of cellular DNA damage.

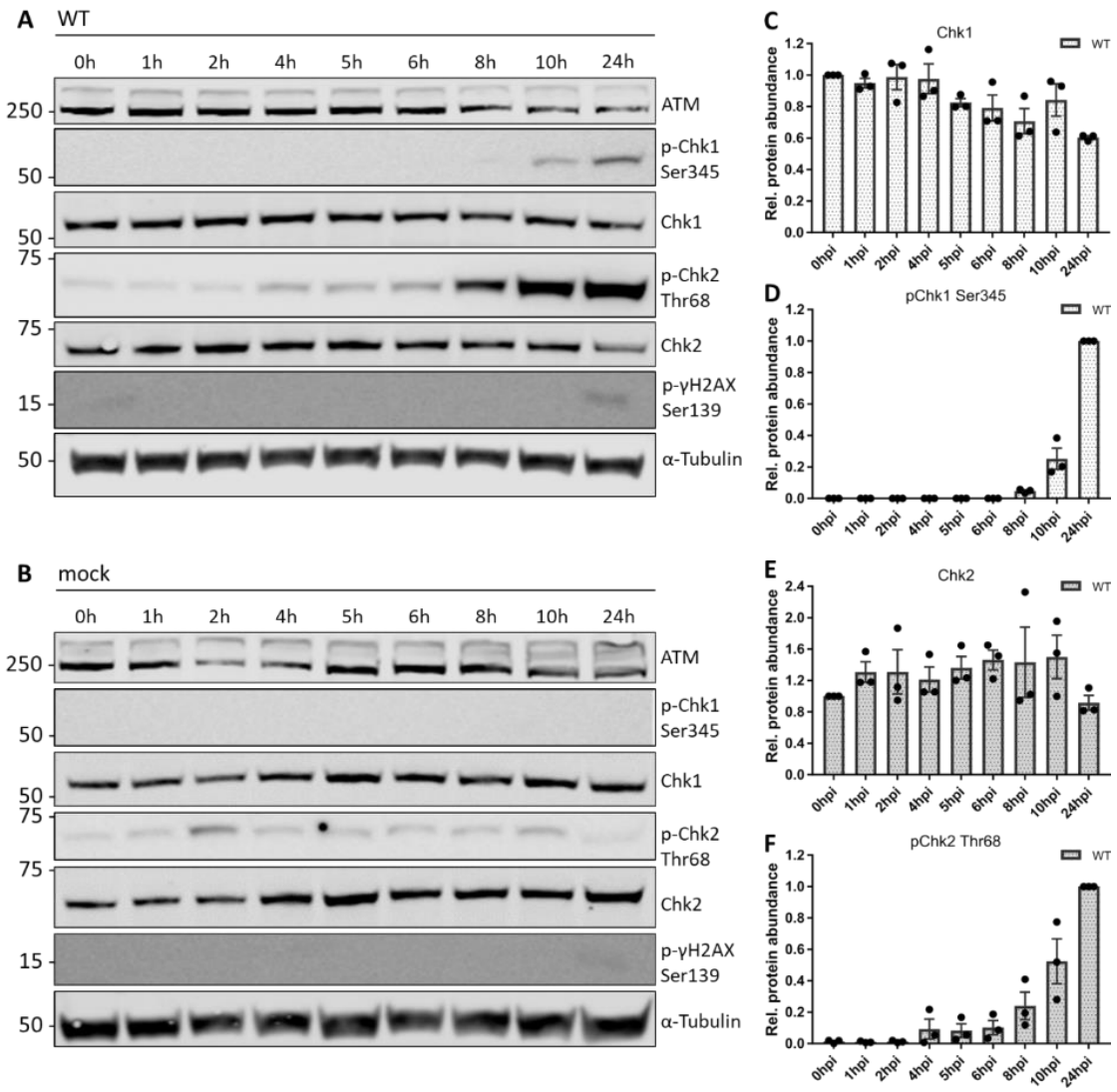

Figure 5-2 VACV infection activates the cellular DNA damage response.

HeLa cells were either mock infected, or infected with WT VACV (MOI 5) and samples were harvested at 0, 1, 2, 4, 5, 6, 8, 10, 24hpi. [A-B] Whole cell lysates were resolved via SDS-PAGE and immunoblotted for ATM, activating phosphorylation Chk1 (Ser345), Chk2 (Thr 68), and γH2AX (Ser139), the early viral protein I3, the late viral protein F17, and α-Tubulin as loading control. A representative blot of three biological replicates is shown. [C-D] Total and phosphorylated protein abundance was quantified and normalized to 0hpi, or 24hpi respectively. Data represent three biological replicates with one technical replicate each and are displayed as mean ± S.E.M.

As I found that VACV triggers DDR, I next aimed to define the subcellular localization of activated Chk1 and Chk2. Previously, ATR and Chk1 were described to be activated in the cytosol of infected cells. Immunoblots of cytosolic and nuclear cell fractions showed increased levels of phosphorylated ATR and Chk1 in the cytosol after infection (Postigo et al., 2017). In order to characterize the cytosolic location of activated Chk1 and Chk2 in more detail, I decided to analyse infected cells by confocal immunofluorescence.

HeLa cells were either mock infected, or infected with WR HA-D5 (MOI, 2) and fixed at 0, 2, 3, 4, 5, 6, 7, 8, 10, and 24hpi. Cells were stained for immunofluorescence with Hoechst (DNA), anti-HA (viral D5, red), and either anti-pChk2 Thr68 (green), or anti-pChk1 Ser345 (green). Both activated Chk1 and Chk2 were found to co-localized with viral replication sites (Figure 5-3 and Figure 5-4). Mirroring the pattern and timing observed by immunoblotting, phosphorylated Chk2 was detected to co-localize with viral replication sites as early as 5hpi, whereas the co-localization with phosphorylated Chk1 was less pronounced and was only observed after 8hpi.

In order to further characterize the spatiotemporal dynamics of Chk2 activation, I aimed to describe the kinetics of co-localization between pChk2 (Thr68) and VACV replication sites. To this end, a minimum of 100 cells per timepoint was analysed. First, the amount of individual VACV replication sites (DNA and HA-D5 positive) per cell was counted (Figure 5-3, A), classifying the replication sites according to their morphology either as speckles, dense, or as decondensed (Figure 5-3, B). Second, the number of pChk2 (Thr68) positive replication sites was determined for each of the three morphology groups (Figure 5-3, C). As infection progresses, foci of viral DNA grow from small speckles into dense replication sites which then transition to become areas of decondensed viral DNA, or so-called viral factories. Based on this analysis I discovered that activated Chk2 increasingly associates with maturing replication sites and nearly 100% of viral factories stained positive phosphorylated Chk2. While further experiments are needed to clarify whether Chk2 physically interacts with viral DNA, and how it is activated, this data demonstrates that active Chk2 localizes at sites of viral DNA replication.

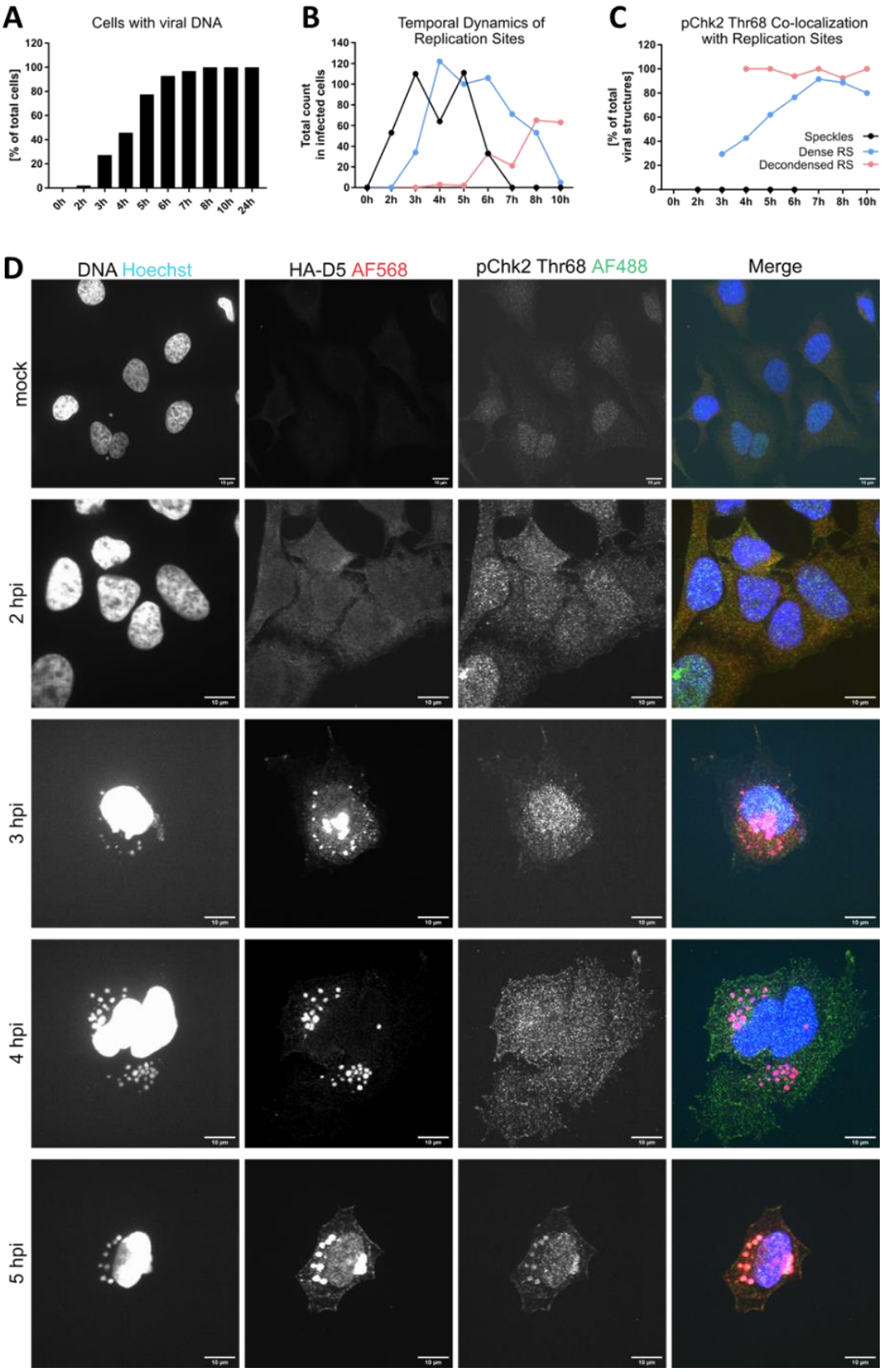
A
Cells with viral DNA
[% of total cells]
0h 2h 3h 4h 5h 6h 7h 8h 10h 24h
B
Temporal Dynamics of Replication Sites
Total count in infected cells
0h 2h 3h 4h 5h 6h 7h 8h 10h
C
pChk2 Thr68 Co-localization with Replication Sites
[% of total viral structures]
Speckles
Dense RS
Decondensed RS
0h 2h 3h 4h 5h 6h 7h 8h 10h
D
DNA Hoechst
HA-D5 AF568
pChk2 Thr68 AF488
Merge
mock
2 hpi
3 hpi
4 hpi
5 hpi

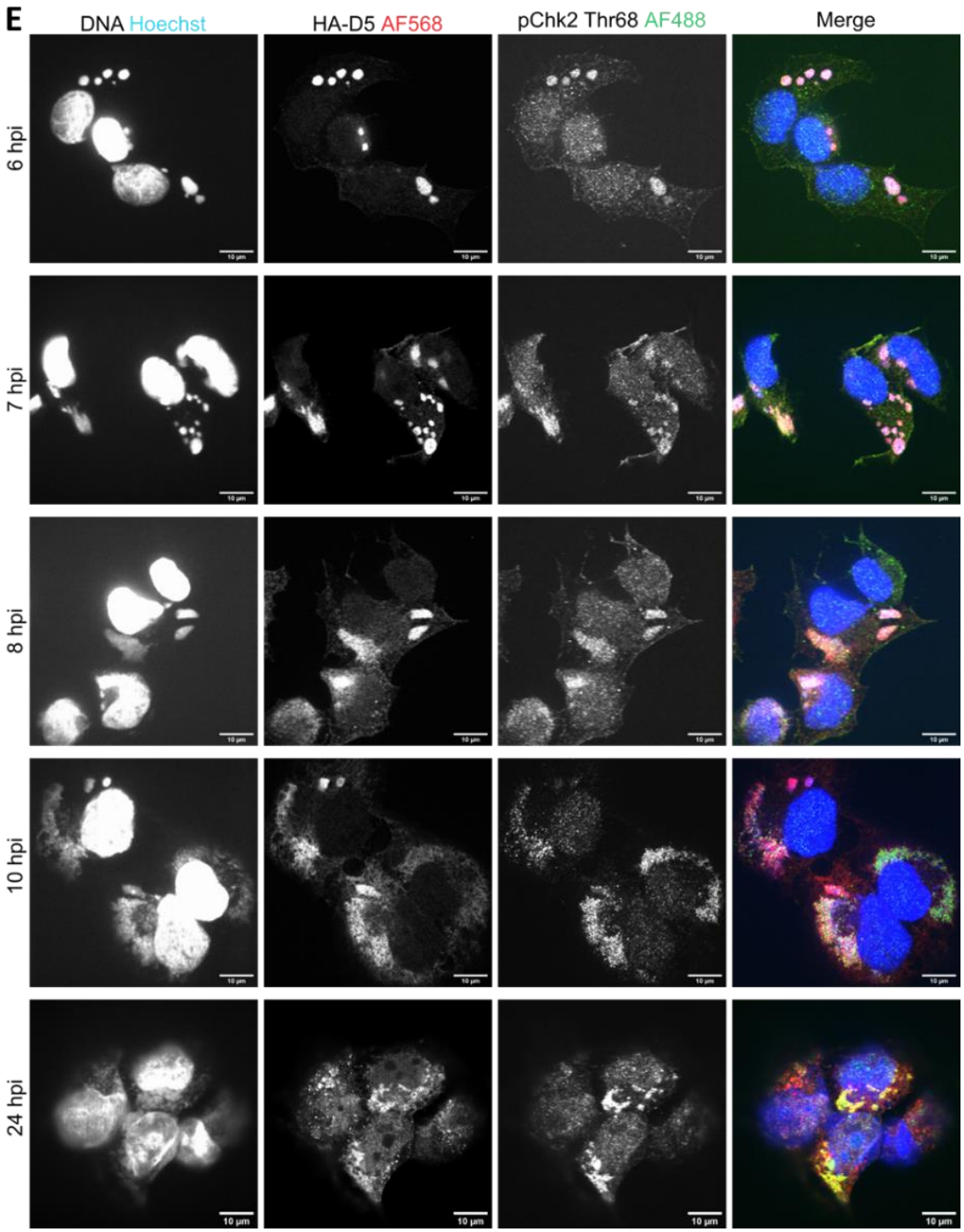

Figure 5-3 Activated Chk2 (pChk Thr68) is enriched in VACV replication sites.

HeLa cells were either mock infected, or infected with WR HA-D5 (MOI 2) and samples were fixed at 2, 3, 4, 5, 6, 7, 8, 10, and 24hpi. Cells were stained for immunofluorescence with Hoechst (DNA), anti-HA (viral D5, red), and anti pChk2 Thr68 (green). [A-B] A minimum of 100 cells was manually analysed, counting the amount of individual VACV replication sites (DNA and HA-D5 positive) per cell, and classifying the replication sites according to their morphology either as speckles, dense, or decondensed. [C] The number of pChk2 Thr68 co-localizing replication sites was counted and displayed percentage of total replication sites for each morphology (speckles, dense, and decondensed). [E-F] Representative confocal images of mock and WR HA-D5 infected samples at the indicated time post infection. Scale bar represents 10µm.

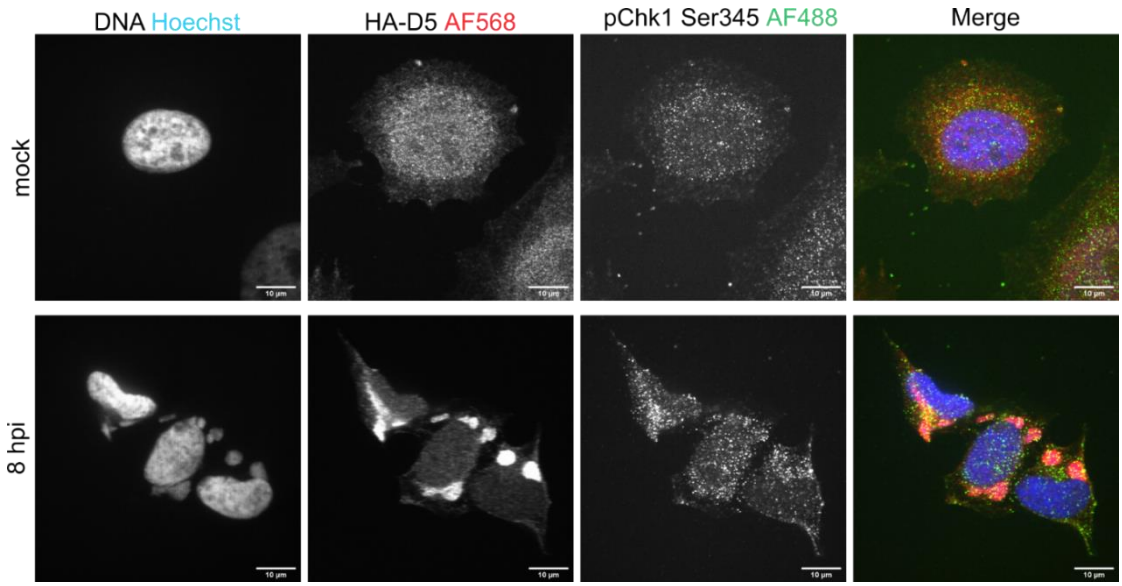

Figure 5-4 Activated Chk1 (pChk Ser345) is enriched in VACV replication sites.

HeLa cells were either mock infected, or infected with WR HA-D5 (MOI 2) and samples were fixed at 8 hpi. Cells were stained for immunofluorescence with Hoechst (DNA), anti-HA (viral D5, red), and anti pChk1 Ser345 (green). Representative confocal images of mock and WR HA-D5 infected samples at the indicated time post infection. Scale bar represents 10μm.

2.2 VACV early gene expression is not sufficient to activate the cellular DNA Damage Response

VACV-induced activation of DDR kinases ATR and Chk1 was previously shown to rely on viral early gene expression with activation observed in the absence of viral uncoating but requiring de novo protein synthesis (Postigo et al., 2017). While I could confirm that VACV promotes phosphorylation of Chk1 and Chk2, activation was only observed after the onset of viral late gene expression (Figure 5-2). This suggested the involvement of a late, rather than an early, viral protein. To establish which wave of viral gene expression accounted for DDR activation, I first tested whether expression of early genes was sufficient to promote phosphorylation of Chk2. To this end, viral intermediate and late gene expression were inhibited by treatment with the DNA synthesis inhibitor AraC.

HeLa cells were either mock infected, or infected with WT VACV (MOI 5), in the presence or absence of AraC (10μM) and samples were harvested at 0, 1, 2, 4, 5, 6, 8, 10, and 24hpi. Whole cell lysates were resolved via SDS-PAGE and immunoblotted for pChk2 (Thr68), the viral early protein I3, the viral late protein F17, and α-Tubulin as a loading control. While viral early genes are expressed before genome replication, intermediate and late viral gene transcription

requires replication of the released genome (Oda and Joklik, 1967). Therefore, viral late but not early gene transcription is inhibited by AraC, which was confirmed by expression of early I3 in the absence of late F17 (Figure 5-5).

In line with the above discussed results, VACV infection strongly induced Chk2 phosphorylation on Thr68 in untreated samples. While AraC treatment increased the baseline activation of Chk2 in uninfected as well as infected samples, the amount of Chk2 phosphorylation stayed below that of untreated, WT infected samples at 24hpi. However, VACV failed to further activate the DDR in the presence of AraC. Consistent with this, Chk2 phosphorylation levels at 24hpi remained comparable to uninfected AraC controls. Contrary to previous findings, these data indicate that expression of early viral genes does not account for activation of the cellular DDR during VACV infection.

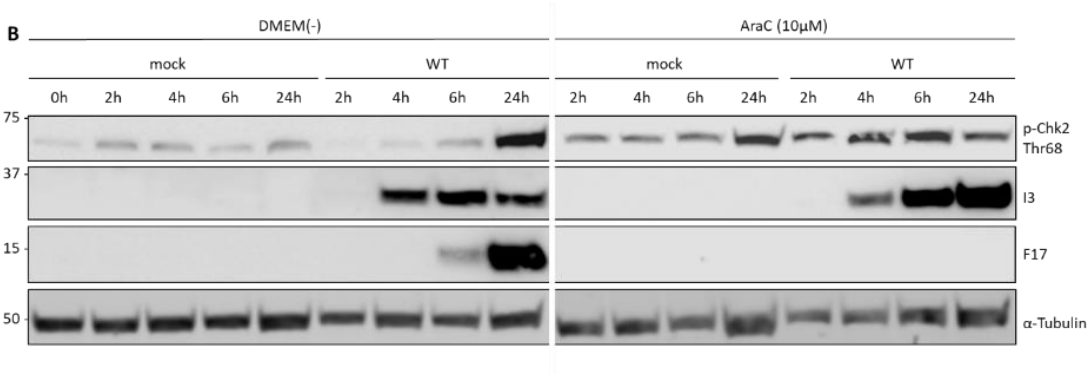

Figure 5-5 Early viral gene expression is not sufficient to activate the cellular DDR.

HeLa cells were either mock infected, or infected with WT VACV (MOI 5) in either DMEM(-) only, or DMEM containing the replication inhibitor AraC (10µM). Samples were harvested at 0, 2, 4, 6, and 24hpi and whole cell lysates were resolved via SDS-PAGE and immunoblotted for pChk2 (Thr68), the early viral protein I3, the late viral protein F17, and α-Tubulin as loading control.

2.3 VACV kinase F10 is required to activate the cellular DNA Damage Response

In the previous section, I showed that viral early gene expression and genome uncoating were not sufficient to activate the cellular DDR. Therefore, I next aimed to determine which of the post-uncoating steps was required to promote DDR activation. After release, the viral genome is replicated in the cytosol which induces the cascaded transcription of intermediate and late viral genes. To identify which of these steps are essential, I monitored phosphorylation of Chk2 upon knockdown of the viral DNA-dependent RNA polymerase subunit A24. As described

before, silencing of A24 by siRNA (siA24R) allows for transcription of early viral genes, and genome replication, whereas intermediate and late transcription are inhibited (Baroudy and Moss, 1980; Hooda-Dhingra et al., 1990; Resch et al., 2007). Since activation of the DDR signalling pathway is regulated by dynamic phosphorylation, I hypothesised that the viral candidate protein was likely to be either a kinase or a phosphatase. VACV encodes two late proteins that have phospho-enzymatic activity: the phosphatase H1, and the kinase F10 which together form a phosphoregulatory network that drives viral morphogenesis and transcriptional competence (Liu et al., 1995; Novy et al., 2018) . As WT infection causes phosphorylation rather than dephosphorylation of Chk2 I first focused on the kinase F10. To test the involvement of F10 in triggering the DDR signalling cascade, F10L was silenced by siRNA (siF10L). The knockdown efficiency was assessed by infecting cells with a recombinant VACV strain that expresses F10 with a C-terminal streptavidin-HA tag in the endogenous F10 locus (WR F10-SH EL EGFP).

HeLa cells were reverse transfected with scrambled control siRNA (Scr), siA24R, or siF10L. After 48h, cells were either mock infected, or infected with WR F10-SH EL EGFP (MOI 1) and samples were harvested at 0, 8, and 24hpi. Whole cell lysates were resolved via SDS-PAGE and immunoblotted for pChk2 (Thr68), HA, the viral early protein I3, the viral late protein F17, and α-Tubulin as a loading control (Figure 5-6). Knockdown of A24 was indirectly assessed by expression of early I3 and the absence of late F17.

As observed before, scrambled control siRNA did not affect the ability of VACV to activate the cellular DDR and robust phosphorylation of Chk2 at residue Thr68 was observed after 24hpi. On the contrary, knockdown of A24 prevented the virus from inducing activation of Chk2, and no increase in phosphorylation was observed at 24hpi. This data demonstrates that replicating viral genomes are not sufficient to trigger DDR activation, which suggested either the direct involvement of A24, or that viral intermediate or late genes are required in activating the DDR. While silencing of A24 completely prevented viral late gene transcription, knockdown of the viral kinase F10 was permissive for late expression, albeit at reduced levels compared to Scr control. Despite expression of late viral genes, Chk2 remained unphosphorylated during VACV infection in the absence of F10. This shows that knockdown of a late protein, F10 kinase is sufficient to reproduce the phenotype caused by inhibition of intermediate and late genes. From this data I conclude that the late expressed viral kinase F10 is required to activate the cellular DDR during VCAV infection.

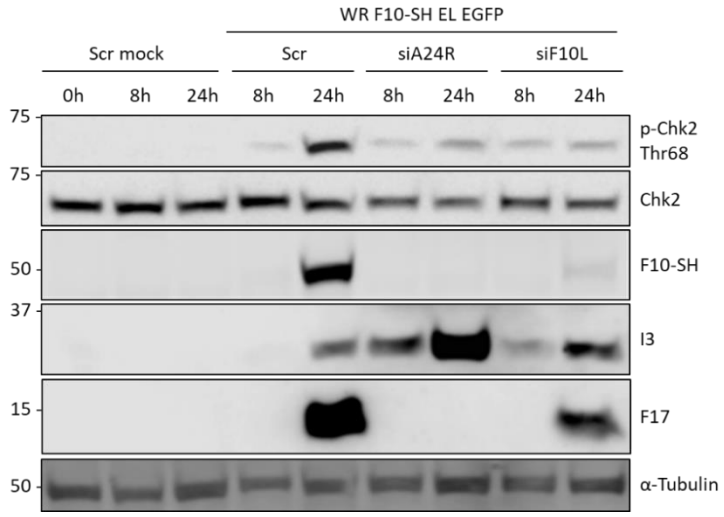

Figure 5-6 The viral kinase F10 is required to activate the cellular DDR during WT VACV infection.

HeLa cells were reverse transfected with scrambled control siRNA (Scr), siA24R, or siF10L. 48h after transfection, cells were either mock infected, or infected with WR F10-SH EL EGFP (MOI 1) and samples were harvested at 0, 8, and 24hpi. Whole cell lysates were resolved via SDS-PAGE and immunoblotted for pChk2 (Thr68), Chk2, HA to detect expression of viral F10-SH, the early viral protein I3, the late viral protein F17, and α-Tubulin as loading control. A representative blot of three biological replicates is shown.

2.4 VACV kinase F10 is sufficient to activate the cellular DNA Damage Response

Knockdown of the viral kinase F10 demonstrated that it is essential for VACV-induced activation of the DDR. However, this experiment does not distinguish between F10 directly phosphorylating the DDR effector Chk2, and a scenario where F10 functions as part of a signalling cascade, involving several viral proteins. Therefore, to test whether F10 is the only viral protein required for activating the DDR, I expressed a codon-optimized version of F10 in uninfected cells and monitored the phosphorylation status of Chk2 (Figure 5-7).

HeLa cells were incubated with DMEM(-), or were transfected with either a pMAX GFP control vector, or a codon-optimized version of F10 carrying an N-terminal 3xFLAG tag (3xFLAGco). Samples were harvested at 0h, 12h, and 24h post transfection. Whole cell lysates were resolved via SDS-PAGE and immunoblotted for activating phosphorylation of Chk2 (Chk2 Thr68), Chk2, and α-Tubulin as a loading control. Efficient expression of the 3xFLAG-F10co construct was confirmed by blotting for the FLAG tag.

Background levels of activated Chk2 were confirmed to be low, as shown by a faint band in the DMEM(-) control. Expression of GFP was found to slightly increase phosphorylation of Chk2 at residue Thr68, while it did not affect Chk2 protein abundance. On the other hand, expression of the viral kinase F10 induced robust phosphorylation of Chk2 despite decreased overall Chk2 protein levels. These data demonstrate that F10 is sufficient to activate the cellular DDR effector kinase Chk2 and does not require co-expression of another viral protein. Further experiments are needed to determine whether F10 directly phosphorylates Chk2, or whether it functions through activation of a cellular kinase.

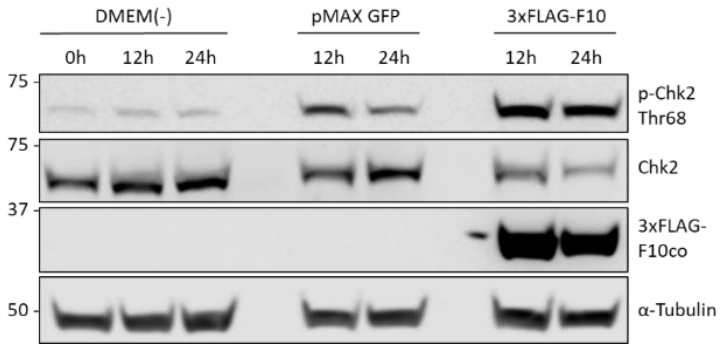

Figure 5-7 Expression of 3xFLAG-F10co is sufficient to activate the cellular DDR.

HeLa cells were transfected with either a DMEM(-) control, pMAX GFP control vector, or codon-optimized 3xFLAG-F10co. Samples were harvested at 0h, 12h, and 24h post transfection. Whole cell lysates were resolved via SDS-PAGE and immunoblotted for activating phosphorylation of Chk2 (Chk2 Thr68), Chk2, FLAG to monitor expression of 3xFLAG-F10co, and α-Tubulin as loading control. A representative blot of three biological replicates is shown.

3 VACV alters cellular levels of p53 and its effector p21

As discussed above, damaged DNA causes activation of the two transducer kinases ATR and ATM, which then induce a signalling cascade by phosphorylating their downstream kinases Chk1, and Chk2, respectively. The DNA damage signal is then translated by effector proteins into cellular responses such as DNA repair, apoptosis, and inhibition of cell cycle progression. The major effector orchestrating these responses is the transcription factor and tumour suppressor p53.

In the absence of DNA damage or other stress signals, p53 is rapidly turned over by proteasomal degradation, which is mediated by its negative regulator, the E3 ubiquitin ligase Mdm2 (Haupt et al., 1997; Kubbutat et al., 1997). Upon DNA damage, p53 is phosphorylated

on several residues by the DDR kinases ATR/ATM (Ser15) and Chk1/Chk2 (Thr18 and Ser20) which inhibits binding to Mdm2 (reviewed in (Ashcroft et al., 1999; Hafner et al., 2019)). Additionally, p53 is further stabilized by ATR/ATM directed degradation of Mdm2 (Khosravi et al., 1999; Maya et al., 2001). Induction and acetylation of p53 promotes transcription of p53-responsive genes such as *CDN1A,* which encodes the CDK inhibitor p21 (Waf1/Cip1) (Dornan et al., 2003; Sherr and Roberts, 1999; Waldman et al., 1995). p21 is a member of the Cip/Kip family of CDK inhibitor (CKI) proteins which bind and inactivate CDK2 – cyclin E/A, and CDK1 – cyclin B complexes, thus preventing cell cycle progression and cell proliferation (Harper and Brooks, 2005; Sherr, 1994; Vermeulen et al., 2003). In addition to negatively regulating CDK activity, p21 also prevents cellular DNA replication by directly inhibiting the DNA-polymerase processivity factor PCNA (Waga et al., 1994).

Due to its central role in cell cycle control, modulation of p53 expression and activity is a common strategy of viruses to create a pro-viral environment. Poxviruses, including VACV, have also been implicated by individual studies to either induce or prevent p53 expression (Wali and Strayer, 1996, 1999b; Yoo et al., 2008). Therefore, I decided to investigate whether p53 expression is upregulated in response to VACV-induced activation of the DDR signalling cascade.

3.1 VACV infection causes degradation of cellular p53 and Mdm2

Previous studies have described poxviruses to modulate the expression of p53: Malignant rabbit fibroma virus (MV), a Leporipoxvirus, encodes the early transcription factor C7 which was reported to induce direct transcription of the *TP53* gene during early stages of infection (Wali and Strayer, 1996). The same group has also observed temporal regulation of p53 in response to VACV infection in pre-synchronized cells. After initial upregulation during the first 4hpi, p53 levels were later found to drop below uninfected control levels (Wali and Strayer, 1999b). Similarly, VACV has been shown to cause decreased p53 levels at 30 and 48hpi in pre-synchronized osteosarcoma cells (Yoo et al., 2008). Increased transcription of the negative regulator *Mdm2* was suggested to promote the observed downregulation of p53 during VACV infection. Although these studies hint at a connection between VACV infection and the p53-Mdm2 signalling pathway, mechanistic understanding remained limited, p53 regulation during early stages of VACV infection remained unclear, and the (viral) effector protein remained

undefined. Therefore, I aimed at describing VACV-induced alterations of p53 and Mdm2 in unsynchronized cells, focusing on early stages during infection.

HeLa cells were either mock infected, or infected with WT VACV (MOI 5) and samples were harvested at 0, 1, 2, 4, 5, 6, 8, 10, and 24hpi. Whole cell lysates were resolved via SDS-PAGE and immunoblotted for p53, Mdm2, and α-Tubulin as a loading control (Figure 5-8, A, B). Protein abundance was quantified and normalized to 0hpi (Figure 5-8, C, D).

In mock infected samples, fluctuating levels of Mdm2 and p53 were detected throughout the timecourse, albeit at low levels in the case of p53. In contrast to previous findings, VACV infection promoted robust downregulation of both p53 and its regulator Mdm2. While Mdm2 was found to immediately decrease upon viral entry, p53 degradation was only observed after an initial lag phase of 4hpi. These findings show that VACV infection directs effective downregulation of not only p53 but also its negative regulator Mdm2.

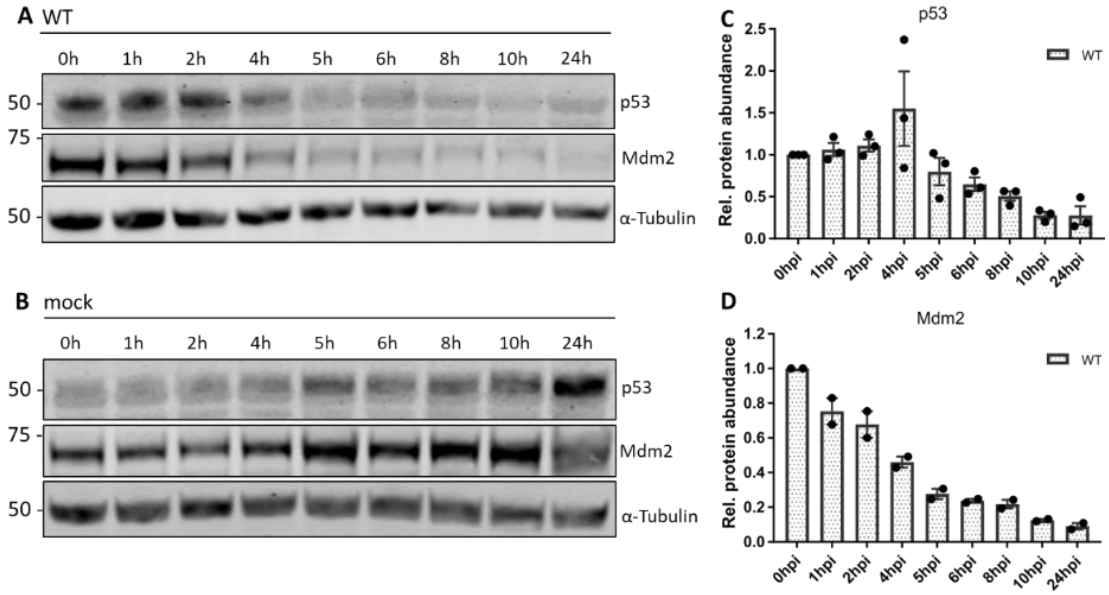

Figure 5-8 VACV infection induces degradation of p53 and Mdm2.

Unsynchronized HeLa cells were either mock infected, or infected with WT VACV (MOI 5) and samples were harvested at 0, 1, 2, 4, 5, 6, 8, 10, 24hpi. Whole cell lysates were resolved via SDS-PAGE and immunoblotted for p53, Mdm2, the early viral protein I3, the late viral protein F17, and α-Tubulin as loading control. [A-B] A representative blot of three biological replicates (p53), or of two biological replicates (Mdm2) is shown. [C-D] The protein abundance of infected samples was quantified and normalized to 0hpi. Data represent three (p53), or two (Mdm2) biological replicates with one technical replicate each and are displayed as mean ± S.E.M.

3.2 B1 depletion increases p53 levels

Having shown that VACV infection destabilizes p53 and Mdm2, I next looked to identify the essential virus life cycle stage.

In uninfected cells, the activity and stability of p53 is regulated by a complex combination of post-translational modifications (PTMs) including acetylation, ubiquitination, sumoylation, and phosphorylation. Phosphorylation of several residues, including Ser15, Thr18, and Ser20, in the N-terminus of p53 control the interaction of p53 with its negative regulator Mdm2 (reviewed in (Hafner et al., 2019)).

Given that p53 stability is regulated by dynamic (de)phosphorylation, I hypothesised that a viral kinase or phosphatase destabilized p53. VACV encodes one phosphatase (H1), and two kinases (B1 and F10). The kinase B1 is expressed early during infection, whereas the phosphatase H1 and the kinase F10 are expressed late. H1 and F10 form a phospho-signaling network that orchestrates transcriptional competence, maturation and assembly of new progeny virions (Liu et al., 2000; Novy et al., 2018). On the other hand, B1 functions early during the virus life cycle and is essential for viral genome replication (Condit et al., 1983; Hooda-Dhingra et al., 1990; Olson et al., 2017).

Taking a candidate-based approach, I decided to focus on B1 as a potential mediator of p53 degradation, due to the following reasons: first, p53 is degraded before the onset of late viral gene expression, which argues for an early expressed viral protein. Second, B1 shares homology with the cellular kinases VRK1 (Vaccinia related kinase 1) which is known to modulate p53 stability by phosphorylating Thr18 (Vega et al., 2004). Third, expression of B1 in uninfected cells was shown to be sufficient to phosphorylate p53 in its N-terminus, which was suggested to promote binding to Mdm2 and proteasome-dependent degradation (Santos et al., 2004).

Therefore, B1 was silenced by RNAi in order to elucidate its role in VACV-mediated destabilization of p53. HeLa cells were reverse transfected with either scrambled control siRNA (Scr), or siRNA targeting B1 mRNA (siB1R). After 48h, cells were either mock infected, or infected with WT (MOI 1) and samples were harvested at 0, 8, and 24 hpi. Whole cell lysates were resolved via SDS-PAGE and immunoblotted for p53, the early viral protein I3, and the late viral protein F17 (Figure 5-9). As discussed above, B1 is required for viral genome replication. Therefore, B1R silencing allows for early gene expression, while late gene expression is inhibited. B1 knockdown efficiency was determined by expression of early I3 and

the reduction of late F17. As F17 expression was reduced but not completely abolished in the siB1R treated sample, this indicates that knockdown of B1 was incomplete and sufficient B1 was produced to allow for late F17 expression, albeit at severely reduced levels.

While control siRNA did not affect p53 levels, VACV infection was confirmed to completely degrade p53 by 24hpi. On the other hand, infection after silencing of B1R led to accumulation of p53, which exceeded uninfected levels at 8 and 24hpi. Additionally, depletion of B1 caused a second, lower molecular p53 band (Figure 5-9, *). The altered molecular weight might be explained by changes in the posttranslational modifications of p53 such as a reduction in phosphorylation. Taken together, these findings suggest that depletion of B1 stabilizes p53 and alters its PTM pattern.

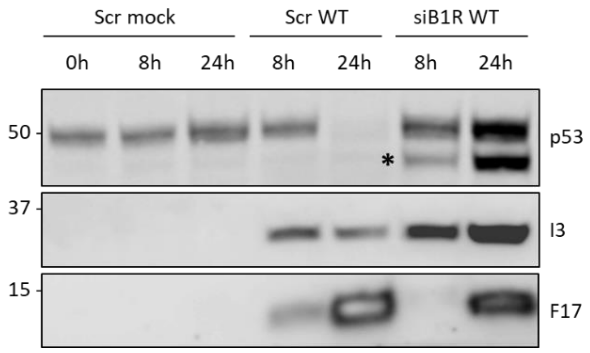

Figure 5-9 Depletion of the viral kinase B1 stabilized p53.

HeLa cells were reverse transfected with either scrambled control siRNA (Scr), or siB1R. After 48h, cells were either mock infected, or infected with WT (MOI 1) and samples were harvested at 0, 8, and 24 hpi. Whole cell lysates were resolved via SDS-PAGE and immunoblotted for p53, the early viral protein I3, and the late viral protein F17.

As B1 is essential for viral genome replication, silencing not only depletes B1 but also inhibits genome replication and subsequent late viral gene expression. Therefore, the previous experiment cannot distinguish between the effect of knocking down B1 and the effect of suppressing viral replication. In order to differentiate the two, viral replication was inhibited by either blocking viral uncoating (siD5R), or by specifically silencing the viral polymerase (siE9L). In both conditions, viral early genes, including B1, are expressed in the absence of viral genome replication. As before, HeLa cells were reverse transfected with either scrambled control siRNA (Scr), siD5R, or siE9L. After 48h, cells were either mock infected, or infected with WT MOI (2, 10) and samples were harvested at 0, 8, and 24 hpi. Whole cell lysates were resolved via SDS-PAGE and immunoblotted for p53, the early viral protein I3, the late viral

protein F17, and α-Tubulin as a loading control (Figure 5-10). As discussed above, D5 and E9 are required for viral genome replication. Therefore, D5R and E9L silencing allows for early gene expression, while late gene expression is inhibited. D5 and E9 knockdown efficiency was confirmed by expression of early I3 and the absence of late F17.

Infection of siD5R or siE9L treated cells caused accumulation of p53, which was comparable to the increase in p53 levels observed after siB1R silencing. In contrast to knockdown of B1, a second, lower molecular p53 band was not detected after depletion of either D5 or E9 (Figure 5-10, *). This data suggests that repression of viral genome replication is sufficient to increase p53 levels, even in the presence of the viral kinase B1.

In summary, although the above described RNAi experiments do not allow for any definitive conclusions they hint at a potential PTM of p53 which depends on expression of B1.

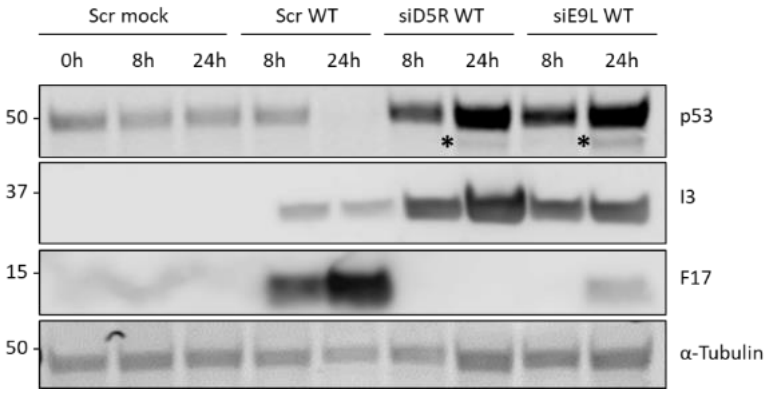

Figure 5-10 Inhibition of post-uncoating steps cause accumulation of p53.

HeLa cells were reverse transfected with a scrambled control siRNA (Scr), siD5R, or siE9L. After 48h, cells were either mock infected, or infected with WT MOI (1) and samples were harvested at 0, 8, and 24 hpi. Whole cell lysates were resolved via SDS-PAGE and immunoblotted for p53, the early viral protein I3, the late viral protein F17, and α-Tubulin as loading control.

3.3 VACV ΔB1mutB12 fails to degrade p53 and / or Mdm2

Interpretation of the above described siRNA silencing experiments was inconclusive, as potential pre-replication functions of B1 could not be separated from its essential role in viral genome replication. Highlighting its requirement in the virus life cycle, full genetic deletion of B1 abrogates the production of infectious virions. The resulting ΔB1 VACV strain can therefore only be produced in the presence of transient complementation e.g. in a B1 expressing cell line (Olson et al., 2017). However, in order to study the role of B1 in (de)stabilizing p53, I

needed a system which decoupled B1 activity and viral DNA replication. Such a replication competent B1 deletion VACV strain was published earlier this year by the Wiebe lab (Olson et al., 2019). Through experimental evolution of the severely attenuated ΔB1 virus (Olson et al., 2017), a mutation in the B12R pseudokinase gene was discovered that rescued the ΔB1 replication defect (Olson et al., 2019). Although the function of B12 remains to be established, B1 seems to promote VACV replication, at least in part, by suppressing the inhibitory function of its paralog pseudokinase B12. Importantly, the resulting ΔB1mutB12 VACV strain allowed me to study replication-independent functions of B1, such as its potential effect on p53 stability.

To monitor p53 levels in the absence of the kinase B1, HeLa cells were infected with ΔB1mutB12 and harvested 0, 1, 2, 4, 5, 6, 8, 10, and 24 hpi. Whole cell lysates were resolved via SDS-PAGE and immunoblotted for p53, Mdm2, the early viral protein I3, the late viral protein F17, and α-Tubulin as a loading control (Figure 5-11**, B**).

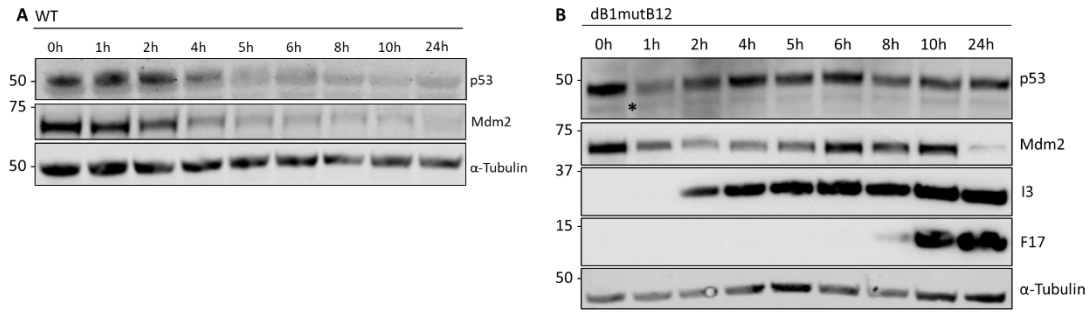

Figure 5-11 VACV ΔB1mutB12 fails to degrade cellular p53 and Mdm2.

[A] WT infection for comparison. Blot reproduced from previous section. [B] Unsynchronized HeLa cells were either mock infected, or infected with VACV ΔB1 mutB12 (MOI 5) and samples were harvested at 0, 1, 2, 4, 5, 6, 8, 10, 24hpi. Whole cell lysates were resolved via SDS-PAGE and immunoblotted for p53, Mdm2, the early viral protein I3, the late viral protein F17, and α-Tubulin as loading control.

In contrast to WT VACV infection, p53 was not degraded by ΔB1mutB12 infection. During the 24hpi, p53 abundance was found to fluctuate but was neither completely diminished, nor upregulated to the same extent as previously observed after repression of viral replication. Similarly, during the first 10hpi Mdm2 was not degraded by ΔB1mutB12, although by 24hpi Mdm2 levels were strongly reduced. Degradation of Mdm2 at this late timepoint could be caused by F10-mediated activation of ATR and ATM, since these two DDR components were shown to negatively regulate Mdm2 stability (Khosravi et al., 1999; Maya et al., 2001). The

differences in p53 and Mdm2 stability in WT and ΔB1mutB12 infections are not caused by a replication defect of ΔB1mutB12, as is indicated by normal timing of early (I3) and late (F17) viral gene expression. Therefore, this data demonstrates that B1 and/or B12 are required to mediate degradation of p53 during VACV infection.

3.4 VACV dynamically modulates levels of cellular p21

In the above sections I have shown that the viral kinase F10 activates the cellular DDR pathway while the viral kinase B1 and/or its paralog pseudokinase B12 cause degradation of the main DDR effector p53.

Canonical ATR/ATM signalling causes a delay or arrest in cell cycle progression by inducing p53 to transactivate the CDK inhibitor p21 (Dornan et al., 2003; Harper and Brooks, 2005; Sherr, 1994; Sherr and Roberts, 1999; Vermeulen et al., 2003; Waldman et al., 1995). The broad range inhibitory effect of p21 on cell cycle progression parallels the cell cycle alterations observed after VACV infection: Apart from mediating a systemic cell cycle arrest, p21 also negatively regulates the cellular DNA-polymerase processivity factor PCNA and thus inhibits cellular DNA replication (Waga et al., 1994). Therefore, I next aimed to investigate p21 as a potential cellular effector that mediates the virus-induced cell cycle arrest.

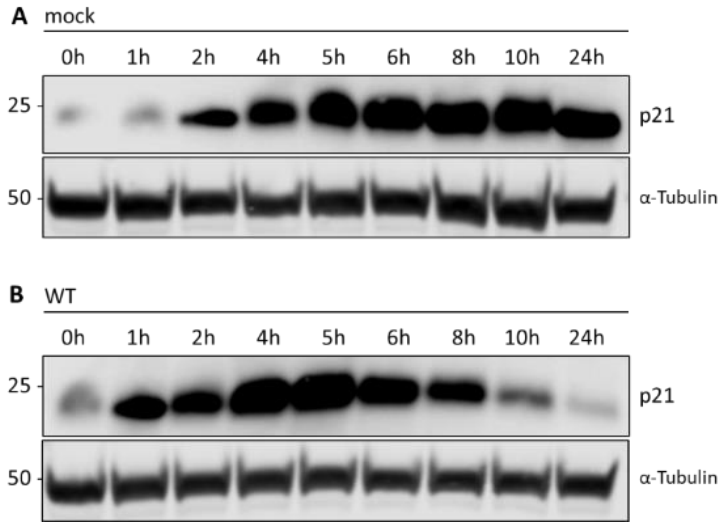

Figure 5-12 VACV infection dynamically regulates levels of cellular p21.

Unsynchronized HeLa cells were either mock infected, or infected with WT VACV (MOI 5) and samples were harvested at 0, 1, 2, 4, 5, 6, 8, 10, 24hpi. Whole cell lysates were resolved via SDS-PAGE and immunoblotted for p21, and α-Tubulin as loading control. [A-B] A representative blot of two biological replicates is shown.

First, I characterized the cellular levels of p21 in response to VACV infection. To this end, HeLa cells were infected with WT VACV (MOI 5) and harvested 0, 1, 2, 4, 5, 6, 8, 10, and 24 hpi. Whole cell lysates were resolved via SDS-PAGE and immunoblotted for p21, and α-Tubulin as a loading control (Figure 5-12, A, B).

In uninfected samples, the initially low levels of p21 strongly increased between 1 and 6 hpi (Figure 5-12, A). Thereafter, p21 expression levelled out and remained elevated until 24hpi. Conversely, VACV infection induced a strong upregulation of p21 already at 1hpi, which was found to peak around 5hpi (Figure 5-12, B). While levels stayed elevated in uninfected samples, VACV directed a strong downregulation of p21 after 6hpi until it was almost completely degraded by 24hpi. These results demonstrate that VACV infection accounts for a biphasic modulation of p21 expression. Interestingly, this parallels the kinetics of the early established VACV block in host cell cycle progression.

3.5 VACV kinase F10 is required for degradation of p21

Having found VACV infection to dynamically modulate expression of the CDK inhibitor p21, I next looked to define the essential viral effector protein. In uninfected cells, the half-life of p21 is regulated by phosphorylation on different residues and nuclear export into the cytosol. Stabilization of p21 has been shown to involve phosphorylation on Thr145 by the two cellular kinases PIM1 and PIM2 (Wang et al., 2002, 2010), whereas phosphorylation at Thr57 or Ser114 by GSK3-beta (Lee et al., 2007; Rössig et al., 2002), as well as phosphorylation on Thr145 and Ser146 by AKT (Zhou et al., 2001) are associated with degradation of p21 (Abbas et al., 2008; Esteve-Puig et al., 2014).

Additionally, since I observed p21 levels to decrease concurrently with the onset of intermediate and late viral gene expression around 6hpi, I hypothesised that the viral candidate protein was likely to be either a late expressed kinase or phosphatase. As previously discussed, VACV encodes one late expressed kinase (F10), and one phosphatase (H1).

To identify whether intermediate and late gene expression were required, I monitored p21 levels upon knockdown of the viral DNA-dependent RNA polymerase subunit A24. As described before, silencing of A24 by siRNA (siA24R) allows for transcription of early viral genes, and genome replication, whereas intermediate and late transcription are inhibited (Baroudy and Moss, 1980; Hooda-Dhingra et al., 1990; Resch et al., 2007). To test the

involvement of F10 in directing p21 degradation, F10L was silenced by siRNA (siF10L). The knockdown efficiency was assessed by infecting cells with a recombinant VACV strain that expresses F10 with a C-terminal streptavidin-HA tag in the endogenous F10 locus (WR F10-SH EL EGFP).

HeLa cells were reverse transfected with scrambled control siRNA (Scr), siA24R, or siF10L. After 48h, cells were either mock infected, or infected with WR F10-SH EL EGFP (MOI 1) and samples were harvested at 0, 8, and 24hpi. Whole cell lysates were resolved via SDS-PAGE and immunoblotted for p21, HA, the viral early protein I3, the viral late protein F17, and α-Tubulin as a loading control (Figure 5-13). Knockdown of A24 was indirectly was confirmed by expression of early I3 and the absence of late F17.

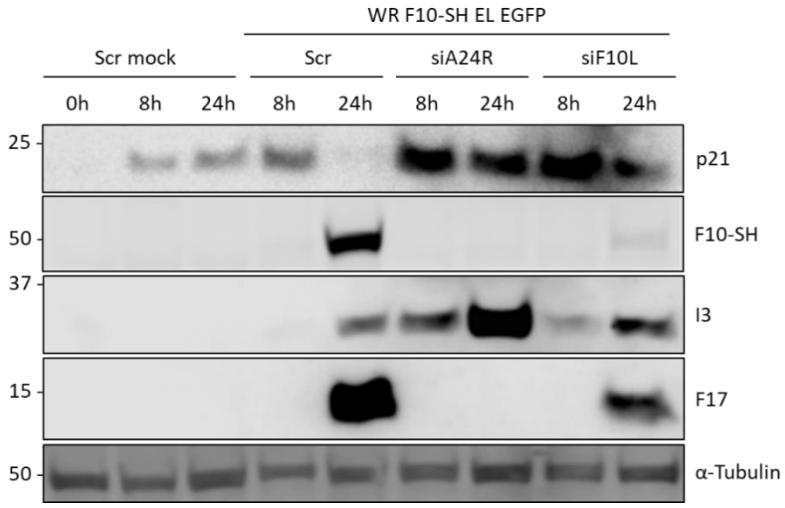

Figure 5-13 Knockdown of F10 prevents VACV-induced degradation of p21.

HeLa cells were reverse transfected with a scrambled control siRNA (Scr), siA24R, or siF10L. After 48h, cells were either mock infected, or infected with WR F10-SH EL EGFP (MOI 1) and samples were harvested at 0, 8, and 24hpi. Whole cell lysates were resolved via SDS-PAGE and immunoblotted for p21, HA to detect expression of viral F10-SH, the early viral protein I3, the late viral protein F17, and α-Tubulin as loading control. A representative blot of two biological replicates is shown.

As observed before, scrambled control siRNA did not affect the ability of VACV to direct downregulation p21 by 24hpi. In contrast, knockdown of A24 prevented degradation of p21, which was found to accumulate to levels surpassing uninfected controls. While these data suggested that viral early gene expression induces p21 upregulation, it demonstrated that intermediate and/or late viral gene expression are required to direct degradation of p21.

While silencing of A24 completely prevented viral late gene transcription, knockdown of the viral kinase F10 was permissive for late expression, albeit at reduced levels compared to Scr control. In the absence of F10 kinase, p21 was found to accumulate despite expression of late viral genes. Whilst expression of p21 was reduced between 8hpi and 24hpi in siF10L treated cells, p21 levels were still markedly higher than in the Scr control infection. Taken together, this shows that knockdown of the kinase F10 is sufficient to reproduce the phenotype caused by inhibition of intermediate and late genes. From this data I conclude that the late expressed viral kinase F10 is required to degrade p21 during late stages of VACV infection.

3.6 VACV kinase F10 is sufficient to cause degradation of p21

siRNA silencing of the viral kinase F10 demonstrated its essential function in inducing degradation of p21. However, as previously described for F10-mediated activation of the DDR, this experiment does not distinguish between direct function of F10, and a scenario where F10 acts as part of a signalling cascade, involving several viral proteins. Therefore, to test whether F10 is the only viral protein required to direct downregulation of p21, I expressed a codon-optimized version of F10 in uninfected cells (Figure 5-7) and monitored levels of p21.

HeLa cells were incubated with DMEM(-), or were transfected with either a pMAX GFP control vector, or a codon-optimized version of F10 carrying an N-terminal 3xFLAG tag (3xFLAGco). Samples were harvested at 0h, 12h, and 24h post transfection. Whole cell lysates were resolved via SDS-PAGE and immunoblotted for p21, and α-Tubulin as a loading control. Efficient expression of the 3xFLAG-F10co construct was confirmed by blotting for FLAG (Figure 5-14).

As seen before in uninfected samples, p21 strongly increased in untransfected DMEM(-) controls over 24hrs. While p21 was also observed to accumulate strongly in GFP control expressing cells, p21 levels at 24h were slightly reduced compared to untransfected controls. On the other hand, expression of the viral kinase F10 induced robust degradation of p21 at 24h post transfection. These data demonstrate that F10 is sufficient to direct degradation of p21 and does not require co-expression of another viral protein. Further experiments are needed to determine whether F10 directly phosphorylates p21 to stimulate its degradation, or whether it functions through activation of a cellular signalling cascade.

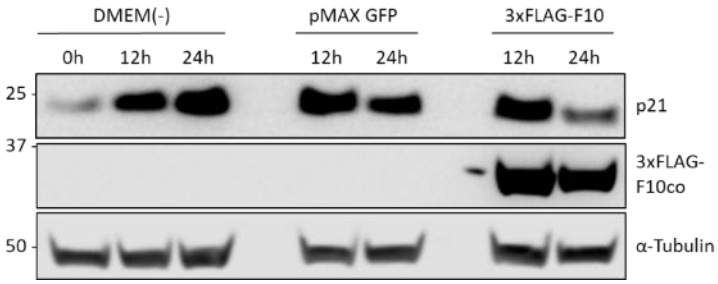

Figure 5-14 Expression of 3xFLAG-F10co is sufficient to promote a reduction of p21 levels.

HeLa cells were transfected with a DMEM(-) control, or a pMAX GFP expression control, or 3xFLAG-F10co expressing a codon-optimized version of the viral kinase F10 carrying an N-terminal triple FLAG tag. Cells were harvested at 0, 12, and 24h post transfection. Whole cell lysates were resolved via SDS-PAGE and immunoblotted for p21, FLAG to monitor expression of 3xFLAG-F10co, and α-Tubulin as loading control. A representative blot of two biological replicates is shown.

4 Functional relevance of modulating the host cell cycle

In the previous sections, I have used recombinant VACV strains, RNAi, biochemistry, and super-resolution microscopy to demonstrate that VACV early gene expression inhibits cell proliferation after viral entry. Concurrently, the cellular CDK inhibitor p21 was upregulated, while the tumour suppressor p53 was targeted for degradation by the viral kinase B1 and/or its paralog pseudokinase B12. The second wave of viral gene expression was found to shift the cell cycle from G1 to S/G2/M, while still inhibiting cell proliferation. Additionally, the viral kinase F10 was shown to be necessary and sufficient to cause degradation of p21, and for activation of the cellular DNA damage response (DDR). However, so far I have not addressed the relevance of cell cycle subversion for VACV replication. Therefore, I next aimed to define how VACV uses the cell cycle to promote its own replication.

4.1 VACV arrests p53 null cells

Having found that VACV infection directs degradation of p53 and its negative regulator Mdm2, I next aimed to identify the functional relevance of this for the viral life cycle. p53 is well-studied as a key regulator of cell cycle progression and apoptosis (Debbas and White, 1993; Lowe et al., 1993; Wagner et al., 1994; Wu and Levine, 1994). It integrates different stress signals such as DNA damage, and nutrient starvation into a transcriptional response that controls G1/S transition, as well as the G0 and G2/M checkpoints (Cross et al., 1995; Del Sal et al., 1995; El-Deiry et al., 1993; Fukasawa et al., 1996; Kastan et al., 1992; Linke et al., 1996). Due to its essential role in cell cycle control, I investigated the functional link between VACV-induced p53 manipulation and cell cycle dysregulation. Therefore, I characterized how up-, or downregulation of intracellular p53 levels affected the ability of VACV to alter cell cycle progression.

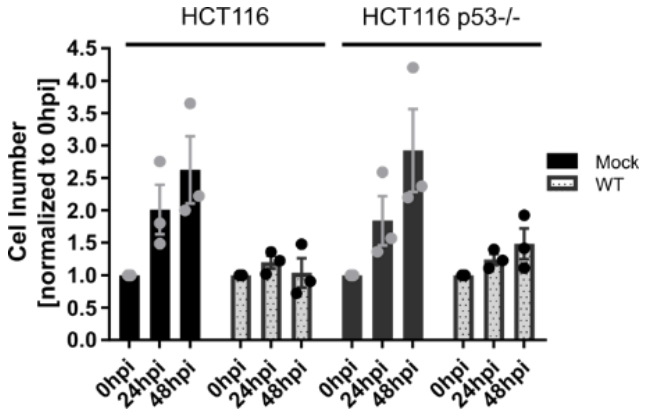

Figure 5-15 VACV infection inhibits proliferation of p53-/- cells.

Relative increase in HCT116 and HCT116 p53-/- cell numbers in mock (black), and VACV WT infected (grey) samples. Unsynchronized HCT116 or HCT116 p53-/- cells were either mock infected, or infected with WT VACV (MOI 5). Cells were harvested and counted at 0, 24, and 48hpi. Cell counts were normalized to 0hpi. Data represent three biological replicates with one technical replicate each and are displayed as mean ± S.E.M.

In section 3.1 of this chapter, I have shown that VACV rapidly induces increased levels of the cell cycle inhibitor p21 after entry, whereas its upstream regulator p53 is degraded after 4hpi. Since transcription of p21 is mediated by p53, I decided to test whether p53 is required during the first 4hpi for VACV to arrest the host cell cycle. To address this question, I measured the proliferation of a genetically engineered p53 double negative HCT116 cell line (generously provided by Dr. Miranda Wilson) in the presence and absence of VACV. WT HCT116, and HCT116 p53 -/- cells were mock infected, or infected with WT VACV (MOI 5). Cells were counted at 0, 24, and 48hpi and cell counts were normalized to 0hpi (Figure 5-15). Proliferation of uninfected cells was not affected by deletion of p53 and WT HCT116, as well as HCT116 p53-/- cell numbers nearly tripled over 48hpi. Similarly, WT infection blocked cell proliferation independent of the presence or absence of p53. However, the efficiency of the cell cycle block

varied between the WT and deletion cell line: while infected WT HCT116 numbers remained constant, infected HCT116 p53-/- cell numbers increased 1.5 ± 0.2 fold over 48hpi. This data shows that VACV does not require p53 to inhibit cell cycle progression.

4.2 The VACV kinase B1 and degradation of p53 are not required to arrest the cell cycle

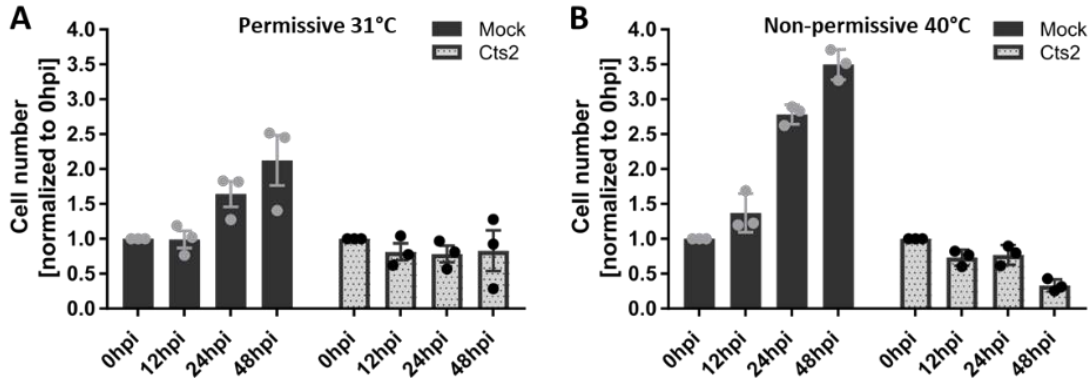

Figure 5-16 The viral kinase B1 is not required to inhibit host cell proliferation.

BSC40 cells were either mock infected, or infected with the temperature sensitive VACV strain Cts2 (MOI 5) either at the permissive, or non-permissive temperature. Cells were counted at 0, 10, 24, and 48hpi and counts were normalized to 0hpi. [A] Normalized counts of mock (black) and infected (grey) samples at the permissive temperature (31°C). [B] Normalized counts of mock (black) and infected (grey) samples at the non-permissive temperature (40°C). Data represent three biological replicates with two technical replicates each and are displayed as mean ± S.E.M.

Since I have found VACV to inhibit proliferation in the absence of p53, I next asked the opposite question and assayed whether degradation of p53 was required for VACV to block the host cell cycle. Previously in this chapter, I showed that p53 is degraded in a B1 and/or B12 dependent manner during infection. Therefore, to test the role of p53 degradation, I utilized the temperature sensitive VACV strain Cts2 that encodes a mutant of B1 that is non-functional at non-permissive temperatures (Condit et al., 1983; Rempel and Traktman, 1992; Rempel et al., 1990). BSC40 cells were either mock infected, or infected with the ts mutant Cts2 (MOI 5). After viral entry at the permissive temperature, cells were either kept at 31°C, or shifted to 40°C and samples were counted at 0, 12, 24, and 48hpi (Figure 5-16). While uninfected cells were found to proliferate faster at 40°C than at 31°C, neither of the temperature regimes inhibited cell proliferation. On the other hand, infected cells failed to proliferate, independent of the temperature conditions. Under permissive conditions, infected cell numbers slightly decreased, compared to a 2.1-fold increase in uninfected samples (Figure 5-16, A). Similarly,

under non-permissive conditions, Cts2 infected cell numbers decreased, whereas uninfected controls more than tripled during 48h (Figure 5-16, B). Concluding, this data demonstrates that neither degradation of p53, nor expression of the viral kinase B1 are required to arrest host cell proliferation.

However, similar to silencing B1 by siRNA, infection with Cts2 at non-permissive temperatures cannot distinguish between the potential function of B1 in targeting p53 for degradation and its essential role in viral genome replication. Additionally, results discussed in section 3.2 of this chapter showed that repression of viral genome replication is sufficient to increase p53 levels, even in the presence of the viral kinase B1. Therefore, the above described Cts2 experiment does not allow for any definite conclusions whether B1-mediated degradation is required for arresting the host cell cycle.

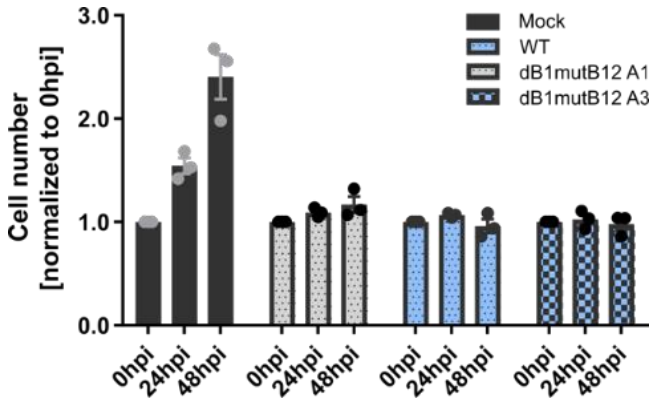

Figure 5-17 Neither the viral kinase B1, nor the pseudokinase B12 are required to inhibit host cell proliferation.

Relative increase in HeLa cell numbers after mock, VACV WT or ΔB1mutB12 infection. Unsynchronized HeLa cells were mock infected, or infected with WT VACV (MOI 1), or two different isolates (A1, A3) of the B1 deletion virus ΔB1mutB12. Cells were harvested and counted at 0, 24, and 48hpi. Cell counts were normalized to 0hpi. Data represent three biological replicates with one technical replicate each and are displayed as mean ± S.E.M.

In order to study the effect of loss of B1 activity in the presence of viral replication, I again used the previously introduced ΔB1mutB12 strain (Olson et al., 2019). To test whether ΔB1mutB12 could inhibit host proliferation, HeLa cells were mock infected, or infected with either WT VACV (MOI 1), or two different isolates (A1, A3) of the ΔB1mutB12 strain. Samples were counted at 0, 24, and 48hpi and normalized to cell counts at 0hpi (Figure 5-17). As observed before, uninfected cells were found to increase 2.4-fold in numbers over 48hpi. On the other hand, both WT VACV and ΔB1mutB12 infection blocked host cell progression and cell numbers remained constant. Concluding, neither the viral kinase B1, nor its paralog

pseudokinase B12 are required to arrest the host cell cycle. As ΔB1mutB12 fails to reduce p53 levels, this experiment also shows that p53 degradation is neither essential for the virus-induced cell cycle block, nor for viral replication.

4.3 Neither VACV kinase B1 nor degradation of p53 are required to shift the cell cycle

p53 controls correct timing and progression of the cell cycle by integrating several different damage response pathways. Under steady state conditions, p53 is continuously degraded due to Mdm2-dependent ubiquitination. However, under stress conditions such as DNA damage or depletion of ribonucleoside pools p53 is stabilized and can activate different checkpoints to arrest the cell cycle (El-Deiry et al., 1993; Linke et al., 1996). Since VACV infection shifts the cell cycle from G1 into S/G2/M, I hypothesised that infection mediated degradation of p53 might serve as a mechanism to facilitate G1/S transition.

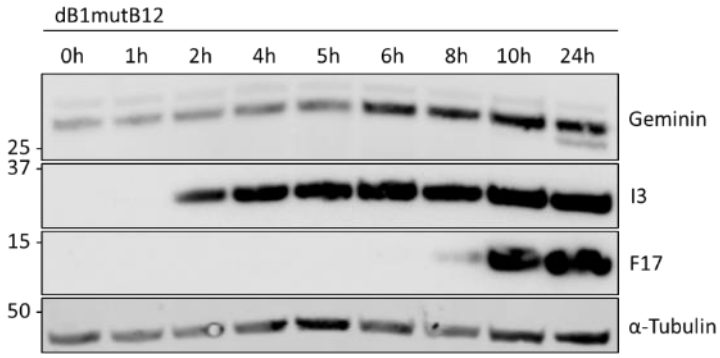

Figure 5-18 Neither the viral kinase B1, nor the pseudokinase B12 are required to shift the host cell cycle.

Unsynchronized HeLa cells were either mock infected, or infected with VACV ΔB1mutB12 (MOI 5) and samples were harvested at 0, 1, 2, 4, 5, 6, 8, 10, 24hpi. Whole cell lysates were resolved via SDS-PAGE and immunoblotted for Geminin, the early viral protein I3, the late viral protein F17, and α-Tubulin as loading control.

To test this hypothesis, I assessed cell cycle alterations after infection with ΔB1mutB12. As this virus contains an mCherry cassette that was used to disrupt the B1R ORF (Olson et al., 2017), I could not use it in combination with the fluorescent HeLa FUCCI reporter system. Instead, I monitored endogenous Geminin levels as a proxy for cell cycle entry. HeLa cells were infected with ΔB1mutB12 and harvested 0, 1, 2, 4, 5, 6, 8, 10, and 24 hpi. Whole cell lysates were resolved via SDS-PAGE and immunoblotted for Geminin, the early viral protein I3, the late viral protein F17, and α-Tubulin as a loading control (Figure 5-18). As was previously observed during WT VACV infection, Geminin levels increased from 6hpi onwards, which indicates an

accumulation of cells in S/G2/M. Therefore, these data suggest that ΔB1mutB12 promotes transition from G1 to S/G2/M. Thus, neither degradation of p53, nor the viral kinase B1, or its paralog pseudokinase B12 are required to shift the host cell cycle.

4.4 Stabilization of p53 by Nutlin-3 prevents the cell cycle shift

So far I have shown that virus-induced cell cycle arrest and shift occurred independently of p53 and were not inhibited by baseline p53 levels. Therefore, I next aimed to characterize how accumulation of p53 influenced the virus life cycle, and VACV's ability to alter host cell cycle progression. In order to address this question, I needed a tool to increase p53 levels in the absence of genotoxic stress.

As described above, p53 abundance is tightly controlled by the E3 ubiquitin ligase Mdm2, which targets p53 for proteasomal degradation (Haupt et al., 1997; Kubbutat et al., 1997). Unless phosphorylated, p53 associates N-terminally with Mdm2 through interaction with an essential p53 binding site (Iwakuma and Lozano, 2003). The small molecule inhibitor Nutlin-3 specifically targets this binding pocket and thereby inhibits interaction of p53 with Mdm2 (Carvajal et al., 2005; Vassilev, 2004; Vassilev et al., 2004). As a consequence, stabilized p53 is no longer targeted for proteasomal degradation and is transcriptionally activated (Thompson et al., 2004). Since Nutlin-3 acts by direct inhibition of Mdm2, it induces accumulation of p53 in the absence of cellular stresses.

First, I defined the effective concentration of Nutlin-3 required to stabilize p53. To this end, levels of p53 and Mdm2 were measured in uninfected HeLa cells over 24h. Cells were continuously incubated with 25µM Nutlin-3 and were harvested at 0, 0.5, 2, 4, 6, and 24h. Whole cells lysates were resolved via SDS-PAGE and immunoblotted for p53, Mdm2, and α-Tubulin as loading control (Figure 5-19, E). As demonstrated by the increase in p53 abundance at 24h, 25µM Nutlin-3 was sufficient to stabilize p53.

Next, to address whether accumulation of p53 affected the VACV-induced shift, the cell cycle distribution of asynchronous HeLa FUCCI cells was monitored during VACV infection in the presence or absence of Nutlin-3. HeLa FUCCI cells were pre-treated with Nutlin-3 (25µM) for 30min before being either mock infected, or infected with WT VACV (MOI 2) in the continued presence of the inhibitor. Samples were harvested at 0, 12, and 24hpi and the cell cycle

distribution was analysed by flow cytometry. Based on their fluorescence, cells were classified as either early G1, G1, early S, or S / G2 / M (Figure 5-19, A-D).

As previously described in chapter 4, untreated and uninfected populations were measured to accumulate in G1, which increased the G1 fraction from 28.5 ± 0.2 % at 0hpi, to 35.2 ± 2.0% at 24hpi (Figure 5-19, B). Concurrently, the amount of cells in S/G2/M decreased between 0 and 24hpi (Figure 5-19, D). Neither the early G1, nor the early S phase fraction was found to fluctuate significantly in mock infected samples (Figure 5-19, B, C). VACV infected samples were confirmed to induce the opposite trend: the fraction of S/G2/M cells was increased at the expense of early G1, and G1 cells, indicating reduced G1 entry.

Conversely, while Nutlin-3 did not affect the cell cycle distribution of uninfected cells, it prevented VACV from shifting cells into S/G2/M. This fraction represented 36.3 ± 0.9% of untreated, infected cells, whereas it made up significantly less (26.0 ± 2.0%) in Nutlin-3 treated, infected populations (Figure 5-19, D). The inhibitory effect of Nutlin-3 was mirrored by the failure of VACV to shift cells out of G1. In the absence of Nutlin-3, VACV infection caused the G1 fraction to decline to 23.8 ± 1.2% of total cells. However, in the presence of Nutlin-3, the amount of G1 cells increased from 28.5 ± 0.2% at 0hpi to 32.1 ± 1.3%, which was comparable to mock infected levels at 24hpi (Figure 5-19, B). Concluding, using the FUCCI reporter system, I found that Nutlin-3 prevented VACV from shifting cells from the G1 phase of the cell cycle into the S/G2/M phase. On the other hand, Nutlin-3 did not affect the cell cycle distribution of uninfected control cells, which were found to shift from S/G2/M into G1.

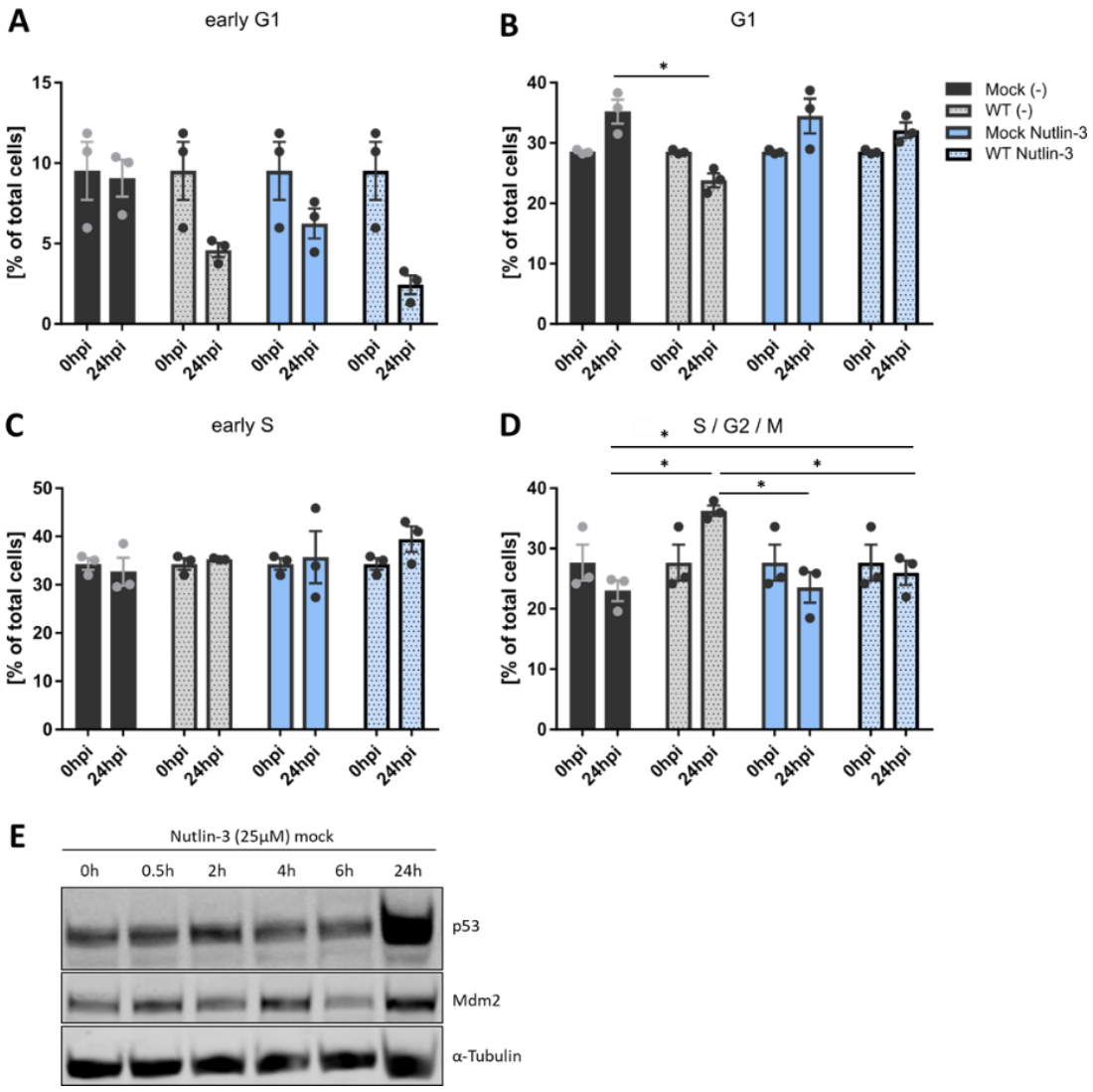

Figure 5-19 Nutlin-3 prevents VACV from shifting the cell cycle distribution.

HeLa FUCCI cells were pre-treated with Nutlin-3 (25µM) for 30min before being either mock infected, or infected with WT VACV (MOI 2) in the continued presence of the inhibitor. Samples were harvested at 0, 12, and 24hpi and the cell cycle distribution was analysed by flow cytometry. Based on their fluorescence, cells were classified as either early G1, G1, early S, or S/G2/M. Individual cell cycle fractions are compared in [A-D]. [A] Percentage of early G1, [B] G1, [C] early S, and [D] S/G2/M cell fractions in untreated mock (black bars), untreated WT VACV (dotted grey bars), Nutlin-3 treated mock (blue bars), and Nutlin-3 WT VACV (dotted, light blue bars) infected samples. Data represent three biological replicates with one technical replicate each and are displayed as mean ± S.E.M. Shown are all statistically significant differences within the G1, and S/G2/M fractions for the 24hpi timepoint. Parametric, paired, two-tailed t-test for significance. ns. $p > 0.05$, * $p < 0.033$. [E] Levels of p53 and Mdm2 after 24h of Nutlin-3 (25µM) treatment. Uninfected HeLa cells were continuously incubated with 25µM Nutlin-3 and were harvested at 0, 0.5, 2, 4, 6, and 24h. Whole cells lysates were resolved via SDS-PAGE and immunoblotted for p53, Mdm2, and α-Tubulin as loading control.

4.5 Nutlin-3 inhibits viral late gene expression

In the previous section I showed that Nutlin-3 causes accumulation of p53 and prevents VACV from shifting the host cell cycle. Next, I aimed to determine whether increased p53 levels and/or inhibition of the cell cycle shift affected the virus life cycle. To address this question, I made use of VACV's temporally cascaded gene transcription. Expressing EGFP under a stage-specific viral promoter allows to monitor progression of the virus life cycle and to detect potential inhibition of intermediate steps (Figure 5-20). In order to monitor expression of viral early genes I used a VACV recombinant that expresses EGFP under an early viral promoter (WR E EGFP). Similarly, to assess viral late gene expression, I used a VACV recombinant that expresses EGFP under a late viral promoter (WR L EGFP).

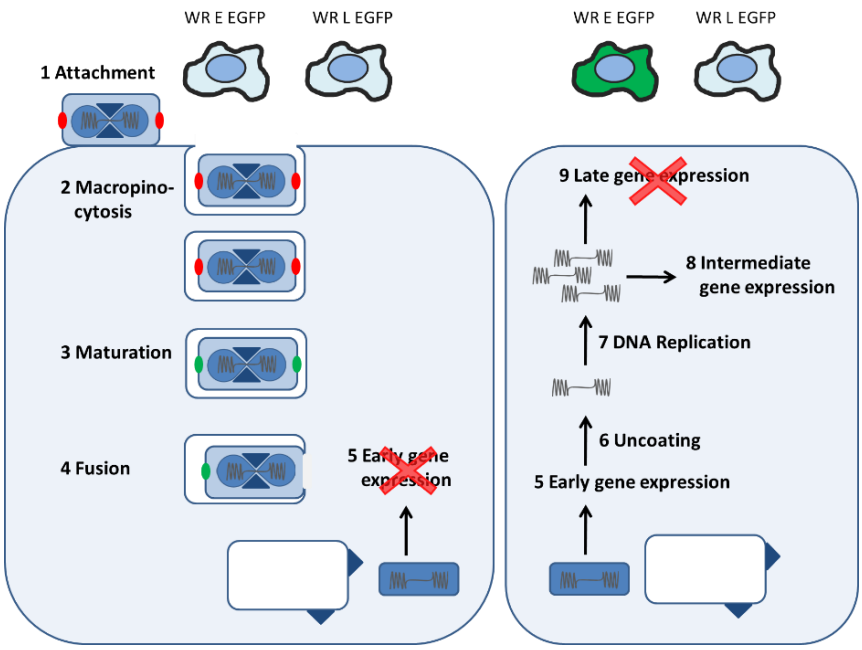

Figure 5-20 Schematic of WR E EGFP and WR L EGFP infection.

Infection with recombinant VACV that expresses EGFP either un an early, or a late viral promoter allows to monitor progression of the virus life cycle and to detect potential inhibition of intermediate steps. Early inhibitors block expression of both early and late viral gene expression (neither E EGFP, nor L EGFP expression), whereas late inhibitors only repress late gene expression (E EGFP expression in the absence of L EGFP expression). An early block indicates inhibition viral entry or protein translation and a late block suggests inhibition viral genome replication and intermediate or early gene transcription.

The combination of these two VACV reporter strains allows to classify a compound as either an early inhibitor (neither E EGFP, nor L EGFP expression), or a late inhibitor (E EGFP expression

in the absence of L EGFP expression) (Figure 5-20). Whereas an early block indicates inhibition of a step before early gene expression, including viral entry and protein translation, a late block suggests inhibition of a step between the two gene expression waves, including viral genome replication and intermediate or early gene transcription.

To determine the effect of Nutlin-3 on the VACV life cycle, HeLa cells pre-treated with Nutlin-3 (25µM) for 30min were infected with either WR E EGFP (MOI 5), or WR L EGFP (MOI 5) in the continued presence of inhibitor. Samples were harvested at 0, 2, 4, 6, 8, 10, and 24hpi and EGFP expression was analysed by flow cytometry (Figure 5-21). Two different infection parameters were measured: the percentage of EGFP expressing cells (Figure 5-21, A, B) and the amount of viral gene expression, as determined by the mean fluorescence intensity (MFI) of the EGFP signal (Figure 5-21, C, D).

Nutlin-3 had no influence on viral entry or viral early gene expression. The percentage of WR E EGFP infected cells was comparable in mock and Nutlin-3 treated cells throughout the infection timecourse (Figure 5-21, A). Under both conditions, approx. 86% of cells were early EGFP positive by 24hpi. Similarly, the amount of early expressed EGFP did not differ in mock and Nutlin-3 treated cells (Figure 5-21, C), indicating that Nutlin-3 does not impact early viral gene expression, or any steps earlier during the virus life cycle.

In contrast, viral late gene expression was severely reduced and delayed by Nutlin-3 treatment. The delay in late viral gene expression was marked by significantly fewer late EGFP positive cells at 6hpi in Nutlin-3 treated samples (Figure 5-21, B). After an initial lag phase, the percentage of late infected cells in treated and untreated samples equalized by 24hpi (Figure 5-21, B). While the percentage of late infected cells caught up by 24hpi, the amount of late gene expression did not (Figure 5-21, C). L EGFP levels were 2.1-fold reduced at 6hpi and continued to stay below untreated controls, so that by 24hpi they were 2.5-fold reduced, compared to controls (Figure 5-21, C).

Taken together, this data shows that Nutlin-3 inhibits a step between viral early and late gene expression. Further experiments are required to define the repressed step in the virus life cycle. Additionally, it remains to be clarified whether Nutlin-3 directly inhibits viral replication, or whether the antiviral activity represent an indirect effect of increased p53 levels.

In the previous chapter (section 3) I have shown that VACV relies on expression of viral intermediate or late gene expression to shift the host cell cycle. Since I have found that Nutlin-3 inhibits late viral gene expression, this might explain why VACV fails to shift the host cell

cycle in the presence of Nutlin-3. Therefore, further experiments are required to determine the utility of shifting the cell cycle, and whether there might exist a positive feedback loop between viral gene expression and the cell cycle shift.

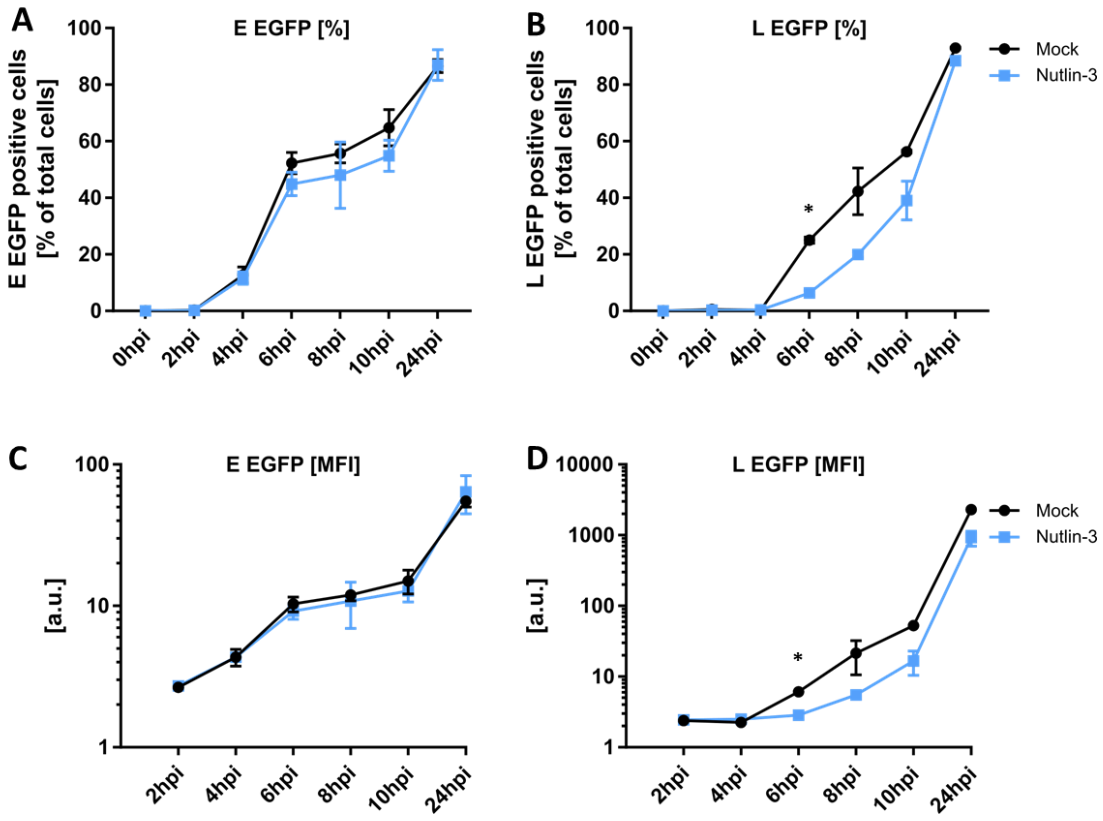

Figure 5-21 Nutlin-3 inhibits late viral gene expression.

HeLa cells were pre-treated with Nutlin-3 (25µM) for 30min before being infected with either WR E EGFP (MOI 5), or WR L EGFP (MOI 5) in the continued presence of the inhibitor. Samples were harvested at 0, 2, 4, 6, 8, 10 and 24hpi and EGFP expression was analysed by flow cytometry. [A-B] Percentage of infected cells in the presence (blue), or absence of Nutlin-3 (black), represented by the amount of cells expressing either early viral genes [A], or late viral genes [B]. [C-D] The amount of viral gene expression in the presence (blue), or absence of Nutlin-3 (black), represented as the mean fluorescence intensity (MFI) of EGFP expressed under an early [C], or late viral promoter [D]. EGFP MFI is indicated on a logarithmic scale. Data represent one biological replicate with two technical replicates and are displayed as mean ± S.D. Only statistically significant differences are indicated. Parametric, paired, two-tailed t-test for significance. ns. $p > 0.05$, * $p < 0.033$.

4.6 Small molecule inhibitor screen identifies cellular G2/M regulators as required for productive VACV infection

Previously published data and my own results presented in this thesis, provide evidence that VACV infection alters cell cycle progression (Jungwirth and Launer, 1968; Kit and Dubbs, 1962; Wali and Strayer, 1999b; Yoo et al., 2008). Using RNAi and different VACV recombinants showed that VACV gene expression modulates the G1/S and G2/M checkpoints and shifts the host cell cycle. While I have shown that VACV targets different cell cycle pathways and regulatory proteins, the utility of this remained to be investigated.

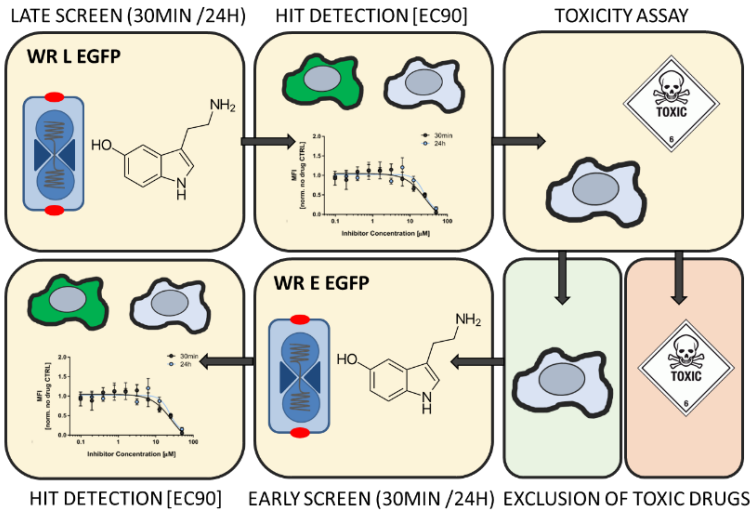

Figure 5-22 Schematic workflow of the cell cycle inhibitor screen.

A small molecule inhibitor library was screened that targets pre-selected cellular kinases implicated in cell cycle control. First, the library was screened for inhibitors of late viral gene expression using the WR L EGFP reporter strain. The drugs were preincubated for either 30min or 24h and the viral late gene expression was measured by flow cytometry. The EC90 concentration was calculated for all preliminary hits and the cytotoxicity was measured by LDH assay. Non-toxic hits were then screen for inhibitors of early viral gene expression using the WR E EGFP reporter strain. The drugs were preincubated for either 30min or 24h and the viral early gene expression was measured by flow cytometry. The EC90 concentrations were again determined for all hits.

To address this question, I screened a small molecule inhibitor library that targeted pre-selected cellular kinases implicated in cell cycle control. The library was assembled based on hits from two previously published siRNA screens (Mercer et al., 2012; Sivan et al., 2013) and unpublished phosphoproteomics data from the Mercer lab. The resulting library contained 19 compounds that targeted several CDKs, Aurora kinases, DDR associated kinases, as well as the negative cell cycle regulator Wee1. For supplementary information about the inhibitors, please refer to Table 8 in the Material and Methods section 3.1.

Extended inhibition of any cell cycle controller is likely to result in aberrant cell cycle progression and/or cell cycle arrest. Therefore, it was essential to differentiate between direct enzymatic involvement of the kinase in the virus life cycle, and an indirect effect caused by interfering with cell cycle progression. To identify the individual contributions, I screened the library with two different preincubation regimes. The cells were either preincubated with inhibitor for 30 min prior to infection to test for the direct enzymatic requirement of the targeted kinase, or for 24 h to assess the indirect effect of perturbing the cell cycle.

Using the two different preincubation regimes, the library was first screened for inhibitors of viral late gene expression (workflow outlined in Figure 5-22). To establish a dose-titration curve, the inhibitors were used at a broad concentration range, based on the reported IC50 values in cell-free assays (Materials and Methods, Table 7). Compounds that repressed viral late gene expression were tested for their cytotoxicity by LDH assay and toxic compounds were discarded as "non-hits". Next, non-toxic hits were screened for inhibitors of early viral gene expression and the hits were classified as either early or late inhibitors. EC90 values were determined for all early and late inhibitors in order to be used in future follow-up studies (for EC90 values, please refer to Table 9).

First, to identify inhibitors of late viral gene expression I again used the WR L EGFP reporter strain that expresses EGFP under a late viral promoter. HeLa cells were preincubated with serially diluted inhibitors for either 30 min, or 24 h and infected with WR L EGFP (MOI 5) in the presence of inhibitor. Samples were harvested at 24 hpi and analysed by flow cytometry. Viral late gene expression was measured as the mean fluorescence intensity (MFI) of the L EGFP signal and normalized to a plate-internal DMSO infection control. Normalized MFI values are plotted against the inhibitor concentrations (logarithmic scale). The dose response curve for each inhibitor was fitted as a non-linear regression curve with a variable slope using the software Prism7.

Of the 19 screened drugs, four were found not to inhibit viral late gene expression and were immediately discarded as non-hits: the DNA-PK inhibitor (Selleckchem catalogue number S2893), the MEK1 inhibitor (S1006) and the ATR inhibitors (S8050 and S8007) (Figure 5-23). For the remaining 15, EC90 values were determined for both the 30min and 24h preincubation regime. The effective concentration 90 (EC90) describes the concentration at which compound displays 90% of its maximum effect. In the case of a repressor, EC90 values therefore indicate the concentration at which the compound reaches 90% of its maximum inhibitory effect (also called IC90). As most of the screened inhibitors were developed as anti-cancer drugs,

considerable cytotoxicity was expected in HeLa cells. Therefore, the cytotoxicity of the EC90 concentrations was determined after 24h incubation by LDH assay. Inhibitors were classified as toxic if they caused more than 30% cell death, compared to a cell lysis control which was set at 100% cell death. This criterion eliminated another five compounds from the hit list as toxic: the ATM inhibitor (S1092), the CDK7 inhibitor (S1572), the CDK1/2/5 inhibitor (S1153), the CDK4/6 inhibitor (S1116), and the Casein Kinase 2 (CK2) inhibitor (S2248). These "non-hit" compounds are grouped in Figure 5-23.

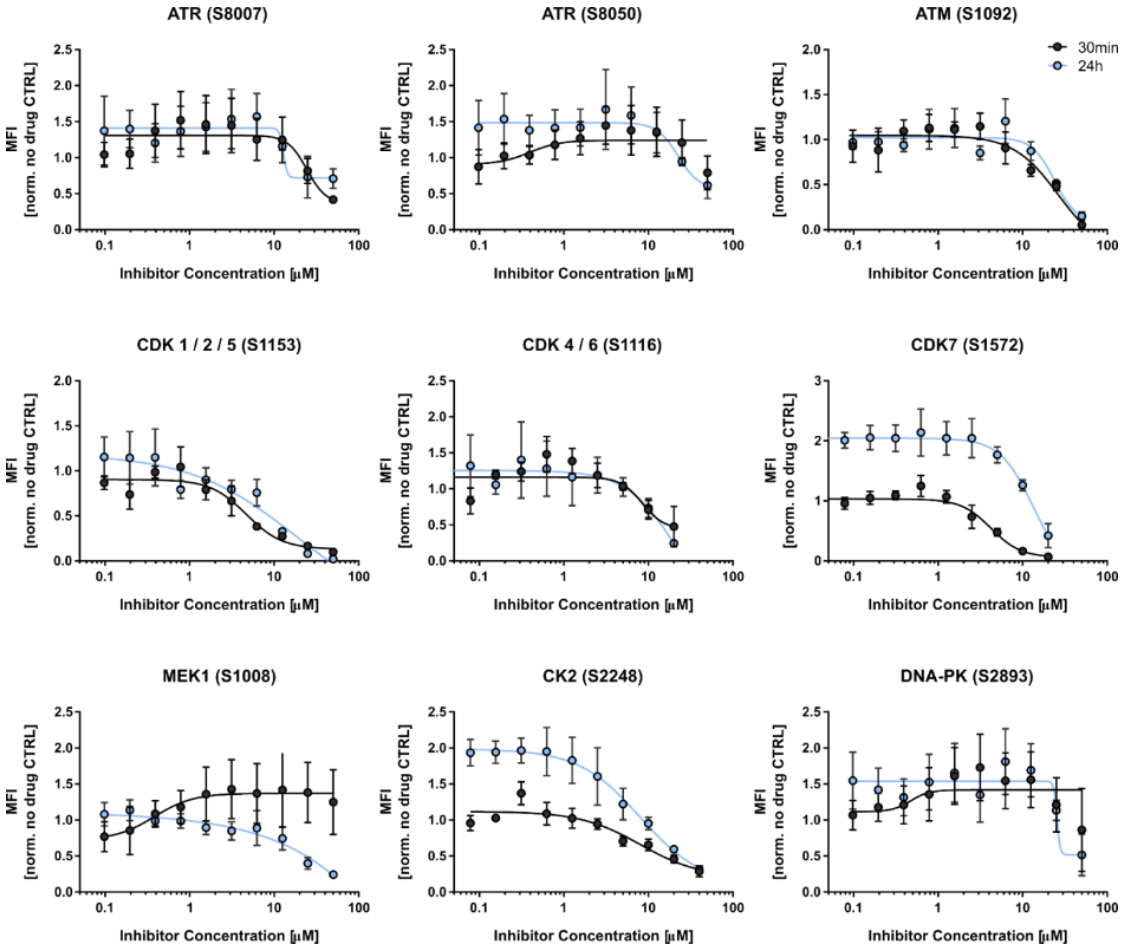

Figure 5-23 Compounds without anti-viral activity.

HeLa cells were pre-incubated with increasing concentrations of the indicated inhibitors for either 30min (black), or 24h (light blue). Cells were infected in the presence of inhibitor with WR L EGFP (MOI 5), expressing EGFP under a late viral promoter and samples were harvested at 24hpi. The mean EGFP fluorescence intensity (MFI) was analysed by flow cytometry and was normalized to the DMSO infection control. Normalized MFI values are plotted against the inhibitor concentrations (logarithmic scale). The dose response curve for each inhibitor is displayed as a solid line and was fitted as a non-linear regression curve with a variable slope using the software Prism7. Data represent three biological replicates with two technical replicates each and are displayed as mean ± S.E.M. Selleckchem catalogue numbers for the respective inhibitor are displayed in brackets.

Next, to identify inhibitors of viral early gene expression I used the WR E EGFP reporter strain that expresses EGFP under an early viral promoter. HeLa cells were preincubated with serially diluted inhibitors for either 30 min, or 24 h and infected with WR L EGFP (MOI 5) in the presence of inhibitor. Samples were harvested at 8 hpi and analysed by flow cytometry. Viral early gene expression was measured as the mean fluorescence intensity (MFI) of the E EGFP signal and normalized to a plate-internal DMSO infection control. Normalized MFI values are plotted against the inhibitor concentrations (logarithmic scale). The dose response curve for each inhibitor was fitted as a non-linear regression curve with a variable slope using the software Prism7.

As before, EC90 values were determined and a second toxicity assay was carried out, if the EC90 for early inhibition was found to be higher than the previously determined EC90 for late inhibition. The hits were grouped into three different functional groups: Aurora Kinases (Figure 5-24), DDR kinases (Figure 5-25), CDKS and Wee1 (Figure 5-26).

The tested Aurora kinase inhibitors did not repress viral early gene expression (Figure 5-24). On the other hand, both pan-Aurora kinase inhibitors were found to negatively affect late viral gene expression after 30min preincubation. With the same preincubation regime, selective inhibition of AuroraA or AuroraB did not prevent viral late gene expression. This might indicate that the kinase function of AuroraA/B is directly required for viral late gene expression and that AuroraA and AuroraB might have redundant functions in the viral life cycle. Additionally, all four inhibitors were found to abolish late gene expression after preincubation for 24h, with a lower EC90 than after 30min preincubation which indicates a stronger inhibitor effect. Since inhibition of Aurora kinases has been linked to cell cycle arrest at G2/M (Li et al., 2010b) and generalized inhibition of cell cycle progression (Kumari et al., 2014), this data suggests that prolonged inhibition of Aurora kinases induces cell cycle changes which are permissive for viral early gene expression but repress viral late gene expression.

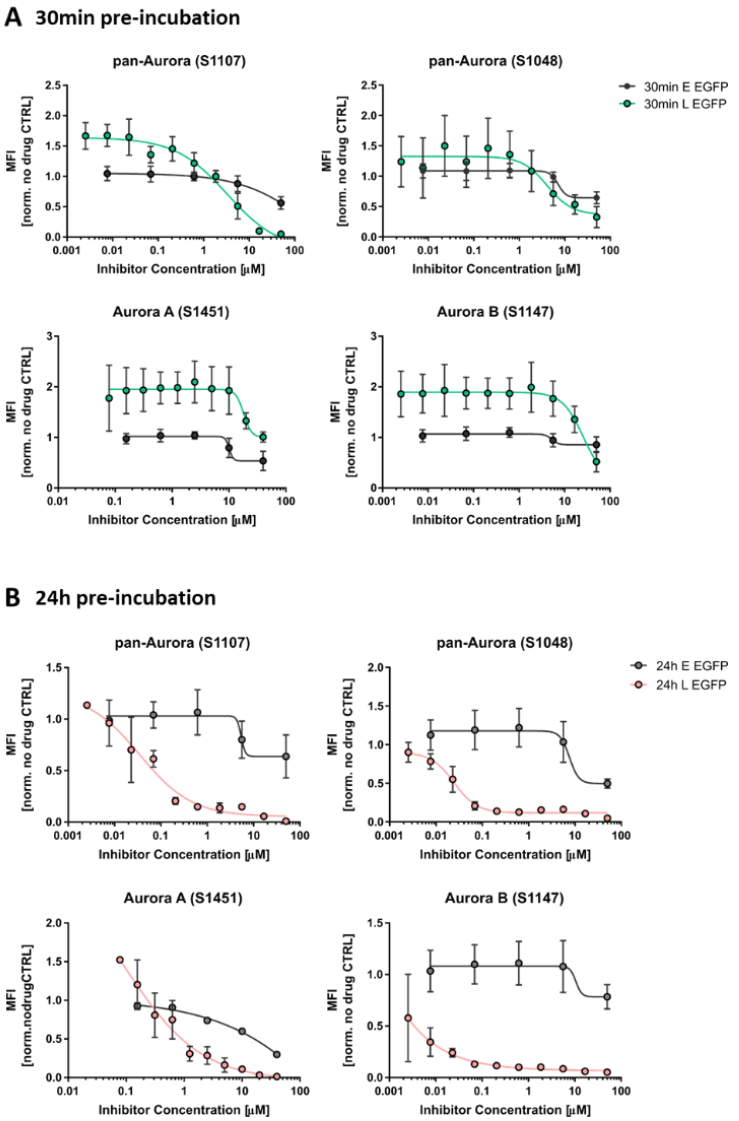

Figure 5-24 Aurora kinase inhibitors prevent VACV late gene expression.

HeLa cells were pre-incubated with increasing concentrations of the indicated inhibitors for either [A] 30min, or [B] 24h. Cells were infected in the presence of inhibitor with either WR E EGFP (MOI 5, black and grey), or WR L EGFP (MOI 5, green and pink). Samples were harvested either at 8hpi (WR E EGFP), or at 24hpi (WR L EGFP). The mean EGFP fluorescence intensity (MFI) was analysed by flow cytometry and was normalized to the DMSO infection control. Normalized MFI values are plotted against the inhibitor concentrations (logarithmic scale). The dose response curve for each inhibitor is displayed as a solid line and was fitted as a non-linear regression curve with a variable slope using the software Prism7. Data represent three biological replicates with two technical replicates each and are displayed as mean ± S.E.M. Selleckchem catalogue numbers for the respective inhibitor are displayed in brackets.

Inhibition of the DDR kinases ATR, Chk1, and Chk2 have previously been shown to inhibit viral genome replication (Postigo et al., 2017). Confirming these results, inhibition of ATR, Chk1, or Chk1/2 represses viral late gene expression in a dose-dependent manner (Figure 5-25). On the other hand, viral early gene expression was less susceptible to ATR, Chk1, or Chk1/2 inhibition after 30min pre-incubation and a strong reduction in EGFP signal was only observed at the

highest tested concentration (20µM) for the Chk1 inhibitor. Pretreatment for 24h lowered the EC90 values for late viral gene inhibition and also affected early viral gene expression, although to a much lesser extent. This data confirms previous findings that enzymatic activity of the DDR kinases ATR, Chk1, and Chk1/2 is required for productive VACV infection (Postigo et al., 2017). While it was published that activation of the DDR was required for viral genome replication, based on my results I can only confirm the block to occur at a stage between viral early and viral late gene expression.

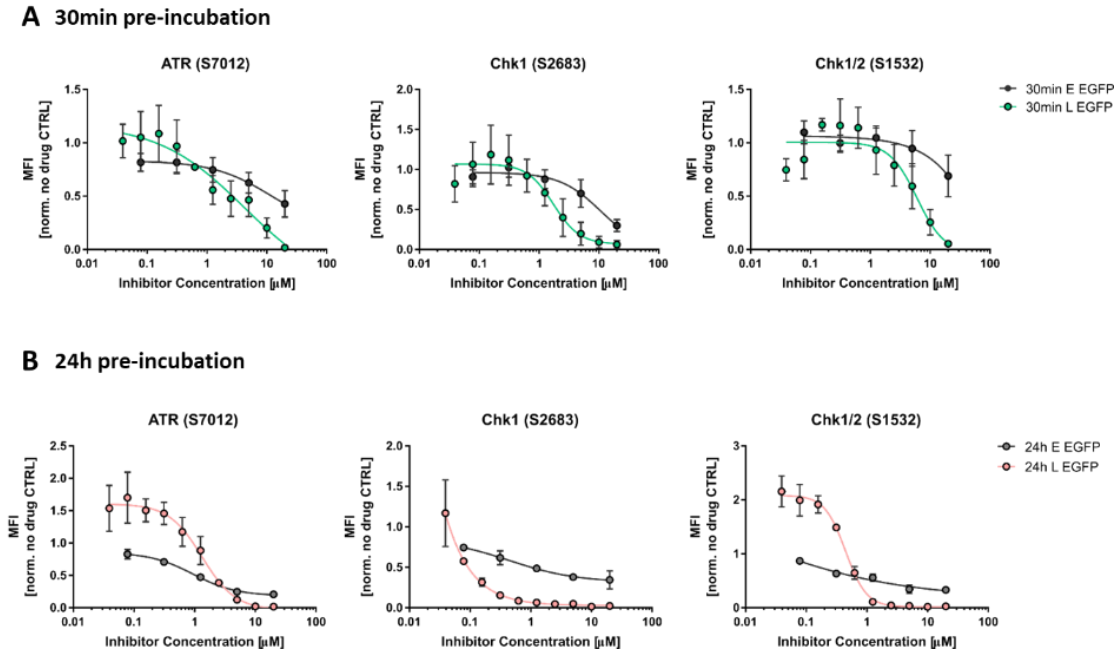

Figure 5-25 DNA damage response inhibitors attenuate VACV late gene expression.

HeLa cells were pre-incubated with increasing concentrations of the indicated inhibitors for either [A] 30min, or [B] 24h. Cells were infected in the presence of inhibitor with either WR E EGFP (MOI 5, black and grey), or WR L EGFP (MOI 5, green and pink). Samples were harvested either at 8hpi (WR E EGFP), or at 24hpi (WR L EGFP). The mean EGFP fluorescence intensity (MFI) was analysed by flow cytometry and was normalized to the DMSO infection control. Normalized MFI values are plotted against the inhibitor concentrations (logarithmic scale). The dose response curve for each inhibitor is displayed as a solid line and was fitted as a non-linear regression curve with a variable slope using the software Prism7. Data represent three biological replicates with two technical replicates each and are displayed as mean ± S.E.M. Selleckchem catalogue numbers for the respective inhibitor are displayed in brackets.

Non-selective inhibition of CDKs (S1249) was found to negatively affect viral gene expression in general, although late gene expression was found to be more susceptible to inhibition as reflected by a lower EC90 value than for early gene expression (Figure 5-26). These data suggest that generalized inhibition of CDKs interferes either with viral entry, fusion, and/or viral early gene transcription or translation. Although anti-viral concentrations of the

compound were not measured to be cytotoxic, pan-CDK inhibition might still non-specifically reduce the host cells ability to support productive viral infection

Inhibition of CDK 2/7/9 (S1145) did not affect viral gene expression after 30min preincubation (Figure 5-26). However, 24 h preincubation was found to repress viral late gene expression at a dose-dependent manner, while early gene expression was less inhibited. These findings indicate that enzymatic activity of the three CDKs 2/7/9 is not directly required for viral gene expression. Inactivation of the CAK CDK7 prevents activation of all other cell cycle regulating CDKs and therefore arrests the cell cycle in G1 and G2 (Nuwayhid et al., 2006). The data suggests that 24h preincubation with the inhibitor induces cell cycle changes which are not permissive for viral late gene expression.

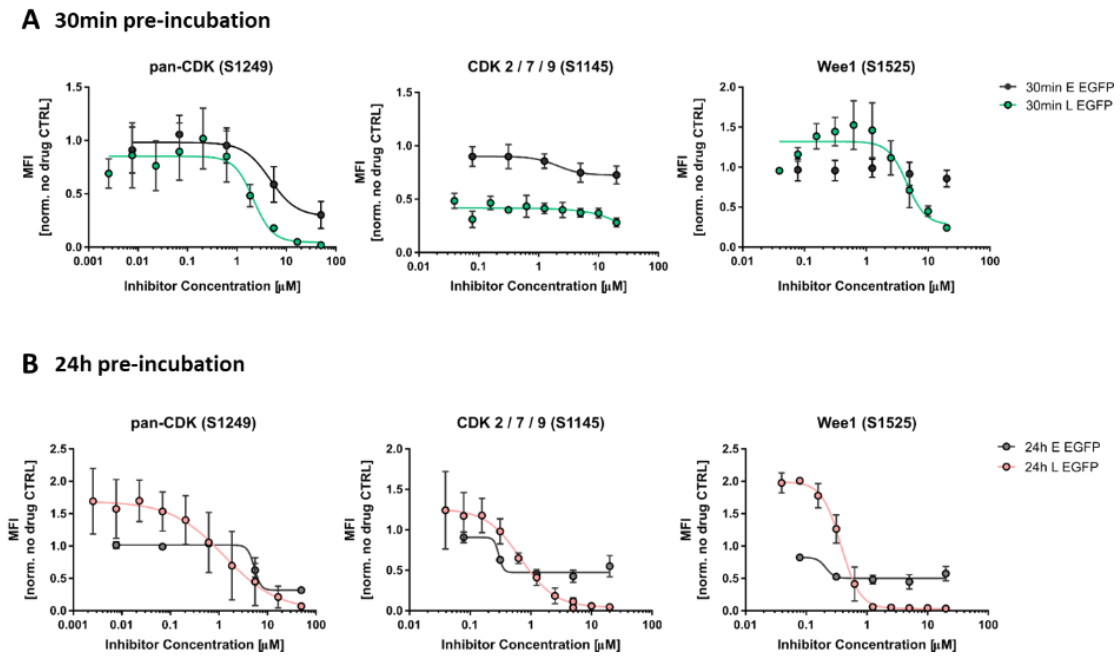

Figure 5-26 Wee1 and selected CDK inhibitors prevent VACV late gene expression.

HeLa cells were pre-incubated with increasing concentrations of the indicated inhibitors for either [A] 30min, or [B] 24h. Cells were infected in the presence of inhibitor with either WR E EGFP (MOI 5, black and grey), or WR L EGFP (MOI 5, green and pink). Samples were harvested either at 8hpi (WR E EGFP), or at 24hpi (WR L EGFP). The mean EGFP fluorescence intensity (MFI) was analysed by flow cytometry and was normalized to the DMSO infection control. Normalized MFI values are plotted against the inhibitor concentrations (logarithmic scale). The dose response curve for each inhibitor is displayed as a solid line and was fitted as a non-linear regression curve with a variable slope using the software Prism7. Data represent three biological replicates with two technical replicates each and are displayed as mean ± S.E.M. Selleckchem catalogue numbers for the respective inhibitor are displayed in brackets.

Inhibition of the kinase Wee1 did not repress early viral gene expression at the tested concentrations, neither after 30min, nor 24h preincubation (Figure 5-26). On the other hand, viral late gene expression was reduced in a dose-dependent manner at both preincubation regimes. This data indicates that the enzymatic activity of Wee1 might directly contribute to

productive viral infection (30min preincubation). However, preincubation for 24h lowered the EC90 ca. 10-fold which indicates that inhibition of Wee1 creates a cellular environment which is not permissive for viral late gene expression. In uninfected cells, Wee1 prevents M phase entry by phosphorylating CDK1 (cf. Introduction, section 3.3.2). Inhibition of Wee1 has been shown to cause an M phase arrest in some cell lines (Kreahling et al., 2013; Lewis et al., 2017). Taken together, these findings might suggest that infection in M phase cells cannot progress to the stage of late viral gene expression.

In summary, I have screened a custom-made small molecule library for inhibitors of viral late and/or early gene expression. To differentiate between direct enzymatic involvement of the kinase in the virus life cycle, and an indirect effect caused by interfering with cell cycle progression, I preincubated the cells with the drugs for 30min, and 24h, respectively. After elimination of toxic compounds, I found nine inhibitors, grouping into three classes, which negatively affect viral late gene expression, while one compound also reduced viral early gene expression. I could confirm previous results that implicate a role of the DDR for productive viral infection. Additionally, I found Aurora kinases to be implicated in viral replication, a connection that has not yet been described in the literature. The inhibited virus life cycle stage(s) between viral early and late gene expression remain to be defined. Also, analysis of the cell cycle distribution after inhibitor treatment will provide further insight into the individual cell cycle phase requirements for VACV replication.

5 Summary chapter 5

In chapters 3 and 4 I have shown that VACV arrests and then shifts the host cell cycle from G1 into S/G2/M. While the cell cycle arrest depends on a pre-uncoating step, shifting the host cell cycle requires expression of an intermediate or late viral gene. In this chapter I show that VACV infection dysregulates the G1/S and G2/M checkpoints (Figure 5-27). Screening a small molecule inhibitor library, I confirmed that DDR activation is required for viral late gene expression. Additionally, I discovered the cell cycle regulators Aurora Kinase A and B to be required for productive infection, which has not been previously described.

I found viral early gene expression to disrupt the G1/S cell cycle checkpoint which is normally controlled by p53 and its effector protein p21 (Waf1). Activation of p53 induces expression of p21 which then elicits a G1 arrest by repressing CDK2 and CDK1 function. I showed that viral early gene expression coincided with accumulation of p21 during early stages of infection. On the other hand, p53 was degraded in a mechanism that depended on the viral kinase B1 and/or its paralog pseudokinase B12. Using temperature sensitive VACV strains and a p53-/- cell line, I found that VACV arrests and shifts the host cell cycle in a p53-independent manner, which also did not require expression of B1 and/or B12. However, stabilization and accumulation of p53 by Nutlin-3 repressed viral late gene expression as well as the VACV-induced cell cycle shift. It remains to be clarified which viral life cycle step is inhibited by Nutlin-3 treatment.

Late gene expression then activated the G2/M checkpoint. The late expressed viral kinase F10 was shown to be required and sufficient for activation of the DDR kinases ATM and Chk2. Confirming previous findings, pharmacological inhibition of the DDR repressed viral late gene expression. In addition to DDR activation, F10 expression negatively regulated p21 levels: overexpression of F10 reduced cellular p21 levels, whereas siRNA knockdown during infection prevented p21 degradation. The mechanism and the role of F10-mediated regulation of p21 remains to be elucidated.

Taken together, in this chapter I have found a mechanism how VACV dysregulates the G1/S and G2/M checkpoint which is indicated to promote infection.

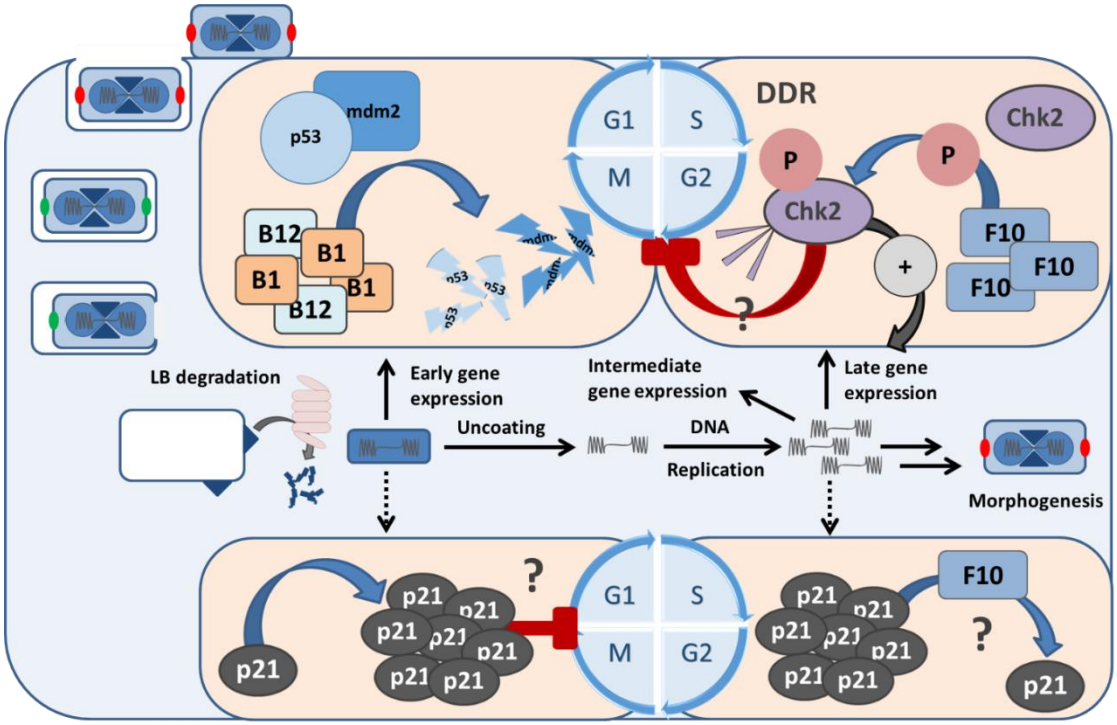

Figure 5-27 A model of VACV induced alterations of the cell cycle and its regulatory proteins.

VACV infection inhibits cell proliferation and shifts the cell cycle from G1 into S/G2M. VACV enters the host cell and expresses a first wave of early genes, which induces a block in cell cycle progression and degradation of the regulatory proteins p53 and Mdm2. Concurrently, the cellular CDK inhibitor p21 accumulates in an infection-dependent manner. As infection progresses to express intermediate and late viral genes, cells are shifted from G1 into S/G2/M. The shift in cell cycle is paralleled by degradation of p21 and viral F10-mediated activation of the DNA damage response (DDR). Activation of the DDR components ATR, Chk1 and Chk2 is required for expression of late viral genes.

6 Discussion

As obligate intracellular parasites, viruses are highly dependent on the host cell environment for productive viral replication. Therefore, they have evolved strategies to make host factors more abundant and accessible, while evading the host's immune response. A common viral strategy is subversion of the host cell's division and growth program, the so-called cell cycle. This process is tightly regulated in normal, uninfected cells and several molecular checkpoints ensure that cells divide in a controlled manner. Uncontrolled division, however, is a hallmark of cancer and cell cycle dysregulation is a major cause for cancer development. Efforts to better understand the mechanisms that promote oncogenesis have identified a small group of oncogenic viruses that drive cancer development. Current estimates by the WHO assume that viral infections account for 20% of human cancers worldwide and virus-induced cell cycle dysregulation has been the focus of intense research over the past years (reviewed in (Bagga and Bouchard, 2014; Fan et al., 2018)). However, viruses have not only been recognized as a cause for cancer but also as a promising biotechnological tool for anti-cancer therapy. These virotherapies exploit a virus' natural or engineered preference for preferentially infecting and thereby destroying tumour cells. Several different virotherapies based on oncolytic viruses such as the poxvirus vaccinia virus (VACV) are currently being tested in clinical trials.

VACV is well-known as the model poxvirus and has gained clinical significance as the vaccine used to successfully eradicate smallpox. The causative agent of smallpox, variola poxvirus, remains the deadliest virus in human history, accounting for more than 500 million deaths. The smallpox vaccination campaign has been discontinued, which leaves the population at risk for smallpox re-emergence by bioterrorism, or zoonotic poxvirus infections such as monkeypox and cowpox. Limited treatment options for poxvirus infections necessitate continued research into this virus family to develop improved anti-virals and vaccines.

Encoding over 200 proteins, Poxviruses are known as master regulators that highjack and control almost every process in their host cells. As the model poxvirus, VACV has been extensively studied for nearly 80 years. Early reports published in the 60ies suggested that VACV alters the host cell cycle and inhibits cellular DNA synthesis (Jungwirth and Launer, 1968). Later, VACV was described to modulate expression of key cell cycle regulators, such as Cyclins and CDKs (Wali and Strayer, 1999b; Yoo et al., 2008), and to activate the cellular DNA damage response (Postigo et al., 2017). However, the relevance of this cell cycle subversion to VACV replication and how it is achieved remained undefined. This PhD project therefore aimed

to provide a more comprehensive understanding of how VACV alters the host cell cycle during infection. Throughout this thesis I combined state of the art techniques with classical assays to determine the (viral) effector proteins, their mode of action, and the contribution of the host cell cycle to productive VACV infection. Although I have discovered novel mechanistic insights and enabled a better understanding of how and why VACV modulates the host cell cycle, my work also highlights the complexity of this host pathogen interaction. In the following I will summarize the major findings of this thesis, discuss open questions and future directions

1 VACV arrests the host cell cycle

I developed a direct, image-based assay to visualize cellular DNA synthesis in VACV infected cells. Using this assay in combination with measuring cell proliferation, I have demonstrated that VACV rapidly arrests the cell cycle and cellular DNA synthesis in a process that relies on either H1, and/or early viral gene expression. However, the viral effector protein remains to be identified.

To address this question, I will first need to distinguish between the requirement for the viral phosphatase H1 and early gene transcription. To test whether H1 is sufficient for preventing cell cycle progression, I will overexpress a codon-optimized version of H1 and monitor cell proliferation. If I find H1 sufficient to prevent cell proliferation, I will look to characterize the underlying mechanism for this.

However, I hypothesise that viral early gene expression rather than H1 accounts for the block, since I found that the H1(-) strain prevents cells cycle progression. Additional, indirect evidence that the viral effector is not H1 but an early viral protein comes from a previous study of UV inactivated VACV. UV-induced crosslinking of viral DNA was shown to inhibit viral genome replication and early gene expression in a dose-dependent manner (Tsung et al., 1996). Importantly, the authors also described a UV regime that rescued cell proliferation while allowing for expression of only a subset of short early viral genes. In this setting, pre-packaged H1 will still have been present in the infected cells but did not seem sufficient for blocking host cell cycle progression. Additionally, this particular UV crosslinking regime was found to inhibit expression in a gene size dependent manner. Therefore, this report predicts the viral effector protein to be encoded by an early gene longer than 0.5 kb. Since the majority

of viral (early) genes fall within this size category, this criterion does not sufficiently reduce the number of candidate proteins.

Hence, if I find that H1 is non-essential in blocking the host cell cycle, I will next screen the Mercer lab early gene siRNA library by automated, high-throughput microscopy, using our previously published protocol (Kilcher et al., 2014; Mercer, 2019). To test specifically the role of early viral proteins, I will screen the siRNA library with the temperature sensitive Cts24 strain under non-permissive conditions to prevent intermediate and late viral gene expression. In combination with the EdC incorporation assay described in Chapter 3, this system will allow me to identify the viral gene(s) which prevent cellular DNA synthesis.

Concurrent with the block in cellular DNA synthesis, I found the cellular CDK inhibitor p21 (Waf1 / Cip1) to be upregulated by VACV infection. However, so far I have not identified how VACV induces p21 accumulation and the (viral) effector protein remains to be defined. Since p21 accumulation was found to coincide with the onset of viral early gene expression, this suggested that VACV encodes an early effector that positively regulates the stability of p21. In uninfected cells, p21 has a very short half-life and is tightly controlled by dynamic phosphorylation that either promotes degradation or stabilizes the protein. VACV encodes only one known kinase that is expressed early during infection, the viral kinase B1. Further implicating a role in stabilizing p21, I found B1 to share > 40% sequence homology with the two cellular kinases PIM1 and PIM2 which are reported to stabilize p21 by phosphorylation at Thr145 (Wang et al., 2002, 2010). This sequence homology seemed specific for B1, since no significant overlap was detected between PIM1/2 and the viral pseudokinase B12, or the late kinase F10 by pBLAST alignment (Figure 6-1).

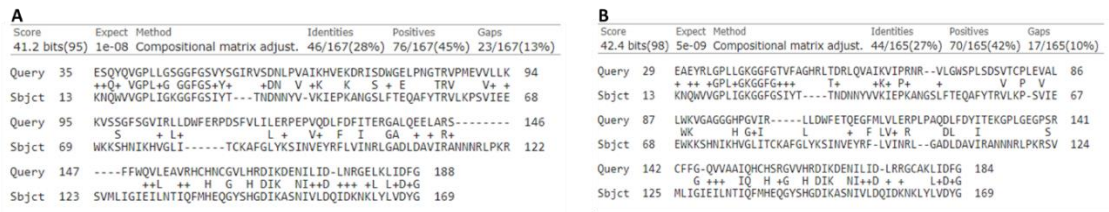

Figure 6-1 pBLAST sequence alignment between the cellular kinases PIM1, PIM2 and the viral kinase B1.

[A] Sequence alignment between the cellular kinase PIM1 and the viral kinase B1. [B] Sequence alignment between the cellular kinase PIM2 and the viral kinase B1.

p21 belongs to the Cip/Kip family of CDK inhibitor (CKI) proteins, which also includes p27 (Kip1), and p57 (Kip2) (Harper and Brooks, 2005; Sherr, 1994; Vermeulen et al., 2003). Members of this CKI family bind and inactivate CDK2 and CDK1 complexes, thus preventing

cell cycle progression and proliferation (Harper and Brooks, 2005; Vermeulen et al., 2003). The broad range inhibitory effect of p21 on cell cycle progression parallels the cell cycle alterations observed after VACV infection: Apart from mediating a systemic cell cycle arrest, p21 also negatively regulates the cellular DNA-polymerase processivity factor PCNA and thus inhibits cellular DNA replication (Waga et al., 1994). Therefore, I hypothesise that p21 might act as the cellular effector that mediates virus-induced cell cycle arrest during early infection.

However, I have found that the ΔB1mutB12 VACV strain inhibits cell proliferation, which implies that B1 is not required to block progression of the host cell cycle. This would either suggest that B1 has no role in stabilizing p21, or that p21 is not the cellular effector protein that mediates the block. These conclusions are based on the assumption that VACV arrests the cell cycle by a single blocking mechanism. However, given that the viral kinase F10 was shown to activate the DDR late during infection, this rather supports the hypothesis that VACV induces two (independent) cell cycle blocks. The first block is established early during infection and might be directed by viral B1 and cellular p21, while the second block is induced late by viral F10-mediated activation of cellular DDR. This model predicts that host cell proliferation should be rescued by silencing the viral kinase F10 in the background of ΔB1mutB12 strain.

In uninfected cells, p21 transcription is regulated by the transcription factor p53. Cellular stress signals such as DNA damage trigger canonical ATR/ATM signalling that in turn promotes p53 to transactivate p21 (Dornan et al., 2003; Harper and Brooks, 2005; Sherr, 1994; Sherr and Roberts, 1999; Vermeulen et al., 2003; Waldman et al., 1995).While I observed a strong increase in p21 levels, p53 was found to be degraded in a process that required either the viral kinase B1, and/or its paralog pseudokinase B12. This finding provides the first evidence that B1 might regulate p53 stability also in the context of infection (Santos et al., 2004), and confirms previous reports that showed p53 degradation at late (>12hpi) timepoints (Wali and Strayer, 1999b; Yoo et al., 2008).

In uninfected cells, p53 is continuously turned over by binding to its negative regulator the E3 ligase Mdm2. Expression of B1 has been shown to direct degradation of p53 which required both Mdm2 and the proteasome (Santos et al., 2004). Mdm2 was further implicated to assist VACV-induced degradation of p53 by the observation that infection induced *Mdm2* transcription (Yoo et al., 2008). Contrasting these findings, I observed complete Mdm2 degradation within 5h of VACV infection in a process that depended on the viral kinase B1 and/or its paralog pseudokinase B12. The role of Mdm2 (degradation) and the proteasome therefore remain to be clarified.

As for Mdm2, the role of p53 also remains to be further clarified. In this thesis I have demonstrated that the VACV-induced cell cycle block and cell cycle shift are independent of p53. Additionally, although B1/B12 -mediated degradation of p53 was found to be dispensable for productive viral infection, pharmacological stabilization of p53 by Nutlin3 inhibited the virus life cycle at a step between viral early and late gene expression. In order to unravel the function of p53 in the VACV life cycle, it will be essential to define the inhibited virus replication step, and whether the inhibition reflects a direct effect of Nutlin3, or an indirect effect mediated by p53. Amongst its "classical" role as apoptosis inducer, p53 has also been described as a cellular anti-viral factor (Takaoka et al., 2003). It was shown that IFN-α/β signalling induces transcription of the *TP53* gene, thus causing elevated p53 protein levels in response to viral infection such as Herpes Simplex virus (HSV). While IFN signalling caused increased protein levels, full activation of p53 required phosphorylation of Thr18 which was suggested to be mediated by the DDR effector kinases ATM and ATR. As the viral kinase F10 was found to activate DDR late (> 6hpi) during infection, this might activate p53 and trigger an antiviral response if p53 degradation is prevented by Nutlin3.

However, given that VACV encodes a whole arsenal of immune-modulating factors, including the IFN-inhibiting factor E3 (Chang et al., 1992), it seems more likely that accumulation of p53 prevents late viral gene expression through an alternative mechanism. Another possibility is the prolonged induction of p21 upon p53 stabilization by Nutlin3. Although I have not yet identified whether VACV-mediated upregulation of p21 requires p53, in uninfected cells, accumulation of p53 transactivates p21 expression. I have found that VACV upregulates p21 early during infection and also directs p21 degradation concurrent with the onset of viral late gene expression (> 6hpi). This late stage degradation of p21 has been found to depend on expression of the viral kinase F10, the same kinase that also activates the DDR. P21 has a dual function during the response to DNA damage: on the one hand it mediates cell cycle arrest by CDK inhibition and on the other hand it prevents DNA replication through direct inhibition of PCNA (Sherr and Roberts, 1999; Waga et al., 1994; Waldman et al., 1995). However, it was observed that ATR-mediated degradation of p21 following DNA damage by low doses of UV was required in order for PCNA-assisted DNA repair to occur (Abbas et al., 2008; Bendjennat et al., 2003). Failure to degrade p21, sequestered PCNA in a complex with p21 and prevented its association with sites of DNA damage, thus preventing efficient repair. Linking the p21-PCNA pathway to VACV replication, it has previously been shown that PCNA associates with the viral polymerase E9 and that inhibition of PCNA prevented viral DNA replication and late gene expression (Postigo et al., 2017). Additionally, I could confirm that chemical inhibition of

the DDR pathway prevented late gene expression. Based on these findings, I propose that F10-mediated activation of DDR is required to degrade p21, so that cellular PCNA can be recruited to viral DNA in order to assist in viral genome replication. Thereby, VACV creates a positive feedback loop which is initiated by low levels of F10 transcription from replicating viral genomes. F10 then activates the DDR which causes degradation of p21, and allows for recruitment of PCNA to viral genome. PCNA in turn enhances viral genome replication which promotes further late viral gene expression.

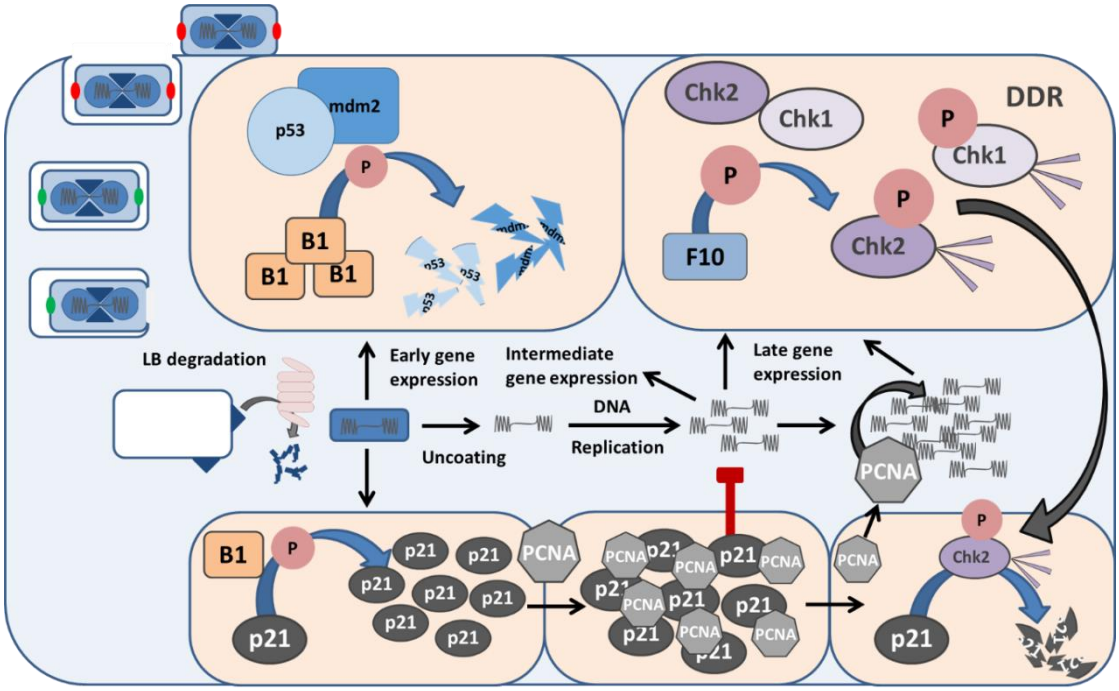

Figure 6-2 A hypothetical model how VACV arrests the host cell cycle.

After viral entry, early expression of the viral kinase B1 phosphorylates the tumour suppressor p53, thus causing its degradation. Concurrently, B1 promotes stability of the CKI p21 by phosphorylation. Increasing levels of p21 repress CDK2 and CDK1 activity, thus arresting the cell cycle. Additionally, p21 prevents cellular DNA synthesis by sequestering the cellular DNA polymerase processivity factor PCNA. Expression of the late viral kinase F10 activates the cellular DDR kinases ATR and Chk2. Next, activated Chk2 causes degradation of p21 and thus relieves the inhibition of PCNA. PCNA is then recruited to viral genomes to facilitate viral DNA synthesis and promote viral late gene expression, which creates a positive feedback loop that leads to complete degradation of p21.

Additionally, the proposed inhibitory effect of p21 on viral genome replication might also explain a previously published observation that both VACV genome uncoating and replication require activity of the proteasome (Mercer et al., 2012). Although the literature is contradictory, it was suggested that DDR-mediated downregulation of p21 requires the ubiquitin and proteasome-dependent degradation pathway (Abbas et al., 2008; Bendjennat et

al., 2003; Lee et al., 2006). Therefore, inhibition of the proteasome might prevent degradation of p21 which could then prevent viral genome replication by the above discussed pathway.

However, this proposed model does not explain why p21 is upregulated if it has such a detrimental effect on viral genome replication. A possible explanation might be that the early upregulation of p21 is required to arrest the cell cycle, in order to create a pro-viral environment e.g. by preventing depletion of nucleotide pools by cellular DNA replication. Taken together, although I have presented evidence that VACV early gene expression inhibits cell proliferation after viral entry, many open questions remain to be addressed.

2 VACV shifts the host cell cycle

In this thesis I have established the HeLa FUCCI system as a method to reliably analyse the cell cycle stage of VACV infected cells. Using this reporter cell line, I have described a VACV-induced shift from G1 into S/G2/M which occurred after the initial cell cycle arrest. This finding poses two problems. First, the virus has to reverse the first cell cycle block to allow for G1 progression. Second, the virus then needs to re-establish a new block to prevent normal cell cycle progression.

To address these questions, I will first look to identify the required viral protein. siRNA experiments described in Chapter 4 of this thesis have shown that either an intermediate and/or a late viral protein is involved in shifting the host cell cycle. Given that the candidate protein needs to provide a mechanism to both relieve and establish a cell cycle block, I will first test the role of the late viral kinase F10. F10 was implicated in downregulation of the cell cycle inhibitor p21, which was found upregulated early during infection. By promoting degradation of p21, F10 might reverse the initial cell cycle block and thus allow for G1 progression. Additionally, I have shown F10 to activate canonical DDR signalling, which might trigger a G2/M checkpoint mediated cell cycle arrest. To assay whether F10 is involved in shifting the cell cycle, I will knock down the viral kinase by siRNA and monitor cell cycle distribution after infection, using the FUCCI cell line. Additionally, if I find F10 to inhibit progression through G2/M, I will have identified two different mechanisms by which VACV blocks the host cell cycle: an early mechanism, depending on an early viral gene (potentially B1) and a late mechanism, potentially depending on F10.

3 VACV requires the host cell cycle machinery for productive infection

Viruses have co-evolved with their host cells for millions of years and have devised strategies to subvert host cell pathways to exploit them for their own replication. Having found that VACV modulates host cell cycle progression, I therefore tried to characterize if and how these changes are required during the virus life cycle.

As VACV depends on its host cell, it is in the interest of the virus to prevent premature cell death. A major inducer of apoptosis is p53. It is activated in response to cellular stress signals such as aberrant DNA replication and pathogen invasion (Takaoka et al., 2003). A common viral strategy for survival is therefore to inhibit p53 activity by promoting its degradation or preventing translocation into the nucleus (Bagga and Bouchard, 2014; Fan et al., 2018). I have found that VACV induces degradation of p53 before the onset of peak viral DNA replication (ca. 4-5hpi). Although VACV encodes several known apoptosis inhibitors (Veyer et al., 2017), degradation of p53 might further assist in preventing premature death of infected cells.

As a DNA virus, VACV requires sufficient dNTP pools for replication of the viral genome. Poxviruses have therefore evolved to encode several enzymes involved in the biogenesis of dNTPs. The VACV proteins I4 and F4 mimick cellular ribonucleotide reductases that catalyse the conversion of NDP precursor molecules to dNDPs, A48 catalyzes phosphorylation of dNMPs to dNDPs, D4 is a uracil DNA glycosylas (UNG), F2 functions as a dUTPase, and J2 is a thymidine kinase (Irwin et al., 2017). This arsenal of enzymes is suggested to promote viral replication in unfavourable environments, such as quiescent cells which have low dNTP pools. In proliferating cells, inactivation of D4 reduced viral replication by one third, while F2 was found to be non-essential. Highlighting the importance of nucleotide metabolism for productive infection, in quiescent cells deletion of both F2 and D4 severely attenuated viral yields (De Silva and Moss, 2008). Additionally, this example shows that viral infection has different enzymatic requirements in quiescent and proliferating cells. Another example is the viral thymidine kinase J2, which is non-essential in (cancer) tissue culture but promotes virulence in vivo (Buller et al., 1985). Since J2 increases the pool of available dNTPs, it promotes infection even under non-optimal conditions. Genetic deletion of J2 therefore makes VACV infection more dependent on the pre-existing cellular dNTPs levels. This increased dependency is exploited in development of oncolytic viruses to target viral replication specifically to cancer cells which are hallmarked by increased dNTP levels (Hanahan and Weinberg, 2000; Kirn and Thorne, 2009). Since I have done all the above described

experiments in cancer cell lines which are known to have deregulated cell cycle progression as well as increased nucleotide levels, these experimental conditions might mask the importance of the VACV induced cell cycle changes for the viral life cycle. It would therefore be interesting to characterize how the cell cycle distribution and progression changed in VACV infected primary cells.

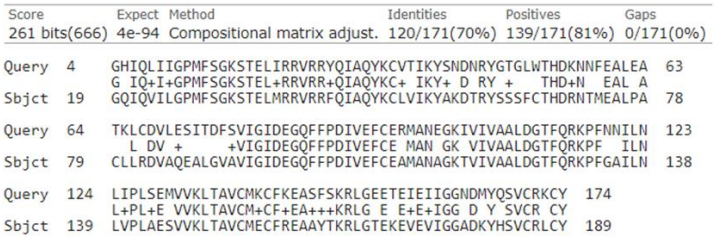

Score	Expect	Method	Identities	Positives	Gaps
261 bits(666)	4e-94	Compositional matrix adjust.	120/171(70%)	139/171(81%)	0/171(0%)

```
Query  4    GHIQLIIGPMFSGKSTELIRRVRRYQIAQYKCVTIKYSNDNRYGTGLWTHDKNNFEALEA  63
            G IQ+I+GPMFSGKSTEL+RRVRR+QIAQYKC+ IKY+ D RY +   THD+N  EAL A
Sbjct  19   GQIQVILGPMFSGKSTELMRRVRRFQIAQYKCLVIKYAKDTRYSSSFCTHDRNTMEALPA  78

Query  64   TKLCDVLESITDFSVIGIDEGQFFPDIVEFCERMANEGKIVIVAALDGTFQRKPFNNILN  123
              L DV +     +VIGIDEGQFFPDIVEFCE MAN GK VIVAALDGTFQRKPF  ILN
Sbjct  79   CLLRDVAQEALGVAVIGIDEGQFFPDIVEFCEAMANAGKTVIVAALDGTFQRKPFGAILN  138

Query  124  LIPLSEMVVKLTAVCMKCFKEASFSKRLGEETEIEIIGGNDMYQSVCRKCY  174
            L+PL+E VVKLTAVCM+CF+EA+++KRLG E E+E+IGG D Y SVCR CY
Sbjct  139  LVPLAESVVKLTAVCMECFREAAYTKRLGTEKEVEVIGGADKYHSVCRLCY  189
```

Figure 6-3 pBLAST sequence alignment of VACV thymidine kinase J2 and human thymidine kinase 1.

VACV J2 is marked as the Query sequence and human TK1 is marked as the Subject sequence.

The observed shift from G1 to S/G2/M might represent a strategy of VACV to protect activity of its viral thymidine kinase J2. In normal, uninfected cells expression and stability of cellular thymidine kinase1 (cTK1) is cell cycle-dependent. While levels are increased during S and G2 phase, cTK1 is actively targeted for degradation by the APC/C –Cdh1 complex during M phase, thus causing barely detectable cTK1 levels in G1 (Kauffman and Kelly, 1991; Ke and Chang, 2004). pBLAST alignment of the viral J2 thymidine kinase and the human cytosolic thymidine kinase 1 shows that the two proteins are 81% identical at the sequence level (Figure 6-3). This might subject the viral protein to recognition and degradation by the cellular APC/C-Cdh1 during M and G1 phase. Shifting infected cells from G1 in S/G2/M phase might prevent degradation of viral thymidine kinase J2.

Throughout this thesis I have described VACV to shift cells from G1 to S/G2/M phase. This is based on analysis of the cell cycle distribution in infected HeLa FUCCI cells. However, this system does not allow for distinction between late S, G2, and M phase without the use of additional markers (cf. section 2.1.2). During the microscopy imaging experiments, I have noted that there are no more mitotic cells after 8hpi. Additionally, I have not observed a single incidence of an actively infected mitotic cell. Although I have not yet systematically quantified this observation, it has previously been published that VACV infection prevents mitosis (Kit

and Dubbs, 1962). I therefore hypothesise that VACV infected cells are shifted from G1 into S/G2, while mitosis is completely inhibited.

In Chapter 3, I described that VACV could arrest pre-synchronized cells in G1, S, and G2. Additionally, I have found in an independent experiment that the block depends on viral early gene expression, or H1. Combining these two findings, I conclude that G1, S, and G2 phases of the cell cycle are permissive for viral early gene expression. However, to gain a more comprehensive understanding of the relationship between viral gene expression or replication and the host cell cycle stage, further experiments are required. I will therefore generate a VACV strain that expresses the far-red fluorescent protein mCardinal under either an early viral promoter (WR E mCard), or under a late viral promoter (WR L mCard). Using these viruses to infect synchronized HeLa FUCCI cells in live cell imaging will allow me to determine whether the kinetics of either early and/or late viral gene expression depends on the host cell cycle stage. Conversely, infecting unsynchronized HeLa FUCCI cells will show how the cell cycle changes in relation to the gene expression stage of the virus.

Given the permissiveness of the other cell cycle phases, the absence of infection in mitotic cells was intriguing. I found that cell cycle dependent activity of the DDR might offer an explanation. Since VACV has been shown to activate and require DDR for productive infection, it would be expected to preferentially infect cells with an intact DDR signalling pathway. However, it was published that the DDR is deactivated or suspended during M phase (Heijink et al., 2013). Additionally, while the VACV activated DDR kinase Chk2 is stably expressed throughout the cell cycle, Chk1 is restricted to S and G2 (Kaneko et al., 1999; Lukas et al., 2001). The absence of a functional DDR pathway during M phase might make mitosis non-permissive for VACV infection.

Screening a pre-selected small molecule inhibitor library, I could confirm the requirement of the DDR for late gene expression. Additionally, I found inhibition of the two kinases Aurora A and Aurora B to negatively affect viral late gene expression, while viral early gene expression was uninhibited. In order to more precisely define the virus life cycle stage where the Aurora kinases might be required, I will monitor the formation of replication sites, and if I find DNA replication to proceed normally I will measure late gene transcription by qPCR. In normal, uninfected cells the Aurora kinases are involved in chromatin remodelling during M phase and progression through the spindle checkpoint. Interestingly, AuroraB has been shown to form a regulatory network with Vaccinia-related kinase 1 (VRK1), which is a cellular homolog of the viral kinase B1 (Nichols and Traktman, 2004). VRK1-mediated phosphorylation of histone 3 at

Thr3 was found to be required for recruitment of Aurora B and subsequent phosphorylation at Ser10. Inhibition of VRK1 thereby prevented localization of Aurora B in centromeres. Importantly, the two kinases were shown to bind each other and cross-inhibit their respective kinase activity. Given that unpublished data from our lab shows that the viral phosphatase dephosphorylates H3Ser10, I would assume that this connection between VRK1 and Aurora B is not of relevance for VACV infection. However, since Aurora B inhibits VRK1, it might also be able to inhibit function of the viral kinase B1. It would therefore be interesting to study the localization of Aurora A and B during infection. Potential co-localization might represent specified areas or times during which B1 needs to be deactivated in order for productive infection to occur.

Having found that VACV requires activation of the DDR, selected CDKs and Aurora kinases, one important point remains to be addressed. These cellular factors are mostly nuclear in uninfected cells but VACV replicates in the cytosol. So this begs the question how VACV activates and/or recruits these factors to sites of VACV replication. One potential option is to send a viral protein into the nucleus to modulate PTM on target proteins to direct their relocalization to the cytoplasm. Another option is to modulate nuclear import and export e.g. promoting export while preventing import. In order to test the importance of nuclear import and export, I will either inhibit nuclear import with Ivermectin, or nuclear export with Leptomycin and monitor the localization of cell cycle regulators (e.g. activated pChk2) in infected cells.

In summary, while I have shown that productive VACV replication is linked to cell cycle phase and does require cell cycle components such as the DDR and the Aurora kinases, their exact involvement in the virus life cycle remains to be established.

4 Conclusions

As obligate intracellular parasites, viruses are highly dependent on host cell environment and resources for productive viral replication. Therefore, viruses have evolved strategies to make host factors more abundant and accessible, including subversion of the host cell cycle. As a

major driver of oncogenesis, virus-induced cell cycle dysregulation has been intensely studied in the past years (reviewed in (Bagga and Bouchard, 2014; Fan et al., 2018)).

While research has focused on tumorigenic viruses such as HPV, KSHV, and EBV, there is comparatively little known about cell cycle regulation of non-oncogenic viruses such as poxviruses. Early research in the 1960s suggested VACV, the model orthopoxvirus, to alter the host cell cycle. In the 1990s, VACV was further described to modulate key cell cycle regulators such as CDK1, p53, and Rb (Jungwirth and Launer, 1968; Wali and Strayer, 1999b; Yoo et al., 2008). However, mechanistic insights and relevance to the viral life cycle were inaccessible due to the then available techniques. Therefore, this PhD project combined state of the art novel techniques with classical assays to address how and why VACV affects the host cell cycle. Here I have described the complex modulation of both the G1/S and G2/M checkpoint by VACV. Identification of (some) involved cellular proteins and their requirement for productive virus replication may provide the basis for new anti-virals through cancer drug repurposing.

Apart from providing new targets for anti-viral therapy, better molecular understanding of VACV-induced cell cycle changes might also advance anti-cancer therapy. VACV has been developed as a oncolytic virus and shown promising results in clinical trials (Antonio Chiocca, 2002; Breitbach et al., 2015). A recently emerging anti-cancer strategy is based on the combination of oncolytic virotherapy with pharmacological targeting of cell cycle checkpoints (LaRocca and Warner, 2018). Virus-induced priming of the cells has been found to pre-sensitize the tumour, thus potentiating the effect of pharmacological checkpoint activation. More comprehensive molecular characterization of how VACV activates the G1/S and G2/M checkpoints might therefore provide new angles for improved oncolytic virotherapy.

7 Bibliography

Abbas, T., Sivaprasad, U., Terai, K., Amador, V., Pagano, M., and Dutta, A. (2008). PCNA-dependent regulation of p21 ubiquitylation and degradation via the CRL4Cdt2 ubiquitin ligase complex. Genes Dev. *22*, 2496–2506.

Agarwal, M.L., Agarwal, A., Taylor, W.R., and Stark, G.R. (1995). p53 controls both the G2/M and the G1 cell cycle checkpoints and mediates reversible growth arrest in human fibroblasts. Proc. Natl. Acad. Sci. U. S. A. *92*, 8493–8497.

Albanese, C., Johnson, J., Watanabe, G., Eklund, N., Vu, D., Arnold, A., and Pestell, R.G. (1995). Transforming p21ras Mutants and c-Ets-2 Activate the Cyclin D1 Promoter through Distinguishable Regions. J. Biol. Chem. *270*, 23589–23597.

Alberts, B., Johnson, A., Lewis, J., Raff, M., Roberts, K., and Walter, P. (2002). Molecular Biology of the Cell (Garland Science).

Alcorta, D.A., Xiong, Y., Phelps, D., Hannon, G., Beach, D., and Barrett, J.C. (1996). Involvement of the cyclin-dependent kinase inhibitor p16 (INK4a) in replicative senescence of normal human fibroblasts. Proc. Natl. Acad. Sci. U. S. A. *93*, 13742–13747.

Andersen, J.L., Le Rouzic, E., and Planelles, V. (2008). HIV-1 Vpr: Mechanisms of G2 Arrest and Apoptosis. Exp. Mol. Pathol. *85*, 2–10.

Ando, T., Kawabe, T., Ohara, H., Ducommun, B., Itoh, M., and Okamoto, T. (2001). Involvement of the Interaction between p21 and Proliferating Cell Nuclear Antigen for the Maintenance of G2/M Arrest after DNA Damage. J. Biol. Chem. *276*, 42971–42977.

Ansarah-Sobrinho, C., and Moss, B. (2004). Vaccinia virus G1 protein, a predicted metalloprotease, is essential for morphogenesis of infectious virions but not for cleavage of major core proteins. J. Virol. *78*, 6855–6863.

Antonio Chiocca, E. (2002). Oncolytic viruses. Nat. Rev. Cancer *2*, 938–950.

Armstrong, J.A., Metz, D.H., and Young, M.R. (1973). The Mode of Entry of Vaccinia Virus into L Cells. J. Gen. Virol. *21*, 533–537.

Ashcroft, M., Kubbutat, M.H.G., and Vousden, K.H. (1999). Regulation of p53 Function and Stability by Phosphorylation. Mol. Cell. Biol. *19*, 1751–1758.

Ashton, N.W., Bolderson, E., Cubeddu, L., O'Byrne, K.J., and Richard, D.J. (2013). Human single-stranded DNA binding proteins are essential for maintaining genomic stability. BMC Mol. Biol. *14*, 9.

Awasthi, P., Foiani, M., and Kumar, A. (2015). ATM and ATR signaling at a glance. J Cell Sci *128*, 4255–4262.

Aylward, R.B., and Birmingham, M. (2005). The human story. BMJ *331*, 1261–1262.

Bacchetti, S., and Whitmore, G.F. (1969). The Action of Hydroxyurea on Mouse L-Cells*. Cell Prolif. *2*, 193–211.

Bagga, S., and Bouchard, M.J. (2014). Cell Cycle Regulation During Viral Infection. In Cell Cycle Control, (Humana Press, New York, NY), pp. 165–227.

Bahar, M.W., Graham, S.C., Stuart, D.I., and Grimes, J.M. (2011). Insights into the Evolution of a Complex Virus from the Crystal Structure of Vaccinia Virus D13. Struct. England1993 *19*, 1011–1020.

Bakkenist, C.J., and Kastan, M.B. (2003). DNA damage activates ATM through intermolecular autophosphorylation and dimer dissociation. Nature *421*, 499.

Balmanno, K., and Cook, S.J. (1999). Sustained MAP kinase activation is required for the expression of cyclin D1, p21Cip1 and a subset of AP-1 proteins in CCL39 cells. Oncogene *18*, 3085–3097.

Banerjee, N.S., Wang, H.-K., Broker, T.R., and Chow, L.T. (2011). Human Papillomavirus (HPV) E7 Induces Prolonged G2 following S Phase Reentry in Differentiated Human Keratinocytes. J. Biol. Chem. *286*, 15473–15482.

Banham, A.H., Leader, D.P., and Smith, G.L. (1993). Phosphorylation of ribosomal proteins by the vaccinia virus B1R protein kinase. FEBS Lett. *321*, 27–31.

Baroudy, B.M., and Moss, B. (1980). Purification and characterization of a DNA-dependent RNA polymerase from vaccinia virions. J. Biol. Chem. *255*, 4372–4380.

Bartz, S.R., Rogel, M.E., and Emerman, M. (1996). Human immunodeficiency virus type 1 cell cycle control: Vpr is cytostatic and mediates G2 accumulation by a mechanism which differs from DNA damage checkpoint control. J. Virol. *70*, 2324–2331.

Beaud, G., and Beaud, R. (1997). Preferential virosomal location of underphosphorylated H5R protein synthesized in vaccinia virus-infected cells. J. Gen. Virol. *78*, 3297–3302.

Beaud, G., Beaud, R., and Leader, D.P. (1995). Vaccinia virus gene H5R encodes a protein that is phosphorylated by the multisubstrate vaccinia virus B1R protein kinase. J. Virol. *69*, 1819–1826.

Behbehani, A.M. (1983). The smallpox story: life and death of an old disease. Microbiol. Rev. *47*, 455–509.

Bendjennat, M., Boulaire, J., Jascur, T., Brickner, H., Barbier, V., Sarasin, A., Fotedar, A., and Fotedar, R. (2003). UV Irradiation Triggers Ubiquitin-Dependent Degradation of p21WAF1 to Promote DNA Repair. Cell *114*, 599–610.

Bengali, Z., Townsley, A.C., and Moss, B. (2009). Vaccinia virus strain differences in cell attachment and entry. Virology *389*, 132–140.

Benmaamar, R., and Pagano, M. (2005). Involvement of the SCF Complex in the Control of Cdh1 Degradation in S-phase. Cell Cycle *4*, 1230–1232.

Betakova, T., Wolffe, E.J., and Moss, B. (1999). Regulation of Vaccinia Virus Morphogenesis: Phosphorylation of the A14L and A17L Membrane Proteins and C-Terminal Truncation of the A17L Protein Are Dependent on the F10L Kinase. J. Virol. *73*, 3534–3543.

Bisht, H., Weisberg, A.S., and Moss, B. (2008). Vaccinia Virus L1 Protein Is Required for Cell Entry and Membrane Fusion. J. Virol. *82*, 8687–8694.

Bisht, H., Weisberg, A.S., Szajner, P., and Moss, B. (2009). Assembly and Disassembly of the Capsid-Like External Scaffold of Immature Virions during Vaccinia Virus Morphogenesis. J. Virol. *83*, 9140–9150.

Black, M.E., and Hruby, D.E. (1991). Structure and function of vaccinia virus thymidine kinase: Biomedical relevance and implications for antiviral drug design. Rev. Med. Virol. *1*, 235–245.

Blasco, R., and Moss, B. (1992). Role of cell-associated enveloped vaccinia virus in cell-to-cell spread. J. Virol. *66*, 4170–4179.

Booher, R.N., Holman, P.S., and Fattaey, A. (1997). Human Myt1 Is a Cell Cycle-regulated Kinase That Inhibits Cdc2 but Not Cdk2 Activity. J. Biol. Chem. *272*, 22300–22306.

Boyer, S.N., Wazer, D.E., and Band, V. (1996). E7 Protein of Human Papilloma Virus-16 Induces Degradation of Retinoblastoma Protein through the Ubiquitin-Proteasome Pathway. Cancer Res. *56*, 4620–4624.

Boyle, K.A., and Traktman, P. (2004). Members of a Novel Family of Mammalian Protein Kinases Complement the DNA-Negative Phenotype of a Vaccinia Virus ts Mutant Defective in the B1 Kinase. J. Virol. *78*, 1992–2005.

Boyle, K.A., Arps, L., and Traktman, P. (2007). Biochemical and genetic analysis of the vaccinia virus d5 protein: Multimerization-dependent ATPase activity is required to support viral DNA replication. J. Virol. *81*, 844–859.

Breitbach, C., Bell, J.C., Hwang, T.-H., Kirn, D., and Burke, J. (2015). The emerging therapeutic potential of the oncolytic immunotherapeutic Pexa-Vec (JX-594). Oncolytic Virotherapy 25.

Brown, N.G., Nick Morrice, D., Beaud, G., Hardie, G., and Leader, D.P. (2000). Identification of sites phosphorylated by the vaccinia virus B1R kinase in viral protein H5R. BMC Biochem. *1*, 2.

Broyles, S.S. (2003). Vaccinia virus transcription. J. Gen. Virol. *84*, 2293–2303.

Broyles, S.S., Yuen, L., Shuman, S., and Moss, B. (1988). Purification of a factor required for transcription of vaccinia virus early genes. J. Biol. Chem. *263*, 10754–10760.

Broyles, S.S., Liu, X., Zhu, M., and Kremer, M. (1999). Transcription Factor YY1 Is a Vaccinia Virus Late Promoter Activator. J. Biol. Chem. *274*, 35662–35667.

Buller, R.M.L., Smith, G.L., Cremer, K., Notkins, A.L., and Moss, B. (1985). Decreased virulence of recombinant vaccinia virus expression vectors is associated with a thymidine kinase-negative phenotype. Nature *317*, 813–815.

Byrd, C.M., and Hruby, D.E. (2005). A conditional-lethal vaccinia virus mutant demonstrates that the I7L gene product is required for virion morphogenesis. Virol. J. *2*, 4.

Byrd, C.M., Bolken, T.C., and Hruby, D.E. (2002). The Vaccinia Virus I7L Gene Product Is The Core Protein Proteinase. J. Virol. *76*, 8973–8976.

Cai, Q., Xiao, B., Si, H., Cervini, A., Gao, J., Lu, J., Upadhyay, S.K., Verma, S.C., and Robertson, E.S. (2012). Kaposi's Sarcoma Herpesvirus Upregulates Aurora A Expression to Promote p53 Phosphorylation and Ubiquitylation. PLOS Pathog. *8*, e1002566.

Canela, N., Rodriguez-Vilarrupla, A., Estanyol, J.M., Díaz, C., Pujol, M.J., Agell, N., and Bachs, O. (2003). The SET Protein Regulates G2/M Transition by Modulating Cyclin B-Cyclin-dependent Kinase 1 Activity. J. Biol. Chem. *278*, 1158–1164.

Carpenter, M.S., and Delange, A.M. (1992). Identification of a temperature-sensitive mutant of vaccinia virus defective in late but not intermediate gene expression. Virology *188*, 233–244.

Carpentier, D.C.J., Gao, W.N.D., Ewles, H., Morgan, G.W., and Smith, G.L. (2015). Vaccinia Virus Protein Complex F12/E2 Interacts with Kinesin Light Chain Isoform 2 to Engage the Kinesin-1 Motor Complex. PLOS Pathog. *11*, e1004723.

Carson, C.T., Schwartz, R.A., Stracker, T.H., Lilley, C.E., Lee, D.V., and Weitzman, M.D. (2003). The Mre11 complex is required for ATM activation and the G2/M checkpoint. EMBO J. *22*, 6610–6620.

Carter, G.C., Law, M., Hollinshead, M., and Smith, G.L. (2005). Entry of the vaccinia virus intracellular mature virion and its interactions with glycosaminoglycans. J. Gen. Virol. *86*, 1279–1290.

Carvajal, D., Tovar, C., Yang, H., Vu, B.T., Heimbrook, D.C., and Vassilev, L.T. (2005). Activation of p53 by MDM2 Antagonists Can Protect Proliferating Cells from Mitotic Inhibitors. Cancer Res. *65*, 1918–1924.

Cassetti, M.C., Merchlinsky, M., Wolffe, E.J., Weisberg, A.S., and Moss, B. (1998). DNA Packaging Mutant: Repression of the Vaccinia Virus A32 Gene Results in Noninfectious, DNA-Deficient, Spherical, Enveloped Particles. J. Virol. *72*, 5769–5780.

Chakrabarti, S., Sisler, J.R., and Moss, B. (1997). Compact, Synthetic, Vaccinia Virus Early/Late Promoter for Protein Expression. BioTechniques *23*, 1094–1097.

Chang, H.W., Watson, J.C., and Jacobs, B.L. (1992). The E3L gene of vaccinia virus encodes an inhibitor of the interferon-induced, double-stranded RNA-dependent protein kinase. Proc. Natl. Acad. Sci. U. S. A. *89*, 4825–4829.

Chang, S.-J., Shih, A.-C., Tang, Y.-L., and Chang, W. (2012). Vaccinia Mature Virus Fusion Regulator A26 Protein Binds to A16 and G9 Proteins of the Viral Entry Fusion Complex and Dissociates from Mature Virions at Low pH. J. Virol. *86*, 3809–3818.

Chang, Y., Moore, P.S., Talbot, S.J., Boshoff, C.H., Zarkowska, T., Godden-Kent, D., Paterson, H., Weiss, R.A., and Mittnacht, S. (1996). Cyclin encoded by KS herpesvirus. Nature *382*, 410–410.

Chaturvedi, P., Eng, W.K., Zhu, Y., Mattern, M.R., Mishra, R., Hurle, M.R., Zhang, X., Annan, R.S., Lu, Q., Faucette, L.F., et al. (1999). Mammalian Chk2 is a downstream effector of the ATM-dependent DNA damage checkpoint pathway. Oncogene *18*, 4047–4054.

Chauhan, V., Rungta, T., Goyal, K., and Singh, M.P. (2019). Designing a multi-epitope based vaccine to combat Kaposi Sarcoma utilizing immunoinformatics approach. Sci. Rep. *9*, 1–15.

Cheevers, W.P., O'Callaghan, D.J., and Randall, C.C. (1968). Biosynthesis of Host and Viral Deoxyribonucleic Acid During Hyperplastic Fowlpox Infection In Vivo. J. Virol. *2*, 421.

Chellappan, S., Kraus, V.B., Kroger, B., Munger, K., Howley, P.M., Phelps, W.C., and Nevins, J.R. (1992). Adenovirus E1A, simian virus 40 tumor antigen, and human papillomavirus E7 protein share the capacity to disrupt the interaction between transcription factor E2F and the retinoblastoma gene product. Proc. Natl. Acad. Sci. U. S. A. *89*, 4549–4553.

Chen, J., Jackson, P.K., Kirschner, M.W., and Dutta, A. (1995). Separate domains of p21 involved in the inhibition of Cdk kinase and PCNA. Nature *374*, 386–388.

Chen, J., Peters, R., Saha, P., Lee, P., Theodoras, A., Pagano, M., Wagner, G., and Dutta, A. (1996). A 39 amino acid fragment of the cell cycle regulator p21 is sufficient to bind PCNA and partially inhibit DNA replication in vivo. Nucleic Acids Res. *24*, 1727–1733.

Chernos, V.I., Belanov, E.F., and Vasilieva, N.N. (1978). Temperature-sensitive mutants of vaccinia virus. I. Isolation and preliminary characterization. Acta Virol. *22*, 81–90.

Chiu, W.-L., and Chang, W. (2002). Vaccinia virus J1R protein: a viral membrane protein that is essential for virion morphogenesis. J. Virol. *76*, 9575–9587.

Chiu, W.-L., Szajner, P., Moss, B., and Chang, W. (2005). Effects of a temperature sensitivity mutation in the J1R protein component of a complex required for vaccinia virus assembly. J. Virol. *79*, 8046–8056.

Chiu, W.-L., Lin, C.-L., Yang, M.-H., Tzou, D.-L.M., and Chang, W. (2007). Vaccinia Virus 4c (A26L) Protein on Intracellular Mature Virus Binds to the Extracellular Cellular Matrix Laminin. J. Virol. *81*, 2149–2157.

Chou, W., Ngo, T.V., and Gershon, P.D. (2012). An overview of the vaccinia virus infectome: a survey of the proteins of the poxvirus-infected cell. J. Virol. *86*, 1487–1499.

Chung, C.-S., Hsiao, J.-C., Chang, Y.-S., and Chang, W. (1998). A27L Protein Mediates Vaccinia Virus Interaction with Cell Surface Heparan Sulfate. J. Virol. *72*, 1577–1585.

Cimprich, K.A., and Cortez, D. (2008). ATR: an essential regulator of genome integrity. Nat. Rev. Mol. Cell Biol. *9*, 616–627.

Clifford, B., Beljin, M., Stark, G.R., and Taylor, W.R. (2003). G2 Arrest in Response to Topoisomerase II Inhibitors: The Role of p53. Cancer Res. *63*, 4074–4081.

Coller, H.A., Sang, L., and Roberts, J.M. (2006). A new description of cellular quiescence. PLoS Biol. *4*, e83.

Condit, R.C., and Motyczka, A. (1981). Isolation and preliminary characterization of temperature-sensitive mutants of vaccinia virus. Virology *113*, 224–241.

Condit, R.C., Motyczka, A., and Spizz, G. (1983). Isolation, characterization, and physical mapping of temperature-sensitive mutants of vaccinia virus. Virology *128*, 429–443.

Condit, R.C., Moussatche, N., and Traktman, P. (2006). In A Nutshell: Structure and Assembly of the Vaccinia Virion. B.-A. in V. Research, ed. (Academic Press), pp. 31–124.

Cono, J., Casey, C.G., Bell, D.M., and Centers for Disease Control and Prevention (2003). Smallpox vaccination and adverse reactions. Guidance for clinicians. MMWR Recomm. Rep. Morb. Mortal. Wkly. Rep. Recomm. Rep. *52*, 1–28.

Cribier, A., Descours, B., Valadão, A.L.C., Laguette, N., and Benkirane, M. (2013). Phosphorylation of SAMHD1 by Cyclin A2/CDK1 Regulates Its Restriction Activity toward HIV-1. Cell Rep. *3*, 1036–1043.

Crighton, D., Woiwode, A., Zhang, C., Mandavia, N., Morton, J.P., Warnock, L.J., Milner, J., White, R.J., and Johnson, D.L. (2003). p53 represses RNA polymerase III transcription by targeting TBP and inhibiting promoter occupancy by TFIIIB. EMBO J. *22*, 2810–2820.

Cross, S.M., Sanchez, C.A., Morgan, C.A., Schimke, M.K., Ramel, S., Idzerda, R.L., Raskind, W.H., and Reid, B.J. (1995). A p53-dependent mouse spindle checkpoint. Science *267*, 1353–1356.

Cyrklaff, M., Risco, C., Fernández, J.J., Jiménez, M.V., Estéban, M., Baumeister, W., and Carrascosa, J.L. (2005). Cryo-electron tomography of vaccinia virus. Proc. Natl. Acad. Sci. U. S. A. *102*, 2772–2777.

Czarnecki, M.W., and Traktman, P. (2017). The vaccinia virus DNA polymerase and its processivity factor. Virus Res. *234*, 193–206.

Dales, S., and Siminovitch, L. (1961). The development of vaccinia virus in Earle's L strain cells as examined by electron microscopy. J. Biophys. Biochem. Cytol. *10*, 475–503.

Dales, S., Milovanovitch, V., Pogo, B.G., Weintraub, S.B., Huima, T., Wilton, S., and McFadden, G. (1978). Biogenesis of vaccinia: isolation of conditional lethal mutants and electron microscopic characterization of their phenotypically expressed defects. Virology *84*, 403–428.

Darzynkiewicz, Z., Gong, J., Juan, G., Ardelt, B., and Traganos, F. (1996). Cytometry of cyclin proteins. Cytometry *25*, 1–13.

Darzynkiewicz, Z., Huang, X., and Zhao, H. (2017). Analysis of Cellular DNA Content by Flow Cytometry. Curr. Protoc. Immunol. *119*, 5.7.1-5.7.20.

Dash, B.C., and El-Deiry, W.S. (2005). Phosphorylation of p21 in G2/M Promotes Cyclin B-Cdc2 Kinase Activity. Mol. Cell. Biol. *25*, 3364–3387.

De Clercq, E. (2002). Cidofovir in the treatment of poxvirus infections. Antiviral Res. *55*, 1–13.

De Silva, F.S., and Moss, B. (2008). Effects of vaccinia virus uracil DNA glycosylase catalytic site and deoxyuridine triphosphatase deletion mutations individually and together on replication in active and quiescent cells and pathogenesis in mice. Virol. J. *5*, 145.

Debbas, M., and White, E. (1993). Wild-type p53 mediates apoptosis by E1A, which is inhibited by E1B. Genes Dev. *7*, 546–554.

DeHart, J.L., Zimmerman, E.S., Ardon, O., Monteiro-Filho, C.M., Argañaraz, E.R., and Planelles, V. (2007). HIV-1 Vpr activates the G2 checkpoint through manipulation of the ubiquitin proteasome system. Virol. J. *4*, 57.

Del Sal, G., Ruaro, E.M., Utrera, R., Cole, C.N., Levine, A.J., and Schneider, C. (1995). Gas1-induced growth suppression requires a transactivation-independent p53 function. Mol. Cell. Biol. *15*, 7152–7160.

Delacroix, S., Wagner, J.M., Kobayashi, M., Yamamoto, K., and Karnitz, L.M. (2007). The Rad9–Hus1–Rad1 (9–1–1) clamp activates checkpoint signaling via TopBP1. Genes Dev. *21*, 1472–1477.

DeLange, A.M., and McFadden, G. (1987). Efficient resolution of replicated poxvirus telomeres to native hairpin structures requires two inverted symmetrical copies of a core target DNA sequence. J. Virol. *61*, 1957–1963.

Derrien, M., Punjabi, A., Khanna, M., Grubisha, O., and Traktman, P. (1999). Tyrosine Phosphorylation of A17 during Vaccinia Virus Infection: Involvement of the H1 Phosphatase and the F10 Kinase. J. Virol. *73*, 7287–7296.

Dilla, M.A.V., Truiullo, T.T., Mullaney, P.F., and Coultex, J.R. (1969). Cell Microfluorometry: A Method for Rapid Fluorescence Measurement. Science *163*, 1213–1214.

Direkze, S., and Laman, H. (2004). Regulation of growth signalling and cell cycle by Kaposi's sarcoma-associated herpesvirus genes. Int. J. Exp. Pathol. *85*, 305.

Dittmer, D.P., and Damania, B. (2013). Kaposi sarcoma associated herpesvirus pathogenesis (KSHV) – an update. Curr. Opin. Virol. *3*, 238.

Doceul, V., Hollinshead, M., Breiman, A., Laval, K., and Smith, G.L. (2012). Protein B5 is required on extracellular enveloped vaccinia virus for repulsion of superinfecting virions. J. Gen. Virol. *93*, 1876–1886.

Dodding, M.P., Mitter, R., Humphries, A.C., and Way, M. (2011). A kinesin-1 binding motif in vaccinia virus that is widespread throughout the human genome. EMBO J. *30*, 4523–4538.

Dornan, D., Shimizu, H., Burch, L., Smith, A.J., and Hupp, T.R. (2003). The proline repeat domain of p53 binds directly to the transcriptional coactivator p300 and allosterically controls DNA-dependent acetylation of p53. Mol. Cell. Biol. *23*, 8846–8861.

Dove, B., Brooks, G., Bicknell, K., Wurm, T., and Hiscox, J.A. (2006). Cell Cycle Perturbations Induced by Infection with the Coronavirus Infectious Bronchitis Virus and Their Effect on Virus Replication. J. Virol. *80*, 4147–4156.

Draetta, G., and Eckstein, J. (1997). Cdc25 protein phosphatases in cell proliferation. Biochim. Biophys. Acta BBA - Rev. Cancer *1332*, M53–M63.

Du, S., and Traktman, P. (1996). Vaccinia virus DNA replication: two hundred base pairs of telomeric sequence confer optimal replication efficiency on minichromosome templates. Proc. Natl. Acad. Sci. *93*, 9693–9698.

Dulić, V., Kaufmann, W.K., Wilson, S.J., Tisty, T.D., Lees, E., Harper, J.W., Elledge, S.J., and Reed, S.I. (1994). p53-dependent inhibition of cyclin-dependent kinase activities in human fibroblasts during radiation-induced G1 arrest. Cell *76*, 1013–1023.

Dupré, A., Boyer-Chatenet, L., and Gautier, J. (2006). Two-step activation of ATM by DNA and the Mre11–Rad50–Nbs1 complex. Nat. Struct. Mol. Biol. *13*, 451–457.

Dyson, N., Howley, P.M., Munger, K., and Harlow, E. (1989). The human papilloma virus-16 E7 oncoprotein is able to bind to the retinoblastoma gene product. Science *243*, 934–937.

Easterbrook, K.B. (1966). Controlled degradation of vaccinia virions in vitro: an electron microscopic study. J. Ultrastruct. Res. *14*, 484–496.

El-Deiry, W.S., Tokino, T., Velculescu, V.E., Levy, D.B., Parsons, R., Trent, J.M., Lin, D., Mercer, W.E., Kinzler, K.W., and Vogelstein, B. (1993). WAF1, a potential mediator of p53 tumor suppression. Cell *75*, 817–825.

Elder, R.T., Yu, M., Chen, M., Zhu, X., Yanagida, M., and Zhao, Y. (2001). HIV-1 Vpr Induces Cell Cycle G2 Arrest in Fission Yeast (Schizosaccharomyces pombe) through a Pathway Involving Regulatory and Catalytic Subunits of PP2A and Acting on Both Wee1 and Cdc25. Virology *287*, 359–370.

Ellis, M., Chew, Y.P., Fallis, L., Freddersdorf, S., Boshoff, C., Weiss, R.A., Lu, X., and Mittnacht, S. (1999). Degradation of p27(Kip) cdk inhibitor triggered by Kaposi's sarcoma virus cyclin-cdk6 complex. EMBO J. *18*, 644–653.

Ellison, V., and Stillman, B. (2003). Biochemical Characterization of DNA Damage Checkpoint Complexes: Clamp Loader and Clamp Complexes with Specificity for 5' Recessed DNA. PLOS Biol. *1*, e33.

Esteve-Puig, R., Gil, R., González-Sánchez, E., Bech-Serra, J.J., Grueso, J., Hernández-Losa, J., Moliné, T., Canals, F., Ferrer, B., Cortés, J., et al. (2014). A Mouse Model Uncovers LKB1 as an UVB-Induced DNA Damage Sensor Mediating CDKN1A (p21WAF1/CIP1) Degradation. PLoS Genet. *10*, e1004721.

Evans, E., and Traktman, P. (1992). Characterization of vaccinia virus DNA replication mutants with lesions in the D5 gene. Chromosoma *102*, S72–S82.

Fallon, R.J., and Cox, R.P. (1979). Cell cycle analysis of sodium butyrate and hydroxyurea, inducers of ectopic hormone production in HeLa cells. J. Cell. Physiol. *100*, 251–261.

Fan, Y., Sanyal, S., and Bruzzone, R. (2018). Breaking Bad: How Viruses Subvert the Cell Cycle. Front. Cell. Infect. Microbiol. *8*.

Fenner, F., Henderson, D.A., Arita, I., Jezek, Z., Ladnyi, I.D., and Organization, W.H. (1988). Smallpox and its eradication (World Health Organization).

Ferguson, B.J., Mansur, D.S., Peters, N.E., Ren, H., and Smith, G.L. (2012). DNA-PK is a DNA sensor for IRF-3-dependent innate immunity. ELife *1*, e00047.

Fesquet, D., Labbé, J.C., Derancourt, J., Capony, J.P., Galas, S., Girard, F., Lorca, T., Shuttleworth, J., Dorée, M., and Cavadore, J.C. (1993). The MO15 gene encodes the catalytic subunit of a protein kinase that activates cdc2 and other cyclin-dependent kinases (CDKs) through phosphorylation of Thr161 and its homologues. EMBO J. *12*, 3111–3121.

Flemington, E.K. (2001). Herpesvirus Lytic Replication and the Cell Cycle: Arresting New Developments. J. Virol. *75*, 4475–4481.

Foloppe, J., Kintz, J., Futin, N., Findeli, A., Cordier, P., Schlesinger, Y., Hoffmann, C., Tosch, C., Balloul, J.-M., and Erbs, P. (2008). Targeted delivery of a suicide gene to human colorectal tumors by a conditionally replicating vaccinia virus. Gene Ther. *15*, 1361–1371.

Foo, C.H., Lou, H., Whitbeck, J.C., Ponce-de-León, M., Atanasiu, D., Eisenberg, R.J., and Cohen, G.H. (2009). Vaccinia virus L1 binds to cell surfaces and blocks virus entry independently of glycosaminoglycans. Virology *385*, 368–382.

Freed, E.O., and Martin, M.A. (2013). Human immunodeficiency viruses: Replication. p.

Friborg, J., Kong, W., Hottiger, M.O., and Nabel, G.J. (1999). p53 inhibition by the LANA protein of KSHV protects against cell death. Nature *402*, 889–894.

Fukasawa, K., Choi, T., Kuriyama, R., Rulong, S., and Woude, G.F.V. (1996). Abnormal Centrosome Amplification in the Absence of p53. Science *271*, 1744–1747.

Furth, J.J., and Cohen, S.S. (1968). Inhibition of Mammalian DNA Polymerase by the 5'-Triphosphate of 1-β-d-Arabinofuranosylcytosine and the 5'-Triphosphate of 9-β-d-Arabinofuranosyladenine. Cancer Res. *28*, 2061–2067.

Gammon, D.B., Gowrishankar, B., Duraffour, S., Andrei, G., Upton, C., and Evans, D.H. (2010). Vaccinia Virus–Encoded Ribonucleotide Reductase Subunits Are Differentially Required for Replication and Pathogenesis. PLOS Pathog. *6*, e1000984.

Garcia, A.D., Aravind, L., Koonin, E.V., and Moss, B. (2000). Bacterial-type DNA holliday junction resolvases in eukaryotic viruses. Proc. Natl. Acad. Sci. U. S. A. *97*, 8926–8931.

Garcia, A.D., Otero, J., Lebowitz, J., Schuck, P., and Moss, B. (2006). Quaternary Structure and Cleavage Specificity of a Poxvirus Holliday Junction Resolvase. J. Biol. Chem. *281*, 11618–11626.

Gatza, M.L., Chandhasin, C., Ducu, R.I., and Marriott, S.J. (2005). Impact of transforming viruses on cellular mutagenesis, genome stability, and cellular transformation. Environ. Mol. Mutagen. *45*, 304–325.

Gilbert, P.B., McKeague, I.W., Eisen, G., Mullins, C., Guéye-NDiaye, A., Mboup, S., and Kanki, P.J. (2003). Comparison of HIV-1 and HIV-2 infectivity from a prospective cohort study in Senegal. Stat. Med. *22*, 573–593.

Girard, F., Strausfeld, U., Fernandez, A., and Lamb, N.J.C. (1991). Cyclin a is required for the onset of DNA replication in mammalian fibroblasts. Cell *67*, 1169–1179.

Gnant, M.F.X., Noll, L.A., Irvine, K.R., Puhlmann, M., Terrill, R.E., Alexander, H.R., and Bartlett, D.L. (1999). Tumor-Specific Gene Delivery Using Recombinant Vaccinia Virus in a Rabbit Model of Liver Metastases. JNCI J. Natl. Cancer Inst. *91*, 1744–1750.

Godden-Kent, D., Talbot, S.J., Boshoff, C., Chang, Y., Moore, P., Weiss, R.A., and Mittnacht, S. (1997). The cyclin encoded by Kaposi's sarcoma-associated herpesvirus stimulates cdk6 to phosphorylate the retinoblastoma protein and histone H1. J. Virol. *71*, 4193–4198.

Goebel, S.J., Johnson, G.P., Perkus, M.E., Davis, S.W., Winslow, J.P., and Paoletti, E. (1990). The complete DNA sequence of vaccinia virus. Virology *179*, 247–266, 517–563.

Goh, W.C., Manel, N., and Emerman, M. (2004). The human immunodeficiency virus Vpr protein binds Cdc25C: implications for G2 arrest. Virology *318*, 337–349.

Goldstone, D.C., Ennis-Adeniran, V., Hedden, J.J., Groom, H.C.T., Rice, G.I., Christodoulou, E., Walker, P.A., Kelly, G., Haire, L.F., Yap, M.W., et al. (2011). HIV-1 restriction factor SAMHD1 is a deoxynucleoside triphosphate triphosphohydrolase. Nature *480*, 379–382.

Gray, R., Albrecht, D., Beerli, C., Cohen, G., Henriques, R., and Mercer, J. (2018). Nanoscale Polarization of the Vaccinia Virus Entry Fusion Complex Drives Efficient Fusion. BioRxiv 360073.

Gray, R.D.M., Beerli, C., Pereira, P.M., Scherer, K.M., Samolej, J., Bleck, C.K.E., Mercer, J., and Henriques, R. (2016). VirusMapper: open-source nanoscale mapping of viral architecture through super-resolution microscopy. Sci. Rep. *6*.

Gray-Bablin, J., Rao, S., and Keyomarsi, K. (1997). Lovastatin Induction of Cyclin-dependent Kinase Inhibitors in Human Breast Cells Occurs in a Cell Cycle-independent Fashion. Cancer Res. *57*, 604–609.

Greber, U.F., Singh, I., and Helenius, A. (1994). Mechanisms of virus uncoating. Trends Microbiol. *2*, 52–56.

Greseth, M.D., Boyle, K.A., Bluma, M.S., Unger, B., Wiebe, M.S., Soares-Martins, J.A., Wickramasekera, N.T., Wahlberg, J., and Traktman, P. (2012). Molecular Genetic and Biochemical Characterization of the Vaccinia Virus I3 Protein, the Replicative Single-Stranded DNA Binding Protein. J. Virol. *86*, 6197–6209.

Greseth, M.D., Carter, D.C., Terhune, S.S., and Traktman, P. (2017). Proteomic Screen for Cellular Targets of the Vaccinia Virus F10 Protein Kinase Reveals that Phosphorylation of mDia Regulates Stress Fiber Formation. Mol. Cell. Proteomics *16*, S124–S143.

Greseth, M.D., Czarnecki, M.W., Bluma, M.S., and Traktman, P. (2018). Isolation and Characterization of vΔI3 Confirm that Vaccinia Virus SSB Plays an Essential Role in Viral Replication. J. Virol. *92*.

Griffiths, G., Wepf, R., Wendt, T., Locker, J.K., Cyrklaff, M., and Roos, N. (2001). Structure and Assembly of Intracellular Mature Vaccinia Virus: Isolated-Particle Analysis. J. Virol. *75*, 11034–11055.

Gross, C.H., and Shuman, S. (1996). Vaccinia virions lacking the RNA helicase nucleoside triphosphate phosphohydrolase II are defective in early transcription. J. Virol. *70*, 8549–8557.

Gu, W., and Roeder, R.G. (1997). Activation of p53 Sequence-Specific DNA Binding by Acetylation of the p53 C-Terminal Domain. Cell *90*, 595–606.

Guan, K.L., Jenkins, C.W., Li, Y., Nichols, M.A., Wu, X., O'Keefe, C.L., Matera, A.G., and Xiong, Y. (1994). Growth suppression by p18, a p16INK4/MTS1- and p14INK4B/MTS2-related CDK6 inhibitor, correlates with wild-type pRb function. Genes Dev. *8*, 2939–2952.

Guerra, S., Lopez-Fernandez, L.A., Pascual-Montano, A., Munoz, M., Harshman, K., and Esteban, M. (2003). Cellular Gene Expression Survey of Vaccinia Virus Infection of Human HeLa Cells. J. Virol. *77*, 6493–6506.

Gunasinghe, S.K., Hubbs, A.E., and Wright, C.F. (1998). A Vaccinia Virus Late Transcription Factor with Biochemical and Molecular Identity to a Human Cellular Protein. J. Biol. Chem. *273*, 27524–27530.

Hafner, A., Bulyk, M.L., Jambhekar, A., and Lahav, G. (2019). The multiple mechanisms that regulate p53 activity and cell fate. Nat. Rev. Mol. Cell Biol. *20*, 199.

Hall, M., Bates, S., and Peters, G. (1995). Evidence for different modes of action of cyclin-dependent kinase inhibitors: p15 and p16 bind to kinases, p21 and p27 bind to cyclins. Oncogene *11*, 1581–1588.

Han, Y.H., Moon, H.J., You, B.R., and Park, W.H. (2009). The effect of MG132, a proteasome inhibitor on HeLa cells in relation to cell growth, reactive oxygen species and GSH. Oncol. Rep. *22*, 215–221.

Hanahan, D., and Weinberg, R.A. (2000). The Hallmarks of Cancer. Cell *100*, 57–70.

Hannon, G.J., and Beach, D. (1994). pl5 INK4B is a potentia| effector of TGF-β-induced cell cycle arrest. Nature *371*, 257–261.

Harper, J.V., and Brooks, G. (2005). The mammalian cell cycle: an overview. Methods Mol. Biol. Clifton NJ *296*, 113–153.

Hartlerode, A.J., Morgan, M.J., Wu, Y., Buis, J., and Ferguson, D.O. (2015). Recruitment and activation of the ATM kinase in the absence of DNA-damage sensors. Nat. Struct. Mol. Biol. *22*, 736–743.

Haupt, Y., Maya, R., Kazaz, A., and Oren, M. (1997). Mdm2 promotes the rapid degradation of p53. Nature *387*, 296–299.

He, J., Choe, S., Walker, R., Di Marzio, P., Morgan, D.O., and Landau, N.R. (1995). Human immunodeficiency virus type 1 viral protein R (Vpr) arrests cells in the G2 phase of the cell cycle by inhibiting p34cdc2 activity. J. Virol. *69*, 6705–6711.

Heijink, A.M., Krajewska, M., and van Vugt, M.A.T.M. (2013). The DNA damage response during mitosis. Mutat. Res. Mol. Mech. Mutagen. *750*, 45–55.

Heljasvaara, R., Rodríguez, D., Risco, C., Carrascosa, J.L., Esteban, M., and Rodríguez, J.R. (2001). The Major Core Protein P4a (A10L Gene) of Vaccinia Virus Is Essential for Correct Assembly of Viral DNA into the Nucleoprotein Complex To Form Immature Viral Particles. J. Virol. *75*, 5778–5795.

Helt, C.E., Cliby, W.A., Keng, P.C., Bambara, R.A., and O'Reilly, M.A. (2005). Ataxia Telangiectasia Mutated (ATM) and ATM and Rad3-related Protein Exhibit Selective Target Specificities in Response to Different Forms of DNA Damage. J. Biol. Chem. *280*, 1186–1192.

Hengstschläger, M., Knöfler, M., Müllner, E.W., Ogris, E., Wintersberger, E., and Wawra, E. (1994). Different regulation of thymidine kinase during the cell cycle of normal versus DNA tumor virus-transformed cells. J. Biol. Chem. *269*, 13836–13842.

Heuser, J. (2005). Deep-etch EM reveals that the early poxvirus envelope is a single membrane bilayer stabilized by a geodetic "honeycomb" surface coat. J. Cell Biol. *169*, 269–283.

Hiller, G., and Weber, K. (1985). Golgi-derived membranes that contain an acylated viral polypeptide are used for vaccinia virus envelopment. J. Virol. *55*, 651–659.

Hollinshead, M., Vanderplasschen, A., Smith, G.L., and Vaux, D.J. (1999). Vaccinia Virus Intracellular Mature Virions Contain only One Lipid Membrane. J. Virol. *73*, 1503–1517.

Holowczak, J.A., Thomas, V.I., and Flores, L. (1975). Isolation and characterization of vaccinia virus "nucleoids." Virology *67*, 506–519.

Hooda-Dhingra, U., Patel, D.D., Pickup, D.J., and Condit, R.C. (1990). Fine structure mapping and phenotypic analysis of five temperature-sensitive mutations in the second largest subunit of vaccinia virus DNA-dependent RNA polymerase. Virology *174*, 60–69.

Horsington, J., Lynn, H., Turnbull, L., Cheng, D., Braet, F., Diefenbach, R.J., Whitchurch, C.B., Karupiah, G., and Newsome, T.P. (2013). A36-dependent Actin Filament Nucleation Promotes Release of Vaccinia Virus. PLOS Pathog. *9*, e1003239.

Howard, A.R., Senkevich, T.G., and Moss, B. (2008). Vaccinia Virus A26 and A27 Proteins Form a Stable Complex Tethered to Mature Virions by Association with the A17 Transmembrane Protein. J. Virol. *82*, 12384–12391.

Howley, P.M., and Livingston, D.M. (2009). Small DNA Tumor Viruses: Large Contributors to Biomedical Sciences. Virology *384*, 256–259.

Hoy, S.M. (2018). Tecovirimat: First Global Approval. Drugs *78*, 1377–1382.

Hrecka, K., Hao, C., Gierszewska, M., Swanson, S.K., Kesik-Brodacka, M., Srivastava, S., Florens, L., Washburn, M.P., and Skowronski, J. (2011). Vpx relieves inhibition of HIV-1 infection of macrophages mediated by the SAMHD1 protein. Nature *474*, 658–661.

Hruby, D.E., Guarino, L.A., and Kates, J.R. (1979). Vaccinia Virus Replication I. Requirement for the Host-Cell Nucleus. J. Virol. *29*, 705–715.

Hsiao, J.-C., Chung, C.-S., and Chang, W. (1998). Cell Surface Proteoglycans Are Necessary for A27L Protein-Mediated Cell Fusion: Identification of the N-Terminal Region of A27L Protein as the Glycosaminoglycan-Binding Domain. J. Virol. *72*, 8374–8379.

Hsiao, J.-C., Chung, C.-S., and Chang, W. (1999). Vaccinia Virus Envelope D8L Protein Binds to Cell Surface Chondroitin Sulfate and Mediates the Adsorption of Intracellular Mature Virions to Cells. J. Virol. *73*, 8750–8761.

Hu, X., Wolffe, E.J., Weisberg, A.S., Carroll, L.J., and Moss, B. (1998). Repression of the A8L Gene, Encoding the Early Transcription Factor 82-Kilodalton Subunit, Inhibits Morphogenesis of Vaccinia Virions. J. Virol. *72*, 104–112.

Hutin, S., Ling, W.L., Round, A., Effantin, G., Reich, S., Iseni, F., Tarbouriech, N., Schoehn, G., and Burmeister, W.P. (2016). Domain Organization of Vaccinia Virus Helicase-Primase D5. J. Virol. *90*, 4604–4613.

Ibrahim, N., Wicklund, A., and Wiebe, M.S. (2011). Molecular Characterization of the Host Defense Activity of the Barrier to Autointegration Factor against Vaccinia Virus. J. Virol. *85*, 11588–11600.

Ibrahim, N., Wicklund, A., Jamin, A., and Wiebe, M.S. (2013). Barrier to autointegration factor (BAF) inhibits vaccinia virus intermediate transcription in the absence of the viral B1 kinase. Virology *444*, 363–373.

Ichihashi, Y. (1996). Extracellular Enveloped Vaccinia Virus Escapes Neutralization. Virology *217*, 478–485.

Irwin, C.R., Hitt, M.M., and Evans, D.H. (2017). Targeting Nucleotide Biosynthesis: A Strategy for Improving the Oncolytic Potential of DNA Viruses. Front. Oncol. *7*.

Iwakuma, T., and Lozano, G. (2003). MDM2, An Introduction. Mol. Cancer Res. *1*, 993–1000.

Iwanaga, R., Ozono, E., Fujisawa, J., Ikeda, M.A., Okamura, N., Huang, Y., and Ohtani, K. (2008). Activation of the *cyclin D2* and *cdk6* genes through NF-κB is critical for cell-cycle progression induced by HTLV-I Tax. Oncogene *27*, 5635–5642.

Iyer, L.M., Aravind, L., and Koonin, E.V. (2001). Common Origin of Four Diverse Families of Large Eukaryotic DNA Viruses. J. Virol. *75*, 11720–11734.

Izumiya, Y., Lin, S.-F., Ellison, T.J., Levy, A.M., Mayeur, G.L., Izumiya, C., and Kung, H.-J. (2003). Cell Cycle Regulation by Kaposi's Sarcoma-Associated Herpesvirus K-bZIP: Direct Interaction with Cyclin-CDK2 and Induction of G1 Growth Arrest. J. Virol. *77*, 9652–9661.

James, M.K., Ray, A., Leznova, D., and Blain, S.W. (2008). Differential modification of p27Kip1 controls its cyclin D-cdk4 inhibitory activity. Mol. Cell. Biol. *28*, 498–510.

Järviluoma, A., and Ojala, P.M. (2006). Cell signaling pathways engaged by KSHV. Biochim. Biophys. Acta BBA - Rev. Cancer *1766*, 140–158.

JavanMoghadam-Kamrani, S., and Keyomarsi, K. (2008). Synchronization of the cell cycle using Lovastatin. Cell Cycle *7*, 2434–2440.

Jesus, D.M., Moussatche, N., McFadden, B.D., Nielsen, C.P., D'Costa, S.M., and Condit, R.C. (2015). Vaccinia virus protein A3 is required for the production of normal immature virions and for the encapsidation of the nucleocapsid protein L4. Virology *481*, 1–12.

Jin, S., Antinore, M.J., Lung, F.D., Dong, X., Zhao, H., Fan, F., Colchagie, A.B., Blanck, P., Roller, P.P., Fornace, A.J., et al. (2000). The GADD45 inhibition of Cdc2 kinase correlates with GADD45-mediated growth suppression. J. Biol. Chem. *275*, 16602–16608.

Johnston, J.B., Wang, G., Barrett, J.W., Nazarian, S.H., Colwill, K., Moran, M., and McFadden, G. (2005). Myxoma Virus M-T5 Protects Infected Cells from the Stress of Cell Cycle Arrest through Its Interaction with Host Cell Cullin-1. J. Virol. *79*, 10750–10763.

Jr, F.M.S. (1968). The Antiviral Activity of 9-β-D-Arabinofuranosyladenine (ARA-A). Chemotherapy *13*, 321–338.

Jungwirth, C., and Dawid, I.B. (1967). Vaccinia DNA: Separation of viral from host cell DNA. Arch. F�r Gesamte Virusforsch. *20*, 464–468.

Jungwirth, C., and Launer, J. (1968). Effect of Poxvirus Infection on Host Cell Deoxyribonucleic Acid Synthesis. J. Virol. *2*, 401–408.

Kajioka, R., Siminovitch, L., and Dales, S. (1964). The cycle of multiplication of vaccinia virus in Earle's strain L cells II. Initiation of DNA synthesis and morphogenesis. Virology *24*, 295–309.

Kaldis, P., Ojala, P.M., Tong, L., Mäkelä, T.P., and Solomon, M.J. (2001). CAK-independent Activation of CDK6 by a Viral Cyclin. Mol. Biol. Cell *12*, 3987–3999.

Kamata, M., Watanabe, N., Nagaoka, Y., and Chen, I.S.Y. (2008). Human Immunodeficiency Virus Type 1 Vpr Binds to the N Lobe of the Wee1 Kinase Domain and Enhances Kinase Activity for Cdc2. J. Virol. *82*, 5672–5682.

Kaneko, Y., Watanabe, N., Morisaki, H., Akita, H., Fujimoto, A., Tominaga, K., Terasawa, M., Tachibana, A., Ikeda, K., and Nakanishi, M. (1999). Cell cycle-dependent and ATM-independent expression of human Chk1 kinase. Oncogene *18*, 3673–3681.

Kardinal, C., Dangers, M., Kardinal, A., Koch, A., Brandt, D.T., Tamura, T., and Welte, K. (2006). Tyrosine phosphorylation modulates binding preference to cyclin-dependent kinases and subcellular localization of p27Kip1 in the acute promyelocytic leukemia cell line NB4. Blood *107*, 1133–1140.

Kastan, M.B., Onyekwere, O., Sidransky, D., Vogelstein, B., and Craig, R.W. (1991). Participation of p53 Protein in the Cellular Response to DNA Damage. Cancer Res. *51*, 6304–6311.

Kastan, M.B., Zhan, Q., El-Deiry, W.S., Carrier, F., Jacks, T., Walsh, W.V., Plunkett, B.S., Vogelstein, B., and Fornace, A.J. (1992). A mammalian cell cycle checkpoint pathway utilizing p53 and GADD45 is defective in ataxia-telangiectasia. Cell *71*, 587–597.

Kates, J.R., and McAuslan, B.R. (1967). Poxvirus DNA-dependent RNA polymerase. Proc. Natl. Acad. Sci. U. S. A. *58*, 134–141.

Kates, J., Dahl, R., and Mielke, M. (1968). Synthesis and Intracellular Localization of Vaccinia Virus Deoxyribonucleic Acid-dependent Ribonucleic Acid Polymerase. J. Virol. *2*, 894–900.

Katsafanas, G.C., and Moss, B. (2004). Vaccinia Virus Intermediate Stage Transcription Is Complemented by Ras-GTPase-activating Protein SH3 Domain-binding Protein (G3BP) and Cytoplasmic Activation/Proliferation-associated Protein (p137) Individually or as a Heterodimer. J. Biol. Chem. *279*, 52210–52217.

Katsafanas, G.C., and Moss, B. (2007). Linkage of Transcription and Translation within Cytoplasmic Poxvirus DNA Factories Provides a Mechanism to Coordinate Viral and Usurp Host Functions. Cell Host Microbe *2*, 221–228.

Katz, E., and Moss, B. (1970). Formation of a Vaccinia Virus Structural Polypeptide from a Higher Molecular Weight Precursor: Inhibition by Rifampicin. Proc. Natl. Acad. Sci. U. S. A. *66*, 677–684.

Kauffman, M.G., and Kelly, T.J. (1991). Cell cycle regulation of thymidine kinase: residues near the carboxyl terminus are essential for the specific degradation of the enzyme at mitosis. Mol. Cell. Biol. *11*, 2538–2546.

Kaushik, R., Zhu, X., Stranska, R., Wu, Y., and Stevenson, M. (2009). A cellular restriction dictates the permissivity of non-dividing monocyte/ macrophage to lentivirus and gammaretrovirus infection. Cell Host Microbe *6*, 68–80.

Ke, P.-Y., and Chang, Z.-F. (2004). Mitotic Degradation of Human Thymidine Kinase 1 Is Dependent on the Anaphase-Promoting Complex/Cyclosome-Cdh1-Mediated Pathway. Mol. Cell. Biol. *24*, 514–526.

Keck, J.G., Baldick, C.J., and Moss, B. (1990). Role of DNA replication in vaccinia virus gene expression: A naked template is required for transcription of three late trans-activator genes. Cell *61*, 801–809.

Khosravi, R., Maya, R., Gottlieb, T., Oren, M., Shiloh, Y., and Shkedy, D. (1999). Rapid ATM-dependent phosphorylation of MDM2 precedes p53 accumulation in response to DNA damage. Proc. Natl. Acad. Sci. U. S. A. *96*, 14973–14977.

Khuperkar, D., Kamble, A., Singh, A., Ghate, A., Nawadkar, R., Sahu, A., and Joseph, J. (2017). Selective recruitment of nucleoporins on vaccinia virus factories and the role of Nup358 in viral infection. Virology *512*, 151–160.

Kilcher, S., and Mercer, J. (2015). DNA virus uncoating. Virology *479–480*, 578–590.

Kilcher, S., Schmidt, F.I., Schneider, C., Kopf, M., Helenius, A., and Mercer, J. (2014). siRNA Screen of Early Poxvirus Genes Identifies the AAA+ ATPase D5 as the Virus Genome-Uncoating Factor. Cell Host Microbe *15*, 103–112.

Kim, J.H., Oh, J.Y., Park, B.H., Lee, D.E., Kim, J.S., Park, H.E., Roh, M.S., Je, J.E., Yoon, J.H., Thorne, S.H., et al. (2006). Systemic Armed Oncolytic and Immunologic Therapy for Cancer with JX-594, a Targeted Poxvirus Expressing GM-CSF. Mol. Ther. *14*, 361–370.

Kirn, D.H., and Thorne, S.H. (2009). Targeted and armed oncolytic poxviruses: a novel multi-mechanistic therapeutic class for cancer. Nat. Rev. Cancer *9*, 64–71.

Kit, S., and Dubbs, D.R. (1962). Biochemistry of vaccinia-infected mouse fibroblasts (strain L-M): I. Effects on nuclei acid and protein synthesis. Virology *18*, 274–285.

Knight, J.S., and Robertson, E.S. (2004). Epstein-Barr Virus Nuclear Antigen 3C Regulates Cyclin A/p27 Complexes and Enhances Cyclin A-Dependent Kinase Activity. J. Virol. *78*, 1981–1991.

Knutson, B.A., Liu, X., Oh, J., and Broyles, S.S. (2006). Vaccinia Virus Intermediate and Late Promoter Elements Are Targeted by the TATA-Binding Protein. J. Virol. *80*, 6784–6793.

Koh, J., Enders, G.H., Dynlacht, B.D., and Harlow, E. (1995). Tumour-derived p16 alleles encoding proteins defective in cell-cycle inhibition. Nature *375*, 506–510.

Krakoff, I.H., Brown, N.C., and Reichard, P. (1968). Inhibition of Ribonucleoside Diphosphate Reductase by Hydroxyurea. Cancer Res. *28*, 1559–1565.

Kreahling, J.M., Foroutan, P., Reed, D., Martinez, G., Razabdouski, T., Bui, M.M., Raghavan, M., Letson, D., Gillies, R.J., and Altiok, S. (2013). Wee1 Inhibition by MK-1775 Leads to Tumor Inhibition and Enhances Efficacy of Gemcitabine in Human Sarcomas. PLoS ONE *8*.

Krijnse-Locker, J., Schleich, S., Rodriguez, D., Goud, B., Snijder, E.J., and Griffiths, G. (1996). The Role of a 21-kDa Viral Membrane Protein in the Assembly of Vaccinia Virus from the Intermediate Compartment. J. Biol. Chem. *271*, 14950–14958.

Kubbutat, M.H.G., Jones, S.N., and Vousden, K.H. (1997). Regulation of p53 stability by Mdm2. Nature *387*, 299–303.

Kumari, G., Ulrich, T., Krause, M., Finkernagel, F., and Gaubatz, S. (2014). Induction of p21CIP1 Protein and Cell Cycle Arrest after Inhibition of Aurora B Kinase Is Attributed to Aneuploidy and Reactive Oxygen Species. J. Biol. Chem. *289*, 16072–16084.

LaBaer, J., Garrett, M.D., Stevenson, L.F., Slingerland, J.M., Sandhu, C., Chou, H.S., Fattaey, A., and Harlow, E. (1997). New functional activities for the p21 family of CDK inhibitors. Genes Dev. *11*, 847–862.

Laguette, N., Sobhian, B., Casartelli, N., Ringeard, M., Chable-Bessia, C., Ségéral, E., Yatim, A., Emiliani, S., Schwartz, O., and Benkirane, M. (2011). SAMHD1 is the dendritic– and myeloid–cell–specific HIV–1 restriction factor counteracted by Vpx. Nature *474*, 654–657.

Lahouassa, H., Daddacha, W., Hofmann, H., Ayinde, D., Logue, E.C., Dragin, L., Bloch, N., Maudet, C., Bertrand, M., Gramberg, T., et al. (2012). SAMHD1 restricts HIV-1 by reducing the intracellular pool of deoxynucleotide triphosphates. Nat. Immunol. *13*, 223–228.

Lai, M., Zimmerman, E.S., Planelles, V., and Chen, J. (2005). Activation of the ATR Pathway by Human Immunodeficiency Virus Type 1 Vpr Involves Its Direct Binding to Chromatin In Vivo. J. Virol. *79*, 15443–15451.

Larminie, C.G., Cairns, C.A., Mital, R., Martin, K., Kouzarides, T., Jackson, S.P., and White, R.J. (1997). Mechanistic analysis of RNA polymerase III regulation by the retinoblastoma protein. EMBO J. *16*, 2061–2071.

LaRocca, C.J., and Warner, S.G. (2018). Oncolytic viruses and checkpoint inhibitors: combination therapy in clinical trials. Clin. Transl. Med. *7*, 35.

Lavia, P., Mileo, A.M., Giordano, A., and Paggi, M.G. (2003). Emerging roles of DNA tumor viruses in cell proliferation: new insights into genomic instability. Oncogene *22*, 6508–6516.

Law, M., Carter, G.C., Roberts, K.L., Hollinshead, M., and Smith, G.L. (2006). Ligand-induced and nonfusogenic dissolution of a viral membrane. Proc. Natl. Acad. Sci. U. S. A. *103*, 5989–5994.

Lee, D.H., and Goldberg, A.L. (1998). Proteasome inhibitors: valuable new tools for cell biologists. Trends Cell Biol. *8*, 397–403.

Lee, J.-H., and Paull, T.T. (2004). Direct Activation of the ATM Protein Kinase by the Mre11/Rad50/Nbs1 Complex. Science *304*, 93–96.

Lee, J.-H., and Paull, T.T. (2005). ATM Activation by DNA Double-Strand Breaks Through the Mre11-Rad50-Nbs1 Complex. Science *308*, 551–554.

Lee, H., Zeng, S.X., and Lu, H. (2006). UV Induces p21 Rapid Turnover Independently of Ubiquitin and Skp2. J. Biol. Chem. *281*, 26876–26883.

Lee, J.Y., Yu, S.J., Park, Y.G., Kim, J., and Sohn, J. (2007). Glycogen Synthase Kinase 3β Phosphorylates p21WAF1/CIP1 for Proteasomal Degradation after UV Irradiation. Mol. Cell. Biol. *27*, 3187–3198.

Lehman, J.M., Laffin, J., and Friedrich, T.D. (2000). Simian Virus 40 Induces Multiple S Phases with the Majority of Viral DNA Replication in the G2 and Second S Phase in CV-1 Cells. Exp. Cell Res. *258*, 215–222.

Leite, F., and Way, M. (2015). The role of signalling and the cytoskeleton during Vaccinia Virus egress. Virus Res. *209*, 87–99.

Lewis, C.W., Jin, Z., Macdonald, D., Wei, W., Qian, X.J., Choi, W.S., He, R., Sun, X., Chan, G., Lewis, C.W., et al. (2017). Prolonged mitotic arrest induced by Wee1 inhibition sensitizes breast cancer cells to paclitaxel. Oncotarget *5*.

Li, G., Elder, R.T., Qin, K., Park, H.U., Liang, D., and Zhao, R.Y. (2007). Phosphatase Type 2A-dependent and -independent Pathways for ATR Phosphorylation of Chk1. J. Biol. Chem. *282*, 7287–7298.

Li, G., Park, H.U., Liang, D., and Zhao, R.Y. (2010a). Cell cycle G2/M arrest through an S phase-dependent mechanism by HIV-1 viral protein R. Retrovirology *7*, 59.

Li, Y., Zhang, Z.-F., Chen, J., Huang, D., Ding, Y., Tan, M.-H., Qian, C.-N., Resau, J.H., Kim, H., and Teh, B.T. (2010b). VX680/MK-0457, a potent and selective Aurora kinase inhibitor, targets both tumor and endothelial cells in clear cell renal cell carcinoma. Am. J. Transl. Res. *2*, 296–308.

Lin, S., and Broyles, S.S. (1994). Vaccinia protein kinase 2: a second essential serine/threonine protein kinase encoded by vaccinia virus. Proc. Natl. Acad. Sci. *91*, 7653–7657.

Lin, C.-L., Chung, C.-S., Heine, H.G., and Chang, W. (2000). Vaccinia Virus Envelope H3L Protein Binds to Cell Surface Heparan Sulfate and Is Important for Intracellular Mature Virion Morphogenesis and Virus Infection In Vitro and In Vivo. J. Virol. *74*, 3353–3365.

Lin, Y.-C.J., Li, J., Irwin, C.R., Jenkins, H., DeLange, L., and Evans, D.H. (2008). Vaccinia Virus DNA Ligase Recruits Cellular Topoisomerase II to Sites of Viral Replication and Assembly. J. Virol. *82*, 5922–5932.

Linke, S.P., Clarkin, K.C., Di Leonardo, A., Tsou, A., and Wahl, G.M. (1996). A reversible, p53-dependent G0/G1 cell cycle arrest induced by ribonucleotide depletion in the absence of detectable DNA damage. Genes Dev. *10*, 934–947.

Liu, F., Stanton, J.J., Wu, Z., and Piwnica-Worms, H. (1997). The human Myt1 kinase preferentially phosphorylates Cdc2 on threonine 14 and localizes to the endoplasmic reticulum and Golgi complex. Mol. Cell. Biol. *17*, 571–583.

Liu, K., Lemon, B., and Traktman, P. (1995). The dual-specificity phosphatase encoded by vaccinia virus, VH1, is essential for viral transcription in vivo and in vitro. J. Virol. *69*, 7823–7834.

Liu, Q., Guntuku, S., Cui, X.-S., Matsuoka, S., Cortez, D., Tamai, K., Luo, G., Carattini-Rivera, S., DeMayo, F., Bradley, A., et al. (2000). Chk1 is an essential kinase that is regulated by Atr and required for the G2/M DNA damage checkpoint. Genes Dev. *14*, 1448–1459.

Locker, J.K., and Griffiths, G. (1999). An Unconventional Role for Cytoplasmic Disulfide Bonds in Vaccinia Virus Proteins. J. Cell Biol. *144*, 267–279.

Lowe, S.W., Schmitt, E.M., Smith, S.W., Osborne, B.A., and Jacks, T. (1993). p53 is required for radiation-induced apoptosis in mouse thymocytes. Nature *362*, 847–849.

Lucas-Lenard, J.M., and Cohen, S.S. (1966). The inhibition of polynucleotide phosphorylase by certain substrate analogues. Biochim. Biophys. Acta BBA - Nucleic Acids Protein Synth. *123*, 471–477.

Lukas, C., Bartkova, J., Latella, L., Falck, J., Mailand, N., Schroeder, T., Sehested, M., Lukas, J., and Bartek, J. (2001). DNA Damage-activated Kinase Chk2 Is Independent of Proliferation or Differentiation Yet Correlates with Tissue Biology. Cancer Res. *61*, 4990–4993.

Lukas, J., Lukas, C., and Bartek, J. (2004). Mammalian cell cycle checkpoints: signalling pathways and their organization in space and time. DNA Repair *3*, 997–1007.

Lundberg, A.S., and Weinberg, R.A. (1998). Functional inactivation of the retinoblastoma protein requires sequential modification by at least two distinct cyclin-cdk complexes. Mol. Cell. Biol. *18*, 753–761.

Luo, Y., Hurwitz, J., and Massagué, J. (1995). Cell-cycle inhibition by independent CDK and PCNA binding domains in p21 Cip1. Nature *375*, 159–161.

Ma, H.T., and Poon, R.Y.C. (2011). Synchronization of HeLa cells. Methods Mol. Biol. Clifton NJ *761*, 151–161.

Ma, D., Zhou, P., and Harbour, J.W. (2003). Distinct Mechanisms for Regulating the Tumor Suppressor and Antiapoptotic Functions of Rb. J. Biol. Chem. *278*, 19358–19366.

Magee, W.E., and Sagik, B.P. (1959). The synthesis of deoxyribonucleic acid by HeLa cells infected with vaccinia virus. Virology *8*, 134–137.

Magee, W.E., Sheek, M.R., and Burrous, M.J. (1960). The synthesis of vaccinial deoxyribonucleic acid. Virology *11*, 296–299.

Mailand, N., Podtelejnikov, A.V., Groth, A., Mann, M., Bartek, J., and Lukas, J. (2002). Regulation of G2/M events by Cdc25A through phosphorylation-dependent modulation of its stability. EMBO J. *21*, 5911–5920.

Malkin, A.J., McPherson, A., and Gershon, P.D. (2003). Structure of Intracellular Mature Vaccinia Virus Visualized by In Situ Atomic Force Microscopy. J. Virol. *77*, 6332–6340.

Mansky, L.M. (1996). The Mutation Rate of Human Immunodeficiency Virus Type 1 Is Influenced by thevprGene. Virology *222*, 391–400.

Mantovani, F., and Banks, L. (2001). The human papillomavirus E6 protein and its contribution to malignant progression. Oncogene *20*, 7874–7887.

Maréchal, A., Li, J.-M., Ji, X.Y., Wu, C.-S., Yazinski, S.A., Nguyen, H.D., Liu, S., Jiménez, A.E., Jin, J., and Zou, L. (2014). PRP19 Transforms into a Sensor of RPA-ssDNA after DNA Damage and Drives ATR Activation via a Ubiquitin-Mediated Circuitry. Mol. Cell *53*, 235–246.

Marmelzat, W.L. (1968). Malignant Tumors in Smallpox Vaccination Scars: A Report of 24 Cases. Arch. Dermatol. *97*, 400–406.

Matsuoka, S., Edwards, M.C., Bai, C., Parker, S., Zhang, P., Baldini, A., Harper, J.W., and Elledge, S.J. (1995). p57KIP2, a structurally distinct member of the p21CIP1 Cdk inhibitor family, is a candidate tumor suppressor gene. Genes Dev. *9*, 650–662.

Matsuoka, S., Huang, M., and Elledge, S.J. (1998). Linkage of ATM to Cell Cycle Regulation by the Chk2 Protein Kinase. Science *282*, 1893–1897.

Matsuoka, S., Rotman, G., Ogawa, A., Shiloh, Y., Tamai, K., and Elledge, S.J. (2000). Ataxia telangiectasia-mutated phosphorylates Chk2 in vivo and in vitro. Proc. Natl. Acad. Sci. *97*, 10389–10394.

Mauck, J.C., and Green, H. (1974). Regulation of pre-transfer RNA synthesis during transition from resting to growing state. Cell *3*, 171–177.

Maya, R., Balass, M., Kim, S.-T., Shkedy, D., Leal, J.-F.M., Shifman, O., Moas, M., Buschmann, T., Ronai, Z., Shiloh, Y., et al. (2001). ATM-dependent phosphorylation of Mdm2 on serine 395: role in p53 activation by DNA damage. Genes Dev. *15*, 1067–1077.

McConnell, B.B., Gregory, F.J., Stott, F.J., Hara, E., and Peters, G. (1999). Induced Expression of p16INK4a Inhibits Both CDK4- and CDK2-Associated Kinase Activity by Reassortment of Cyclin-CDK-Inhibitor Complexes. Mol. Cell. Biol. *19*, 1981–1989.

McFadden, G. (2005). Poxvirus tropism. Nat. Rev. Microbiol. *3*, 201–213.

McFadden, G., Graham, K., Ellison, K., Barry, M., Macen, J., Schreiber, M., Mossman, K., Nash, P., Lalani, A., and Everett, H. (1995). Interruption of cytokine networks by poxviruses: lessons from myxoma virus. J. Leukoc. Biol. *57*, 731–738.

McGarry, T.J., and Kirschner, M.W. (1998). Geminin, an Inhibitor of DNA Replication, Is Degraded during Mitosis. Cell *93*, 1043–1053.

McMahon, D. (1975). Cycloheximide Is Not a Specific Inhibitor of Protein Synthesis in Vivo1. Plant Physiol. *55*, 815–821.

MD, R.P. (1970). Molluscum Contagiosum. Arch. Environ. Health Int. J. *21*, 432–452.

Meade, N., Furey, C., Li, H., Verma, R., Chai, Q., Rollins, M.G., DiGiuseppe, S., Naghavi, M.H., and Walsh, D. (2018). Poxviruses evade cytosolic sensing through disruption of an mTORC1-mTORC2 regulatory circuit. Cell *174*, 1143-1157.e17.

Medema, R.H., Herrera, R.E., Lam, F., and Weinberg, R.A. (1995). Growth suppression by p16ink4 requires functional retinoblastoma protein. Proc. Natl. Acad. Sci. U. S. A. *92*, 6289–6293.

Mercer, J. (2019). Vaccinia virus: methods and protocols.

Mercer, J., and Helenius, A. (2008a). Vaccinia Virus Uses Macropinocytosis and Apoptotic Mimicry to Enter Host Cells. Science *320*, 531–535.

Mercer, J., and Helenius, A. (2008b). Vaccinia Virus Uses Macropinocytosis and Apoptotic Mimicry to Enter Host Cells. Science *320*, 531–535.

Mercer, J., and Traktman, P. (2003). Investigation of Structural and Functional Motifs within the Vaccinia Virus A14 Phosphoprotein, an Essential Component of the Virion Membrane. J. Virol. *77*, 8857–8871.

Mercer, J., and Traktman, P. (2005). Genetic and cell biological characterization of the vaccinia virus A30 and G7 phosphoproteins. J. Virol. *79*, 7146–7161.

Mercer, J., Knébel, S., Schmidt, F.I., Crouse, J., Burkard, C., and Helenius, A. (2010). Vaccinia virus strains use distinct forms of macropinocytosis for host-cell entry. Proc. Natl. Acad. Sci. U. S. A. *107*, 9346–9351.

Mercer, J., Snijder, B., Sacher, R., Burkard, C., Bleck, C.K.E., Stahlberg, H., Pelkmans, L., and Helenius, A. (2012). RNAi Screening Reveals Proteasome- and Cullin3-Dependent Stages in Vaccinia Virus Infection. Cell Rep. *2*, 1036–1047.

Mesri, E.A., Cesarman, E., and Boshoff, C. (2010). Kaposi's sarcoma and its associated herpesvirus. Nat. Rev. Cancer *10*, 707–719.

Miller, J.D., van der Most, R.G., Akondy, R.S., Glidewell, J.T., Albott, S., Masopust, D., Murali-Krishna, K., Mahar, P.L., Edupuganti, S., Lalor, S., et al. (2008). Human Effector and Memory CD8+ T Cell Responses to Smallpox and Yellow Fever Vaccines. Immunity *28*, 710–722.

Mitra, J., Dai, C.Y., Somasundaram, K., El-Deiry, W.S., Satyamoorthy, K., Herlyn, M., and Enders, G.H. (1999). Induction of p21WAF1/CIP1 and Inhibition of Cdk2 Mediated by the Tumor Suppressor p16INK4a. Mol. Cell. Biol. *19*, 3916–3928.

Mlcochova, P., Sutherland, K.A., Watters, S.A., Bertoli, C., de Bruin, R.A., Rehwinkel, J., Neil, S.J., Lenzi, G.M., Kim, B., Khwaja, A., et al. (2017). A G1-like state allows HIV-1 to bypass SAMHD1 restriction in macrophages. EMBO J. *36*, 604–616.

Mo, M., Fleming, S.B., and Mercer, A.A. (2009). Cell cycle deregulation by a poxvirus partial mimic of anaphase-promoting complex subunit 11. Proc. Natl. Acad. Sci. U. S. A. *106*, 19527–19532.

Moore, P.S. (2007). KSHV manipulation of the cell cycle and apoptosis (Cambridge University Press).

Moore, P.S., and Chang, Y. (1998). Antiviral activity of tumor-suppressor pathways: clues from molecular piracy by KSHV. Trends Genet. *14*, 144–150.

Morizono, K., Xie, Y., Olafsen, T., Lee, B., Dasgupta, A., Wu, A.M., and Chen, I.S.Y. (2011). The soluble serum protein Gas6 bridges virion envelope phosphatidylserine to the TAM receptor tyrosine kinase Axl to mediate viral entry. Cell Host Microbe *9*, 286–298.

Morse, L., Chen, D., Franklin, D., Xiong, Y., and Chen-Kiang, S. (1997). Induction of Cell Cycle Arrest and B Cell Terminal Differentiation by CDK Inhibitor p18 INK4c and IL-6. Immunity *6*, 47–56.

Moss, B. (1990). Regulation of Vaccinia Virus Transcription. Annu. Rev. Biochem. *59*, 661–688.

Moss, B. (2006). Poxvirus entry and membrane fusion. Virology *344*, 48–54.

Moss, B. (2007). Poxviridae: the viruses and their replication. In Fields Virology, D. Knipe, and P. Howley, eds. (Philadelphia: Lippincott-Raven), p. 2906.

Moss, B. (2012). Poxvirus Cell Entry: How Many Proteins Does it Take? Viruses *4*, 688–707.

Moss, B. (2013). Poxvirus DNA Replication. Cold Spring Harb. Perspect. Biol. *5*.

Moss, B. (2018). Origin of the poxviral membrane: A 50-year-old riddle. PLOS Pathog. *14*, e1007002.

Moss, B., and Rosenblum, E.N. (1973). Protein cleavage and poxvirus morphogenesis: Tryptic peptide analysis of core precursors accumulated by blocking assembly with rifampicin. J. Mol. Biol. *81*, 267–269.

Moussatche, N., and Condit, R.C. (2015). Fine structure of the vaccinia virion determined by controlled degradation and immunolocalization. Virology *475*, 204–218.

Moyer (1987). The role of the host cell nucleus in vaccinia virus morphogenesis. Virus Research.

Moyer, R.W., and Graves, R.L. (1981). The mechanism of cytoplasmic orthopoxvirus DNA replication. Cell *27*, 391–401.

Müller, G., and Peters, D. (1963). Substrukturen des Vaccinevirus dargestellt durch Negativkontrastierung. Arch. Für Gesamte Virusforsch. *13*, 435–451.

Munyon, W., Paoletti, E., and Grace, J.T. (1967). RNA polymerase activity in purified infectious vaccinia virus. Proc. Natl. Acad. Sci. U. S. A. *58*, 2280–2287.

Musahl, C., Holthoff, H.P., Lesch, R., and Knippers, R. (1998). Stability of the Replicative Mcm3 Protein in Proliferating and Differentiating Human Cells. Exp. Cell Res. *241*, 260–264.

Nagler, F.P.O., and Rake, G. (1948). The Use of the Electron Microscope in Diagnosis of Variola, Vaccinia, and Varicella. J. Bacteriol. *55*, 45–51.

Najarro, P., Traktman, P., and Lewis, J.A. (2001). Vaccinia Virus Blocks Gamma Interferon Signal Transduction: Viral VH1 Phosphatase Reverses Stat1 Activation. J. Virol. *75*, 3185–3196.

Nakamura, H., Li, M., Zarycki, J., and Jung, J.U. (2001). Inhibition of p53 Tumor Suppressor by Viral Interferon Regulatory Factor. J. Virol. *75*, 7572–7582.

Nakanishi, M., Robetorye, R.S., Adami, G.R., Pereira-Smith, O.M., and Smith, J.R. (1995). Identification of the active region of the DNA synthesis inhibitory gene p21Sdi1/CIP1/WAF1. EMBO J. *14*, 555–563.

Nallamshetty, S., Crook, M., Boehm, M., Yoshimoto, T., Olive, M., and Nabel, E.G. (2005). The cell cycle regulator p27Kip1 interacts with MCM7, a DNA replication licensing factor, to inhibit initiation of DNA replication. FEBS Lett. *579*, 6529–6536.

Narasimha, A.M., Kaulich, M., Shapiro, G.S., Choi, Y.J., Sicinski, P., and Dowdy, S.F. (2014). Cyclin D activates the Rb tumor suppressor by mono-phosphorylation. ELife *3*.

Nghiem, P., Park, P.K., Kim, Y., Vaziri, C., and Schreiber, S.L. (2001). ATR inhibition selectively sensitizes G1 checkpoint-deficient cells to lethal premature chromatin condensation. Proc. Natl. Acad. Sci. U. S. A. *98*, 9092–9097.

Nichols, R.J., and Traktman, P. (2004). Characterization of Three Paralogous Members of the Mammalian Vaccinia Related Kinase Family. J. Biol. Chem. *279*, 7934–7946.

Nishitani, H., Lygerou, Z., and Nishimoto, T. (2004). Proteolysis of DNA Replication Licensing Factor Cdt1 in S-phase Is Performed Independently of Geminin through Its N-terminal Region. J. Biol. Chem. *279*, 30807–30816.

Nishitani, H., Sugimoto, N., Roukos, V., Nakanishi, Y., Saijo, M., Obuse, C., Tsurimoto, T., Nakayama, K.I., Nakayama, K., Fujita, M., et al. (2006). Two E3 ubiquitin ligases, SCF-Skp2 and DDB1-Cul4, target human Cdt1 for proteolysis. EMBO J. *25*, 1126–1136.

Niven, J.S.F., Armstrong, J.A., Andrewes, C.H., Pereira, H.G., and Valentine, R.C. (1961). Subcutaneous “growths” in monkeys produced by a Poxvirus. J. Pathol. Bacteriol. *81*, 1–14.

Nolen, L.D., Osadebe, L., Katomba, J., Likofata, J., Mukadi, D., Monroe, B., Doty, J., Hughes, C.M., Kabamba, J., Malekani, J., et al. (2016). Extended Human-to-Human Transmission during a Monkeypox Outbreak in the Democratic Republic of the Congo. Emerg. Infect. Dis. *22*, 1014–1021.

Nourse, J., Firpo, E., Flanagan, W.M., Coats, S., Polyak, K., Lee, M.-H., Massague, J., Crabtree, G.R., and Roberts, J.M. (1994). Interleukin-2-mediated elimination of the p27 Kipl cyclin-dependent kinase inhibitor prevented by rapamycin. Nature *372*, 570–573.

Novy, K., Kilcher, S., Omasits, U., Bleck, C.K.E., Beerli, C., Vowinckel, J., Martin, C.K., Syedbasha, M., Maiolica, A., White, I., et al. (2018). Proteotype profiling unmasks a viral signalling network essential for poxvirus assembly and transcriptional competence. Nat. Microbiol. *3*, 588.

Noyce, R.S., Lederman, S., and Evans, D.H. (2018). Construction of an infectious horsepox virus vaccine from chemically synthesized DNA fragments. PLoS ONE *13*.

Nuwayhid, S., Stockett, D., Hyde, J., Aleshin, A., Walker, D.H., and Arkin, M.R. (2006). SNS-032 Is a Potent and Selective Inhibitor of CDK2, 7 and 9 and Induces Cell Death by Inhibiting Cell Cycle Progression and the Expression of Antiapoptotic Proteins. 1.

Oda, K.-I., and Joklik, W.K. (1967). Hybridization and sedimentation studies on “early” and “late” vaccinia messenger RNA. J. Mol. Biol. *27*, 395–419.

Oh, J., and Broyles, S.S. (2005). Host Cell Nuclear Proteins Are Recruited to Cytoplasmic Vaccinia Virus Replication Complexes. J. Virol. *79*, 12852–12860.

Ohtsubo, M., Theodoras, A.M., Schumacher, J., Roberts, J.M., and Pagano, M. (1995). Human cyclin E, a nuclear protein essential for the G1-to-S phase transition. Mol. Cell. Biol. *15*, 2612–2624.

Ojala, P.M., Tiainen, M., Salven, P., Veikkola, T., Castaños-Vélez, E., Sarid, R., Biberfeld, P., and Mäkelä, T.P. (1999). Kaposi’s Sarcoma-associated Herpesvirus-encoded v-Cyclin Triggers Apoptosis in Cells with High Levels of Cyclin-dependent Kinase 6. Cancer Res. *59*, 4984–4989.

Ojeda, S., Domi, A., and Moss, B. (2006). Vaccinia Virus G9 Protein Is an Essential Component of the Poxvirus Entry-Fusion Complex. J. Virol. *80*, 9822–9830.

Okwo-Bele, J.-M., and Cherian, T. (2011). The expanded programme on immunization: A lasting legacy of smallpox eradication. Vaccine *29*, D74–D79.

Olson, A.T., Rico, A.B., Wang, Z., Delhon, G., and Wiebe, M.S. (2017). Deletion of the Vaccinia Virus B1 Kinase Reveals Essential Functions of This Enzyme Complemented Partly by the Homologous Cellular Kinase VRK2. J. Virol. *91*.

Olson, A.T., Wang, Z., Rico, A.B., and Wiebe, M.S. (2019). A poxvirus pseudokinase represses viral DNA replication via a pathway antagonized by its paralog kinase. PLOS Pathog. *15*, e1007608.

Pagano, M., Dürst, M., Joswig, S., Draetta, G., and Jansen-Dürr, P. (1992). Binding of the human E2F transcription factor to the retinoblastoma protein but not to cyclin A is abolished in HPV-16-immortalized cells. Oncogene *7*, 1681–1686.

Paoletti, E., and Moss, B. (1974). Two Nucleic Acid-dependent Nucleoside Triphosphate Phosphohydrolases from Vaccinia Virus NUCLEOTIDE SUBSTRATE AND POLYNUCLEOTIDE COFACTOR SPECIFICITIES. J. Biol. Chem. *249*, 3281–3286.

Parker, L.L., and Piwnica-Worms, H. (1992). Inactivation of the p34cdc2-cyclin B complex by the human WEE1 tyrosine kinase. Science *257*, 1955–1957.

Patel, D., Huang, S.-M., Baglia, L.A., and McCance, D.J. (1999). The E6 protein of human papillomavirus type 16 binds to and inhibits co-activation by CBP and p300. EMBO J. *18*, 5061–5072.

Payne, L. (1978). Polypeptide composition of extracellular enveloped vaccinia virus. J. Virol. *27*, 28–37.

Payne, L.G. (1979). Identification of the vaccinia hemagglutinin polypeptide from a cell system yielding large amounts of extracellular enveloped virus. J. Virol. *31*, 147–155.

Payne, L.G. (1980). Significance of Extracellular Enveloped Virus in the in vitro and in vivo Dissemination of Vaccinia. J. Gen. Virol. *50*, 89–100.

Peng, C.-Y., Graves, P.R., Thoma, R.S., Wu, Z., Shaw, A.S., and Piwnica-Worms, H. (1997). Mitotic and G2 Checkpoint Control: Regulation of 14-3-3 Protein Binding by Phosphorylation of Cdc25C on Serine-216. Science *277*, 1501–1505.

Pennington, T.H., and Follett, E.A.C. (1974). Vaccinia Virus Replication in Enucleate BSC-1 Cells: Particle Production and Synthesis of Viral DNA and Proteins. J. Virol. *13*, 488–493.

Peters, N.E., Ferguson, B.J., Mazzon, M., Fahy, A.S., Krysztofinska, E., Arribas-Bosacoma, R., Pearl, L.H., Ren, H., and Smith, G.L. (2013). A Mechanism for the Inhibition of DNA-PK-Mediated DNA Sensing by a Virus. PLOS Pathog. *9*, e1003649.

Phelps, D.E., and Xiong, Y. (1998). Regulation of cyclin-dependent kinase 4 during adipogenesis involves switching of cyclin D subunits and concurrent binding of p18INK4c and p27Kip1. Cell Growth Differ. *9*, 595.

Pogo, B.G., Berkowitz, E.M., and Dales, S. (1984). Investigation of vaccinia virus DNA replication employing a conditional lethal mutant defective in DNA. Virology *132*, 436–444.

Polyak, K., Lee, M.-H., Erdjument-Bromage, H., Koff, A., Roberts, J.M., Tempst, P., and Massagué, J. (1994a). Cloning of p27Kip1, a cyclin-dependent kinase inhibitor and a potential mediator of extracellular antimitogenic signals. Cell *78*, 59–66.

Polyak, K., Kato, J.Y., Solomon, M.J., Sherr, C.J., Massague, J., Roberts, J.M., and Koff, A. (1994b). p27Kip1, a cyclin-Cdk inhibitor, links transforming growth factor-beta and contact inhibition to cell cycle arrest. Genes Dev. *8*, 9–22.

Poon, R.Y., Yamashita, K., Adamczewski, J.P., Hunt, T., and Shuttleworth, J. (1993). The cdc2-related protein p40MO15 is the catalytic subunit of a protein kinase that can activate p33cdk2 and p34cdc2. EMBO J. *12*, 3123–3132.

Postigo, A., Ramsden, A.E., Howell, M., and Way, M. (2017). Cytoplasmic ATR Activation Promotes Vaccinia Virus Genome Replication. Cell Rep. *19*, 1022–1032.

Pozarowski, P., and Darzynkiewicz, Z. (2004). Analysis of Cell Cycle by Flow Cytometry. In Checkpoint Controls and Cancer: Volume 2: Activation and Regulation Protocols, A.H. Schönthal, ed. (Totowa, NJ: Humana Press), pp. 301–311.

Prescott, D.M., Kates, J., and Kirkpatrick, J.B. (1971). Replication of vaccinia virus DNA in enucleated L-cells. J. Mol. Biol. *59*, 505–508.

Punjabi, A., and Traktman, P. (2005). Cell biological and functional characterization of the vaccinia virus F10 kinase: implications for the mechanism of virion morphogenesis. J. Virol. *79*, 2171–2190.

Pütz, M.M., Midgley, C.M., Law, M., and Smith, G.L. (2006). Quantification of antibody responses against multiple antigens of the two infectious forms of Vaccinia virus provides a benchmark for smallpox vaccination. Nat. Med. *12*, 1310–1315.

Radkov, S.A., Kellam, P., and Boshoff, C. (2000). The latent nuclear antigen of Kaposi sarcoma-associated herpesvirus targets the retinoblastoma–E2F pathway and with the oncogene Hras transforms primary rat cells. Nat. Med. *6*, 1121–1127.

Rao, S., Porter, D.C., Chen, X., Herliczek, T., Lowe, M., and Keyomarsi, K. (1999). Lovastatin-mediated G1 arrest is through inhibition of the proteasome, independent of hydroxymethyl glutaryl-CoA reductase. Proc. Natl. Acad. Sci. U. S. A. *96*, 7797–7802.

Re, F., Braaten, D., Franke, E.K., and Luban, J. (1995). Human immunodeficiency virus type 1 Vpr arrests the cell cycle in G2 by inhibiting the activation of p34cdc2-cyclin B. J. Virol. *69*, 6859–6864.

Reinson, T., Henno, L., Toots, M., Jr, M.U., and Ustav, M. (2015). The Cell Cycle Timing of Human Papillomavirus DNA Replication. PLOS ONE *10*, e0131675.

Rempel, R.E., and Traktman, P. (1992). Vaccinia virus B1 kinase: phenotypic analysis of temperature-sensitive mutants and enzymatic characterization of recombinant proteins. J. Virol. *66*, 4413–4426.

Rempel, R.E., Anderson, M.K., Evans, E., and Traktman, P. (1990). Temperature-sensitive vaccinia virus mutants identify a gene with an essential role in viral replication. J. Virol. *64*, 574–583.

Resch, W., and Moss, B. (2005). The Conserved Poxvirus L3 Virion Protein Is Required for Transcription of Vaccinia Virus Early Genes. J. Virol. *79*, 14719–14729.

Resch, W., Hixson, K.K., Moore, R.J., Lipton, M.S., and Moss, B. (2007). Protein composition of the vaccinia virus mature virion. Virology *358*, 233–247.

Reyes, E.D., Kulej, K., Pancholi, N.J., Akhtar, L.N., Avgousti, D.C., Kim, E.T., Bricker, D.K., Spruce, L.A., Koniski, S.A., Seeholzer, S.H., et al. (2017). Identifying Host Factors Associated with DNA Replicated During Virus Infection. Mol. Cell. Proteomics MCP *16*, 2079–2097.

Reynisdóttir, I., and Massagué, J. (1997). The subcellular locations of p15(Ink4b) and p27(Kip1) coordinate their inhibitory interactions with cdk4 and cdk2. Genes Dev. *11*, 492–503.

Reynisdóttir, I., Polyak, K., Iavarone, A., and Massagué, J. (1995). Kip/Cip and Ink4 Cdk inhibitors cooperate to induce cell cycle arrest in response to TGF-beta. Genes Dev. *9*, 1831–1845.

Rico, A.B., Wang, Z., Olson, A.T., Linville, A.C., Bullard, B.L., Weaver, E.A., Jones, C., and Wiebe, M.S. (2019). The Vaccinia B1 and Cellular VRK2 Kinases Promote Vaccinia Replication Factory Formation through Phosphorylation Dependent Inhibition of Vaccinia B12. J. Virol. JVI.00855-19.

Rivas, C., Aaronson, S.A., and Munoz-Fontela, C. (2010). Dual Role of p53 in Innate Antiviral Immunity. Viruses *2*, 298–313.

Rizopoulos, Z., Balistreri, G., Kilcher, S., Martin, C.K., Syedbasha, M., Helenius, A., and Mercer, J. (2015a). Vaccinia Virus Infection Requires Maturation of Macropinosomes. Traffic Cph. Den. *16*, 814–831.

Rizopoulos, Z., Balistreri, G., Kilcher, S., Martin, C.K., Syedbasha, M., Helenius, A., and Mercer, J. (2015b). Vaccinia Virus Infection Requires Maturation of Macropinosomes. Traffic Cph. Den. *16*, 814–831.

Roberts, K.L., and Smith, G.L. (2008). Vaccinia virus morphogenesis and dissemination. Trends Microbiol. *16*, 472–479.

Roberts, K.L., Breiman, A., Carter, G.C., Ewles, H.A., Hollinshead, M., Law, M., and Smith, G.L. (2009). Acidic residues in the membrane-proximal stalk region of vaccinia virus protein B5 are required for glycosaminoglycan-mediated disruption of the extracellular enveloped virus outer membrane. J. Gen. Virol. *90*, 1582–1591.

Rochester, S.C., and Traktman, P. (1998). Characterization of the Single-Stranded DNA Binding Protein Encoded by the Vaccinia Virus I3 Gene. J. Virol. *72*, 2917–2926.

Rodriguez, J.F., and Smith, G.L. (1990). IPTG-dependent vaccinia virus: identification of a virus protein enabling virion envelopment by Golgi membrane and egress. Nucleic Acids Res. *18*, 5347–5351.

Rodríguez, D., Esteban, M., and Rodríguez, J.R. (1995). Vaccinia virus A17L gene product is essential for an early step in virion morphogenesis. J. Virol. *69*, 4640–4648.

Rodríguez, J.R., Risco, C., Carrascosa, J.L., Esteban, M., and Rodríguez, D. (1998). Vaccinia Virus 15-Kilodalton (A14L) Protein Is Essential for Assembly and Attachment of Viral Crescents to Virosomes. J. Virol. *72*, 1287–1296.

Rohrmann, G., Yuen, L., and Moss, B. (1986). Transcription of vaccinia virus early genes by enzymes isolated from vaccinia virions terminates downstream of a regulatory sequence. Cell *46*, 1029–1035.

Romani, B., Shaykh Baygloo, N., Aghasadeghi, M.R., and Allahbakhshi, E. (2015). HIV-1 Vpr Protein Enhances Proteasomal Degradation of MCM10 DNA Replication Factor through the Cul4-DDB1[VprBP] E3 Ubiquitin Ligase to Induce G2/M Cell Cycle Arrest. J. Biol. Chem. *290*, 17380–17389.

Roos, N., Cyrklaff, M., Cudmore, S., Blasco, R., Krijnse-Locker, J., and Griffiths, G. (1996). A novel immunogold cryoelectron microscopic approach to investigate the structure of the intracellular and extracellular forms of vaccinia virus. EMBO J. *15*, 2343–2355.

Rosales, R., Sutter, G., and Moss, B. (1994). A cellular factor is required for transcription of vaccinia viral intermediate-stage genes. Proc. Natl. Acad. Sci. U. S. A. *91*, 3794–3798.

Roshal, M., Kim, B., Zhu, Y., Nghiem, P., and Planelles, V. (2003). Activation of the ATR-mediated DNA Damage Response by the HIV-1 Viral Protein R. J. Biol. Chem. *278*, 25879–25886.

Rössig, L., Badorff, C., Holzmann, Y., Zeiher, A.M., and Dimmeler, S. (2002). Glycogen Synthase Kinase-3 Couples AKT-dependent Signaling to the Regulation of p21Cip1 Degradation. J. Biol. Chem. *277*, 9684–9689.

Rozelle, D.K., Filone, C.M., Kedersha, N., and Connor, J.H. (2014). Activation of stress response pathways promotes formation of antiviral granules and restricts virus replication. Mol. Cell. Biol. *34*, 2003–2016.

Rustum, Y.M., and Raymakers, R.A. (1992). 1-β-arabinofuranosylcytosine in therapy of leukemia: Preclinical and clinical overview. Pharmacol. Ther. *56*, 307–321.

Sakaguchi, K., Herrera, J.E., Saito, S., Miki, T., Bustin, M., Vassilev, A., Anderson, C.W., and Appella, E. (1998). DNA damage activates p53 through a phosphorylation-acetylation cascade. Genes Dev. *12*, 2831–2841.

Sakaue-Sawano, A., Kurokawa, H., Morimura, T., Hanyu, A., Hama, H., Osawa, H., Kashiwagi, S., Fukami, K., Miyata, T., Miyoshi, H., et al. (2008). Visualizing Spatiotemporal Dynamics of Multicellular Cell-Cycle Progression. Cell *132*, 487–498.

Sanchez, Y., Wong, C., Thoma, R.S., Richman, R., Wu, Z., Piwnica-Worms, H., and Elledge, S.J. (1997). Conservation of the Chk1 Checkpoint Pathway in Mammals: Linkage of DNA Damage to Cdk Regulation Through Cdc25. Science *277*, 1497–1501.

Sanderson, C.M., Hollinshead, M., and Smith, G.L. (2000). The vaccinia virus A27L protein is needed for the microtubule-dependent transport of intracellular mature virus particles. J. Gen. Virol. *81*, 47–58.

Santos, C.R., Vega, F.M., Blanco, S., Barcia, R., and Lazo, P.A. (2004). The vaccinia virus B1R kinase induces p53 downregulation by an Mdm2-dependent mechanism. Virology *328*, 254–265.

Sanz, P., and Moss, B. (1999). Identification of a transcription factor, encoded by two vaccinia virus early genes, that regulates the intermediate stage of viral gene expression. Proc. Natl. Acad. Sci. U. S. A. *96*, 2692–2697.

Sarek, G., Järviluoma, A., and Ojala, P.M. (2006). KSHV viral cyclin inactivates p27KIP1 through Ser10 and Thr187 phosphorylation in proliferating primary effusion lymphomas. Blood *107*, 725–732.

Sarid, R., Flore, O., Bohenzky, R.A., Chang, Y., and Moore, P.S. Transcription Mapping of the Kaposi's Sarcoma-Associated Herpesvirus (Human Herpesvirus 8) Genome in a Body Cavity-Based Lymphoma Cell Line (BC-1). J VIROL 8.

Sarov, I., and Joklik, W.K. (1972). Studies on the nature and location of the capsid polypeptides of vaccinia virions. Virology *50*, 579–592.

Satheshkumar, P.S., Anton, L.C., Sanz, P., and Moss, B. (2009). Inhibition of the ubiquitin-proteasome system prevents vaccinia virus DNA replication and expression of intermediate and late genes. J. Virol. *83*, 2469–2479.

Scheffner, M., Huibregtse, J.M., Vierstra, R.D., and Howley, P.M. (1993). The HPV-16 E6 and E6-AP complex functions as a ubiquitin-protein ligase in the ubiquitination of p53. Cell *75*, 495–505.

Schmidt, F.I., Bleck, C.K.E., Helenius, A., and Mercer, J. (2011a). Vaccinia extracellular virions enter cells by macropinocytosis and acid-activated membrane rupture. EMBO J. *30*, 3647–3661.

Schmidt, F.I., Bleck, C.K.E., Helenius, A., and Mercer, J. (2011b). Vaccinia extracellular virions enter cells by macropinocytosis and acid-activated membrane rupture. EMBO J. *30*, 3647–3661.

Schmidt, F.I., Bleck, C.K.E., Reh, L., Novy, K., Wollscheid, B., Helenius, A., Stahlberg, H., and Mercer, J. (2013). Vaccinia Virus Entry Is Followed by Core Activation and Proteasome-Mediated Release of the Immunomodulatory Effector VH1 from Lateral Bodies. Cell Rep. *4*, 464–476.

Schmidt, S., Schenkova, K., Adam, T., Erikson, E., Lehmann-Koch, J., Sertel, S., Verhasselt, B., Fackler, O.T., Lasitschka, F., and Keppler, O.T. (2015). SAMHD1's protein expression profile in humans. J. Leukoc. Biol. *98*, 5–14.

Scutts, S.R., Ember, S.W., Ren, H., Ye, C., Lovejoy, C.A., Mazzon, M., Veyer, D.L., Sumner, R.P., and Smith, G.L. (2018). DNA-PK Is Targeted by Multiple Vaccinia Virus Proteins to Inhibit DNA Sensing. Cell Rep. *25*, 1953-1965.e4.

Seaman, W.T., Ye, D., Wang, R.X., Hale, E.E., Weisse, M., and Quinlivan, E.B. (1999). Gene Expression from the ORF50/K8 Region of Kaposi's Sarcoma-Associated Herpesvirus. Virology *263*, 436–449.

Selgelid, M. (2004). Bioterrorism and smallpox planning: information and voluntary vaccination. J. Med. Ethics *30*, 558–560.

Senkevich, T.G., and Moss, B. (2005). Vaccinia Virus H2 Protein Is an Essential Component of a Complex Involved in Virus Entry and Cell-Cell Fusion. J. Virol. *79*, 4744–4754.

Senkevich, T.G., Bruno, D., Martens, C., Porcella, S.F., Wolf, Y.I., and Moss, B. (2015). Mapping vaccinia virus DNA replication origins at nucleotide level by deep sequencing. Proc. Natl. Acad. Sci. U. S. A. *112*, 10908–10913.

Seo, T., Park, J., Lee, D., Hwang, S.G., and Choe, J. (2001). Viral Interferon Regulatory Factor 1 of Kaposi's Sarcoma-Associated Herpesvirus Binds to p53 and Represses p53-Dependent Transcription and Apoptosis. J. Virol. *75*, 6193–6198.

Serrano, M., Hannon, G.J., and Beach, D. (1993). A new regulatory motif in cell-cycle control causing specific inhibition of cyclin D/CDK4. Nature *366*, 704–707.

Sharp, P.M., and Hahn, B.H. (2011). Origins of HIV and the AIDS Pandemic. Cold Spring Harb. Perspect. Med. *1*.

Sheaff, R.J., Groudine, M., Gordon, M., Roberts, J.M., and Clurman, B.E. (1997). Cyclin E-CDK2 is a regulator of p27Kip1. Genes Dev. *11*, 1464–1478.

Shen, Y., and Nemunaitis, J. (2005). Fighting Cancer with Vaccinia Virus: Teaching New Tricks to an Old Dog. Mol. Ther. *11*, 180–195.

Sherr, C.J. (1993). Mammalian G1 cyclins. Cell *73*, 1059–1065.

Sherr, C.J. (1994). G1 phase progression: Cycling on cue. Cell *79*, 551–555.

Sherr, C.J., and Roberts, J.M. (1999). CDK inhibitors: positive and negative regulators of G1-phase progression. Genes Dev. *13*, 1501–1512.

Shope, R.E. (1932). A Filtrable Virus Causing a Tumor-Like Condition in Rabbits and Its Relationship to Virus Myxomatosum. J. Exp. Med. *56*, 803–822.

Si, H., and Robertson, E.S. (2006). Kaposi's Sarcoma-Associated Herpesvirus-Encoded Latency-Associated Nuclear Antigen Induces Chromosomal Instability through Inhibition of p53 Function. J. Virol. *80*, 697–709.

Sivan, G., Martin, S.E., Myers, T.G., Buehler, E., Szymczyk, K.H., Ormanoglu, P., and Moss, B. (2013). Human genome-wide RNAi screen reveals a role for nuclear pore proteins in poxvirus morphogenesis. Proc. Natl. Acad. Sci. U. S. A. *110*, 3519–3524.

Sivan, G., Weisberg, A.S., Americo, J.L., and Moss, B. (2016). Retrograde Transport from Early Endosomes to the trans-Golgi Network Enables Membrane Wrapping and Egress of Vaccinia Virus Virions. J. Virol. *90*, 8891–8905.

Smith, G.L., Vanderplasschen, A., and Law, M. (2002). The formation and function of extracellular enveloped vaccinia virus. J. Gen. Virol. *83*, 2915–2931.

Smith, G.L., Murphy, B.J., and Law, M. (2003). Vaccinia Virus Motility. Annu. Rev. Microbiol. *57*, 323–342.

So, W.-K., and Cheung, T.H. (2018). Molecular Regulation of Cellular Quiescence: A Perspective from Adult Stem Cells and Its Niches. In Cellular Quiescence: Methods and Protocols, H.D. Lacorazza, ed. (New York, NY: Springer New York), pp. 1–25.

So, S., Davis, A.J., and Chen, D.J. (2009). Autophosphorylation at serine 1981 stabilizes ATM at DNA damage sites. J. Cell Biol. *187*, 977–990.

Sodeik, B., and Krijnse-Locker, J. (2002). Assembly of vaccinia virus revisited: de novo membrane synthesis or acquisition from the host? Trends Microbiol. *10*, 15–24.

Spruck, C., and Strohmaier, H.M. (2002). Seek and Destroy: SCF Ubiquitin Ligases in Mammalian Cell Cycle Control. Cell Cycle *1*, 248–252.

Stiefel, P., Schmidt, F.I., Dörig, P., Behr, P., Zambelli, T., Vorholt, J.A., and Mercer, J. (2012). Cooperative Vaccinia Infection Demonstrated at the Single-Cell Level Using FluidFM. Nano Lett. *12*, 4219–4227.

Sun, Y., Xu, Y., Roy, K., and Price, B.D. (2007). DNA Damage-Induced Acetylation of Lysine 3016 of ATM Activates ATM Kinase Activity. Mol. Cell. Biol. *27*, 8502–8509.

Suzan-Monti, M., La Scola, B., and Raoult, D. (2006). Genomic and evolutionary aspects of Mimivirus. Virus Res. *117*, 145–155.

Swanton, C., Mann, D.J., Fleckenstein, B., Neipel, F., Peters, G., and Jones, N. (1997). Herpes viral cyclin/Cdk6 complexes evade inhibition by CDK inhibitor proteins. Nature *390*, 184–187.

Szajner, P., Weisberg, A.S., Wolffe, E.J., and Moss, B. (2001). Vaccinia virus A30L protein is required for association of viral membranes with dense viroplasm to form immature virions. J. Virol. *75*, 5752–5761.

Szajner, P., Jaffe, H., Weisberg, A.S., and Moss, B. (2003). Vaccinia Virus G7L Protein Interacts with the A30L Protein and Is Required for Association of Viral Membranes with Dense Viroplasm To Form Immature Virions. J. Virol. *77*, 3418–3429.

Szajner, P., Weisberg, A.S., and Moss, B. (2004). Evidence for an Essential Catalytic Role of the F10 Protein Kinase in Vaccinia Virus Morphogenesis. J. Virol. *78*, 257–265.

Szajner, P., Weisberg, A.S., Lebowitz, J., Heuser, J., and Moss, B. (2005). External scaffold of spherical immature poxvirus particles is made of protein trimers, forming a honeycomb lattice. J. Cell Biol. *170*, 971–981.

Takaoka, A., Hayakawa, S., Yanai, H., Stoiber, D., Negishi, H., Kikuchi, H., Sasaki, S., Imai, K., Shibue, T., Honda, K., et al. (2003). Integration of interferon-α/β signalling to p53 responses in tumour suppression and antiviral defence. Nature *424*, 516–523.

Tan, L., Ehrlich, E., and Yu, X.-F. (2007). DDB1 and Cul4A Are Required for Human Immunodeficiency Virus Type 1 Vpr-Induced G2 Arrest. J. Virol. *81*, 10822–10830.

Tattersall, P., and Ward, D.C. (1976). Rolling hairpin model for replication of parvovirus and linear chromosomal DNA. Nature *263*, 106–109.

Taylor, W.R., and Stark, G.R. (2001). Regulation of the G2/M transition by p53. Oncogene *20*, 1803–1815.

Taylor, W.R., Schönthal, A.H., Galante, J., and Stark, G.R. (2001). p130/E2F4 Binds to and Represses the cdc2 Promoter in Response to p53. J. Biol. Chem. *276*, 1998–2006.

Terzi, M.Y., Izmirli, M., and Gogebakan, B. (2016). The cell fate: senescence or quiescence. Mol. Biol. Rep. *43*, 1213–1220.

Thompson, T., Tovar, C., Yang, H., Carvajal, D., Vu, B.T., Xu, Q., Wahl, G.M., Heimbrook, D.C., and Vassilev, L.T. (2004). Phosphorylation of p53 on Key Serines Is Dispensable for Transcriptional Activation and Apoptosis. J. Biol. Chem. *279*, 53015–53022.

Thorne, S.H. (2014). Immunotherapeutic Potential of Oncolytic Vaccinia Virus. Front. Oncol. *4*.

Thorne, S.H., Hwang, T.-H.H., O'Gorman, W.E., Bartlett, D.L., Sei, S., Kanji, F., Brown, C., Werier, J., Cho, J.-H., Lee, D.-E., et al. (2007). Rational strain selection and engineering creates a broad-spectrum, systemically effective oncolytic poxvirus, JX-963. J. Clin. Invest. *117*, 3350–3358.

Tolonen, N., Doglio, L., Schleich, S., and Locker, J.K. (2001). Vaccinia Virus DNA Replication Occurs in Endoplasmic Reticulum-enclosed Cytoplasmic Mini-Nuclei. Mol. Biol. Cell *12*, 2031–2046.

Townsley, A.C., Weisberg, A.S., Wagenaar, T.R., and Moss, B. (2006). Vaccinia Virus Entry into Cells via a Low-pH-Dependent Endosomal Pathway. J. Virol. *80*, 8899–8908.

Toyoshima, H., and Hunter, T. (1994). p27, a novel inhibitor of G1 cyclin-Cdk protein kinase activity, is related to p21. Cell *78*, 67–74.

Tseng, M., Palaniyar, N., Zhang, W., and Evans, D.H. (1999). DNA Binding and Aggregation Properties of the Vaccinia Virus I3L Gene Product. J. Biol. Chem. *274*, 21637–21644.

Tsung, K., Yim, J.H., Marti, W., Buller, R.M.L., and Norton, J.A. (1996). Gene Expression and Cytopathic Effect of Vaccinia Virus Inactivated by Psoralen and Long-Wave UV Light. J VIROL *70*, 7.

Tsuruga, H., Yabuta, N., Hashizume, K., Ikeda, M., Endo, Y., and Nojima, H. (1997). Expression, Nuclear Localization and Interactions of Human MCM/P1 Proteins. Biochem. Biophys. Res. Commun. *236*, 118–125.

Ulaeto, D., Grosenbach, D., and Hruby, D.E. (1996). The vaccinia virus 4c and A-type inclusion proteins are specific markers for the intracellular mature virus particle. J. Virol. *70*, 3372–3377.

Unger, B., Mercer, J., Boyle, K.A., and Traktman, P. (2013). Biogenesis of the Vaccinia Virus Membrane: Genetic and Ultrastructural Analysis of the Contributions of the A14 and A17 Proteins. J. Virol. *87*, 1083–1097.

Vanderplasschen, A., and Smith, G.L. (1997). A novel virus binding assay using confocal microscopy: demonstration that the intracellular and extracellular vaccinia virions bind to different cellular receptors. J. Virol. *71*, 4032–4041.

Vanderplasschen, A., Hollinshead, M., and Smith, G.L. (1998). Intracellular and extracellular vaccinia virions enter cells by different mechanisms. J. Gen. Virol. *79*, 877–887.

Vanslyke, J.K., and Hruby, D.E. (1994). Immunolocalization of Vaccinia Virus Structural Proteins during Virion Formation. Virology *198*, 624–635.

Vanslyke, J.K., Whitehead, S.S., Wilson, E.M., and Hruby, D.E. (1991). The multistep proteolytic maturation pathway utilized by vaccinia virus P4a protein: A degenerate conserved cleavage motif within core proteins. Virology *183*, 467–478.

Vassilev, L.T. (2004). Small-Molecule Antagonists of p53-MDM2 Binding: Research Tools and Potential Therapeutics. Cell Cycle *3*, 417–419.

Vassilev, L.T., Vu, B.T., Graves, B., Carvajal, D., Podlaski, F., Filipovic, Z., Kong, N., Kammlott, U., Lukacs, C., Klein, C., et al. (2004). In Vivo Activation of the p53 Pathway by Small-Molecule Antagonists of MDM2. Science *303*, 844–848.

Vassilev, L.T., Tovar, C., Chen, S., Knezevic, D., Zhao, X., Sun, H., Heimbrook, D.C., and Chen, L. (2006). Selective small-molecule inhibitor reveals critical mitotic functions of human CDK1. Proc. Natl. Acad. Sci. U. S. A. *103*, 10660–10665.

Vaughan, A., Aarons, E., Astbury, J., Balasegaram, S., Beadsworth, M., Beck, C.R., Chand, M., O'Connor, C., Dunning, J., Ghebrehewet, S., et al. (2018). Two cases of monkeypox imported to the United Kingdom, September 2018. Eurosurveillance *23*, 1800509.

Vega, F.M., Sevilla, A., and Lazo, P.A. (2004). p53 Stabilization and accumulation induced by human vaccinia-related kinase 1. Mol. Cell. Biol. *24*, 10366–10380.

Vermeulen, K., Bockstaele, D.R.V., and Berneman, Z.N. (2003). The cell cycle: a review of regulation, deregulation and therapeutic targets in cancer. Cell Prolif. *36*, 131–149.

Verschuren, E.W., Klefstrom, J., Evan, G.I., and Jones, N. (2002). The oncogenic potential of Kaposi's sarcoma-associated herpesvirus cyclin is exposed by p53 loss in vitro and in vivo. Cancer Cell *2*, 229–241.

Verschuren, E.W., Hodgson, J.G., Gray, J.W., Kogan, S., Jones, N., and Evan, G.I. (2004). The Role of p53 in Suppression of KSHV Cyclin-induced Lymphomagenesis. Cancer Res. *64*, 581–589.

Veyer, D.L., Carrara, G., Maluquer de Motes, C., and Smith, G.L. (2017). Vaccinia virus evasion of regulated cell death. Immunol. Lett. *186*, 68–80.

Vlach, J., Hennecke, S., and Amati, B. (1997). Phosphorylation-dependent degradation of the cyclin-dependent kinase inhibitor p27. EMBO J. *16*, 5334–5344.

Vodermaier, H.C. (2004). APC/C and SCF: Controlling Each Other and the Cell Cycle. Curr. Biol. *14*, R787–R796.

Waga, S., Hannon, G.J., Beach, D., and Stillman, B. (1994). The p21 inhibitor of cyclin-dependent kinases controls DNA replication by interaction with PCNA. Nature *369*, 574–578.

Wagner, A.J., Kokontis, J.M., and Hay, N. (1994). Myc-mediated apoptosis requires wild-type p53 in a manner independent of cell cycle arrest and the ability of p53 to induce p21waf1/cip1. Genes Dev. *8*, 2817–2830.

Waldman, T., Kinzler, K.W., and Vogelstein, B. (1995). p21 Is Necessary for the p53-mediated G1 Arrest in Human Cancer Cells. Cancer Res. *55*, 5187–5190.

Wali, A., and Strayer, D.S. (1996). Regulation of p53 Gene Expression by a Poxviral Transcription Factor. Virology *224*, 63–72.

Wali, A., and Strayer, D.S. (1999a). Comparative Effects of Virulent and Avirulent Poxviruses on Cell Cycle Progression. Exp. Mol. Pathol. *66*, 31–38.

Wali, A., and Strayer, D.S. (1999b). Infection with Vaccinia Virus Alters Regulation of Cell Cycle Progression. DNA Cell Biol. *18*, 837–843.

Walker, D.H., and Maller, J.L. (1991). Role for cyclin A in the dependence of mitosis on completion of DMA replication. Nature *354*, 314–317.

Walsh, D., Arias, C., Perez, C., Halladin, D., Escandon, M., Ueda, T., Watanabe-Fukunaga, R., Fukunaga, R., and Mohr, I. (2008). Eukaryotic Translation Initiation Factor 4F Architectural Alterations Accompany Translation Initiation Factor Redistribution in Poxvirus-Infected Cells. Mol. Cell. Biol. *28*, 2648–2658.

Wang, S., and Shuman, S. (1995). Vaccinia virus morphogenesis is blocked by temperature-sensitive mutations in the F10 gene, which encodes protein kinase 2. J. Virol. *69*, 6376–6388.

Wang, I.-H., Suomalainen, M., Andriasyan, V., Kilcher, S., Mercer, J., Neef, A., Luedtke, N.W., and Greber, U.F. (2013). Tracking Viral Genomes in Host Cells at Single-Molecule Resolution. Cell Host Microbe *14*, 468–480.

Wang, S.E., Wu, F.Y., Yu, Y., and Hayward, G.S. (2003a). CCAAT/Enhancer-Binding Protein-α Is Induced during the Early Stages of Kaposi's Sarcoma-Associated Herpesvirus (KSHV) Lytic Cycle Reactivation and Together with the KSHV Replication and Transcription Activator (RTA) Cooperatively Stimulates the Viral RTA, MTA, and PAN Promoters. J. Virol. *77*, 9590–9612.

Wang, S.E., Wu, F.Y., Fujimuro, M., Zong, J., Hayward, S.D., and Hayward, G.S. (2003b). Role of CCAAT/Enhancer-Binding Protein Alpha (C/EBPα) in Activation of the Kaposi's Sarcoma-Associated Herpesvirus (KSHV) Lytic-Cycle Replication-Associated Protein (RAP) Promoter in Cooperation with the KSHV Replication and Transcription Activator (RTA) and RAP. J. Virol. *77*, 600–623.

Wang, T.S., Wong, S.W., and Korn, D. (1989). Human DNA polymerase alpha: predicted functional domains and relationships with viral DNA polymerases. FASEB J. *3*, 14–21.

Wang, Z., Bhattacharya, N., Mixter, P.F., Wei, W., Sedivy, J., and Magnuson, N.S. (2002). Phosphorylation of the cell cycle inhibitor p21Cip1/WAF1 by Pim-1 kinase. Biochim. Biophys. Acta BBA - Mol. Cell Res. *1593*, 45–55.

Wang, Z., Zhang, Y., Gu, J.J., Davitt, C., Reeves, R., and Magnuson, N.S. (2010). Pim-2 phosphorylation of p21Cip1/WAF1 enhances its stability and inhibits cell proliferation in HCT116 cells. Int. J. Biochem. Cell Biol. *42*, 1030–1038.

Warbrick, E., Lane, D.P., Glover, D.M., and Cox, L.S. (1995). A small peptide inhibitor of DNA replication defines the site of interaction between the cyclin-dependent kinase inhibitor p21WAF1 and proliferating cell nuclear antigen. Curr. Biol. *5*, 275–282.

Watanabe, H., Pan, Z.-Q., Schreiber-Agus, N., DePinho, R.A., Hurwitz, J., and Xiong, Y. (1998). Suppression of cell transformation by the cyclin-dependent kinase inhibitor p57KIP2 requires binding to proliferating cell nuclear antigen. Proc. Natl. Acad. Sci. *95*, 1392–1397.

Wei, W., Ayad, N.G., Wan, Y., Zhang, G.-J., Kirschner, M.W., and Kaelin, W.G. (2004). Degradation of the SCF component Skp2 in cell-cycle phase G1 by the anaphase-promoting complex. Nature *428*, 194–198.

Weisberg, A.S., Maruri-Avidal, L., Bisht, H., Hansen, B.T., Schwartz, C.L., Fischer, E.R., Meng, X., Xiang, Y., and Moss, B. (2017). Enigmatic origin of the poxvirus membrane from the endoplasmic reticulum shown by 3D imaging of vaccinia virus assembly mutants. Proc. Natl. Acad. Sci. U. S. A. *114*, E11001–E11009.

Welsch, S., Doglio, L., Schleich, S., and Krijnse Locker, J. (2003). The Vaccinia Virus I3L Gene Product Is Localized to a Complex Endoplasmic Reticulum-Associated Structure That Contains the Viral Parental DNA. J. Virol. *77*, 6014–6028.

White, R.J. (2004). RNA polymerase III transcription and cancer. Oncogene *23*, 3208–3216.

White, R.J., Gottlieb, T.M., Downes, C.S., and Jackson, S.P. (1995). Cell cycle regulation of RNA polymerase III transcription. Mol. Cell. Biol. *15*, 6653–6662.

White, T.E., Brandariz-Nuñez, A., Valle-Casuso, J.C., Amie, S., Nguyen, L.A., Kim, B., Tuzova, M., and Diaz-Griffero, F. (2013). The Retroviral Restriction Ability of SAMHD1, but Not Its Deoxynucleotide Triphosphohydrolase Activity, Is Regulated by Phosphorylation. Cell Host Microbe *13*.

Whitehead, S.S., and Hruby, D.E. (1994). A transcriptionally controlled trans-processing assay: putative identification of a vaccinia virus-encoded proteinase which cleaves precursor protein P25K. J. Virol. *68*, 7603–7608.

WHO (2015). The Independent Advisory Group on Public Health Implications of Synthetic Biology Technology Related to Smallpox.

Wickramasekera, N.T., and Traktman, P. (2010). Structure/Function Analysis of the Vaccinia Virus F18 Phosphoprotein, an Abundant Core Component Required for Virion Maturation and Infectivity. J. Virol. *84*, 6846–6860.

Wiebe, M.S., and Traktman, P. (2007). Poxviral B1 Kinase Overcomes Barrier to Autointegration Factor, a Host Defense against Virus Replication. Cell Host Microbe *1*, 187–197.

Wittek, R., Richner, B., and Hiller, G. (1984). Mapping of the genes coding for the two major vaccinia virus core polypeptides. Nucleic Acids Res. *12*, 4835–4848.

Wright, C.F., Oswald, B.W., and Dellis, S. (2001). Vaccinia Virus Late Transcription Is Activated in Vitro by Cellular Heterogeneous Nuclear Ribonucleoproteins. J. Biol. Chem. *276*, 40680–40686.

Wu, X., and Levine, A.J. (1994). p53 and E2F-1 cooperate to mediate apoptosis. Proc. Natl. Acad. Sci. U. S. A. *91*, 3602–3606.

Yang, Z., and Moss, B. (2009). Interaction of the Vaccinia Virus RNA Polymerase-Associated 94-Kilodalton Protein with the Early Transcription Factor. J. Virol. *83*, 12018–12026.

Yang, X., Huang, B., Deng, L., and Hu, Z. (2018). Progress in gene therapy using oncolytic vaccinia virus as vectors. J. Cancer Res. Clin. Oncol.

Yang, Z., Reynolds, S.E., Martens, C.A., Bruno, D.P., Porcella, S.F., and Moss, B. (2011). Expression Profiling of the Intermediate and Late Stages of Poxvirus Replication ▿. J. Virol. *85*, 9899–9908.

Yoo, N.-K., Pyo, C.-W., Kim, Y., Ahn, B.-Y., and Choi, S.-Y. (2008). Vaccinia virus-mediated cell cycle alteration involves inactivation of tumour suppressors associated with Brf1 and TBP. Cell. Microbiol. *10*, 583–592.

You, Z., Chahwan, C., Bailis, J., Hunter, T., and Russell, P. (2005). ATM Activation and Its Recruitment to Damaged DNA Require Binding to the C Terminus of Nbs1. Mol. Cell. Biol. *25*, 5363–5379.

Young, C.W., and Hodas, S. (1964). Hydroxyurea: Inhibitory Effect on DNA Metabolism. Science *146*, 1172–1174.

Yuan, H., Kamata, M., Xie, Y.-M., and Chen, I.S.Y. (2004). Increased Levels of Wee-1 Kinase in G2 Are Necessary for Vpr- and Gamma Irradiation-Induced G2 Arrest. J. Virol. *78*, 8183–8190.

Zerjatke, T., Gak, I.A., Kirova, D., Fuhrmann, M., Daniel, K., Gonciarz, M., Müller, D., Glauche, I., and Mansfeld, J. (2017). Quantitative Cell Cycle Analysis Based on an Endogenous All-in-One Reporter for Cell Tracking and Classification. Cell Rep. *19*, 1953–1966.

Zhan, Q., Antinore, M.J., Wang, X.W., Carrier, F., Smith, M.L., Harris, C.C., and Fornace, A.J. (1999). Association with Cdc2 and inhibition of Cdc2/Cyclin B1 kinase activity by the p53-regulated protein Gadd45. Oncogene *18*, 2892–2900.

Zhang, Y.F., and Moss, B. (1991). Vaccinia virus morphogenesis is interrupted when expression of the gene encoding an 11-kilodalton phosphorylated protein is prevented by the Escherichia coli lac repressor. J. Virol. *65*, 6101–6110.

Zhang, Q., Yu, Y.A., Wang, E., Chen, N., Danner, R.L., Munson, P.J., Marincola, F.M., and Szalay, A.A. (2007). Eradication of Solid Human Breast Tumors in Nude Mice with an Intravenously Injected Light-Emitting Oncolytic Vaccinia Virus. Cancer Res. *67*, 10038–10046.

Zhang, Y., Keck, J.G., and Moss, B. (1992). Transcription of viral late genes is dependent on expression of the viral intermediate gene G8R in cells infected with an inducible conditional-lethal mutant vaccinia virus. J. Virol. *66*, 6470–6479.

Zhao, H., and Piwnica-Worms, H. (2001). ATR-Mediated Checkpoint Pathways Regulate Phosphorylation and Activation of Human Chk1. Mol. Cell. Biol. *21*, 4129–4139.

Zhao, R.Y., and Elder, R.T. (2005). Viral infections and cell cycle G2/M regulation. Cell Res. *15*, 143–149.

Zhao, R.Y., Li, G., and Bukrinsky, M.I. (2011). Vpr-Host Interactions during HIV-1 Viral Life Cycle. J. Neuroimmune Pharmacol. Off. J. Soc. NeuroImmune Pharmacol. *6*, 216–229.

Zhou, B.P., Liao, Y., Xia, W., Spohn, B., Lee, M.-H., and Hung, M.-C. (2001). Cytoplasmic localization of p21 Cip1/WAF1 by Akt-induced phosphorylation in HER-2/neu -overexpressing cells. Nat. Cell Biol. *3*, 245–252.

Zimmerman, E.S., Sherman, M.P., Blackett, J.L., Neidleman, J.A., Kreis, C., Mundt, P., Williams, S.A., Warmerdam, M., Kahn, J., Hecht, F.M., et al. (2006). Human Immunodeficiency Virus Type 1 Vpr Induces DNA Replication Stress In Vitro and In Vivo. J. Virol. *80*, 10407–10418.

Zimmermann, H., Degenkolbe, R., Bernard, H.-U., and O'Connor, M.J. (1999). The Human Papillomavirus Type 16 E6 Oncoprotein Can Down-Regulate p53 Activity by Targeting the Transcriptional Coactivator CBP/p300. J. Virol. *73*, 6209–6219.

Zindy, F., Quelle, D.E., Roussel, M.F., and Sherr, C.J. (1997). Expression of the p16 INK4a tumor suppressor versus other INK4 family members during mouse development and aging. Oncogene *15*, 203–211.

Zmasek, C.M., Knipe, D.M., Pellett, P.E., and Scheuermann, R.H. (2019). Classification of human Herpesviridae proteins using Domain-architecture Aware Inference of Orthologs (DAIO). Virology *529*, 29–42.

Zou, L., and Elledge, S.J. (2003). Sensing DNA Damage Through ATRIP Recognition of RPA-ssDNA Complexes. Science *300*, 1542–1548.

Zwartouw, H.T. (1964). THE CHEMICAL COMPOSITION OF VACCINIA VIRUS. J. Gen. Microbiol. *34*, 115–123.

(1975). Rapid flow cytofluorometric analysis of mammalian cell cycle by propidium iodide staining. J. Cell Biol. *66*, 188–193.